Université de Montréal

Implication des inhibiteurs de PARP dans le cancer de l'ovaire

par
Hubert Fleury

Programmes de biologie moléculaire
Faculté de Médecine

Thèse présentée à la Faculté des études supérieures et post-doctorales
en vue de l'obtention du grade de Ph.D
en Biologie moléculaire

Directrice de thèse
Dre Anne-Marie Mes-Masson

Co-directrice de thèse
Dre Diane Provencher

Mai 2017

Résumé

Le cancer épithélial de l'ovaire (EOC) est le cancer gynécologique le plus létal en Amérique du Nord. Les inhibiteurs de poly (ADP-Ribose) Polymérase (PARP) ont été utilisés pour en améliorer le traitement ; deux d'entre eux dont l'Olaparib sont approuvés par la FDA. L'Olaparib démontre une bonne efficacité (30% de réponse) en tant qu'agent unique pour les patientes atteintes du cancer de l'ovaire et encore plus pour celles présentant une mutation dans les gènes *BRCA1/2* (45%). Ce résultat a été expliqué comme étant un effet de létalité synthétique entre les mutations *BRCA1/2* qui sont les acteurs principaux du système de réparation de l'ADN par recombinaison homologue (RH) et l'inhibition de PARP qui est l'acteur principal du système de réparation de l'ADN par excision de base (BER). Chez les patientes ne présentant pas de mutation *BRCA1/2* (25%), la réponse observée s'explique également par un effet de létalité synthétique mais cette fois-ci dû soit à la baisse d'expression des gènes *BRCA1/2*, soit à l'inhibition d'autres protéines spécifiques de la RH (effet BRCAness). A contrario, 55% des patientes mutées *BRCA1/2* ne répondent pas au traitement. La réponse globale est seulement de 30% alors que 50% des patientes EOC séreux de haut grade (HGS) présentent une déficience en RH. Pour tenter d'expliquer cette contradiction, cette thèse cherche à définir et à améliorer la réponse à l'Olaparib dans les EOC HGS. Premièrement, il a fallu établir un modèle permettant d'étudier les différentes réponses aux inhibiteurs de PARP. Aux 12 lignées cellulaires d'EOC HGS préexistantes au laboratoire, 6 nouvelles lignées présentant des caractéristiques spécifiques à la réponse aux inhibiteurs de PARP ont été caractérisées et ajoutées [TOV2978G, TOV3041G, TOV3291G, OV866 (2), OV4453 (mutation non-sens récurrente *BRCA2* d'origine germinale) et OV4485 (mutation du site d'épissage *BRCA1*)]. À partir de ce modèle cellulaire, un nouveau schéma prédictif de la sensibilité à l'Olaparib a été déterminé. On y expose l'idée que les patientes y répondant présentent une déficience en RH (BRCAness) mais qu'elle doit être combinée à une déficience en NER ou en MMR. Malgré les efforts pour cibler ces patientes et pour produire de nouveaux inhibiteurs de PARP plus efficaces, la réponse globale reste toujours autour de 30%, les cas de résistance acquise sont de plus en plus nombreux et le traitement drastique de maintenance

reste encore le seul moyen d'obtenir une réponse clinique. Tout cela nous a amené, comme troisième objectif, à nous concentrer sur le type de destin cellulaire induit par les inhibiteurs de PARP nous permettant de déterminer une combinaison thérapeutique pour améliorer la réponse. Nous démontrons que l'Olaparib conduit à un état sénescent réversible dans les lignées cellulaires de EOC HGS malgré leurs mutations *TP53*. Cet état peut être ciblé par des sénolytiques (principalement un inhibiteur de Bcl2/Bcl-XL) pour créer une réponse synergique lorsqu'ils sont associés à des inhibiteurs de PARP. Les expériences *in vivo* confirment l'efficacité de la combinaison thérapeutique. Ces travaux ont contribué à donner une meilleure identification des patientes susceptibles de répondre aux inhibiteurs de PARP et à déterminer une nouvelle thérapie combinée particulièrement efficace.

Mots clés : Séreux de haut grade, Cancer épithélial de l'ovaire, lignée cellulaire, mutation BRCA, inhibiteurs de PARP, Olaparib, réparation de l'ADN, NER, MMR, sénescence, arrêt du cycle cellulaire, combinaison thérapeutique.

Abstract

Epithelial ovarian cancer (EOC) is the most lethal gynaecological cancer in North America. Poly (ADP-Ribose) Polymerase (PARP) inhibitors have been used to improve treatment; two of which including Olaparib are approved by the FDA. Olaparib demonstrates good efficacy (30% response) as a single agent for patients with ovarian cancer and even more so for those with a mutation in the BRCA1/2 (45%) genes. This result was explained as a consequence of synthetic lethality between the mutants BRCA1/2; which are the principal actors of the DNA repair system by homologous recombination (HR), and the inhibition of PARP, which is the main actor of DNA repair by base excision repair (BER). In patients with no BRCA1/2 mutation (25%), the observed response is also explained by an effect of synthetic lethality, but this time due to either a decline in BRCA1/2 gene expression or the inhibition of other proteins specific to HR (BRCAness effect). In contrast, 55% of BRCA1/2 mutated patients did not respond to treatment. The overall response is only 30%, while 50% of high-grade serous (HGS) EOC patients have an HR deficiency. To try to explain this contradiction, this thesis seeks to define and improve the response to Olaparib in the HGS EOCs. First, a model was developed to study the different responses to PARP inhibitors. To the 12 pre-existing EOC HGS cell lines in the laboratory, 6 new lines presenting with characteristics specific to PARP inhibitors response were characterized and added [TOV2978G, TOV3041G, TOV3291G, OV866 (2), OV4453 (recurrent BRCA2 nonsense mutation of germinal origin) and OV4485 (splice-site mutation BRCA1)]. From this cell model, a new predictive pattern of susceptibility to Olaparib was determined. The idea presented is that the responding patients have an HR deficiency (BRCAness) but that it must be combined with a NER or MMR deficiency. Despite efforts to target these patients and to produce new, more effective PARP inhibitors, the overall response is still around 30%; cases of acquired resistance are increasing and drastic maintenance treatment is still the only way to obtain a clinical response. All this has led us as a third objective to focus on the type of cellular fate induced by the PARP inhibitors allowing us to determine a combination therapy for an improved response. We demonstrate that Olaparib leads to a reversible senescent state in the HGS EOC cell lines

despite their TP53 mutations. This condition can be targeted by senolytics (mainly a Bcl2 / Bcl-XL inhibitor) to create a synergistic response when combined with PARP inhibitors. The in vivo experiments confirm the efficacy of the therapeutic combination. This work has contributed to the better identification of patients who are able to respond to PARP inhibitors and to determine a new and particularly effective combination therapy.

Keywords: high-grade serous, ovarian epithelial cancer, cell line, BRCA mutation, PARP inhibitors, Olaparib, DNA repair, NER, MMR, senescence, cell cycle arrest, therapeutic combination.

Liste des publications et contributions

Hubert Fleury*, Laudine Communal*, Euridice Carmona, Lise Portelance, Suzanna L. Arcand, Kurosh Rahimi, Patricia N. Tonin, Diane Provencher, Anne-Marie Mes-Masson (2015) Novel high-grade serous epithelial ovarian cancer cell lines that reflect the molecular diversity of both the sporadic and hereditary disease. Genes & Cancer, Vol. 6 (9-10) * These authors contributed equally (1)

Maud Marques*, Marie-Claude Beauchamp*, **Hubert Fleury**, Ido Laskov, Sun Qiang, Manuela Pelmus, Diane Provencher, Anne-Marie Mes-Masson, Walter H Gotlieb, Michael Witcher (2015) Chemotherapy reduces PARP1 in cancers of the ovary: implications for future clinical trials involving PARP inhibitors. BMC medicine 13 (1), 217. * These authors contributed equally to the work (2)

Hubert Fleury, Euridice Carmona, Vincent G. Morin, Liliane Meunier, Jean-Yves Masson, Patricia N. Tonin, Diane Provencher, Anne-Marie Mes-Masson (2016) Cumulative defects in DNA repair pathways drive the PARP inhibitor response in high-grade serous epithelial ovarian cancer cell lines. Oncotarget. 2016;8(25):40152(3)

Lydia Edjekouane, Samira Benhadjeba, Maïka Jangal, **Hubert Fleury**, Nicolas Gévry, Euridice Carmona, André Tremblay (2016) Proximal and distal regulation of the HYAL1 gene cluster by the estrogen receptor α in breast cancer cells. Oncotarget 7 (47), 77276. (4)

Anthony M Couturier, **Hubert Fleury**, Anne-Marie Patenaude, Victoria L Bentley, Amélie Rodrigue, Yan Coulombe, Joshi Niraj, Joris Pauty, Jason N Berman, Graham Dellaire, Javier M Di Noia, Anne-Marie Mes-Masson, Jean-Yves Masson (2016) Roles for APRIN (PDS5B) in homologous recombination and in ovarian cancer prediction. Nucleic Acids Research 44 (22), 10879-10897. (5)

Yi Kan Wang, Ali Bashashati, Michael S Anglesio, Dawn R Cochrane, Diljot S Grewal, Gavin Ha, Andrew McPherson, Hugo M Horlings, Janine Senz, Leah M Prentice, Anthony N Karnezis, Daniel Lai, Mohamed R Aniba, Allen W Zhang, Karey Shumansky, Celia Siu, Adrian Wan, Melissa K McConechy, Hector Li-Chang, Alicia Tone, Diane Provencher, Manon de Ladurantaye, **Hubert Fleury**, Aikou Okamoto, Satoshi Yanagida, Nozomu Yanaihara, Misato Saito, Andrew J Mungall, Richard Moore, Marco A Marra, C Blake Gilks, Anne-Marie Mes-Masson, Jessica N McAlpine, Samuel Aparicio, David G Huntsman, Sohrab P Shah (2017) Genomic consequences of aberrant DNA repair mechanisms stratify ovarian cancer histotypes. Nat Genet. 2017;49(6):856-65(6)

Manuscrit en preparation

Hubert Fleury*, Nicolas Malaquin*, Aurelie Martinez, Alexandre Sauriol, Euridice Carmona, Diane Provencher, Anne-Marie Mes-Masson and Francis Rodier. PARP inhibitors elicit a reversible cancer senescence state targetable by senolytics. En preparation pour Nature.
* These authors contributed equally

Publications inclues dans cette these

Hubert Fleury[*], Laudine Communal[*], Euridice Carmona, Lise Portelance, Suzanna L. Arcand, Kurosh Rahimi, Patricia N. Tonin, Diane Provencher, Anne-Marie Mes-Masson (2015) Novel high-grade serous epithelial ovarian cancer cell lines that reflect the molecular diversity of both the sporadic and hereditary disease Genes & Cancer, Vol. 6 (9-10) * These authors contributed equally

– Inclue comme Chapitre 1

Auteurs	Contributions
Hubert Fleury (Candidat)	Mise au point des expériences (40%)
	Analyses et interprétation des données (40%)
	Ecriture du papier (20%)
Laudine Communal	Mise au point des expériences (35%)
	Analyses et interprétation des données (40%)
	Ecriture du papier (20%)
Euridice Carmona	Mise au point des expériences (10%)
	Analyses et interprétation des données (20%)
	Ecriture du papier (25%)
Lise Portelance	Mise au point des expériences (5%)
	Analyses et interprétation des données (0%)
	Ecriture du papier (0%)
SuzannaL. Aracand	Mise au point des expériences (5%)
	Analyses et interprétation des données (0%)
	Ecriture du papier (0%)
Kurosh Rahimi	Mise au point des expériences (0%)
	Analyses et interprétation des données (0%)
	Ecriture du papier (5%)
Patricia N. Tonin	Mise au point des expériences (0%)
	Analyses et interprétation des données (0%)
	Ecriture du papier (10%)
Diane Provencher	Mise au point des expériences (0%)
	Analyses et interprétation des données (0%)
	Ecriture du papier (5%)
Anne-Marie Mes-Masson	Mise au point des expériences (5%)
	Analyses et interprétation des données (0%)
	Ecriture du papier (15%)

Hubert Fleury, Euridice Carmona, Vincent G. Morin, Liliane Meunier, Jean-Yves Masson, Patricia N. Tonin, Diane Provencher, Anne-Marie Mes-Masson (2016) Cumulative defects in DNA repair pathways drive the PARP inhibitor response in high-grade serous epithelial ovarian cancer cell lines. Oncotarget. 2016;8(25):40152

– Inclue comme Chapitre 2

Auteurs	Contributions
Hubert Fleury (Candidat)	Mise au point des expériences (85%)
	Analyses et interprétation des données (50%)
	Ecriture du papier (30%)
Euridice Carmona	Mise au point des expériences (5%)
	Analyses et interprétation des données (35%)
	Ecriture du papier (25%)
Vincent G.Morin	Mise au point des expériences (5%)
	Analyses et interprétation des données (0%)
	Ecriture du papier (0%)
Liliane Meunier	Mise au point des expériences (5%)
	Analyses et interprétation des données (0%)
	Ecriture du papier (0%)
Jean-Yves Masson	Mise au point des expériences (0%)
	Analyses et interprétation des données (5%)
	Ecriture du papier (10%)
Patrica N.Tonin	Mise au point des expériences (0%)
	Analyses et interprétation des données (0%)
	Ecriture du papier (10%)
Diane Provencher	Mise au point des expériences (0%)
	Analyses et interprétation des données (0%)
	Ecriture du papier (5%)
Anne-Marie Mes-Masson	Mise au point des expériences (0%)
	Analyses et interprétation des données (10%)
	Ecriture du papier (20%)

Hubert Fleury*, Nicolas Malaquin*, Aurelie Martinez, Alexandre Sauriol, Euridice Carmona, Diane Provencher, Anne-Marie Mes-Masson# and Francis Rodier# (en préparation pour début 2018) PARP inhibitors elicit a reversible cancer senescence state targetable by senolytics. En préparation pour Nature. * These authors contributed equally

– Inclue comme Chapitre 3

Auteurs	Contributions
Hubert Fleury (Candidat)	Mise au point des expériences (45%)
	Analyses et interprétation des données (35%)
	Ecriture du papier (25%)
Nicolas Malaquin	Mise au point des expériences (45%)
	Analyses et interprétation des données (35%)
	Ecriture du papier (25%)
Aurélie Martinez	Mise au point des expériences (5%)
	Analyses et interprétation des données (0%)
	Ecriture du papier (0%)
Alexandre Suariol	Mise au point des expériences (5%)
	Analyses et interprétation des données (0%)
	Ecriture du papier (0%)
Euridice Carmona	Mise au point des expériences (0%)
	Analyses et interprétation des données (10%)
	Ecriture du papier (25%)
Diane Provencher	Mise au point des expériences (0%)
	Analyses et interprétation des données (0%)
	Ecriture du papier (5%)
Anne-Marie Mes-Masson	Mise au point des expériences (0%)
	Analyses et interprétation des données (10%)
	Ecriture du papier (10%)
Francis Rodier	Mise au point des expériences (0%)
	Analyses et interprétation des données (10%)
	Ecriture du papier (10%)

Remerciements

Je tiens à remercier tout d'abord ma directrice de recherche, Dre. Anne-Marie MES-MASSON, professeure à l'Université de Montréal, qui m'a initié au monde de la recherche et sans qui tout simplement cette thèse n'éxisterait pas. Merci d'avoir misé puis par la suite cru en moi en me laissant réaliser cette thèse. Son support durant mon cheminement fut ni trop ni pas assez, me permettant de finir ma thèse mais aussi de me sentir indépendant ; merci chaleureusement pour cela Anne-Marie. Je remercie également ma co-directrice de recherche, Dre. Diane Provencher, professeure à l'Université de Montréal, pour m'avoir apporté le côté clinique du cancer. Dre Euridice Carmona, merci pour ton soutien, merci pour tes idées, tes conseils ; c'est une personne sur qui j'ai pu compter durant toutes ces années, merci Euridice. Je remercie aussi Dr. R Bertrand, Dr F Rodier, Dr. JY Masson, Dre P Tonin. Merci également à tous les membres de l'équipe (Louise, Ben, Cécile, Véro, Mélissa, Jackie, Amine, Lateef, Patra, Nathalie, Claudia, Geneviève, Chantale, Jennifer, Monique, Christine, René, Doris, Gabriela, Maxime, Kayla, Adriana et Alexandre) qui ont participé à rendre ma vie au laboratoire agréable, facile et joyeuse. De plus, les personnes qui, en plus, ont eu le malheur de travailler avec moi, je leur tire mon chapeau et m'excuse pour toutes les blagues ou retards qu'elles ont eu à subir en travaillant avec moi, je parle particulièrement de Lise, Manon, Kim et Liliane. Un grand merci à ceux qui ont fait que ma vie au laboratoire va terriblement me manquer, ceux sans qui toutes ces années au laboratoire m'auraient paru très longues, je parle ici de Gany, Laudine, Zied, Nicolas M., Nicolas L., Yannick, Sylvie, Aurélie, Sophie, David, merci à vous, merci les amis. Une pensée aussi aux amis extérieurs au laboratoire, extérieurs à la science, une bouffée d'air frais permettant de vivre à côté de la recherche, merci d'avoir été là. Enfin, je remercie mes parents, Christine et Luc et ma sœur Lise d'avoir toujours cru en moi, de m'avoir soutenu, un pilier important et solide que j'ai la chance d'avoir. Finalement, je tiens à remercier un autre pilier de ma vie, ma conjointe Julie Betelu pour simplement être la personne la plus chouette que j'ai pu rencontrer dans ma vie. Julie, merci pour ton support, ta patience immense et merci d'avoir toujours été présente même dans mes moments les plus désagréables.

Tables des matières

Liste des figures

Chapitre 2 : Cumulative defects in DNA repair pathways drive the PARP inhibitor response in high-grade serous epithelial ovarian cancer cell lines

Chapitre 3 : PARP inhibitors induce a reversible senescence-like state in cancer cells that renders them susceptible to elimination by the Bcl2 family of inhibitors

Liste des tableaux

Liste des abréviations

53BP1	53 binding protein
ADN	Acide désoxyribonucléique
AKT	Serine/threonine kinase
ARNm	Acide ribonucléique message
ATP	Adenosine triphosphate
ATP7A -B:	ATPase copper transporting alpha A-B
BAX	BCL2 associated X, apoptosis regulator
BER	Base excision repair
BRCA1	Breast Cancer 1
BRCA2	Breast Cancer 2
CDK12	Cyclin dependent kinase 12
CGH	Comparative genomic hybridization
CHEK1-2	Checkpoint kinase 1
CK7-8-18-19	Cytokératine 7-8-18-19
CREBBP	CREB binding protein
CSA/CSB	Cockayne syndrome A/B
CSMD3	CUB and Sushi multiple domains 3
CTR1	Solute carrier family 31 member 1
DDB1	Damage specific DNA binding factor 1
DNA-PK	DNA phospho kinase
DSB	Double strand break
EGFR	Epidermal growth factor receptor
EMSY	EMSY, *BRCA2* interacting transcriptional repressor
EOC	Cancer épithélial de l'ovaire
ERCC1-6	ERCC excision repair 1-6
FANCA-I-L-C	Fanconi anemia complementation group A-I-L-C
FANCJ	*BRCA1* interacting protein C-terminal helicase 1
FAT3	FAT atypical cadherin 3
FDA	Federal drug association
FOXO3A	AKT-associated phosphorylation of forkhead box O
GABRA6	Gamma-aminobutyric acid type 1 receptor alpha 6
HER2	Erb-b2 receptor tyrosine kinase 2
HGS	Séreux de haut grade
HIF1	Basic helix-loop-helix proteins
HSP90	Heat shock protein 90
IC50	Inhibition concentration 50

IL-6-8	Interleukine-6-8
JNK	Jun N-terminal kinase
KU70-80	X-ray repair cross complementing 6-5
LGS	Séreux de bas grade
MAPK1	Mitogen-activated protein kinase 1
MECOM	MDS1 and EVI1 complex locus
MLH1	mutL homolog 1
MMR	Mismatch repair
MSH2-6	mutS homolog 2-6
mTOR	Mechanistic target of rapamycin
MUC16	mucin 16
NAD+	Nicotinamide adénine dinucléotide
NER	Nucléotide excision repair
NF1	Neurofibromin 1
NHEJ	Non Homologous end joining
NOXA	BCL2 homology region 3 (BH3) only
OGG1	8-oxoguanine DNA glycosylase
p16-21-27	Cyclin dependent kinase inhibitor 2A-1A-1B
p53	Tumor protein p53
PALB2	Partner and localizer of *BRCA2*
PAR	Poly ADP ribose
PARP	Poly (ADP-Ribose) polymerase
PML	Promyelocytic leukemia
PMS2	MutL homologs
PTEN	Phosphatase and tensin homolog
RAD23	Homolog A, nucleotide excision repair protein
RFC1	Replication factor C subunit 1
RH	Recombinaison Homologue
RPA	Replication protein A
RRH	Réparation par Recombinaison Homologue
SA-b-Gal	Senescence-associated beta galactosidase
SCID	Severe combined immunodefeciency
Slug	snail family transcriptional repressor 2
Snail	SNAG transcriptional repressors
TCGA	The Cancer Genome Atlas
TEM	Transition epithélio-mésenchymateuse
Timp-1	TIMP metallopeptidase inhibitor 1
UV	Ultra violet
VEGF	Vascular endothelial growth factor A
XPF	ERCC excision repair 4, endonuclease catalytic subunit
Zeb1	zinc finger E-box binding homeobox 1

1 INTRODUCTION

1.1 Cancer de l'ovaire

1.1.1 Statistiques

Selon la Société canadienne du cancer, le cancer de l'ovaire est le cancer gynécologique le plus létal. Chez la femme, ce cancer est le 5ème plus mortel après celui du poumon, du sein, colorectal et pancréatique. En Amérique du Nord environ 65% des femmes diagnostiquées avec un cancer de l'ovaire vont en décéder (22280 nouveaux cas dont 14240 qui en mourront en 2016) (7). La survie nette après 5 ans est de 46% en Amérique du Nord et s'améliore à environ 90% si le cancer est diagnostiqué à des stades précoces. Malheureusement, seulement 20-30% des cas sont découverts lorsque le cancer est encore limité aux ovaires, ce qui démontre bien la nécessité d'un diagnostic précoce.

1.1.2 Anatomie de l'ovaire

Les ovaires sont les organes de l'appareil reproducteur chez la femme. Ils sont situés de chaque côté de l'utérus symétriquement à la paroi pelvienne. Ils sont responsables de la production des œufs (ovules) et des hormones féminines comme l'estrogène et la progestérone. Ils mesurent environ 3 à 5 cm en longueur et pèsent environ 2 à 4 grammes. Les ovaires sont principalement formés de cellules épithéliales, stromales et germinales. Les cellules épithéliales vont former une monocouche à la surface externe des ovaires, les cellules stromales forment les follicules et le tissu conjonctif servant à maintenir les composantes de l'ovaire ensemble et les germinales ou ovocytes sont les cellules reproductives et se trouvent à la périphérie des ovaires (8) (Figure 1).

1.1.3 Symptômes et méthodes de détection du cancer de l'ovaire

Cliniquement, les différents cancers de l'ovaire se présentent souvent comme une masse pouvant atteindre une taille importante au niveau du bassin. En général, les symptômes peuvent être ressentis au niveau abdominal, gastro-intestinal, génito-urinaire. Ils se caractérisent par une augmentation de la taille abdominale, des ballonnements, une fatigue accrue, des douleurs abdominales, dorsales et/ou pelviennes, de l'indigestion, une fréquence urinaire augmentée, de la constipation, une incontinence urinaire, de la douleur ou des saignements lors des rapports sexuels, de la satiété précoce, une perte de poids, des nausées, de la thrombose veineuse profonde et de la diarrhée (9, 10). Si l'un de ces symptômes est présent à une fréquence inhabituelle, il devrait inciter un médecin à soupçonner un cancer de l'ovaire (11). Ces symptômes ressemblent à des problèmes bénins, ce qui retarde le diagnostique. La recherche doit donc découvrir de nouvelles techniques pour détecter le cancer de l'ovaire à des stades plus précoces. La méthode d'examen pelvien annuel ne fonctionne pas pour la détection précoce de cancer de l'ovaire (12). L'analyse de biomarqueurs spécifiques dans le sérum, comme l'antigène tumoral CA 125 (MUC16), est une méthode largement utilisée en clinique pour le cancer de l'ovaire car non invasive et relativement fiable. L'antigène tumoral CA 125 est une glycoprotéine de grand poids moléculaire (200-2000 kDa) de la famille des mucines transmembranaires. L'expression de MUC16 est retrouvée dans la majorité des cancers épithéliaux de l'ovaire (EOC) mais pas dans l'épithélium ovarien normal (13). On observe un haut niveau de CA 125 (>35U/mL) chez plus de 80% des patientes présentant un stade avancé du cancer épithélial de l'ovaire. Ce marqueur peut être augmenté dans d'autres cas créant ainsi des faux positifs, son expression varie selon les différents types et sous-types du cancer de l'ovaire et il n'est pas toujours corrélé avec la malignité de la tumeur. Il peut être cependant utilisé comme test d'accompagnement lors du diagnostic ou pour suivre la maladie pendant le traitement de chimiothérapie (14). Le cancer de l'ovaire est donc asymptomatique et reste difficile à détecter précocément et donc à traiter.

1.1.4 Types de cancer de l'ovaire

Le cancer de l'ovaire est classifié en trois grands groupes en fonction du type cellulaire d'origine de la tumeur (Figure 1). Les tumeurs germinales représentent 10-15% et sont dérivées des cellules germinales de l'ovaire. Les tumeurs stromales proviennent des follicules ou des cellules des tissus du stroma qui soutiennent les ovaires et représentent environ 8% de toutes les tumeurs ovariennes. Plus de 75% des tumeurs germinales et stromales sont détectées chez les jeunes patientes de moins de 20 ans et dans la plupart des cas restent confinées au niveau de l'ovaire. De plus, elles sont souvent détectées à des stades précoces permettant un excellent pronostic après chirurgie et traitements (15, 16). Les tumeurs épithéliales, décrites comme dérivées de la monocouche épithéliale de l'ovaire (17), sont les cancers ovariens les plus létaux et les plus fréquents (80%). Ce fort taux explique qu'il soit le plus étudié.

Récemment l'origine des tumeurs épithéliales de l'ovaire pour certains sous-types est remise en question, entre autres, par la découverte de la mutation *TP53* au niveau de la couche épithéliale des trompes de Fallope (18) (19). Dans d'autres cas, l'endométriose pourrait être aussi une origine du cancer. Sachant que l'ovaire est une niche importante pour le développement de la tumeur (20), on peut envisager un modèle mixte de trompes de Fallope et d'épithélium ovarien. Dans cette thèse on s'intéressera principalement au cancer épithélial de l'ovaire.

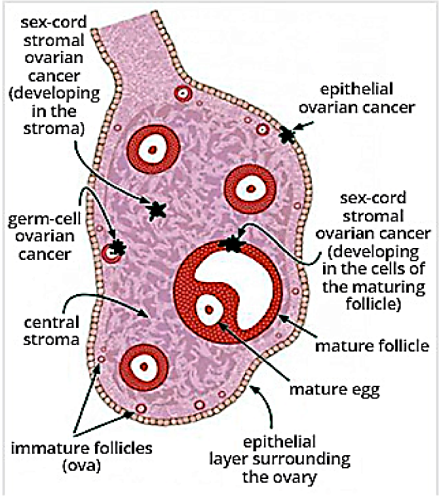

Figure 1: Types du cancer de l'ovaire et leurs précurseurs
https://canceraustralia.gov.au/affected-cancer/cancertypes/gynaecological-cancers/ovarian-cancer/about-ovarian-cancer. ***©****Commonwealth of Australia 2016*

1.2 Cancer épithélial de l'ovaire

Les EOCs sont hétérogènes et peuvent être divisés en quatre principaux sous-types. Les sous-types séreux (représentant 60-70%), endométrioïdes (10-20%), mucineux (5-20%) et de cellules claires (3-10%) avec des taux de survie à 5 ans respectivement de 20 à 35%, de 40 à 63%, de 40 à 69%, de 35 à 50% sont les plus courants (Figures 2) (21-23). Chacun de ces sous-types est génétiquement distinct avec des caractérisations moléculaires uniques et une susceptibilité aux agents chimiothérapeutique différente. Les mécanismes sous-jacents à cette hétérogénéité restent encore mal documentés. Au cours des dernières années, la compréhension de la pathologie et de l'initiation des évènements moléculaires dans les différents sous-types du EOC s'est considérablement améliorée (24, 25). Malgré cette hétérogénéité, les exigences de Santé Canada font qu'à l'heure actuelle, nous ne différencions pas assez ces sous-types pour les traiter comme des groupes indépendants. Il est impératif pour les chercheurs et les cliniciens d'accroître les connaissances concernant les caractéristiques de ces sous-types du EOC.

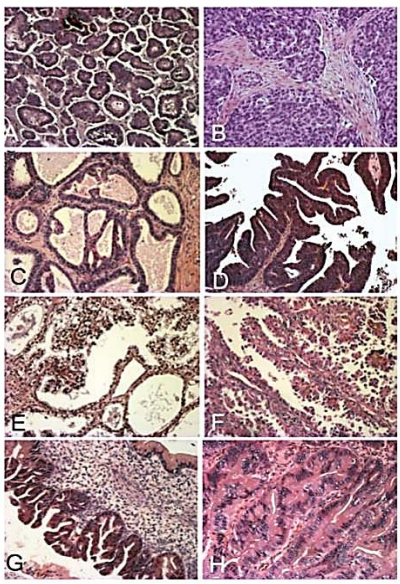

Figure 2 : Représentation des quatre sous-types histologiques les plus communs d'EOC
Ovarian cancer: pathology, biology, and disease models; Daniel G. Rosen, Front Bioscience, 2010 (A) Carcinome séreux de l'ovarien montrant la formation de papilles. B : Carcinome séreux de l'ovaire avec une croissance prédominant. (C) Tumeur endométrioïde de l'ovaire à faible potentiel malin présentant des glandes semblables à l'hyperplasie complexe de l'endomètre utérin. (D) Intérêt sur carcinome endométrioïde de l'ovaire morphologiquement similaire au carcinome endométrioïde de l'utérus. (E) Carcinome clair de l'ovaire illustrant la clairance cellulaire et le modèle de croissance kystique. (F) Intérêt sur carcinome ovarien à cellules claires de l'ovaire avec un modèle de croissance de cellules ''hobnail''. (G) Tumeur mucineuse de l'ovaire à faible potentiel malin. (H) Carcinome mucineux de l'ovaire bien différencié.

1.2.1 Caractéristiques générales:

Le sous-type séreux, représentant environ 65% des EOCs, est le plus fréquent et est considéré comme le plus létal (26). Les tumeurs séreuses sont classées en bas ou haut grade selon plusieurs critères (17, 27). Le sous-type endométrioïde représente 10 à 20% des EOCs, il est plus fréquemment diagnostiqué chez les femmes âgées d'environ 50 ans (28). Tout comme les EOCs séreux, les endométrioïdes sont classés de bas ou haut grade (29). Le sous-type de cellules claires, relativement peu fréquent, représente environ 5 à 10% des cancers épithéliaux de l'ovaire avec un taux de survie plus faible que les autres sous-types (30). Au Japon, ce sous-type est bien plus fréquent (25% des EOC) que dans les pays de l'ouest comme l'Amérique du Nord (31). Finalement, les tumeurs mucineuses représentent environ 5-10% des cas intégrant des tumeurs bénignes et malignes pour respectivement 85% et 10% (17). Les recherches suggèrent que de nombreux carcinomes ovariens peuvent provenir de l'extérieur des ovaires mais des questions demeurent quant à leur origine et leur progression (Figure 3).

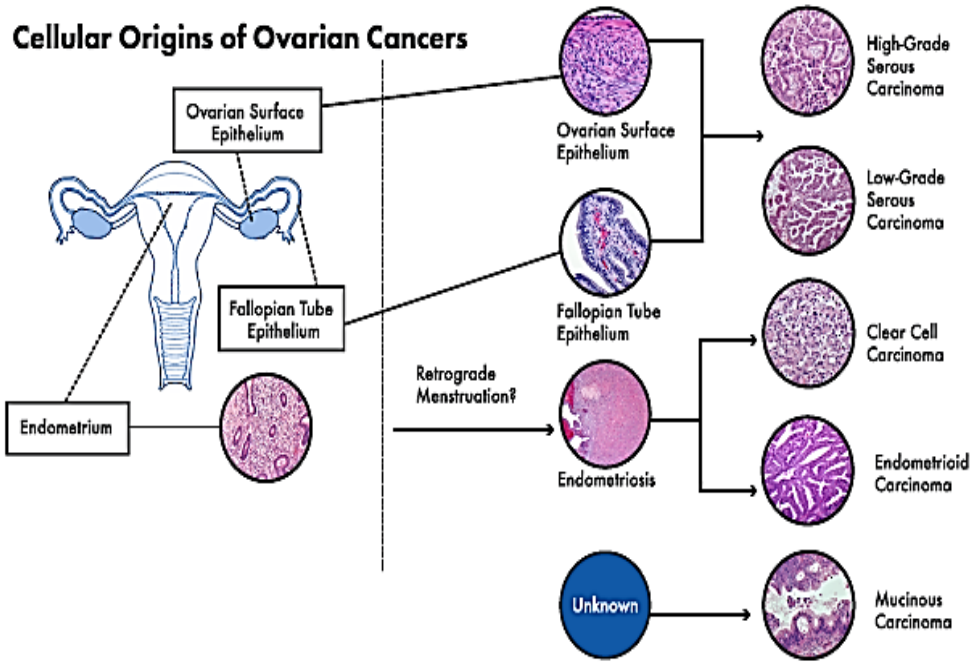

Figure 3: Origine cellulaire du cancer de l'ovaire
The national Academies of Sciences, engineering, medecine, 2016
(http://resources.nationalacademies.org/Infographics/OvarianCancers/Research-Guide.html)

1.2.2 Facteurs de risque héréditaires

Connaître les facteurs influençant le développement d'un cancer de l'ovaire facilite sa prévention et sa détection précoce. L'âge, comme pour la plupart des cancers, est l'un des principaux facteurs de risque. L'âge médian des patientes au moment du diagnostic est compris entre 60 à 70 ans (32). L'historique familial du cancer de l'ovaire et/ou du sein est un autre facteur significatif, cette hérédité représente 5 à 15% des cas (33). Deux principaux types de prédisposition héréditaire du cancer de l'ovaire ont été largement documentés. Le plus important, représentant 90% des patientes atteintes du cancer ovarien héréditaire, est caractérisé par des mutations germinales des gènes Breast Cancer 1 (*BRCA1*) / Breast Cancer 2 (*BRCA2*). Pour une femme ayant une mutation *BRCA1*, le risque de cancer de l'ovaire épithélial est de 39 à 46% et, avec une mutation *BRCA2*, de 12 à 20% (32, 34, 35) (36). Les autres 10% sont dus à des mutations dans certains gènes de la réparation par mésappariements (Mismatch Repair, MMR) comme *MLH1, MSH2, MSH6* associés à un syndrome de Lynch II, dans le gène *TP53* et dans plusieurs autres gènes impliqués dans la recombinaison homologue (RH) tels que *CHEK2, RAD51, BRIP1* (*BRCA1* interacting protein C-terminal helicase 1) et *PALB2* (32, 37, 38).

1.2.3 Caractéristiques moléculaires

La caractérisation moléculaire des différents sous-types des EOCs distingue les cancers séreux de haut grade (HGS) des autres sous-types. Par exemple, comparativement au HGS, les EOCs à cellules claires présentent peu de mutations *TP53* mais des mutations *ARID1A* (AT-rich interaction domain 1A) et *PIK3CA* (Phosphatidylinositol-4,5-biphosphate 3-kinase catalytic) récurrentes (39). Les tumeurs endométrioïdes ont fréquemment des mutations pour *CTNNB1* (Catenin beta 1), *ARID1A* et *PIK3CA*. Enfin, les tumeurs mucineuses sont mutées au niveau du gène *KRAS* (KRAS proto-oncogene, GTPase) (40) (41).

1.2.3.1 Séreux

Le sous-type séreux est divisé en HGS et en séreux de bas grade (low grade serous, LGS). Morphologiquement, les LGS sont caractérisées par peu d'atypie nucléaire et un nombre de mitoses plus faible que pour les HGS (42). Mais les HGS et LGS se distinguent

surtout aux niveaux génomique et moléculaire ; des analyses à la fois cytogénétique et du polymorphisme nucléotidique démontrent de plus faibles anomalies moléculaires pour les LGS (43-45). De plus, des études d'hybridation génomique comparative (CGH) ont démontré une fréquence significativement plus élevée d'anomalies du nombre de copies chez les HGS (40, 46). Les tumeurs LGS se caractérisent par des mutations dans la voie KRAS ou BRAF, retrouvées dans 68% (45, 47).

Comme beaucoup d'études le prouvent, le gène *TP53* est presque toujours muté dans les tumeurs HGS (97% des tumeurs). Cette mutation se produit au début de la genèse du cancer de l'ovaire et est la mutation dominante (''driver'') des HGS procurant une instabilité génétique et donc une importante hétérogénéciété (48). Cette mutation se retrouve dans le cancer du sein de type triple négatif. Les autres gènes les plus fréquemment affectés sont les gènes *BRCA1* et *BRCA2*. Plus précisément, les mutations germinales *BRCA1* et *BRCA2* sont les altérations les plus courantes et sont présentes dans environ 9% des HGS, alors que les mutations somatiques représentent 3% (40). La majorité des mutations *BRCA1/2* sont également suivies d'une perte d'hétérozygotie, ce qui indique une inactivation du gène dans 75% des cas (49). De plus, des modifications épigénétiques de *BRCA1* sont présentes dans 11% des cas. Des mutations germinales et somatiques ont également été identifiées dans d'autres gènes à des taux inférieurs (<6%) mais statistiquement significatifs, tels que *NF1, RB1 (*RB transcriptional corepressor 1*), CDK12, FAT3, CSMD3* et *GABRA6*. Des études complémentaires sont nécessaires pour confirmer ces taux sur des cohortes de patientes indépendantes. Certaines études s'intéressent à la kinase cyclin dépendante (CDK12) comme une cible potentielle par, entre autres, son rôle dans la RH (50).

Des défauts dans la réparation par recombinaison homologue (RRH) sont retrouvés dans 50% des cas d'EOC HGS (40). Ils sont principalement causés par des mutations génétiques, somatiques et épigénétiques des gènes *BRCA1/2* (51). D'autres altérations de la RRH entraînent sa déficience [mutations dans les gènes de l'Anémie de Fanconi (*PALB2, FANCA, FANCI, FANCL et FANCC*), spécifiques de l'ADN (*RAD50, RAD51, RAD51C et RAD54L*), responsables de la réponse aux dommages à l'ADN (*ATM, ATR, CHEK1* et *CHEK2*) et non impliqués directement dans la RRH (*PTEN*, l'amplification *EMSY)]* (50) (52). En plus des altérations de la voie RH, d'autres voies de réparation de l'acide désoxyribonucléique (ADN), telles que la réparation par excision des nucléotides (Nucléotides

Excision Repair, NER) et la MMR, peuvent être affectées par certains gènes spécifiques de ces voies de la réparation (*ERCC2-6, DDB1, XPC, RFC1, RAD23B*). L'étude de ''The Cancer Genome Atlas'' (TCGA) rapporte qu'on retrouve ceci dans 8% des tumeurs de HGS (40).

En plus des mutations, les variations du nombre de copies sont remarquablement communes dans les HGS (environ 46%). Les amplifications focales les plus courantes, fortement amplifiées dans plus de 20% des EOC HGS, sont *CCNE1* (Cyclin E1), *MYC, MECOM, MAPK1 et KRAS*. Les gènes suppresseurs de tumeurs connus *PTEN, RB1* et *NF1* étaient localisés dans des régions de délétions homozygotes dans au moins 2% des tumeurs (Table I).

Toutes les recherches actuelles et antérieures démontrent bien que l'EOC HGS présente une importante instabilité génomique apportant une biologie moléculaire et cellulaire très altérée. Cette instabilité génomique promeut une grande hétérogénéité entre les différentes patientes et donc n'a pas de voie prédominante dérégulée qui permettrait de déterminer des cibles thérapeutiques efficaces pour l'ensemble des patientes.

1.2.3.2 Endométrioïdes

Les EOC endométriaux se caractérisent par des mutations bien distinctes dans *PTEN, ARID1A, PIK3CA, PIK3R1, CTNNB1 et KRAS* (53). Des modifications épigénétiques de MLH1 entrainent une instabilité des microsatellites pour 13-50% des cas d'EOC endométrioïdes (54). Ses altérations moléculaires les plus courantes et caractéristiques sont les mutations de β-catenine et *PTEN,* représentant respectivement 30% et 20% des cas. Elles sont détectées dans des tumeurs de stade 1 bien différenciées et considérées comme un événement précoce (29). La mutation de *KRAS* est retrouvée à une fréquence de seulement 10% des cas, tout comme celle de *TP53* qui reste rare pour ce sous-type. En outre, les EOC endométriaux présentent une dérégulation de la cadhérine E, p16, cycline E (53).

1.2.3.3 Cellules claires

Bien que le carcinome ovarien à cellules claires soit le sous-type le moins courant en Amérique du Nord (12% des cas), il est la deuxième cause de décès par cancer de l'ovaire. Pourtant, il reste peu étudié. Les EOC à cellules claires ont un taux mitotique faible et sont génétiquement stables. D'ailleurs, ils ne présentent pas le caryotype complexe et l'instabilité chromosomique caractéristique des EOC HGS, ce qui pourrait expliquer leur faible sensibilité à la chimiothérapie. La mutation *ARD1A* est retrouvée dans 46% et cela est corrélé avec la perte d'expression de BAF250a qui a été observée dans 73% des cas d'EOC à cellules claires (39). De plus, ce sous-type présente une forte instabilité des microsatellites, associée à une diminution de l'expression *MLH1* et *MSH2* (syndrome de Lynch). Des niveaux significativement élevés d'acide ribonucléique messager (ARNm) de *ERCC1* et *XPB*, deux gènes clés impliqués dans la voie de réparation de l'excision des nucléotides et dans la résistance aux traitements de chimiothérapie, ont été observés dans le EOC à cellules claires seulement (55).

	Frequency (%)
Gene mutations	
TP53	>95
BRCA1/2 germline	17–22
BRCA 1/2 somatic	6–7
NF1	4
CDK12	3
RB1, FA genes, HR DNA-damage gene	2[b]
Core RAD gene	1.5
Copy number alterations	
CCNE1, MYC, MECOM amplifications	≥20
NF1 loss	12
RB1 loss	10
PTEN loss	8
EMSY amplification	8
PAX8 amplification	3
Gene expression subtypes	
Proliferative	21
Immunoreactive	23
Differentiated	26
Mesenchymal	30

Table I: Résumé des principales modifications moléculaires dans les cancers HGS
Genomic Characterization of High-Grade Serous Ovarian Cancer: Dissecting Its Molecular Heterogeneity as a Road Towards Effective Therapeutic Strategies; Lorenza Mittempergher; Curr Oncol Rep (2016) 18: 44 DOI 10.1007/s11912-016-0526-9

1.2.3.4 Mucineux

Des mutations du gène *TP53* (37% des cas), de la voie MAP Kinase (49% de mutations en *KRAS* et 3,5% en *BRAF*) et de la voie mTOR (*PIK3CA* dans 12% et *PTEN* dans 6%) ont été démontrées dans les EOC mucineux. La surexpression de cMET est observée dans 33% des cas, mais aucune amplification de ce gène n'a été mise en évidence. Celle des gènes *EGFR* et *HER2* est observée dans respectivement 50% et 11% des cas par hybridation fluorescente in situ (Fluorescente In situ Hybridation, FISH) (41). Il est actuellement mis en doute que le sous-type mucineux provienne de l'ovaire. Il semblerait qu'il puisse avoir une origine gastro-intestinale (56).

1.2.4 Prise en charge du cancer épithélial de l'ovaire

1.2.4.1 Traitement chirurgical du EOC

La chirurgie du cancer de l'ovaire a deux objectifs principaux. Le premier est d'éliminer le maximum de la tumeur - c'est ce qu'on appelle la cytoréduction. On dit alors que la chirurgie est complète et cela apporte une meilleure chance de survie aux patientes concernées, surtout lorsque le cancer de l'ovaire déjà répandu largement dans l'abdomen (57). Le deuxième objectif est de connaître le stade de la maladie. En fonction du résultat, il est courant d'éliminer l'utérus (hystérectomie), les ovaires, les trompes de Fallope (opération appelée salpingo-ovarectomie bilatérale) et l'omentum, couche de tissu adipeux couvrant le contenu abdominal (omentectomie). De plus, certains ganglions lymphatiques dans le bassin et l'abdomen sont biopsiés, afin de voir si le cancer s'est propagé. Finalement, s'il y a de l'ascite dans le bassin ou la cavité abdominale, il sera également retiré. Tout le matériel récupéré durant la chirurgie est analysé en laboratoire (Figure 4) (15).

1.2.4.2 Classification de la maladie par le stade

Le stade décrit l'avancement du cancer et sa propagation au moment du diagnostic. La Fédération internationale de gynécologie et d'obstétrique (FIGO) a classé les EOC en quatre stades (Table II) (58). Ces stades sont définis par la taille tumorale au niveau des ovaires, l'extension à d'autres tissus pelviens et à la cavité péritonéale, l'impact sur les ganglions lymphatiques et le développement de métastases à distance. Il peut être utilisé comme un

facteur pronostique significatif : plus le stade du EOC est précoce, meilleure est la chance de survie. Lorsque les EOC sont diagnostiqués et traités au stade I et II, les taux de survie à 5 ans sont encourageants avec respectivement > 90% et 70-80%. En revanche, si la maladie s'étend au-delà des ovaires aux stades III et IV, les taux de survie à 5 ans peuvent chuter respectivement à 20-30% et <5% (59). La décision du traitement approprié se base encore, malgré les caractéristiques différentes que présentent chacun des types et sous-types, seulement sur le stade de la maladie (Figure 4).

Stage	Characteristics
I	Growth limited to the ovaries
IA	Growth limited to one ovary; no ascites; no tumor on the external surfaces, capsule intact
IB	Growth limited to both ovaries; no ascites; no tumor on the external surfaces, capsule intact
IC	Tumor either stage IA or IB but on the surface of one or both ovaries; capsule ruptured; ascites-containing malignant cells present; or positive peritoneal washings
II	Growth involving one or both ovaries with pelvic extension of disease
IIA	Extension of disease and/or metastases to the uterus and/or fallopian tubes
IIB	Extension of disease to other pelvic tissues
IIC	Tumor either stage IIA or IIB but on the surface of one or both ovaries; capsule(s) ruptured; ascites-containing malignant cells present; or positive peritoneal washings
III	Tumor involving one or both ovaries with peritoneal implants outside the pelvis and/or positive retroperitoneal or inguinal nodes; superficial liver metastasis equals stage III; tumor is limited to the true pelvis but with histologically verified malignant extension to the small bowel or omentum
IIIA	Tumor grossly limited to the true pelvis with negative nodes but with histologically confirmed microscopic seeding of abdominal peritoneal surfaces
IIIB	Tumor of one or both ovaries; histologically confirmed implants on abdominal peritoneal surfaces, none > 2 cm in diameter; nodes negative
IIIC	Abdominal implants > 2 cm in diameter and/or positive retroperitoneal or inguinal nodes
IV	Growth involving one or both ovaries with distant metastases; if pleural effusion is present, there must be positive cytologic test results to allot a case to stage IV; parenchymal liver metastasis equals stage IV

FIGO = International Federation of Gynecology and Obstetrics

Table II : Stadification du cancer de l'ovaire selon FIGO (2014) *https://www.sgo.org/wp-content/uploads/2012/09/FIGO-Ovarian-Cancer Staging_1.10.14.pdf*

1.2.4.3 Traitements standards de première ligne

Les molécules de chimiothérapie à base de platine (cisplatin et carboplatine) représentent le noyau de thérapie de première intention pour les patientes atteintes d'un cancer ovarien avancé. Ces médicaments à base de platine sont des agents formant des adduits inter ou intra brins d'ADN pouvant être réparés par les voies de la réparation de l'ADN ou, le cas échéant, provoquer l'arrêt du cycle cellulaire en phases S et G2 et faire entrer la cellule en apoptose (60). Les dérivés de taxane [paclitaxel (Taxol) et docétaxel (Taxotère)] sont la plupart du temps combinés à la chimiothérapie en première ligne. Leur action consiste à perturber la dynamique des microtubules en liant de manière permanente les sous-unités β-tubuline dans les cellules se divisant activement, conduisant à l'arrêt mitotique et finalement à la mort cellulaire (61). Il a été montré que plus de 80% des patientes répondent initialement au traitement, cependant, la majorité des patientes avec un cancer de l'ovaire rechute (Figure 4).

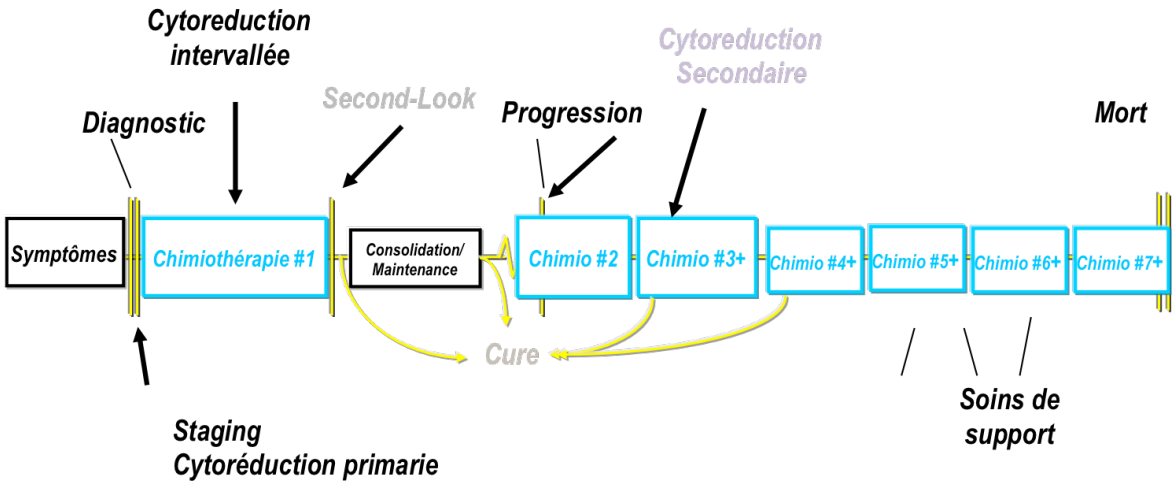

Figure 4 : Cancer de l'ovaire : sa *trajectoire.*
Après le diagnostic du carcinome de l'ovaire, l'évolution clinique suit généralement une voie qui inclut la chirurgie cytoréductrice et les cycles multiples de traitement de chimiothérapie si la maladie progresse. Pour distinguer entre la thérapie de consolidation et la thérapie d'entretien, la «consolidation» implique. un traitement très court d'une forme différente de thérapie, et la «maintenance» implique un déroulement plus long d'un type similaire de thérapie. Après le diagnostic du carcinome de l'ovaire, l'évolution clinique suit généralement une voie qui inclut la chirurgie cytoréductrice et les cycles multiples de traitement de chimiothérapie si la maladie progresse. Pour distinguer entre la thérapie de consolidation et la thérapie d'entretien, la «consolidation» implique un traitement très court d'une forme différente de thérapie, et la «maintenance» implique un déroulement plus long d'un type similaire de thérapie.
Donnée par Omit Oza et traduit par Diane Provencher

1.3 Mécanismes de réponse aux traitements et nouvelles thérapies

1.3.1 Principales voies de la réparation de l'ADN.

La machinerie de réparation de l'ADN cellulaire est cruciale pour maintenir l'intégrité du génome humain, qui est constamment remise en question par une variété de facteurs endogènes et exogènes, y compris les rayonnements ultraviolets (UV) et les produits chimiques cancérogènes. Ces mécanismes de réparation peuvent être généralement divisés en cinq voies distinctes: la RH, l'assemblage final non homologue (NHEJ), la NER, la réparation de l'excision de base (BER) et la MMR (Figure 5). Les défauts dans ces voies de réparation prédisposent les individus à une variété de cancers. L'état cellulaire de ces voies de réparation peut être déterminant pour les résultats de chimiothérapie, radiothérapie et certaines thérapies ciblées sur la survie de la tumeur. Ces différentes voies de réparation sont généralement présentées de façon indépendante les unes des autres, pourtant il existe une interaction entre les voies de réparation de l'ADN (telles que la réaction croisée entre la RH et le NHEJ dans la réparation des ruptures d'ADN à double brin), la réparation d'excision de base, les alkyltransférases et les dioxygénases d'ADN dans la réparation, ou encore entre les protéines des voies de la réparation simple brin et celles de la réparation double brin. Cette interaction entre les différentes voies de la réparation de l'ADN joue probablement un rôle dans les mécanismes de résistance des tumeurs ou, à l'inverse, pour minimiser les effets secondaires de l'inhibition d'une seule voie de réparation de l'ADN dans les cellules normales (62).

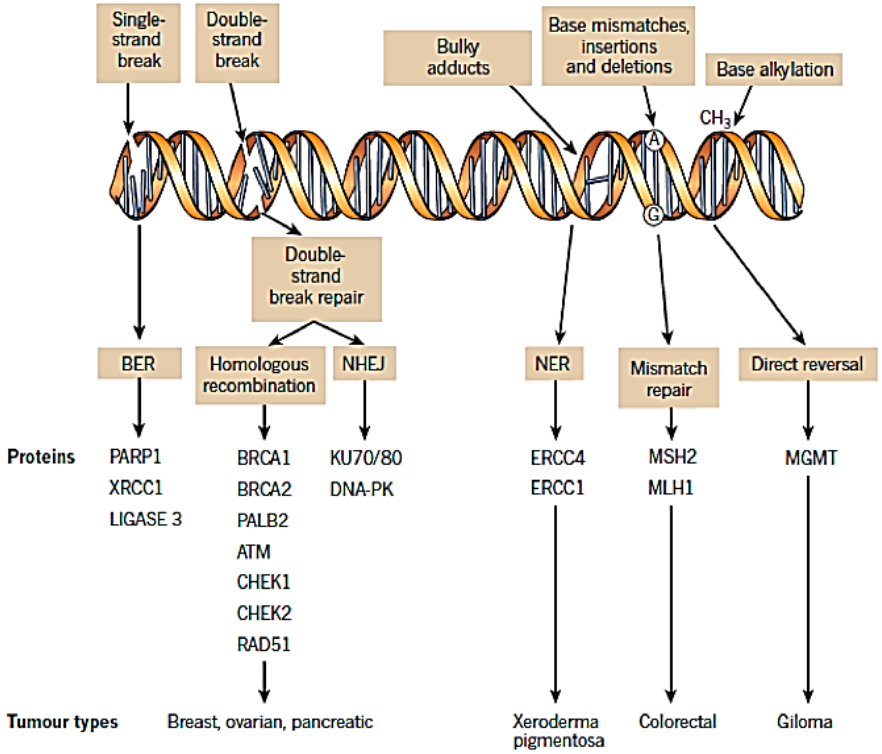

Figure 5: Schéma des différents mécanismes de réparation de l'ADN maintenant la stabilité génomique

The DNA damage response and cancer therapy Christopher J. Lord ; Alan AshworthNature 481,287–294 (19 January 2012) doi:10.1038/nature10760

1.3.1.1 La NHEJ:

La présence d'une cassure double brin dans l'ADN génomique est une situation très dangereuse pour une cellule. Par conséquent, différents mécanismes ont évolué dans les cellules eucaryotes pour antagoniser ces lésions. La NHEJ est l'un de ces mécanismes, elle peut réparer rapidement les cassures double brins de l'ADN. Ce processus de réparation est initié par l'hétérodimètre Ku (Ku70 et Ku80) qui se lie à l'ADN et se termine en quelques secondes après la formation de cassures double brin. La protéine forme une structure en forme d'anneau qui peut encercler l'extrémité de l'ADN. Elle sert de plate-forme pour le recrutement de nouveaux facteurs de NHEJ de base qui sont nécessaires pour la réparation, dont la protéine kinase dépendant de l'ADN (DNAPK). Différentes protéines peuvent être nécessaires pour

rendre les extrémités permissives à la réparation : non seulement des nucléases comme Artemis, WRN ou APLF, mais aussi des polymérases. Enfin, le complexe ADN Ligase IV / XRCC4 / XLF scelle ensemble l'ADN pour rétablir l'intégrité génomique.

La réparation d'une cassure double brin via la voie NHEJ n'est pas limitée à une phase particulière du cycle cellulaire, mais elle est propice à l'erreur en raison de l'étape de traitement final et contribue à l'instabilité génomique à travers des translocations et des suppressions chromosomiques. Pour maintenir la stabilité génomique, les cellules peuvent contrecarrer les cassures double brin de l'ADN via la voie de recombinaison homologue qui fournit une réparation fidèle. Cependant, contrairement à la RH, qui emploie un mécanisme sophistiqué pour assurer la précision de la réparation, la NHEJ est plus rapide. Le choix entre NHEJ et RH est principalement dépendant de l'étape du cycle cellulaire – la RH se produit normalement pendant les phases S et G2 du cycle cellulaire car elle nécessite une chromatide soeur homologue pour servir de modèle pour la réparation, alors que la NHEJ fonctionne principalement dans le G0 et G1, même si elle peut également entrer en jeu dans d'autres phases du cycle cellulaire, en particulier lorsque la réparation des RH devient compromise (63). Les altérations génétiques des principaux gènes NHEJ ont été liées à la préposition du cancer. Par exemple, des mutations *Ku70* ont été associées à la susceptibilité au cancer du sein, au cancer colorectal et au cancer du poumon (64). En outre, l'activité accrue de NHEJ a été proposée comme principale source de réarrangements génomiques observés dans divers cancers (65).

1.3.1.2 La réparation par recombinaison homologue (RRH)

La RRH représente un mécanisme principalement dédié à la réparation des cassures double brin (Double Strand Break, DSB) pendant la réplication de l'ADN. La première étape de la RRH est d'entamer l'extrémité de l'ADN, ce qui conduit à la génération de ``surplombs'' de l'ADN en 3' qui sont ensuite recouverts par la protéine RPA. On sait que plusieurs nucléases sont impliquées dans ce processus : le complexe Mre11-Rad50-Xrs2, Exo1 et Sae2. Des protéines médiatrices comme Rad51 ou *BRCA2* chargent alors la recombinase Rad51 sur l'ADNc en éliminant ainsi le RPA de l'ADN. Cela stabilise le filament nucléoprotéique qui effectue ensuite une recherche d'homologie sur le chromosome soeur ou homologue. Ensuite, le Rad51-ssDNA-filament effectue une recherche d'homologie sur un modèle d'ADN

approprié comme la chromatide sœur. L'invasion de fil subséquente est alors complétée par la formation d'une boucle de déplacement (boucle D). Ensuite, les polymérases distinctes utilisent le brin envahissant comme amorce pour commencer la synthèse de l'ADN. Chez l'homme, on sait que les polymérases peuvent également servir de médiateur à cette étape d'extension d'ADN en plus de la polymérase réplicative δ. Un acteur clé dans ce processus est la protéine motrice Rad54. Elle stabilise le filament de la nucléoprotéine Rad51 et favorise la formation de la D-boucle. Finalement, Rad54 perturbe le filament Rad51 pour permettre l'initiation de la synthèse de l'ADN. De nombreux gènes de susceptibilité au cancer de l'ovaire et du sein sont impliqués dans cette voie comme *BRCA1* et *BRCA2* ainsi que *ATM*, *PALB2*, *BRIP1* et *RAD51*. Les défauts en RRH prédisposent également à de nombreux autres cancers, y compris le cancer de la prostate et du pancréas (64, 66-68). La RRH est la voie de réparation de l'ADN la plus compliquée, contenant le plus grand nombre de protéines de réparation. Beaucoup de ces protéines ont été exploitées intensivement en tant que cibles thérapeutiques ou biomarqueurs parce que les défauts de RRH sensibilisent les tumeurs aux agents inducteurs de DSB tels que les rayonnements ionisants, les poisons de la topoisomérase I. De façon indirecte, les agents à base de platine comme le cisplatin et la carboplatine après la phase S si le NER est défectueux en font aussi partie (64).

1.3.1.3 La réparation par excision de nucléotide

La voie NER traite des dommages induits à la double hélice d'ADN, par exemple ceux induits par la lumière UV ou la fumée du tabac. Un défaut de la NER prédispose les individus à différents syndromes pouvant causer le cancer, comme le xeroderma pigmentosum et le syndrome de cockayne qui est caractérisé par un risque élevé de cancer de la peau et du colon (69). Des altérations génétiques dans les gènes NER clés peuvent également donner lieu à d'autres cancers. Par exemple, la méthylation ERCC1 et les polymorphismes observés dans XPA et XPC ont été impliqués dans la genèse du cancer du poumon et du cancer de la vessie, respectivement (70). La carence en NER confère une sensibilité à divers agents chimiothérapeutiques, y compris le cisplatin, la mitomycine et la moutarde azotée (64). Les adduits qui faussent l'hélice de l'ADN comme ceux générés par la lumière UV (6-4 photoproduits et les dimères de pyrimidine), sont éliminés par la réparation d'excision nucléotidique (NER). La NER se divise en deux sous-voies: NER (TC-NER) couplé à la

transcription et le génome global NER (GG-NER). Ces deux voies sont mécaniquement semblables, mais l'initiation de la voie et la façon dont elles reconnaissent la lésion de l'ADN est différente. Le GG-NER agit sur le génome global en détectant et liant les distorsions de l'ADN par la protéine XPC. La TC-NER est activée lorsque l'ARN-Polymerase II est bloquée en raison de la présence de dommages à l'ADN. Cela va initier le recrutement des protéines CSA et CSB.

1.3.1.4 La réparation par excision de base

La voie BER est responsable de l'élimination de petites lésions de base non déformantes de l'hélice, causées par l'oxydation, l'alkylation ou la désamination, qui induisent souvent des cassures simple brin (Single Strand Break, SSB). La BER se divise en deux voies distinctes, la courte et la longue. La première entraîne la réparation d'un seul nucléotide tandis que la longue échange au moins deux nucléotides. Pour initier la courte BER, une glycosylase d'ADN spécifique reconnaît une base endommagée et la supprime en coupant la liaison N-glycosidique. Puis une endonucléase AP1 (APE1) coupe le squelette d'ADN 5'. Ensuite, la polymérase β remplit le nucléotide correspondant. En fin de compte, l'étanchéité de l'espace restant est réalisée par l'ADN Ligase III/XRCC1. La longue BER a une étape d'initiation identique, mais après le clivage APE1, Pol δ ou ε, PCNA, FEN1 et ligase I sont recrutés sur le site dommage. La polymérase insère de nouveaux nucléotides, ce qui génère un brin 5' nécessitant un clivage par FEN1 et une ligation par la Ligase I /PCNA pour une réparation finale. Les défauts génétiques dans les gènes essentiels du BER, comme *OGG1*, sont principalement associés à un risque de cancer colorectal excessif. En outre, les polymorphismes observés dans *OGG1* ont été impliqués dans la sensibilité au cancer du poumon (71). L'activité BER compromise rend les cellules tumorales sensibles au rayonnement ionisant et aux agents alkylants tels que le méthanesulfonate de méthyle et le temozolomide. Les agents alkylants représentent une classe primaire de médicaments chimiothérapeutiques de première ligne, dont l'efficacité est largement influencée par l'état cellulaire des voies BER et MMR (72).

1.3.1.5 Réparation par mésappariement

La voie MMR est le mécanisme majeur pour la réparation des correspondances base-base et des boucles d'insertion / suppression formées lors de la réplication de l'ADN. Bien que les polymérases réplicatives δ et ε ont une fonction de correction du nucléotide inséré, il est estimé qu'une par 109 à 1010 paires de bases se retrouve muté par chaque division cellulaire. Pour détecter et réparer de telles erreurs, le système de réparation par mésappariement vérifie continuellement les brins nouvellement synthétisés. La littérature suggère que MSH2 et MSH6 sont en mesure d'initier la réparation. Parmi les autres acteurs clés du MMR, il existe trois hétérodimères: MutLα (MLH1 / PMS2), MutLβ (MLH1/PMS1) et MutLγ (MLH1/MLH3) servant à la médiation de l'incision endonucléolytique du brin d'ADN contenant des erreurs. L'élimination complète du brin endommagé est ensuite effectuée par Exonuclease1. Enfin, l'intervalle d'ADN monocaténaire résultant est rempli par une ADN polymérase telle que Polδ et scellé par la ligase I. Dans les cellules tumorales déficitaires en MMR, les taux de mutation sont 1000 fois supérieurs aux cellules normales. Les mutations germinales des gènes *MSH2*, *MSH6*, *PMS2* et *MLH1* peuvent provoquer le syndrome de Lynch, un trouble héréditaire associé aux cancers colorectal, de l'endomètre, de l'ovaire et de l'estomac (73). La déficience en MMR peut provoquer une hypersensibilité des tumeurs aux agents alkylants, comme mentionné ci-dessus. En outre, l'état cellulaire du MMR peut affecter la résistance des tumeurs aux rayonnements ionisants et aux agents chimiothérapeutiques tels que le méthotrexate, l'anthracycline et le taxane (74).

Une trop grande accumulation de dommages de l'ADN au sein de la cellule, due à une induction excessive par des agents induisant des dommages de l'ADN, à une déficience dans une des voies de réparation de l'ADN citées préalablement ou à l'addition de ces deux phénomènes, est en temps normal un inducteur puissant de la mort cellulaire déclenchée par l'apoptose (75).

1.3.2 Destin cellulaire des cellules cancéreuses suite à un traitement par des agents endommageant de l'ADN

L'instabilité du génome est une des caractéristiques du cancer. Les cellules ont développé différents mécanismes pour éliminer les cellules défectueuses et génétiquement instables (76). Le principal objectif des traitements induisant des cassures de l'ADN

[chimiothérapie, radiothérapie et de façon indirecte les inhibiteurs de poly (ADP-Ribose) polymerase (PARP)] est de priver les cellules cancéreuses de leur capacité à se diviser et ainsi, normalement, induire leur mort cellulaire. De nos jours, plusieurs recherches révèlent que l'induction de la mort cellulaire est un mécanisme très complexe. En effet, ces dernières années, il est de plus en plus évident que l'inhibition de la capacité proliférative des cellules traitées, en particulier pour les tumeurs solides, peut se produire par différents types de réponse cellulaire tels que l'apoptose, la nécrose, la catastrophe mitotique, l'autophagie et la sénescence (Figure 6) (77). Selon la réponse apportée à la cellule, le résultat sur la tumeur sera soit une diminution de la croissance tumorale due à la mort cellulaire, soit une augmentation de l'agressivité tumorale pouvant mener à une résistance acquise de la tumeur (78).

1.3.2.1 Apoptose

L'apoptose est une mort programmée, caractérisée par un rétrécissement cellulaire et nucléaire, une préservation de la membrane plasmatique, un clivage des protéines du cytosquelette par des protéases pro-apoptotiques provoquant ainsi l'effondrement des composants sous-cellulaires (79). La mort de la cellule apoptotique médiée par plusieurs caspase est réalisée grâce au clivage de plusieurs protéines essentielles requises pour le fonctionnement et la survie cellulaire. PARP-1 est l'un des nombreux substrats cellulaires connus des caspases. Le clivage de PARP-1 par les caspases est considéré comme une caractéristique de l'apoptose. Presque toutes les caspases, y compris la caspase-1, sont connues pour modifier PARP-1 in vitro (80). Hanahan et Weinberg, dans leurs travaux (76, 81), ont souligné que l'une des caractéristiques principale du cancer est la capacité d'échapper à l'apoptose. D'ailleurs plus de 50% des tumeurs présentent des défauts dans la machinerie apoptotique. Ceci est particulièrement pertinent pour les EOC où l'atténuation de l'apoptose dans ces cellules tumorales contribue à la résistance à un traitement ultérieur et joue probablement un rôle important dans la progression (82). Au cours des dernières années, un intérêt accru est né pour comprendre les mécanismes sous-jacents de l'apoptose et ainsi élaborer des stratégies d'interventions thérapeutiques. Beaucoup des caractéristiques affichées par les cellules cancéreuses, telles que l'inactivation des points de contrôle du cycle cellulaire, induiraient normalement l'apoptose chez les cellules saines (83). Parmi les plus caractérisées, notons l'augmentation d'expression de Bcl-2 (anti-apoptotique) et les mutations dans le gène

TP53 qui fait le lien entre les dommages de l'ADN et l'induction transcriptionnelle de nombreuses protéines pro-apoptotiques comprenant PUMA, Noxa et Bax (84). Finalement, environ 50% des cancers humains ont montré une expression élevée de Bcl-2 (85). Les protéines de la famille Bcl-2 sont impliquées dans la régulation de l'apoptose en contrôlant la perméabilité de la membrane mitochondriale. Plusieurs études ont démontré que ces protéines peuvent interagir les unes avec les autres en neutralisant leurs fonctions pro ou anti-apoptotiques. L'équilibre entre les membres anti et pro-apoptotiques dicte le sort de la survie cellulaire ou de la mort. Les membres pro-apoptotiques Bcl-2 peuvent être divisés en 2 groupes selon leur fonction et le nombre de domaines BH qu'ils possèdent. Les protéines contenant des domaines BH 1-3 sont connues sous le nom de protéines pro-apoptotiques multidomaines telles que Bax, Bak et Bok (86). Les protéines pro-apoptotiques BH-3 seulement, comme Bik, Bid, Bad, Bim, Bmf, Noxa, Puma et d'autres, peuvent former des hétérodimères avec les protéines multidomaines Bax et Bak conduisant à l'activation des mitochondries. Les protéines anti-apoptotiques dont Bcl-2, Bcl-XL et Mcl-1 peuvent également former des interactions hétéro-dimériques avec Bax et Bak, neutralisant ainsi leur activité pro-apoptotique. Les protéines anti-apoptotiques peuvent former des hétéro-dimères avec des protéines BH-3 et cette interaction neutralise la fonction pro-survie des protéines anti-apoptotiques. Une approche thérapeutique consiste à activer l'apoptose en ciblant la famille des BCL comme BCL-2, BCL-XL et BCL-W. ABT-737 et ABT-263 étant des inhibiteurs ciblant les BCL actuellement testés en essais cliniques (87). Bien que semblant contre-intuitif, les cellules mourantes peuvent sécréter des facteurs stimulants qui ont des effets favorisant la croissance sur les cellules environnantes. En outre, les cellules cancéreuses concourent pour la nutrition et l'espace; en cas de mort cellulaire, un espace vide est laissé, et les clones plus agressifs peuvent prendre en charge cet espace (88). Ce qui devient de plus en plus clair, cependant, c'est que l'apoptose pourrait ne plus être une barrière étanche à l'eau contre la tumorigène comme on l'avait pensé auparavant.

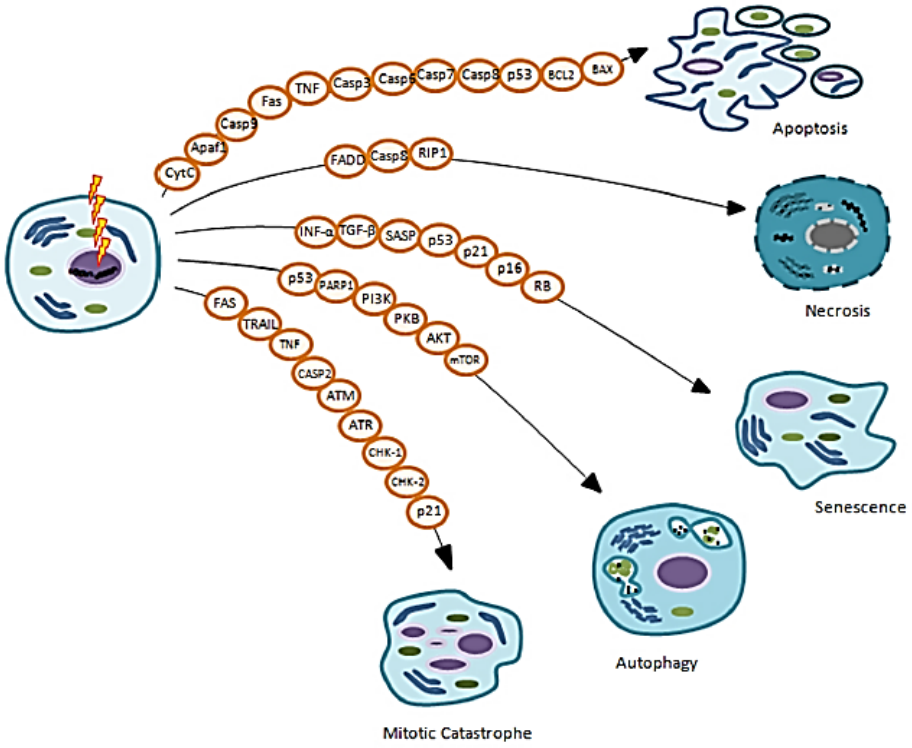

Figure 6: Différents destins cellulaires suite aux dommages de l'ADN
Luigi Minafra et al., Cell and molecular response to IORT treatment, Transl Cancer Res 2014;3(1):32-47

1.3.2.2 Nécrose

La nécrose est caractérisée, contrairement à l'apoptose, par un gonflement des organelles avec une rupture superficielle de la membrane amenant à un déversement du contenu intracellulaire. Cette réponse résulte d'une défaillance métabolique, coïncidant avec l'épuisement rapide de l'adenosine triphosphate (ATP). Parce que les membranes sont compromises, les enzymes dégradantes s'échappent des lysosomes et pénètrent dans le cytosol provoquant ainsi une destruction cellulaire (89). La nécrose est considérée comme une mort cellulaire "accidentelle" à l'inverse de l'apoptose dite ‘’programmée’’.

L'exposition des cellules à des conditions supra-physiologiques, (la force mécanique, la chaleur, le froid ou les toxines perméables à la membrane) induit également la nécrose (90).

1.3.2.3 Autophagie

L'autophagie est un mécanisme de survie qui est rapidement induit pendant le stress cellulaire pour protéger les cellules de la mort cellulaire en éliminant les mitochondries endommagées ou des protéines toxiques (91). L'autophagie joue un rôle complexe dans le cancer mais semble fonctionner comme un suppresseur de tumeur. De nombreux oncogènes comme PI3k / Akt, Bcl-2 et mToR suppriment l'autophagie alors que les suppresseurs de tumeurs, par exemple PTEN et HIF1α, favorisent généralement l'autophagie. Cependant, dans le cadre de la chimiothérapie, l'autophagie semble favoriser la résistance (92).

1.3.2.4 Catastrophe mitotique

La catastrophe mitotique est un processus antiprolifératif réglementé qui survient pendant une mitose défectueuse ou échouée. Bien qu'il ne constitue pas un mécanisme de mort cellulaire en soi, la catastrophe mitotique précède et utilise des mesures antiprolifératives, y compris l'apoptose, la nécrose et la sénescence pour empêcher la prolifération de cellules mitotiques défectueuses (93). La catastrophe mitotique se caractérise par des altérations nucléaires uniques qui mènent à une binucléation et/ou à une micronucléation, utilisées comme marqueurs morphologiques. Les agents antimitotiques induisant une crise mitotique les plus connus sont les agents de ciblage des microtubules comme les taxanes (Paclitaxel et Docétaxel). Les taxanes sont largement utilisés pour traiter les tumeurs du cancer du sein, de l'ovaire et de la prostate (61).

1.3.2.5 Sénescence

La sénescence cellulaire est un état d'arrêt de croissance irréversible décrit en 1961 suite à l'observation des fibroblastes humains primaires subissant un nombre fini de divisions cellulaires en culture avant d'entrer dans un état viable d'arrêt stable de la croissance (94). La sénescence cellulaire est une réponse au stress non létale qui entraîne un arrêt de la division cellulaire persistante et donne un phénotype morphologique et biochimique distinct. La sénescence peut être détectée dans les tumeurs par l'expression dérégulée de certains ARNm et de certaines protéines (95). À ce jour, le biomarqueur de sénescence le plus utilisé est la présence d'une activité de β-Galactosidase associée à la sénescence (SA-β-Gal). Fait intéressant, bien que SA-β-Gal soit un bon biomarqueur de sénescence, il est nécessaire

d'établir d'autres phénotypes pour définir cet état. Par exemple, l'arrêt de la croissance est associé à une activité accrue de divers gènes suppresseurs de tumeur régulant le cycle cellulaire (dont *p16*, *Tp53*, *p21* ou *p27)* (96), mais aussi à un phénotype sécrétoire (incluant l'augmentation de IL-6 et IL-8) responsable des communications des cellules sénescentes avec leur microenvironnement. De plus, les cellules sénescentes présentent, contrairement aux foyers transitoires de dommage de l'ADN, des foyers persistants et localisés, avec des corps nucléaires PML et CHK2 activés (DNA segments with chromatin alterations reinforcing senescence, DNASCARS) (97).

Malgré l'importance de p53 sauvage dans l'induction de la sénescence, il existe plusieurs exemples qui mettent en évidence la possibilité d'une sénescence indépendante de p53. Ainsi, des recherches ont relié p21 avec la sénescence et démontrent qu'une sénescence dépendante de p21 peut se produire dans des cellules embryonnaires normales en l'absence de p53 (98). D'autres études ont montré, dans les cellules pulmonaires cancéreuses p53 et p16 mutés, qu'il y a une induction de p21 et d'un arrêt du cycle cellulaire G2 / M comprenant une morphologie de type sénescence et une activité SA-β-Gal (98).

Les recherches actuelles suggèrent que la sénescence induite par la thérapie représente une nouvelle cible fonctionnelle permettant l'amélioration du traitement du cancer. Les cellules sénescentes sont en arrêt de croissance permanente ; la conséquence est l'inhibition de la prolifération de cellules transformées rendant la sénescence, par définition, un principal suppresseur de tumeur. Cependant, une cellule sénescente non divisée n'est pas une cellule neutre. Les cellules sénescentes sont fortement définies par la présence de leur système sécrétoire. L'impact que cela a sur le microenvironnement tumoral environnant est complexe. Ainsi, il a été discuté et montré que les cellules sénescentes créent un microenvironnement qui favorise simultanément la croissance, l'invasion des tumeurs, et aussi la résistance acquise des tumeurs (96). Une étude réalisée dans un modèle de lymphome a montré que les dommages à l'ADN induits par la thérapie ont déclenché un phénotype sénescent et augmenté la sécrétion des facteurs IL-6 et Timp-1 créant un «niche chimio-résistante» dans le thymus et favorisant ainsi la rechute tumorale. Dans ce cas, IL-6 et Timp-1 ont activé Bcl-XL dans des cellules cancéreuses survivantes favorisant ainsi l'inhibition de l'apoptose dans le microenvironnement de la tumeur (99). Il a aussi été prouvé que la progression des tumeurs résistantes peut être due

à la sénescence induite dans la tumeur primaire par chimiothérapie et cela à travers le phénotype sécrétoire associé à la sénescence (100).

1.3.3 Chimiorésistance

La résistance est généralement due à une combinaison de mécanismes, certains entraînant une réduction des dommages à l'ADN et d'autres agissant dans la prise en charge des lésions de l'ADN. Les médicaments de platine pénètrent dans les cellules soit en utilisant des transporteurs soit par diffusion passive (101). Par exemple, la perte de CTR1 (copper transporteur permettant l'entrée des molécules de platine au sein de la cellule au travers de la membrane plasmique) affaiblit l'entrée de molécules de platine dans les cellules et, par conséquent, entraine la résistance aux agents alkylant (102). Des taux de glutathion et de métallothionéine relativement élevés vont éliminer le platine activé dans le cytoplasme avant que la liaison à l'ADN puisse se produire, provoquant une résistance. L'exportation active des molécules de platine des cellules par les exportateurs de cuivre ATP7A et ATP7B ainsi que par le glutathion S-conjugué d'exportation GS-X pompe (également connu sous le nom ABC-Transporters) peut contribuer aussi à cette résistance (103). La résistance à la chimiothérapie peut être due à une diminution de l'expression ou à la perte de certaines voies de signalisation spécifiques à l'apoptose médié par diverses protéines comme les membres de p53, anti-apoptotiques et pro-apoptotique Bcl2 et JNK (104). Enfin, la résistance peut aussi se produire par des changements dans les voies de réparation de l'ADN comme, par exemple, une augmentation de la NER ou une perte de la MMR (105-107). Inversement, l'hypersensibilité de certaines lignées cellulaires au cisplatin est due à un NER défectueux, par perte ou réduction de l'expression de protéines NER telle que XPA (108). Une étude récente a montré que l'inactivation des gènes suppresseurs de tumeurs *RB1*, *NF1*, *RAD51* et *PTEN* dans les HGS contribue à une résistance acquise. On retrouve le même effet de chimiorésistance avec la réversion de la mutation des gènes *BRCA1/2* (109). Face à tous ces mécanismes de chimiorésistance connus ou en cours de compréhension, de nouvelles thérapies prometteuses surgissent pour traiter le cancer de l'ovaire.

1.3.4 Nouveaux traitements

Actuellement, la thérapie ciblée est un nouveau type de traitement contre le cancer qui utilise le développement d'agents moléculaires plus sophistiqués ciblant les voies clés de la signalisation et de la différenciation cancéreuses pour identifier et attaquer les cellules cancéreuses tout en faisant peu de dommages aux cellules normales (110, 111). Ces traitements attaquent le fonctionnement interne des cellules cancéreuses - la programmation qui les rend différentes des cellules normales et saines. Chaque type de thérapie ciblée fonctionne différemment, mais tous modifient la façon dont une cellule cancéreuse pousse, se divise, se répare ou interagit avec d'autres cellules.

L'angiogénèse est un des mécanismes largement étudié et ciblé pour le développement de nouvelles thérapies. Pour la tumeur, une nouvelle croissance dans le réseau vasculaire est importante car sa prolifération, ainsi que sa propagation métastatique dépend d'un apport suffisant d'oxygène et de nutriments. Les vaisseaux sanguins se forment par un processus appelé angiogenèse qui est régulé principalement par plus d'une douzaine de protéines. Parmi celles-ci, le facteur de croissance endothélial vasculaire (VEGF) favoriserait la croissance et la progression de la tumeur; d'ailleurs des niveaux accrus de VEGF ont été associés à un pronostique défavorable et à une résistance au platine dans les cancers épithéliaux de l'ovaire (112). Le Bevacizumab (commercialement connu sous le nom d'Avastin), un anticorps monoclonal humanisé, se lie au VEGF et l'empêche de se lier à son récepteur. Il a été incorporé dans le traitement de première intention pour les EOC de stade avancé et les essais randomisés de phase III récents ont démontré des taux de réponse améliorés chez les patientes qui ont reçu du bevacizumab en monothérapie ou combiné avec du carboplatine / paclitaxel (113). Plusieurs nouvelles molécules ciblant HER2, Wee tyrosine kinase et les voies de signalisation de PIP3/AKT/mTOR sont actuellement en développement et peuvent fournir des opportunités supplémentaires à l'avenir (114). De plus, parmi les molécules servant de cibles de vulnérabilité spécifique dans le cancer de l'ovaire et du sein, les PARP inhibiteurs constituent une autre découverte majeure (110).

1.4 Poly (ADP-ribose) polymérase

Le système de réponse aux dommages de l'ADN humain englobe un réseau de protéines cellulaires conçu pour détecter et réparer les ruptures d'ADN dans le but de maintenir l'intégrité génomique (115). Les dommages à l'ADN non réparés peuvent conduire à des mutations génétiques, entraînant dans certains cas une transformation maligne. Notre compréhension croissante du processus de réponse aux dommages de l'ADN et des mécanismes qui régissent la réparation de l'ADN a fourni de nouvelles cibles pour les thérapies anticancéreuses.

1.4.1 Généralités sur les Poly (ADP-ribose) polymérases

Il y a plus d'un demi-siècle, la famille des protéines PARP a été découverte. Elle comprend au moins 17 enzymes, la PARP1 étant décrite comme la plus abondante dans les tissus normaux. Seules PARP1 et PARP-2 sont connues pour être impliquées dans la réparation des dommages à l'ADN en sachant que la PARP1 représente au moins 85% de l'activité PARP cellulaire (64, 116, 117). Il a été aussi suggéré que PARP-3 joue également, en partie, un rôle dans la réponse aux dommages de l'ADN en contrôlant l'activité de PARP1 par hétérodimérisation (118).

La PARP1 est une enzyme qui catalyse la formation de polymères ADP-ribose (PAR) sur un réseau de substrats de protéines nucléaires, y compris elle-même (119, 120). Sa fonction principale est de reconnaître, se lier et être activé par une grande variété de dommages à l'ADN ainsi qu'à des structures d'ADN non endommagées. Par conséquent, la fonction principale de PARP1 en réponse à des dommages d'ADN de toute sorte est de détecter le site de lésion et de s'y lier. Ce qu'il fait après la liaison est encore un mystère sur lequel se penche la recherche. Certaines de ces fonctions, comme en réponse à SSB, sont connues depuis 25 ans. (117, 121). Suite à la liaison de ces protéines, l'enzyme PARP subit une ribosylation de l'ADP et, en partenariat avec les histones H1 / H2B, permet le déroulement de la chromatine pour la BER. Ce processus nécessite généralement la consommation de Nicotinamide adénine dinucléotide (NAD+). Cette activation de PARP1 entraîne une production accrue de fragments de PAR avec parylation de protéines cibles comme PARP1

elle-même, générant finalement une charge négative qui permettra la dissociation de PARP à l'ADN (122).

En plus de son rôle dans la réparation des dommages simple brin de l'ADN par BER, il existe d'autres fonctions à la PARP1 comme le remodelage de la chromatine, la régulation de la transcription, l'entretien télomère, la réponse hypoxique, la mort cellulaire et la transition épithéliale-mésenchymateuse (Figure 7) (120). En ce qui concerne la réparation des dommages à l'ADN, la fonction de la PARP1 est complexe et multiforme. En plus de son implication dans la BER, elle joue aussi un rôle dans la RH, la NER et la NHEJ (123, 124). De plus, le profil d'expression du gène *PARP1* dans des échantillons chirurgicaux, provenant de plus de 8 000 tissus primaires malins et normaux, a été considérablement augmenté chez les patients atteints de cancer du sein, de l'utérus, des poumons, des ovaires et de la peau, et le lymphome non-Hodgkinien (125) (126). Mais il a aussi été montré que cette surexpression corrélait avec un mauvais prognostique pour la réponse à la chimiothérapie pour les patientes attientes d'EOC HGS (127).

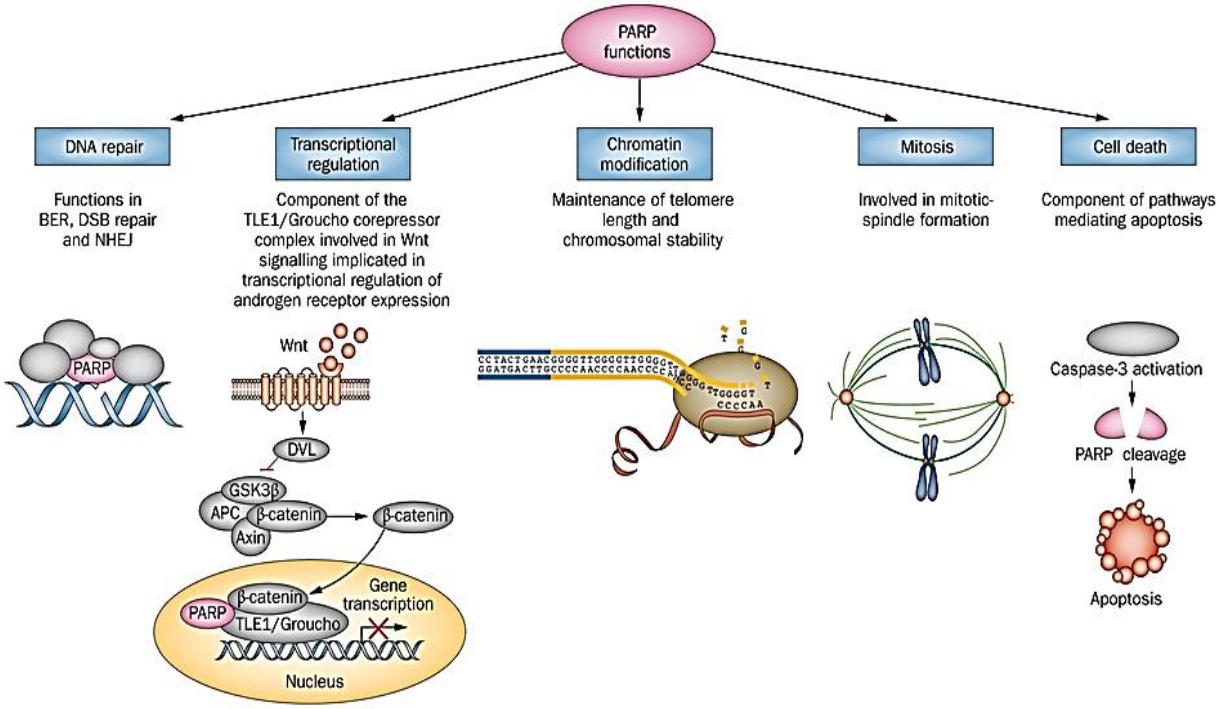

Figure 7 : Différents rôles de PARP.

An update on PARP inhibitors—moving to the adjuvant setting; Amir Sonnenblick, Evandro de Azambuja, Hatem A. Azim Jr & Martine Piccart ; Nature Reviews Clinical Oncology 12, 27–41 (2015) doi:10.1038/nrclinonc.2014.163 (Sonnenblick, 2015, PMID: 25286972)

1.4.2 Les inhibiteurs de PARP

Par le rôle de PARP1 dans la réparation de l'ADN, des inhibiteurs de PARP de première génération pour l'utilisation clinique ont été créés au début des années 1990 : on recherchait leur capacité à inhiber l'activité de PARP et ainsi être utilisé comme agent anti-cancéreux (128, 129). La majorité des inhibiteurs de PARP a été conçue pour inhiber de manière compétitive le domaine catalytique de PARP1, empêchant le substrat NAD + de pénétrer dans le site catalytique. Les inhibiteurs de PARP ont été initialement proposés comme chimio-sensibilisateurs, mais en 2005 deux documents précliniques ont montré que les cellules du cancer du sein déficitaires en BRCA étaient très sensibles à l'inhibition de la PARP par rapport aux cellules de type sauvage, même traitées en monothérapie (130) (131). Bien que le mécanisme exact soit incertain, la théorie la plus courante est que l'inhibition de la PARP1 élimine efficacement la capacité d'une cellule à réparer les SSBs par le biais du BER, obligeant cette dernière à s'appuyer plutôt sur d'autres mécanismes de réparation de l'ADN comme la RH et les voies de la NHEJ en raison de l'effondrement de la fourche de réplication (132, 133). Cependant, les cellules déficitaires en BRCA 1 et 2, impliqués dans la RH, sont incapables d'utiliser pleinement la voie RH et meurent de l'accumulation des cassures d'ADN non réparées causées par l'inhibiteur de PARP, illustrant ainsi le concept de létalité synthétique spécifique au cancer (Figure 8) ((129, 130, 134). Dans les cellules compétentes pour BRCA, les cassures doubles brins sont réparées par la voie RH résultant de la viabilité cellulaire. En raison de la sélectivité des inhibiteurs de la PARP pour les cellules déficitaires en BRCA, ils sont utilisés comme traitement personnalisé présentant une faible toxicité. Les mutations BRCA, qui peuvent être soit héréditées par la lignée germinale, soit se produire de novo dans les cellules somatiques, contribuent à l'instabilité génétique et sont le plus souvent associées aux cancers du sein et des ovaires. Cependant, l'incapacité à subvenir à la RH, donc à avoir une déficience en RH, n'est pas seulement définie par les mutations BRCA 1 et 2, mais aussi par des altérations génomiques et épigénétiques d'autres gènes impliquées dans la RH comme *ATR*, *ATM*, *RAD51/54*, *CHK1/2*, *NBS1*, *PTEN* et *PALB2*. Ces aberrations génétiques et épigénétiques confèrent aux cellules affectées le phénotype de «BRCAness», c'est à dire que la susceptibilité aux traitements pour ces cellules est semblable à celle observée pour les cellules présentant la mutation BRCA et donc sensibles aux inhibiteurs de PARP. L'association du phénotype BRCAness avec une plus large gamme de mutations génétiques

peut étendre l'utilité des inhibiteurs de PARP au-delà des tumeurs malignes de la reproduction pour lesquels ils étaient initialement destinés (135, 136).

Cependant, les données actuelles montrent que d'autres mécanismes de létalité synthétique avec l'inhibition de PARP existent, impliquant l'inhibition ou l'activation d'autres voies de la réparation comme, par exemple, l'activation de la NHEJ (122, 137, 138). La PARP est en compétition avec Ku70 et Ku80, protéines jouant un rôle clé dans la NHEJ, pour se lier aux dommages à l'ADN et supprimer l'activité de la voie NHEJ (139, 140). En outre, l'inhibition de la PARP permet la liaison de la protéine Ku aux DNA DSB afin de servir de médiateur à la voie NHEJ, en particulier dans les cellules déficientes en HR. Il est à noter que les effets cytotoxiques de l'inhibition de la PARP sont diminués par l'inhibition de DNA-PK, ce qui est essentiel pour le NHEJ (122). Ceci suggère que la létalité synthétique observée avec l'inhibition de PARP dans des cellules déficientes en RH peut être attribuée à des erreurs liées à la promotion de NHEJ.

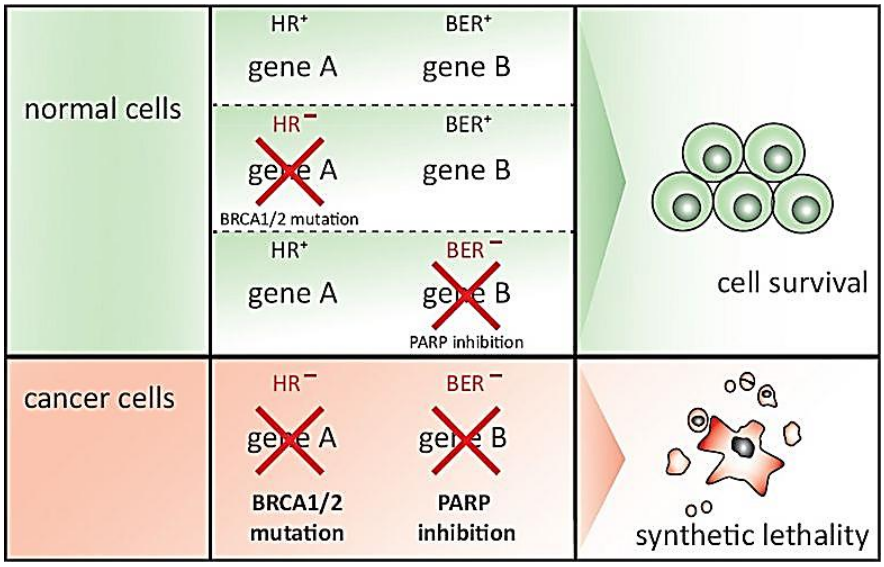

Figure 8 : Principe de la létalité synthétique
Targeting DNA double-strand break signalling and repair: recent advances in cancer therapy; Daniela Hühn, Hella A Bolck, Alessandro A Sartori; DOI: 10.4414/smw.2013.13837 ; 2013 ; Swiss Med Wkly. 2013;143:w1383 ; PMID: 23897299

Depuis quelques années, il est démontré que les inhibiteurs de PARP - en plus de bloquer l'activité catalytique de PARP - induisent le piégeage du complexe ADN-PARP1 au niveau des cassures simple brin induisant une non-dissociation de l'enzyme sur l'ADN

endommagé, ce qui provoque une barrière aux systèmes de réparation de l'ADN lors de la fourche de réplication (141). Cette théorie est basée sur le fait que de nombreux inhibiteurs de PARP présentent des degrés similaires d'inhibition catalytique de PARP mais une différence dans la capacité cytotoxique. Il est proposé que les inhibiteurs de PARP induisent un changement conformationel allostérique dans PARP1 et PARP-2 qui stabilise leur association avec l'ADN. La capacité des inhibiteurs de la PARP à piéger la PARP sur l'ADN apparait corrélée à la cytotoxicité (142). En effet, on remarque que la cytotoxicité des inhibiteurs de PARP est supérieure dans les cellules présentant PARP de type sauvage comparativement aux cellules mutées pour PARP1/2. Ceci n'est pas expliqué par l'inhibition catalytique des inhibiteurs de la PARP (141).

1.4.3 Inhibiteurs de PARP en clinique

Une étude basée sur 232 femmes présentant un EOC HGS a constaté que 50% des patientes étaient déficientes en RH en raison de mutation germinale (15%) ou somatiquement acquis 35% (143). Une étude clinique de phase II, effectuée en 2011, a recruté 91 femmes atteintes du EOC HGS présentant ou pas des mutations *BRCA1/2*. Le taux de réponse globale à l'Olaparib est de 30%, augmente à 45% chez les patientes sélectivement *BRCA1/2* et est à 24% chez les patientes ne présentant pas de mutations *BRCA1/2* (144). Plus tard, d'autres études cliniques internationales de phase II, plus grande, ont recruté plus de 300 femmes spécifiquement atteintes du EOC HGS présentant des mutations BRCA 1/2 (145) (146). Les taux de réponse sont de 33% et 31% selon l'étude clinique, donc un peu plus bas que ce qui avait été déterminé dans la première étude. Sur la base de ces données, la Federal Drug Association (FDA) a donné son approbation, en décembre 2014, pour l'utilisation en clinique de l'Olaparib en monothérapie, avec 400 mg deux fois par jour, pour les patientes atteintes d'un cancer ovarien avancé présentant une mutation BRCA et préalablement traitées avec minimum trois lignes de chimiothérapie. L'inhibition de l'activité de PARP est transitoire et, par conséquent, elle est dosée en continu pour la plupart des essais en utilisant un schéma de dosage deux fois par jour. De plus, il est important de noter que ces réponses sont relatives car elles signifient une augmentation du PFS de 3,6 mois (147). Par la suite, Santé Canada et l'agence européenne des médicaments ont accepté l'Olaparib avec les mêmes règles de traitement. Les effets indésirables associés à l'Olaparib sont des nausées, des vomissements,

une diminution de l'appétit, une anémie, une thrombocytopénie, des arthralgies et des myalgies. Des cas rares de leucémie myéloïde aiguë et de syndrome myélodysplasique ont été signalés chez des patientes fortement traitées (145, 146). Ces effets secondaires poussent les entreprises pharmaceutiques à développer des nouveaux inhibiteurs de PARP présentant une plus grande efficacité à des plus faibles doses, permettant ainsi de diminuer les effets secondaires, d'améliorer la réponse et donc le nombre de patientes pouvant en bénéficier (Table III) (129)).

Drugs	IC_{50} (PARP-1; PARP-2)	Sponsors	Highest stage	Identifiers on clinicaltrials.gov	Combination	Patients	BRCA1/2 testing
2	5 nM; 1 nM[8]	AstraZeneca	Phase III	NCT02000622	No	Breast cancer	Yes
			Phase III	NCT02032823	No	Breast cancer	Yes
			Phase III	NCT01874353	No	Ovarian cancer	Yes
			Phase III	NCT01844986	No	Ovarian cancer	Yes
			Phase III	NCT02282020	No	Ovarian cancer	Yes
			Phase III	NCT02184195	No	Pancreatic cancer	Yes
			Phase III	NCT01924533	+ paclitaxel	Gastric cancer	No
3	NA* [K_i: 1.4 nM (PARP-1)][25]	Clovis Oncology	Phase III	NCT01968213	No	Ovarian cancer	Yes
4	3.8 nM; 2.1 nM[26]	Tesaro	Phase III	NCT01847274	No	Ovarian cancer	Yes
			Phase III	NCT01905592	No	Breast cancer	Yes
5	NA* (K_i: 5 nM; 5 nM)[27]	AbbVie	Phase III	NCT02163694	+ carboplatin + paclitaxel	Breast cancer	Yes
			Phase III	NCT02032277	+ carboplatin	TNBC	No
			Phase III	NCT02106546	+ carboplatin + paclitaxel	NSCLC	No
			Phase III	NCT02152982	+ temozolomide	Glioblastoma	No
6	0.57 nM (PARP-1)[28]	BioMarin	Phase III	NCT01945775	No	Breast cancer	Yes
7	1.0 nM; 1.2 nM[30]	Eisai	Phase Ib / II	NCT01618136	+ temozolomide or carboplatin and paclitaxel	Solid tumors or B-cell lymphoma	No
8	NA*	Eisai	Phase II	NCT01605162	+ temozolomide	Melanoma	No
12	0.83 nM; 0.11 nM[58]	BeiGene	Phase Ia	NCT02361723	No	Solid tumors	No
			Phase Ib	NCT02660034	+ BGB-A317	Solid tumors	Yes
13	NA (K_i: 0.47 nM; 0.85 nM)[32]	AbbVie	Phase I	NCT01339650	No	Solid tumors	Yes
11	5 nM (PARP-1)[22]	AstraZeneca	Phase I	NCT01247168	No	Solid tumors	No
9	20 nM; 6 nM (for its active ingredient CEP-8983)[20]	Cephalon; Teva Pharmaceutical Industries	Phase II	NCT01311713	No	Solid tumors	Yes
10	<15 nM (PARP-1)[21]	Genentech	Phase I	NCT00272415	+ temozolomide	Melanoma	No

[a]The listed clinical trials are for the highest stage of corresponding inhibitors. Gray represents the PARP-1 inhibitors that currently have unknown or terminated clinical trial status. NA*: The IC_{50} values for PARP-1 and/or PARP-2 are not available. Compound 8 was reported to inhibit PARP activity by 84% at 3 μM.[59]

Table III : Les inhibiteurs de PARP qui ont été (gris) ou sont évalués cliniquement pour la thérapie contre le cancer.

An Update on Poly(ADP-ribose)polymerase-1 (PARP-1) Inhibitors: Opportunities and Challenges in Cancer Therapy. Ying-Qing Wang et al., J. Med. Chem. 2016, 59, 9575−9598

1.4.4 Les nouveaux PARP inhibiteurs

Cinq nouveaux inhibiteurs de PARP (Figure 9), actuellement en essais cliniques de phase III, ont été créés par les entreprises pharmaceutiques pour tenter d'améliorer l'inhibition de l'activité de PARP tout en diminuant les effets secondaires. L'Olaparib est le plus largement étudié et était, encore fin 2016 le seul à être approuvé par la Food and Drug Association (FDA). Un autre inhibiteur de PARP prometteur est le Rucaparib qui a récemment reçu, en raison de sa bonne activité, une approbation accélérée par la FDA pour traiter les patientes présentant une mutation germinale ou somatique de BRCA et ayant subi au préalable

au minimum deux lignes de chimiothérapie (https://www.fda.gov/drugs/informationondrugs/approveddrugs/ucm 533891). Tous les inhibiteurs de PARP bloquent principalement l'activité enzymatique de PARP1. Le Talazoparib et le Rucaparib sont extrêmement efficaces pour réduire l'activité de la PARP, suivis par Niraparib, Olaparib et le moins puissant, le Veliparib (148). Par contre, des études ont observé que les inhibiteurs de PARP diffèrent considérablement par leurs capacités de piégeage. Le Talazoparib est l'agent de piégeage le plus puissant, détectable aux concentrations de sous-nmol/L. L'Olaparib est lui de puissance intermédiaire avec un piégeage significatif observable aux alentours de 10 à 100 nmol/L, alors que le Veliparib et le Niraparib sont les agents de piégeage les moins efficaces nécessitant des concentrations > 1 mmol/L (149). Le NMS-P118 est actuellement en développement préclinique et a également démontré une inhibition de la PARP1/2 plus puissante que l'Olaparib (150) (151).

1.4.5 Destin cellulaire après traitement aux inhibiteurs de PARP

La plupart des études montrent que le destin cellulaire induit par la létalité synthétique des inhibiteurs de PARP passe par un processus apoptotique provoqué par une interruption du cycle cellulaire qui est déclenchée par une accumulation de dommages à l'ADN (152). À l'inverse, certaines études ont montré que les inhibiteurs de PARP induisent une nécrose ou une sénescence. Cette sénescence est montrée dans différents types cancéreux comme la prostate, l'ovaire, le sein et les cancers colorectaux, et est à chaque fois dépendante de p53 et précédée d'un traitement induisant des liaisons à l'ADN comme la radiothérapie ou la chimiothérapie (153, 154). Par exemple, une étude montre que l'inhibition de PARP déclenche une sénescence cellulaire dépendante de p53 dans les cellules déficientes PTEN dans la prostate. Ils constatent également que la sénescence cellulaire induite par PARP est transformée en une réponse apoptotique lors de la perte commune de PTEN et de p53 (155).

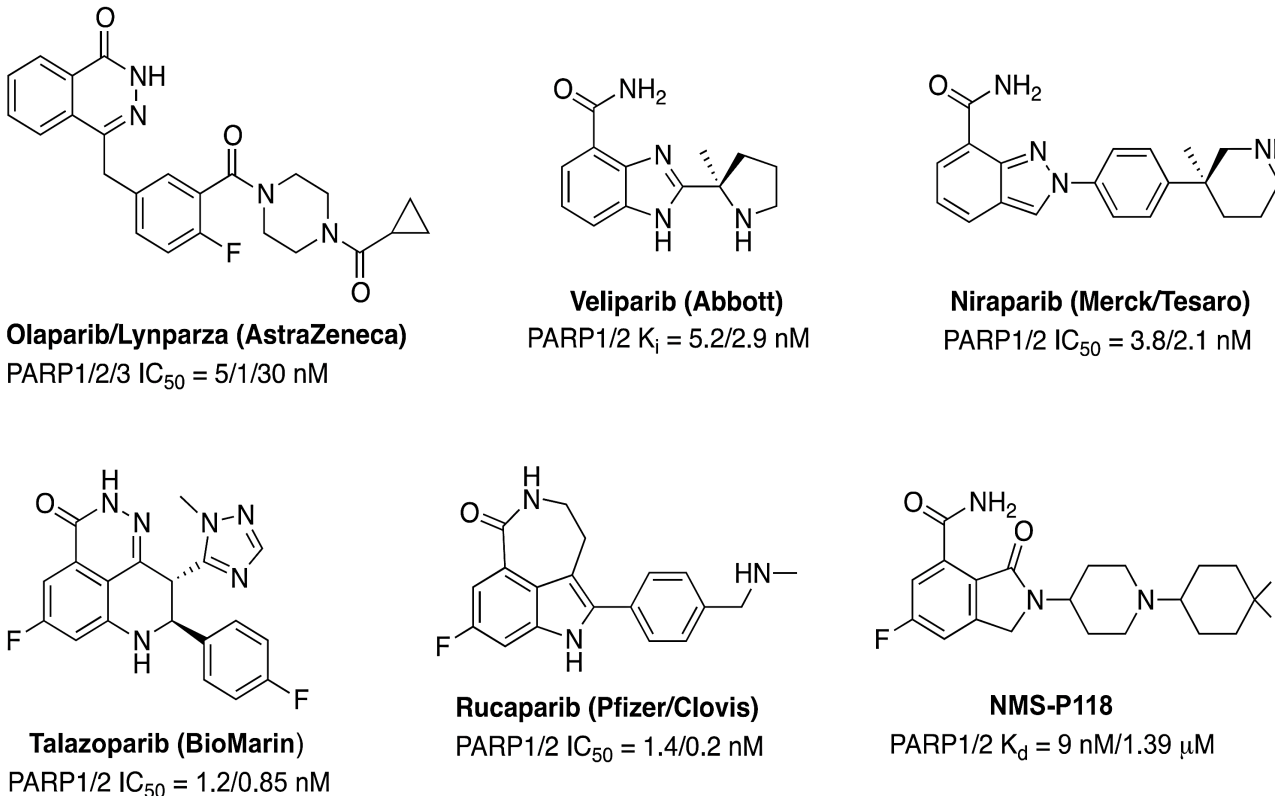

Figure 9: Structures et activités des différents inhbiteurs de PARP
DNA repair targeted therapy: The past or future of cancer treatment? Navnath S. Gavande et al. Pharmacology & Therapeutics 160 (2016) 65–83

1.4.6 Résistance aux inhibiteurs de PARP

Il est démontré que les inhibiteurs de PARP sont efficaces pour les cancers associés à *BRCA1* et *BRCA2*, cependant toutes les patientes ne répondent pas aussi bien et certaines tumeurs peuvent devenir résistantes par différents mécanismes (Figure 10). Les mécanismes moléculaires décrivant la résistance aux inhibiteurs de PARP sont principalement liés à la restauration de la RH comme, par exemple, la récupération de la fonction BRCA. Cette restauration de l'activité de BRCA peut se produire par réversion, restauration de trame de lecture, perte de méthylation du promoteur de BRCA ou stabilisation du domaine BRCA 1 C-terminal par la fonction HSP90 (156, 157). L'inhibition de 53BP1 est un autre mécanisme bien décrit de résistance aux inhibiteurs de PARP dans les tumeurs BRCA mutées. 53BP1 empêche

la mise en place de la RH dans un contexte BRCA muté en phosphorylant RPA et l'empêchant ainsi de se fixer sur l'ADN. Toutefois, si 53BP1 est inhibé, RPA se fixe sur l'ADN et recrute RAD51 qui va induire la RH en contournant le besoin de BRCA fonctionnelle (158). Mais des recherches ont démontré que l'inhibition de RNF8, dans le contexte de résistance par BRCA muté et 53BP1 perdue, permettait de revenir à une déficience de la RH. Cliniquement, l'utilisation d'inhibiteur de RNF8 serait intéressante pour les patientes présentant un profil BRCA mutée et 53BP1 inhibé (159). Un autre mécanisme serait basé sur l'expression de PARP1. PARP peut être diminuée ou complètement perdue en raison de divers mécanismes de régulation, tels que l'hyperméthylation du promoteur. Cette réduction de PARP1 entraîne moins de piégeage de PARP et ainsi diminue l'efficacité des inhibiteurs (160). De plus, la régulation positive des transporteurs ABC, telle que la pompe d'efflux P-gp, est un mécanisme de résistance qui a été décrit pour des agents ciblés multiples et qui peut augmenter l'efflux PARPi des cellules tumorales (161). Dans l'ensemble, la résistance aux PARPi n'est pas inattendue dans le contexte d'une utilisation clinique accrue de ces agents. La connaissance et la compréhension des mécanismes moléculaires pertinents sous-jacents à la résistance PARPi sont pertinentes et peuvent également conduire à de nouvelles cibles ou à de nouvelles combinaisons avec les inhibiteurs de PARP.

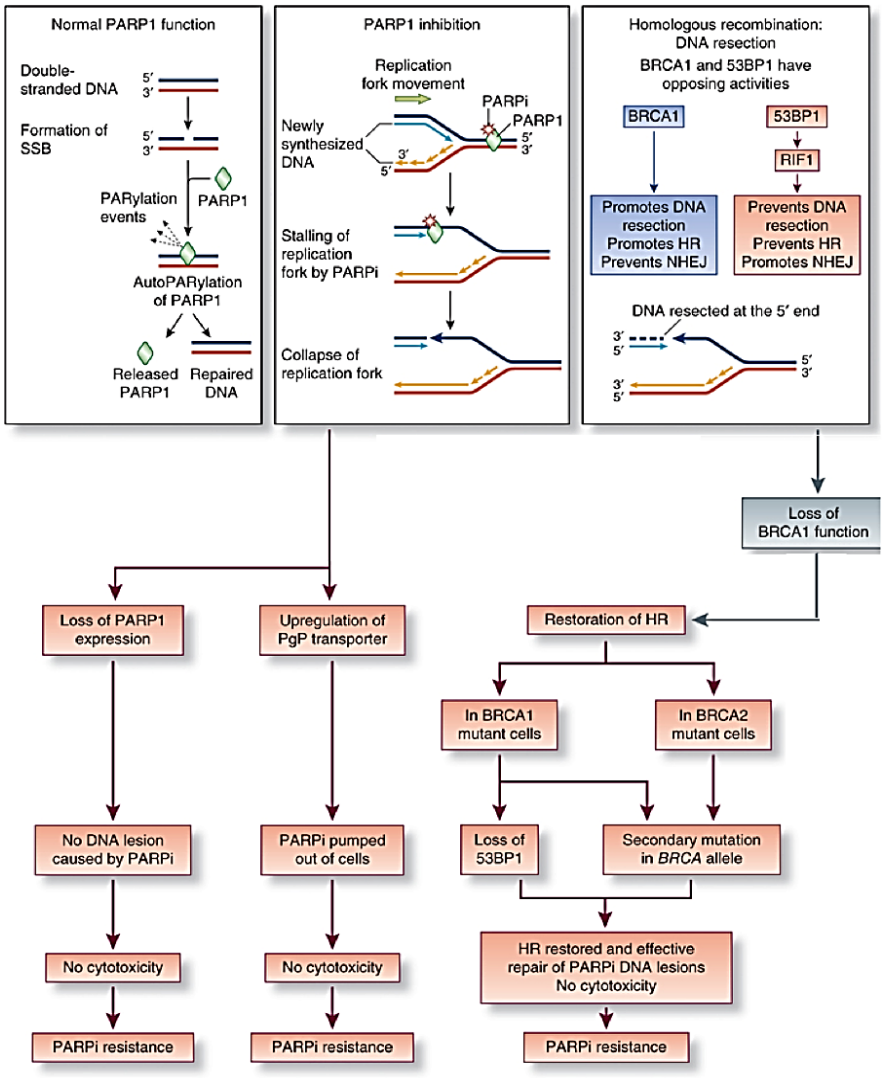

Figure 10: Mécanismes de résistance aux inhibiteurs de PARP
Mechanisms of resistance to therapies targeting BRCA-mutant cancers, Christopher J Lord & Alan Ashworth, Nature Medicine 19, 1381–1388 (2013)

1.4.7 Co-traitements

Les combinaisons d'agents thérapeutiques ciblant des voies moléculaires différentes mais interagissant entre elles ont le potentiel d'améliorer la survie des patientes. Il a déjà été démontré que certains agents ne produisent qu'un effet anti-tumoral minime voire nul lorsqu'ils sont utilisés comme agents uniques, mais peuvent provoquer un effet conséquent

lorsqu'ils sont combinés. Bien que l'utilisation des inhibiteurs de PARP en tant qu'agent unique ait récemment suscité une grande attention, de nombreuses études évaluant le potentiel des inhibiteurs de PARP combinés à d'autres traitements ont eu lieu au cours de la dernière décennie afin d'en augmenter son efficacité et son champ d'action. Plus précisément, des stratégies visant à optimiser l'utilisation du PARPi comme chimio-potentiateurs, ainsi que pour contourner le développement de la résistance, ont été et restent à l'étude.

La découverte et l'optimisation clinique des inhibiteurs de PARP ont été initialement stimulées par leur capacité à améliorer la réponse à la chimiothérapie. L'effet synergique de la combinaison des inhibiteurs de PARP et de TMZ semble être, au moins en partie, dépendant de la capacité de piégeage des inhibiteurs de PARP mais pas de l'état de la RH (141, 162). Dans le même ordre d'idée, la combinaison des inhibiteurs de PARP avec le rayonnement ionisant permet une amélioration de la réponse.

L'erlotinib (un inhibiteur de l'EGFR), combiné avec l'Olaparib augmente l'apoptose dans les cellules de carcinome ovarien surexprimant EGFR et présentant un BRCA de type sauvage (163). Cela s'explique certainement par le fait que certaines mutations EGFR provoquent une déficience en RH par l'intermédiaire de la voie Fanconie Anémie (164). Il en va de même avec les inhibiteurs de VEGFR qui, en induisant un état hypoxique, vont diminuer la RH et donc augmenter la sensibilité aux inhibiteurs de PARP par un effet BRCAness. Par exemple, les thérapies anti-angiogenèses, y compris le Bevacizumab et le Cédiranib, induisent une hypoxie tumorale, une réduction de la RH et donc une sensibilité à l'inhibition de PARP (165). Il est donc clair que la grande majorité des études et des essais portant sur les inhibiteurs de PARP seuls ou en combinaison explore le système de létalité synthétique par la déficience en RH. Cependant, des effets de combinaison des inhibiteurs de PARP ont été démontrés dans des conditions de RH fonctionnelle (166). De telles activités proviennent vraisemblablement des fonctions de PARP non liées à la réparation de l'ADN comme mentionnées ci-dessus ou d'une voie encore inexplorée. Il a été démontré, par exemple, que la combinaison des inhibiteurs de PARP avec des inhibiteurs de CHK1/2 augmente la mort cellulaire dans les cellules mutées *TP53* (167).

1.5 Projet de thèse

1.5.1 Problématique

Les difficultés posées par la prise en charge des patientes atteintes du cancer épithélial de l'ovaire séreux de haut grade nous ont conduit à nous intéresser aux inhibiteurs de PARP. Les premiers essais cliniques démontrent que le taux de réponse globale est de 30%, et augmente à 45% chez les patientes présentant les mutations *BRCA1/2*, amenant le principe que celles-ci répondent aux inhibiteurs de PARP. Or, 24% des patientes ne présentant pas de mutations *BRCA1/2* répondent aux inhibiteurs de PARP, ce qui est expliqué dans la littérature par un effet BRCAness. Pourtant, environ 60% des patientes présentant une mutation *BRCA1/2* ne répondent pas aux inhibiteurs de PARP. Environ 50% des patientes avec un EOC HGS présentent une déficience en RH alors que le taux de réponse globale est seulement de 30%. Donc la mutation *BRCA1/2* ou la BRCAness n'explique pas tous ces résultats. Malgré la mise en place de nouveaux inhibiteurs de plus en plus efficaces, la réponse globale reste toujours autour de 30%. En clinique, le traitement de maintenance aux inhibiteurs de PARP est associé à une résistance acquise, bien qu'il soit le seul moyen d'obtenir une réponse aux traitements. Tout cela oblige les chercheurs à mieux comprendre le mécanisme d'action des inhibiteurs de PARP mais également à les optimiser.

1.5.2 Hypothèses de travail

Les recherches antérieures sur les inhibiteurs de PARP nous ont amené à élaborer les hypothèses suivantes :

1- Le profil fonctionnel de toutes les voies de la réparation de l'ADN (pas seulement la RH et le BRCAness) est important pour prédire la réponse d'un modèle d'étude de lignées cellulaires du cancer de l'ovaire épithélial séreux de haut grade aux inhibiteurs de PARP.

2- Une meilleure compréhension du destin cellulaire suivant un traitement par les inhibiteurs de PARP contribuera non seulement à améliorer nos connaissances, mais aussi à présenter des opportunités pour tester des thérapies combinées capables de potentialiser les réponses et d'éviter les états de résistance.

1.5.3 Objectifs de recherche

Les principaux objectifs ont été déterminés afin de répondre aux hypothèses précédemment citées.

Le premier objectif, constituant le premier chapitre des résultats, est d'améliorer et d'augmenter les modèles cellulaires EOC HGS déjà établis au laboratoire, afin d'avoir un nombre de cellules suffisamment important dont la caractéristique moléculaire principale (statut BRCA1/2) permet de couvrir tous les types de réponses spécifiques aux inhibiteurs de PARP.

Par la suite, nous utiliserons ce nouveau modèle dans un second objectif pour déterminer un modèle spécifique de fonctionnalité des différentes voies de la réparation de l'ADN, permettant de mieux prédire la réponse aux inhibiteurs de PARP.

Le dernier objectif, constituant le troisième chapitre des résultats, est de caractériser le destin cellulaire suite à l'inhibition de PARP et de déterminer si celui-ci peut être exploité pour proposer une nouvelle thérapie combinée.

2 RÉSULTATS

2.1 Chapitre 1 : Novel high-grade serous epithelial ovarian cancer cell lines that reflect the molecular diversity of both the sporadic and hereditary disease

2.1.1 Article #1: Résumé en français

Titre en français : Nouvelles lignées cellulaires de cancer épithélial de l'ovaire de haut grade séreux reflétant la diversité moléculaire de la maladie sporadique et héréditaire.

Peu de modèles cellulaires du cancer épithélial de l'ovaire (EOC) ont été développés pour le sous-type séreux de haut grade (HGS), représentant la forme la plus commune et la plus létale du cancer gynécologique. Nous décrivons ici l'établissement de six nouvelles lignées de cellules EOC dérivées spontanément à partir de tumeurs HGS (TOV2978G, TOV3041G et TOV3291G) ou d'ascites (OV866 (2), OV4453 et OV4485). Un séquençage de l'éxome a révélé des mutations TP53 somatiques dans cinq des lignées cellulaires. La lignée cellulaire OV4485 présente une nouvelle mutation du site d'épissage *BRCA1*, et la OV4453, une mutation non-sens récurrent *BRCA2* d'origine germinale. La nouvelle mutation *BRCA1* induit un épissage anormal et une instabilité de l'ARNm entraînant l'absence de protéine *BRCA1*. Aucune des lignes cellulaires ne présente de mutation dans KRAS ou BRAF, qui sont caractéristiques d'autres sous-types EOC. Les résultats de puce à polymorphisme de nucléotide (SNP-array) montrent que toutes les lignées cellulaires présentent des anomalies chromosomiques structurelles, des altérations du nombre de copies et des régions de perte d'hétérozygotie, en cohérence avec celles décrites pour les HGS. Quatre lignées cellulaires ont pu produire des sphéroïdes en 3D, deux ont montré une croissance indépendante de l'ancrage et trois (y compris les lignées cellulaires mutées *BRCA1* et *BRCA2*) ont formé des tumeurs chez des souris SCID. Ces nouvelles lignées cellulaires EOC-HGS et leurs caractérisations détaillées fournissent de nouveaux outils de recherche pour étudier la forme la plus commune et la plus létale d'EOC.

2.1.2 Article #1: Version originale soumise à Gene and Cancer (Appendice 1)

Genes Cancer. 2015 Sep; 6(9-10):378-98

Novel high-grade serous epithelial ovarian cancer cell lines that reflect the molecular diversity of both the sporadic and hereditary disease

Hubert Fleury[1,2,#], Laudine Communal[1,2,#], Euridice Carmona[1,2], Lise Portelance[1,2], Suzanna L. Arcand[3], Kurosh Rahimi[1,4], Patricia N. Tonin[3,5,6], Diane Provencher[1,2,7,8], Anne-Marie Mes-Masson[1,2,8]

[1] Centre de recherche du Centre hospitalier de l'Université de Montréal (CRCHUM), Montreal, Canada, [2] Institut du cancer de Montréal, Montreal, Canada, [3] The Research Institute of the McGill University Health Centre, Montreal, Canada, [4] Department of Pathology, Centre hospitalier de l'Université de Montréal (CHUM), Montreal, Canada,[5] Department of Human Genetics, McGill University, Montreal, Canada, [6] Department of Medicine, McGill University, Montreal, Canada, [7]Division of Gynecologic Oncology, Université de Montréal, Montreal, Canada,[8] Department of Medicine, Université de Montréal, Montreal, Canada

#These authors contributed equally to the work

Correspondence: Anne-Marie Mes-Masson, Department of Medicine, Université de Montréal, CRCHUM-Institut du cancer de Montréal, 900 rue St-Denis, Montreal, Quebec, Canada, H2X 0A9. Tel: (514) 890-8000 ext. 25496 Fax: (514) 412-7591 E-mail: anne-marie.mes-masson@umontreal.ca

Keywords:high-grade serous, epithelial ovarian cancer, cell lines, *BRCA* mutations

2.1.2.1 Abstract

Few cell line models of epithelial ovarian cancer (EOC) have been developed for the high-grade serous (HGS) subtype, which is the most common and lethal form of gynaecological cancer. Here we describe the establishment of six new EOC cell lines spontaneously derived from HGS tumors (TOV2978G, TOV3041G andTOV3291G) or ascites (OV866(2),OV4453 and OV4485). Exome sequencing revealed somatic *TP53* mutations in five of the cell lines. One cell line has a novel *BRCA1* splice-site mutation, and another, a recurrent *BRCA2* nonsense mutation, both of germline origin. The novel *BRCA1* mutation induced abnormal splicing, mRNA instability, resulting in the absence of *BRCA1* protein. None of the cell lines harbor mutations in *KRAS* or *BRAF*, which are characteristic of other EOC subtypes. SNP arrays showed that all of the cell lines exhibited structural chromosomal abnormalities, copy number alterations and regions of loss of heterozygosity, consistent with those described for HGS. Four cell lines were able to produce 3D-spheroids, two exhibited anchorage-independent growth, and three (including the *BRCA1* and *BRCA2* mutated cell lines) formed tumors in SCID mice. These novelHGS EOC cell lines and their detailed characterization provide new research tools for investigating the most common and lethal form of EOC.

2.1.2.2 Introduction

Ovarian cancer is the fifth cause of cancer-related deaths in the Western world, the second most common gynecological cancer and the leading cause of death from gynecological malignancies [1]. The most common form of cancer of the ovary is epithelial ovarian cancer (EOC) (reviewed in [2, 3]). Largely asymptomatic, over 70% of EOC patients are diagnosed at an advanced stage of the disease. Standard first line therapy consists of tumor de-bulking surgery and treatment with platinum DNA alkylating reagents, such as carboplatin or cisplatin, associated with the microtubule poison paclitaxel [4, 5]. Initial response rates are high butprobably due to innate or acquired chemoresistance the disease recurs in more than 70% of patients [5, 6]. EOCs can be subdivided in different subtypes according to their cell type: serous, mucinous, endometrioid, clear cell, mixed subtypes or undifferentiated adenocarcinomas or carcinomas [2, 7]. For the serous subtype, there is an understanding that distinct molecular events contribute to two possibly non-contiguous diseases, which differentiate low (LGS) and high grade serous (HGS) cancers. Furthermore, it is becoming increasingly clear that distinct molecular events are associated with each particular EOC subtype (discussed in [2, 7-9]).

As a group HGS tumors account for over 60% of all EOCs and are characterized by high genomic instability and chromosomal anomalies with cells exhibiting complex karyotypes, which include intrachromosomal breaks and aneuploidy [10, 11]. It has been proposed that mutations in the *TP53* tumor suppressor gene is one of earliest mutational events in HGS as nearly all cases harbor a somatic mutation in this gene as confirmed by a recent molecular genetic profiling of over 300 HGS samples by The Cancer Genome Atlas Research (TCGA) network [12, 13]. Furthermore, compromised homologous recombination due to loss of *BRCA1* and *BRCA2* function, by the inheritance of a germline pathogenic mutation in approximately 10-20% of HGS cases [12], or through somatic means by acquiring an intragenic mutation or epigenetic silencing [12, 14, 15], occurs in approximately one third of the HGSEOC cases. The prevalence of *TP53*mutations and *BRCA1*/*BRCA2* deficiency likely leads to incompetent DNA repair which in turn contributes to chromosomal instability, resulting in severely aberrant karyotypes. In general, HGS EOCs are highly heterogeneous having widespread inter- and intra-tumoral mutation profiles, although common patterns of

chromosomal regions of gain and loss have been observed [12, 16-18].

The study of processes or pathways relevant to HGS EOC biology, treatment or etiology has been facilitated by cell-based models [19-22]. However, EOC cell lines representative of HGS based on their intragenic mutational spectrum, chromosomal anomalies and gene expression profiles are limited in number [23]. This is surprising given the high frequency of HGS cases relative to the other subtypes of EOC. Indeed the most commonly used cell lines, such as SKOV3 do not exhibit features characteristic of HGS as shown in a recent molecular genetic analysis of 47 ovarian cancer cell line models [23]. It has also been reported that several tumor cell banks lack information of tumor of origin, grade, stage and molecular marker characterization for several ovarian cancer cell lines [24]. Moreover, only a few HGS EOC cell lines harboring *BRCA1* or *BRCA2* mutations have been described [23, 25, 26]. Recently, we reported the characterization of a set of nine matched EOC cell lines derived from tumors at diagnosis and recurrence, andfrom ascites from each of three serous EOC patients [27], and they have been used to characterize some of the molecular genetic features of HGS. In all, it is clear that cell line models that accurately recapitulate HGS EOC characteristics and heterogeneity are in urgent need as they are a starting point to discover and validate new therapeutic targets and biomarkers of this disease.

Here we have described the generation, molecular characterization, and *in vivo* and *in vitro* growth characteristics of six new EOC cell lines all derived from HGS cases. Two of these cell lines were derived from patients harboring a germline *BRCA1* or *BRCA2* mutation. The molecular genetic characterizations of these cell lines suggest that they exhibit features consistent with HGS tumors. Their unique profiles, which include different mechanisms of inactivation of *TP53* and *BRCA1*, reflect the heterogeneity observed in HGS tumors. Therefore, these new cell lines offer a significant contribution to the list of HGS EOC cell lines available for research as they present distinct features characteristic of this multiple-faceted disease.

2.1.2.3 Results

Cell lines derived from HGS EOC patient samples

The clinical characteristics of the patients 866, 2978, 3041, 3291, 4453, and 4485 from which the cell lines were derived are shown in Table I. All patients had late stage (III-IV) and high-grade serous disease. Patients had complete, sub-optimal or optimal surgical debulking, received standard first-line platinum/taxol chemotherapy treatment and died from disease progression.

The cell lines were derived from samples collected at diagnosis or at the time of relapse, from either solid tissue (TOV) or ascites (OV). The TOV2978G, TOV3291G and OV4453 cell lines were derived from primary tissues or ascites from patients that had not had chemotherapy prior to surgery; whereas the OV866(2), TOV3041G and OV4485 cell lines were derived from samples obtained from recurring disease and thus the patients had been treated with chemotherapy before collection. The OV866(2) cell line nomenclature reflects the fact that it was established from a second ascites sample obtained from patient 866. The OV4453 cell line was derived from a patient who received radiotherapy and hormonotherapy treatments for breast cancer five years prior to ovarian cancer diagnosis. Among these six cell lines, OV4453 is the only example of a cell line that was derived from a patient with a personal prior history of cancer.

After 50 passages, the cell lines appeared homogeneous in their morphology, exhibiting a cobblestone appearance characteristic of epithelial cells (Figure 1). Notable is the scarcity or lack of elongated fibroblast-like cells in culture.

Cell lines derived from BRCA1 and BRCA2 mutation positive cases

It is well established that germline mutations in *BRCA1* and *BRCA2* confer susceptibility to breast and ovarian cancers. *BRCA2* and *BRCA1* germline mutations were identified in patients 4453 and 4485, respectively, as a consequence of genetic testing in hereditary cancer clinics due to their breast and ovarian cancer family history (see supplemental Figure S1 for pedigree). The *BRCA2*:G6085T (c.5857G>T) mutation was identified in a screen of the most common *BRCA1* and *BRCA2* mutations found to recur in French Canadians due to common ancestry [28]. Indeed, all of the cell lines were derived from

patients who self reported French Canadian ancestry, a population known to exhibit strong founder effects [29]. This *BRCA2* mutation was found in the homozygous state in OV4453 cell line (Table II) based on DNA sequencing and SNP array analyses (see below). This variant introduces a stop codon (p.E1953X) in the amino acid sequence that is predicted to result in a truncated *BRCA2* protein. This mutation is one of the most common *BRCA2* deleterious mutations found in French Canadians [28, 29].

Following mutation negative findings due to a targeted mutation screen of the most common *BRCA1*/*BRCA2* mutations found in French Canadians, a comprehensive commercial-based mutation analysis performed in the hereditary cancer clinic revealed that patient 4485 harbored the *BRCA1*:IVS14-1G>T (c.4485-1 G>T) mutation. This mutation was also found in OV4485 cell line (Table II) and was found in the homozygous state based on DNA sequencing and SNP array analyses (see below). The pathogenic effect of this new *BRCA1*:IVS14-1G>T mutation is unknown. This unique variant has not been reported in either of the Breast Information Core mutation database (research.nhgri.nih.gov/bic/) or the LOVD-Leiden Open Variation Database (chromium.liacs.nl/LOVD2/cancer/home.php?select_db=*BRCA1*), nor the Exome Aggregation Consortium (ExAC) database (exac.broadinstitute.org). However, an investigation of this mutation in the OV4485 cell line suggests that it probably results in the inactivation of *BRCA1* protein function (Figure 2). A PCR-based assay of cDNA identified the presence of novel transcript in this cell line (Figure 2A) that when sequenced suggested that it was derived from the splicing of exon 13 to an alternative 3' acceptor in exon 15 likely due to the presence of G>T substitution at the splice acceptor site (Figure 2B). When translated to protein, two predicted *BRCA1* proteins could be produced, one having a deletion of 51 amino acids (p.del 1453-1504) (exon 14 splice out + 29bp deletion on exon 15) and another having a premature stop codon (p.S1496X) (29bp deletion of exon 15) (Figure 2B). The p.del1453-1504 mutation would delete part of the coiled coil structure (important for interaction with PALB2, and indirectly *BRCA2*) and some of the ATM target phosphorylation sites of *BRCA1* [30, 31]. The introduction of a stop codon at amino acid position 1496 would also predict a truncated protein with loss of the *BRCA1* C-terminus (BRCT) domain (important for interaction with several phosphorylated proteins that are primarily involved in the DNA damage response) [30, 31]. Rare *BRCA1* codon 1496 truncating mutations (*BRCA1*: p.Ser1496Ter) have been described and are classified as clinically important in the Breast

Information Core mutation database (research.nhgri.nih.gov/bic/). However, it is not known if these predicted transcripts are translated into truncated proteins or are eliminated by other mechanisms such as nonsense-mediated decay. In the OV4485 cell line, no evident *BRCA1* protein band was detected (Figure 2C), and this could be due to low levels of transcribed message (Figure 2A). These results are consistent with the possibility that *BRCA1*:IVS14-1G>T mutation is clinically relevant.

Using a targeted mutation screen, the *BRCA1* and *BRCA2* germline mutations found to recur in French Canadians were not found in normal blood lymphocyte DNA from the patients from which the TOV2978G, TOV3041G and TOV3291G cell line lines were derived. Germline mutations were also not found in a more limited mutation screen of normal blood lymphocyte DNA from the patient from which OV866(2) cell line was derived. These results are consistent with our findings from whole exome sequencing analysis, which also revealed no further evidence for *BRCA1*/*BRCA2* mutations in these cell lines (Table II). During the course of analyzing *BRCA1* gene and protein expression to characterize the consequences of the *BRCA1*:IVS14-1G>T mutation, we were not able to detect *BRCA1* message or protein in TOV2978G and TOV3041G (Figure 2A and C). It is possible that in these cell lines *BRCA1* expression was affected by epigenetic silencing of the promoter, as has been described by the TCGA to have occurred in approximately 12% of316 HGS EOC tumor samples [12].

Cell lines exhibit somatic genetic and genomic features characteristic of HGS EOC

In our initial study of the EOC cell lines, we performed a targeted mutation analysis of selected genes as *TP53* mutations have been found in the majority of HGSEOC tumors and mutually exclusive mutations in *KRAS* and *BRAF* have been found in LGS EOC tumors [12, 32-34]. All cell lines with the exception of TOV3041G harbored an intragenic somatic *TP53* mutation (Table II). All three missense *TP53* mutations are classified as deleterious based on the IARC TP53 mutation database (www-p53.iarc.fr), and the two splice *TP53* mutations are predicted to affect the translation of the encoded protein [18]. Using a targeted mutation analysis, no *KRAS* and *BRAF* mutations affecting common mutation sites in these genes were identified in the cell lines.

SNP array genotyping analysis of each EOC cell line was performed to infer genome-wide chromosomal abnormalities as HGS tumors and cell lines exhibit a high frequency of

chromosomal instability as displayed by copy number anomalies (CNA) across the genome [12, 23, 35]. SNP array analyses of these cell lines showed evidence of extensive chromosomal abnormalities consistent with intrachromosomal breaks and allelic imbalances, which are features characteristics of HGS tumors (Figure 3). Moreover, all cell lines exhibited loss of heterozygosity (LOH) across the *TP53* locus at 17p13, the *BRCA1*locus at 17q12, and the*BRCA2*locus at 13q13.

We also examined SNP array data for *MYC*, *MECOM*, *CCNE1*, *KRAS*, *ALG8*, *SOX17*, and *TACC3*, as regions containing these genes have been shown to exhibit amplification (in order of descending frequency) and for the *NFI*, *RB1* and *PTEN* loci as regions containing these genes have been shown to exhibit homozygous deletions (in order of descending frequency) in HGS tumors [12, 23]. CNA gain was observed for a number of loci in the EOC cell lines, where gain of the *MYC* and *MECOM* loci were observed in all of the EOC cell lines (Table II). CNA gain was also distinctive for the *KRAS* and *CCNE1* loci in the OV866(2) cell line as in to classical gene amplification (Figure 3). Although CNA loss was observed for the *NFI*, *RB1* and *PTEN* loci in all of the EOC cell lines, there was no evidence for homozygous deletions for any of these genes.

We have performed whole exome sequencing analysis to evaluate the presence of somatic anomalies in *TP53*, *BRCA1*, *BRCA2*, *CSMD3*, *NF1*, *CDK12*, and *RB1* in our cell lines as these genes were the most frequently found somatically mutated in HGS EOC samples as reported by the TCGA [12]. This analysis not only verified the presence of somatic *TP53* mutations and germline *BRCA1*/*BRCA2* mutations identified by other means, but also identified mutations in *CSMD3*, *CDK12* and *RB1* (Table II). The splice variants in *RB1* and *CDK12* are predicted to affect the production of the encoded protein. The missense p.S646T mutation in *CSMD3*, has not been reported in the Catalogue of Somatic Mutations in Cancer Database (cancer.sanger.ac.uk/cancergenome/projects/cosmic/). Although this amino acid alteration is predicted to be tolerated by SIFT (http://sift.jcvi.org), it is predicted to be probably damaging by PolyPhen-2 (genetics.bwh.harvard.edu/pph2/), based on computational tools that assess the functional effects of amino acid substitutions. The amino acid substitution occurs in a highly conserved region of the gene based on Genomic Evolutionary Rate Profiling (GERP) for mammalian alignments (genome.ucsc.edu). Finally, we also reviewed *PIK3CA*, *CTNNB1*, and *ARID1A*, as well as *KRAS* and *BRAF*, for somatic mutations in these genes have

been reported to occur in EOC subtypes and corresponding cell lines most often representing other non-HGS subtype cancers [23]. None of our EOC cell lines harbored mutations in these genes (Table II).

Expression of cytokeratin markers, WT-1, TP53, PAX8 and HER2 in tumor tissue and cell lines characteristic of HGS EOC

In order to investigate the epithelial origin of the tumors and corresponding cell lines, cytokeratin expression was investigated by immunohistochemistry (IHC) and Western blot (WB) analyses, respectively. IHC was not performed on tissue samples from patient 4453 since no tumor cells were found in a review of the histology. In this case, surgery was performed during the chemotherapy treatment cycles. It is possible that the tumor mass had regressed having already responded to therapy by the time of surgery. HGS diagnosis of this patient was determined from a pre-chemotherapy omentum biopsy. For the available tumor samples, HGS histopathology was confirmed by hematoxylin-eosin staining and all of the cytokeratins investigated (CK7, CK8, CK18 and CK19) were present in the tissue sections (Figure 4A). Cytokeratin expression was observed in protein extracted from five of six EOC cell lines (Figure 4B). Although the 866 tumor tissue shows positive staining for all the cytokeratins, the corresponding OV866(2) cell line exhibited low or barely detectable levels of cytokeratin expression (Figure 4B). This cell line was established from the ascites of this patient collected at recurrence eight months after the primary tumor was collected. E-cadherin, another epithelial marker, was also not detectable in the cell line (Figure 4B). In contrast, high levels of vimentin, a mesenchymal marker, were observed in the protein extracts of this cell line. All the other cell lines in this study expressed either cytokeratins or E-cadherin or both (Figure 4B).

To further characterize the presently described cell lines, expression of WT1 and PAX8, which are markers specific for the classification of the HGS EOC subtype [36-39], was investigated. All tumors and cell lines exhibited positive staining for these proteins and this was observed at distinct intensity levels for each cell line as observed on WB analyses (Figure 4A-B).

Protein expression of the human epidermal growth factor receptor-2 gene, HER2, which has been implicated in malignant transformation, was also used to characterize the cell

lines, as overexpression has been reported in 10-20% of serous EOC tumors [40, 41]. HER2 staining by IHC was positive in two solid tumors (866, and 3291) (Figure 4A). HER2 expression was detected in protein extracts offour cell lines (Figure 4B), but intensity of the protein bands was not suggestive of overexpression.

Expression of p53 protein is often indicative of mutation type as was observed in our IHC analysis of *TP53* mutated HGS samples, where missense alleles expressed stable mutated protein in contrast to other mutation types which resulted in no detectable protein ("null" alleles) [35]. Protein expression was detected by WB analysis in all three of the cell lines (OV866(2), TOV3291G, and OV4485) that had a missense mutation (Figure 4B). Interestingly, differential p53 expression was observed in cell lines harboring two distinct intronic *TP53* mutations (splice) of unknown function (based on *TP53* IARC Mutation database). While, p53 mRNA and protein are expressed in the OV4453 cell line (*TP53*:c.376-1 G>A mutation), no mRNA or protein was detectable in lysates from the TOV2978G cell line (*TP53*:c.920-2 A>G mutation) (Table II and Figure 4B). Our results showed that despite the absence of p53 protein, the TOV3041G cell line does not harbor a *TP53* mutation by Sanger or whole exome sequencing analyses (Table II and Figure 4B). Our RT-PCR results showed a faint band of *TP53* mRNA in this TOV3041G cell line (Figure 4B), which suggests that the absence of p53 was not due to protein degradation but rather mRNA instability or gene silencing. This mRNA instability was not observed in the non-HGS*TP53* wild-type cell line TOV21G [42] that also has detectable p53 protein (Figure 4B), suggesting that this is a feature specific to HGS EOC. IHC results on p53 expression of tumor samples (Figure 4A) were concordant with those of WB in the HGS EOC cell lines.

Cell lines exhibit aberrant p53 function

The p53 tumor suppressor is a transcription factor that in response to various types of genotoxic stresses transactivates a number of genes by binding to specific DNA sequences [43], thereby arresting cell cycle, repairing damaged DNA, or inducing apoptosis [44]. Among known direct gene targets that are induced by p53 as consequence of genotoxic stress are *CDKN1A*, *PMAIP1* and *MDM2*, which encode the cyclin-dependent kinase inhibitor 1A (p21), phorbol-12-myristate-13-acetate-induced protein 1 (NOXA) and, E3 ubiquitin protein ligase MDM2 proto-oncogene, respectively [45, 46]. Therefore, to further characterize p53 function

in our cell lines, we investigated the expression of these genes after inducing DNA damage by 8 Gy gamma-irradiation. Figure 5 shows that expression of the p53 target genes analyzed by Q-PCR were not significantly increased after gamma-irradiation in any of the cell lines, although a tendency could be observed for NOXA and MDM2 induction in the OV4453 cell line at a later time point (5h). Nevertheless, all three target genes were efficiently induced in the non-HGS*TP53* wild-type TOV21G cell line even 2h after gamma-irradiation, which expresses the *TP53* mRNA and protein (Figure 4B).

Cell lines exhibit altered in vitro cell growth phenotypes characteristic of oncogenic potential

The growth characteristics of the new cell lines were compared to other HGS EOC cell lines previously established in our laboratory [11, 27]. The average doubling time ranged from approximately 1.3 to 2.4 days (Table III), and overlapped the range reported for the other previous HGS cell lines (from 1.5 to 3 days) [11, 27]. Saturation densities were similar for four of the cell lines (OV866(2), TOV2978G, TOV3291G, OV4453) and this was similar to previously described saturation densities (1.5-3.5 $x10^6$ cells) of other HGS EOC cell lines [11, 27]. However, the saturation densities of the TOV3041G and OV4485 cell lines were significantly higher when compared to any of the other cell lines (Table III).

The ability of each cell line to form spheroids was measuredusing the hanging droplet method as previously described [47]. Observed spheroid characteristics include overall shape, compaction, cell aggregates and consistency across multiple experiments, as conducted with other EOC cell lines derived in our laboratory [11, 27, 47]. Although there were some variations among the replicates, only the TOV3041G cell line consistently formed compact spheroids. In contrast, the OV866(2), TOV3291G and OV4485 cell lines formed loosely compact spheroids with irregular margins and the TOV2978G and OV4453 cell lines formed numerous individual small aggregates (Figure 6A, Table III).

We next measured the ability of the cell lines to growin an anchorage independent environment by culturing the cells in soft agar. Only the OV866(2) and OV4453 cell lines were able to clearly form colonies in soft agar (Figure 6B, Table III). The sizes of the colonies were smaller than the previously described HGS TOV1946 cell line but similar to that of the TOV2223G [11]. The number of colonies formed by the OV866(2) and OV4453 cell lines

were in the same range as that of other HGS cell lines derived in our laboratory [11, 27].

The migration potential of the cell lines was measured using an established scratch migration assay [11, 27, 48]. Migration velocity was calculated based on the time it took for the cells to cover the gap created by removing the cells after confluence had been reached. Four of the cell lines, TOV2978G, TOV3041G, TOV3291G and OV4453, had similar migration velocity, exhibiting a range of 15-21 μm/h, and almost filling the gap within 24h. In contrast, the OV866(2) cell line had a significantly higher migration speed (62 μm/h) when compared to any of the other cell lines, completely covering the gap in 24h; and the OV4485 cell line had a significantly lower migration speed (Figure 6C, Table III).

Carboplatin sensitivity of the cell lines

The carboplatin response of the cell lines was measured by a clonogenic assay. Our results indicate that the OV866(2) cell line was strongly resistant to carboplatin, exhibiting the highest IC_{50} (32 μM) among all the tested cell lines (Table III). This finding is consistent with the characteristic of the patient sample from which it was derived, i.e. a second ascites from a recurrent resistant disease. Two other cell lines showed medium resistance to carboplatin (TOV3191G and OV4485) and three were very sensitive (TOV2978G, TOV3041G and OV4453) (Table III). Interestingly, the *BRCA1* mutated cell line (OV4485) shows a strong resistance to carboplatin (IC_{50} = 6 μM), making it a good model to study new therapeutic strategies for platinum resistant BRCA mutated HGS EOC cases.

BRCA1 and BRCA2 mutated cell lines are tumorigenic in mouse xenograft models

The *in vivo* growth potential of all the cell lines was determinedby subcutaneous injection into SCID mice (n = 5 mice for each cell line). Only the HGS cell lines OV4453 and OV4485, which were derived from *BRCA2* and *BRCA1* mutated cases, respectively, formed tumors at subcutaneous injection sites in all the SCID mice (5/5 mice) (Figure 7A-B, Table III). Tumor growth of the OV4485 cell line was significantly faster and mice had a poorer overall survival than that observed with the OV4453 cell line tumorigenicity assays. Tumors started to appear (volume ≥ 300 mm^3) as early as 98 and 138 days for the OV4485 and OV4453 cell lines, respectively, and reached endpoint limits allowable for tumor growth (2500 mm^3) at 170-230 and 190-320 days, respectively. Figure 7A also shows the tumor

growth of the OV866(2), which was the only other cell line to produce tumors. However, the tumor mass at subcutaneous injection sites reached a maximum of 390 mm^3 in 265 days, and this was observed only in two of five mice (Figure 7A-B, Table III).

We also investigated the capacity of the tumorigenic cell lines, OV866(2), OV4453 and OV4485, to form tumors and produce ascites at intraperitoneal injection sites in SCID mice. The experimental endpoints for these experiments were within ethical limits and included palpable peritoneal tumors, bloated abdomen and stress behavior. The survival curves are shown in Figure 7C. For this model, the OV4453 and OV4485 cell lines induced tumors and produced ascites in all mice at a similar rate, and this was faster than that observed with the OV866(2) cell line, which induced intraperitoneal tumors and ascites in four of five mice (Table III).

2.1.2.4 Discussion

The genomic instability and aberrant karyotype of HGS EOC tumors has been well described and is distinct from that observed in the other EOC histotypes, which often exhibit a more stable genome [49, 50]. The recent study from the TCGA also highlighted the high molecular genetic heterogeneity among HGS tumors, although specific genomic anomaliesrecurred at variable frequencies [12]. Their analyses delineated four transcriptional subtypes, three microRNA subtypes, four promoter methylation subtypes and a transcriptional signature associated with survival in an analysis of over 300 HGS cases. There were recognizable features such as high somatic copy number alterations, an overall high frequency (96%) of somatic *TP53* mutations, *BRCA1*/*BRCA2* germline/somatic mutations or silencing of gene expression in approximately 33% of the tumors, and somatic mutations in *CSDM3*, *NF1*, *CDK12*, and *RB1* that each occurred at low frequency [12]. Recently, the genetic and genomic profiles of several EOC cell lines were compared to the TCGA data in order to gather evidence to verify the suitability of these cells as HGS EOC models [23]. As criteria the authors used the presence of the above-mentioned common features of HGS tumors as well as the absence of mutations in seven specific genes (*PIK3CA*, *PTEN*, *KRAS*, *BRAF*, *ERBB2*, *CTNNB1* and *ARID1A*) that have been reported to occur more often in other EOC subtypes. Few cell lines examined in their study exhibited the molecular genetic features characteristic

of HGSEOC samples. In contrast, we have shown that all of our six newly derived cell lines exhibit genetic and genomic features characteristic of HGS samples, suggesting that they have a high probability of being of HGSEOC tumor origin. Namely, that they have high copy number alterations and/or harbour *TP53* mutations. Some of the cell lines were derived from patients with germline *BRCA1*/*BRCA2* mutations. Moreover, some of these cell lines had somatic mutations in *CSDM3*, *RB1*, and *CDK12*, genes that have been shown to exhibit a low but recurrent mutation frequency in HGS EOC tumors. Although we have shown that the molecular genetic spectrum of each of our EOC cell lines is unique, collectively they reflect the heterogeneity of HGSEOC disease. These novel HGS EOC cell lines provide novel research tools for investigating the most common and lethal form of EOC.

The *BRCA1*/*BRCA2* mutation harboring cell lines (OV4485 and OV4453) also each have a somatic *TP53* mutation, and they were the only cell lines that exhibited robust tumorigenic potential in SCID mice. These genetic features makes them attractive models to study novel therapeutics targeting HGS EOC patients harboring *BRCA1*/*BRCA2* mutations, such as the inhibitors of poly (ADP-ribose) polymerase, a class of drugs currently in phase II/III clinical trials in EOC [51-54] that includes Olaparib which has been recently approved by the US Food and Drug Administration as maintenance therapy in *BRCA*-mutated platinum-sensitive HGS EOC [55]. In the present study we also described a new *BRCA1* mutation located at the intron/exon boundary of exon 15 (IVS14-1 G>T). The establishment of the OV4485 cell line made it easier to characterize this mutation and we showed that it induced alternative splicing as well as instability of the *BRCA1* mRNA (Figure 2). The frequency of this mutation is unknown, however no other mutation carriers were reported in a *BRCA1*/*BRCA2* mutation screen of 136 breast and/or ovarian cancer families of French Canadian descendent [56, 57]. Further studies are warranted to investigate the clinical relevance of this new *BRCA1* mutation. In contrast, the nonsense *BRCA2*:G6085T (E1953X) found in the OV4453 patient and corresponding cell line is a pathogenic germline mutation that has been found to recur in the French Canadian population [28, 56]. Until recently, only five HGS EOC cell lines harboring *BRCA1*/*BRCA2* mutations from EOC samples had been described in the literature [23, 25, 26]. During the course of preparing this manuscript, two other *BRCA* mutated HGS EOC cell lines were reported [58]. Nevertheless, none of these cell lines harbor the mutations found in our study. Based on published reports, only the PEO1 (a

BRCA2 mutated) cell line is tumorigenic in xenografted mice [59]. Here we show that both of our *BRCA1* and *BRCA2* mutated cell lines (OV4485 and OV4453 respectively) form tumors in mice. To our knowledge, the OV4485 cell line is the only *BRCA1* mutated HGS EOC cell line with *in vivo* tumorigenic properties in SCID mice. This cell line also showed resistance to carboplatin (Table III), making it a very suitable *in vivo* model to study new therapies for platinum resistant BRCA mutated cases.

The OV866(2) cell line was the only line expressing markers of epithelial-mesenchyme-transition (EMT), as reflected by the absence of cytokeratins (CK7, CK8, CK18, CK19) and E-cadherin expression, and strong vimentin expression (Figure 4). This cell line also showed the highest carboplatin IC_{50}, anchorage-independent growth and cell invasion when compared to the other five cell lines (Figure 6 and Table III). Research has shown that opposing levels of E-Cadherin and vimentin occur in cells that have undergone EMT [60, 61]. Therefore, this new cell line may be an interesting model to study EOC processes related to peritoneal metastasis and invasion, because there is evidence that EMT transition might be involved in this tumor spread [62]. All the other five cell lines showed patterns of epithelial origin as suggested by the presence of cytokeratins and/or E-cadherin expression.

The TOV3041G cell line was derived from a rare case of HGS EOC where a somatic *TP53* mutation was not detected by our mutation screening. However, we have demonstrated the absence of both p53 mRNA and protein as well as the impaired p53 function in this cell line. Therefore, although *TP53* mutation analysis suggests that it harbors a wild-type allele, this cell line has features characteristic of a p53-null mutation. The p53 protein functions as a transcriptional factor with a crucial role in cellular stress response (reviewed in [63-65]). Owing to its critical function in controlling cell survival or death, strict regulation of p53 levels and activity is crucial. At the protein level, p53 is kept under tight control by multiple mechanisms, such as the regulation by MDM2, which ubiquitinates p53 and targets it for proteasome-mediated degradation (reviewed in [66, 67]). Furthermore, mRNA stability and *TP53* transcription is also subject to regulation by a number of factors, such as BCL6, PAX2, PAX8, Wrap53, and specific miRNAs, all of which are reported to repress *TP53* mRNA expression or to render its mRNA unstable [68-70]. Our results suggest that in the TOV3041G cell line, the *TP53* regulation occurs at the mRNA level rather than the protein level, requiring further investigation for the underlying mechanism of inactivation. In the case of the

TOV2978G cell line, the intronic *TP53* mutation seems to also affect transcription, since neither mRNA nor protein were detected in this cell line. Hence, our newly described cell lines also reflect the multi facets of the HGS EOC disease in which *TP53* gene is either mutated or silenced [12, 32, 71].

Interestingly, the two p53-deficient cell lines (TOV2978G and TOV3041G) also did not express *BRCA1* mRNA or protein (Figure 2), despite the fact that they do not harbor *BRCA1* mutations. These cell lines would then represent HGS EOC with silenced *BRCA* gene (possibly by epigenetic mechanisms), which is another very common feature of this disease [12]. Identifying two cell lines with epigenetically silenced *BRCA1* is expected given the apparently high frequency of *BRCA1* promoter hypermethylation, estimated as 12% of HGS EOC tumors observed by the TCGA study [12]. Finally, the TOV3291G harbors a *TP53*mutation, a complex CNA pattern and highest ploidy of the six cell lines, and is the only one to have a *CDK12* mutation. Moreover, we have demonstrated that all of our cell lines do not have a functional p53, a feature characteristic of HGS EOCs.

The presently described EOC cell lines did not exhibit molecular genetic events characteristic of other histological subtypes of EOC. None of them harbored somatic activating mutations in *KRAS* or *BRAF* (Table II), a feature found in LGS tumors and other subtypes of EOC [12, 18, 72]. They also did not harbor mutations in *ARID1A*, *CTNNB1*, or *PIK3CA* that has been observed in other subtypes of EOC, particularly endometrioid adenocarcinomas [23]. HER2 overexpression was not observed in these cell lines, which has been shown to be a feature of clear cell EOC [40, 41, 73, 74]. Therefore, our models can be efficiently distinguished from other EOC sub-types, further highlighting the importance of these cell lines as truly representative HGS EOC models.

2.1.2.5 Materieal and methods

Patient and sample data

Tumor and ascites samples were collected from patients following informed consent from the Centre hospitalier de l'Université de Montréal (CHUM), Division of Gynecologic Oncology. The study was approved by the Comité d'éthique de la recherche du CHUM, the institutional ethics committee. Stage was determined at time of surgery by a gynecologic

oncologist. Histology and tumor grade were determined by a gynecologic-oncology pathologist using criteria consistent with the International Federation of Gynecology and Obstetrics (FIGO) classification [75].

Cell line establishment and culture conditions

In total, six cell lines were derived from samples from six patients, 866, 2978, 3041, 3291, 4453 and 4485. All cell lines were maintained in a low oxygen condition of 5% O_2, and 5% CO_2 and grown in complete OSE medium, which includes OSE medium (Wisent, St-Bruno, QC), 10% FBS, 0.5 μg/mL amphotericin B (Wisent) and 50 μg/mL gentamicin (Gibco®, Life Technologies Inc., Burlington, ON). The solid ovarian tumor (TOV)-derived cell lines (TOV2978G, TOV3041G, TOV3291G) were established using the scrape method as previously described [11, 76]. Briefly, tumor tissue was scraped into a 100 mm plate with complete OSE medium and maintained for 40 days with the medium replaced weekly. Cells were passaged at near confluence, and were considered immortal when passaged over 50 times. The OV cell lines (OV866(2), OV4453, OV4485) were established from the cellular fraction of ascites collected by centrifugation [11, 76]. The cell lines derived from ascites cells were maintained as above for the TOV derived cell lines. Although to date each cell line has reached at least 90-100 passages, most assays were conducted on cell lines between passage 60 and 80.

Cell growth rates

Growth rates were assessed as previously described [11, 42]. Briefly, cells were seeded on day 0 in 100 mm^3dishes (2 x 10^5 cellsper dish). The complete OSE media was replaced every three days for the duration of the experiment. Three times a week from day one to 14, cells were trypsinized, resuspended in media and counted using a hemocytometer. Saturation density was defined as the mean maximum number of cells counted at confluence. Each experiment was performed in triplicate, and repeated twice. Doubling times were determined using a publically available algorithm (www.doubling-time.com).

Antibodies

WB and IHC analyses were performed using the following antibodies: p53 (D0-1, sc-

126, Santa Cruz Biotechnology, Dallas, TX); HER2/ErbB2/Neu (C-18, sc-284, Santa Cruz Biotechnology, for WB; and OP15, Calbiochem®, Millipore (Canada) Ltd., Etobicoke, ON, for IHC); Cytokeratin (CK) 7 (Ab-2, MS-1352-P, Thermo Scientific, Waltham, MA); CK8 (Ab-4, MS-997-P, Thermo Scientific); CK18 (DC-10, sc-6259, Santa Cruz Biotechnology); CK19 (Ab-1, MS198-P, Thermo Scientific),WT1 (6F-H2, 05-753, Millipore (Canada) Ltd.), *BRCA1* (OP92, MS110, Calbiochem®, Millipore (Canada) Ltd.), Vimentin (V9, sc-6260, Santa Cruz Biotechnology), E-cadherin (24E10, #3195, Cell Signaling Technology Inc., Danvers, MA), PAX8 (10336-1-AP, Proteintech, Chicago, IL) and beta-actin (AC-15, ab6276, Abcam Inc., Toronto, ON, Canada).

Western blot analysis

In general (with the exception of *BRCA1* detection, see below), 30 micrograms of total protein extracts were electrophoresed in 10% SDS-polyacrylamide gels. Proteins were then transferred onto nitrocellulose membranes using the Trans-Blot Turbo Transfer System (BioRad, Mississauga, ON) and membranes were blocked with a specific Odyssey® blocking buffer (LIC-927-40010, Mandel Scientific, Guelph, ON) for immunofluorescence detection. Membranes were then probed with primary antibodies in 1% BSA-Phosphate buffered saline (PBS)-Tween at the following dilutions:1/10000 for beta-actin, 1/1000 for CK8, 1/2000 for CK7 and CK18, 1/500 for p53, E-cadherin, and vimentin, 1/200 for HER2, 1/5000 for PAX8 and 1/250 for WT1. Primary antibody labeling was detected with an IR-Dye-fluorochrome conjugated secondary antibody and visualized with the LI-COR Odyssey apparatus (Mandel Scientific). Antibody against beta-actin was used as a loading control.

For *BRCA1*, 60 micrograms of total protein extracts were electrophoresed in 4%-15% pre-cast gels (Bio-Rad). Proteins were then transferred onto nitrocellulose membranes at 400mA (overnight, 4°C) using the conventional blotting system. Membranes were then blocked with 5% milk PBS-Tween and probed with primary antibody diluted 1/1000 in 1% BSA PBS-Tween (overnight, RT). Antibody labeling was detectedwith a HRP-conjugated secondary antibodyand visualized by the enhanced chemiluminescence (ECL) method.

Immunohistochemistry

Tissue sections (4μm) were stained with the Benchmark XT automated stainer

(Ventana Medical System Inc., Tucson, AZ). Antigen retrieval was obtained usingCell Conditioning #1 or #2 (Ventana Medical System Inc.) depending on the protein target (see Supplementary Table S1). Pre-diluted antibodies were manually added to theslides and incubated at 37˚C (see Supplementary Table S1 for details). Reactions were performedusing the UltraView universal DAB detection kit (Ventana Medical System Inc.). Counterstaining was achieved with hematoxylinand bluing reagent (Ventana Medical System Inc.). All sections were scanned using a VS-110 microscope (Olympus, Center Valley, PA) with a 20X 0.75NA objective and resolution of 0.3225 μm, allowing images to be viewed at a 400x magnification. The OlyVIA software (Olympus) was used for image analysis.

Targeted mutation analysis of TP53, KRAS, BRAF, BRCA1 and BRCA2

Mutation analyses were performed using DNA that was extracted from the cell lines (passages 52 to 108) as described previously [76]. Mutation analyseswere designed to detect variants in the protein coding exons 2 to 11, and adjacent splice sites of *TP53*, and the common mutations occurring in either exon 2 of *KRAS*or exons 11 and 15 of *BRAF*. Mutation analysis was performed using PCR-based assays followed by bidirectional sequencing using the 3730XL DNA Analyzer system (Applied Biosystems®, Life Technologies Inc., Burlington, ON) at the McGill University and Genome Quebec Innovation Center (Montreal, QC, Canada) as previously described [18]. Sequence chromatograms were compared with NCBI reference sequence (RefSeq) reported in GenBank: NM_000546.4 (*TP53*), NM_004985.3 (*KRAS*) and NM_004333.4 (*BRAF*), and the genomic structures available from the February 2009 GRCh37/hg19 assembly of the human reference genome. Sequence variants were compared with those reported in the SNP Database (www. ncbi.nlm.nih.gov/SNP). In addition, *TP53* variants were evaluated based on information in the International Agency for Research on Cancer (IARC) TP53 Database (www-p53.iarc.fr).

The ovarian cancer specimens were obtained from French Canadian women, a population known to have specific recurrent *BRCA1* and *BRCA2* mutations due to common ancestors [29]. DNA from peripheral blood lymphocytes was investigated for the most common mutations in *BRCA1* (C4446T and 2953delGTAinsC) and *BRCA2* (8765delAG, G6085T and 3398delAAAAG) using established PCR-based screening assays [29]. Due to limited availability of peripheral lymphocyte DNA from patient 866, the OV866(2) cell line

DNA was also investigated. DNA from peripheral blood lymphocytes of the remaining five patients were also investigated by the Luminex platform, which screens for a broader panel of 19 *BRCA1*/*BRCA2* mutations (including the above recurrent mutations) that represent the majority of pathogenic mutations identified in the French Canadians of Quebec as described [29, 56, 77]. Through the Hereditary Cancer Clinic affiliated with CHUM, DNA from peripheral blood lymphocytes from patients 4453 and 4485 were also genetically tested by BRAC*Analysis*®, a comprehensive mutation analysis for mutations in *BRCA1* and *BRCA2* (www.myriad.com). All variants were verified by bidirectional Sanger sequencing as described above, and compared with *BRCA1* U14680 or *BRCA2* U43746 GenBank sequences (www.ncbi.nlm.nih.gov), and the GRCh37/hg19 assembly of the human reference genome. The Human Genome Variation Society (HGVS) (www.hgvs.org/mutnomen/) designation is provided for all mutations investigated and identified in this study. However, for historical reasons, the original *BRCA1*/*BRCA2* mutation nomenclature is referred to throughout in cases where a recurrent mutation was identified. The variants were also investigated in the patient-matched cell line.

Whole exome sequencing analyses

Libraries for whole exome sequencing were prepared from 500ng of DNA from the six cell lines using the NimbleGen SeqCap EZ Human Exome Library v3.0 kit (Roche NimbleGen, Inc., Madison, WI), followed by paired-end, 100bp sequencing on the HiSeq 2000 (Illumina, Inc., San Diego, CA) at an equivalent of three samples per lane, according to recommended protocols at the McGill University and Genome Quebec Innovation Centre. Alignment to the human genome (NCBI37/hg19) and variant calling was performed using Trimmomatic (to remove adaptors and trimming reads to minimum phred score of 30) (www.usadellab.org/cms/?page=trimmomatic), BWA (alignment) (bio-bwa.sourceforge.net/), GATK (realignment of INDELs, base quality recalibration) (www.broadinstitute.org/gatk/) and Picard (mate-pair recalculation, mark duplicates) (broadinstitute.github.io/picard/) software programs. Variant calling was performed using Samtools and Bcftools (www.htslib.org/), and annotated using SnpEff (snpeff.sourceforge.net/) and dbNSFP (sites.google.com/site/jpopgen/dbNSFP). Additional variant filtering included: minimum read depth of 10 reads, minimum allele frequency of 20%, and a minor allele frequency (MAF) of

less than 2% in European Americans from the Exome Variant Server (evs.gs.washington.edu/EVS/). The sequencing reads for the variants in candidate genes were also reviewed manually using the Integrative Genomics Viewer (IGV) (www.broadinstitute.org/igv).

TP53 and BRCA1 cDNA polymerase chain reaction

Total RNA was extracted from all six cell lines by the TRIzol Reagent (Invitrogen™, Life Technologies Inc., Burlington, ON) followed by the RNeasy kit (Qiagen Inc., Toronto, ON, Canada). One microgram of total RNA was subjected to reverse transcription using the QuantiTect Reverse Transcription Kit (Qiagen Inc.). One microliter of the reverse-transcribed product either diluted (1/10, for *TP53* or beta-actin amplification) or not (for *BRCA1* amplification) was subjected to standard polymerase chain reaction (PCR) using the Phusion High-Fidelity PCR kit (New England BioLabs, Whitby, ON), according to the manufacturer's instructions. Two pairs of primers were used for *BRCA1* amplification, one covering exons 13 to 15: forward, 5'-GACTCTTCTGCCCTTGAGGA-3' and reverse, 5'-CTGTTGCTCCTCCACATCAA-3'; and another covering exons 14-16: forward, 5'-GGCCTTTCTGCTGACAAGTT-3' and reverse, 5'-AATTCTGGCTTCTCCCTGCT-3'. Primers for *TP53* were: forward, 5'-GGAAGACTCCAGTGGTAATCTA-3'and reverse, 5'-TTGGGCAGTGCTCGCTTA-3', which amplify all *TP53* variants; and for the beta-actin control gene: forward, 5'-ACTCTTCCAGCCTTCCTTCC-3'and reverse, 5'-GTACTTGCGCTCAGGAGGAG-3'. PCR products of*BRCA1* amplifications were subjected to bidirectional Sanger sequencing (Centre de recherche du Centre hospitalier de l'Université de Laval), and sequence chromatograms were compared with *BRCA1* U14680 GenBank sequence (www.ncbi.nlm.nih.gov), and the GRCh37/hg19 assembly of the human reference genome.

Genomic analyses using SNP arrays

Genome-wide chromosomal anomalies, such as chromosomal breaks, CNA and LOH, were inferred in the six cell lines using the HumanOmni2.5Exome BeadChip (Illumina, Inc.). This BeadChip assays 2,567,845 markers, with an average spacing of 1.14 Kb per marker (median spacing is 0.57 Kb). Genotyping, using 200 ng of DNA, and scanning were

performed at the McGill University and Genome Quebec Innovation Centre. All samples had call rates (the percentage of valid genotype calls) within the range of 0.945 and 0.993 (average 0.968). Genotyping analysis was performed using the Genome Viewer module in GenomeStudio software (Illumina, Inc.). The software aligns genotyping data for each marker with genomic map coordinates based on the NCBI37/hg19 assembly of the human reference sequence (genome.ucsc.edu/cgi-bin/hgGateway). An image file was created for inferring genomic rearrangements based on the allele frequency (BAF) and copy number (LogR ratio) for each marker assayed. Homozygous deletions were inferred based on Log R ratios less than -2 for at least five adjacently mapped markers. Normalized SNP intensity files were also analyzed by the allele-specific copy number analysis of tumors (ASCAT) algorithm (heim.ifi.uio.no/bioinf/Projects/ASCAT/, and bcb.dfci.harvard.edu/~aedin/courses/Bioconductor/rcourse.r), modified to allow for 100% aberrant cell fraction [78]. ASCAT first segments the genome, and then interprets the abnormalities in each segment to establish the copy number of each parental chromosome, based on the ploidy and aberrant cell fraction. The CNA and LOH status of each segment were visualized with IGV. Gain and loss for loci of interest were inferred relative to ploidy.

Assessment of TP53 function by real time quantitative polymerase chain reaction (Q-PCR)

Cells were seeded on 35 mm^3 plates, grown until 80% confluence, gamma-irradiated at 8Gy, and then harvested at 0h, 2h and 5h after irradiation. Total RNA was extracted using TRIzol Reagent (Invitrogen™, Life Technologies Inc.) followed by the RNeasy kit (Qiagen Inc.). One microgram of total RNA was subjected to reverse transcription using the QuantiTect Reverse Transcription Kit (Qiagen Inc.). One microliter of the reverse-transcribed product was diluted (1:10) and subjected to Q-PCR using sequence-specific primers (400nM) and the SYBR Select Master Mix (Applied Biosystems®, Life Technologies Inc.). Sequence primers for target genes were: p21, forward, 5'-ACCCTAGTTCTACCTCAGGC-3', reverse, 5'-AAGATCTACTCCCCCATCAT-3'; NOXA, forward, 5'-AGAGCTGGAAGTCGAGTGT-3', reverse, 5'-GCACCTTCACATTCCTCTC-3'; MDM2, forward, 5'-ATCTTGGCCAGTATATTATG-3', reverse 5'-GTTCCTGTAGATCATGGTAT-3';and GAPDH, forward, 5'-GGGAAGGTGAAGGTCGGAGT-3', reverse, 5'-TTGAGGTCAATGAAGGGGTCA-3'. The Q-PCR was achieved with the Applied

BioSystems® Step One Plus apparatus. Thermocycling conditions were one UDG activation cycle at 50°C for 2 min and one AmpliTaq activation plus denaturation cycle at 95°C for 2 min followed by 40 cycles at 95°C for 15sec, 60°C for 1 min and 72°C for 30 sec. Gene expression values were normalized to theGAPDH gene. Two or three independent experiments were performed in duplicate.

Spheroid assay

A spheroid assay was performed to determine the ability of cell lines to generate three-dimensional structures in the form of aggregates, as previously described [47, 79]. Briefly, 4,000 cells were suspended in 16 µl of complete OSE medium and placed on the cover of non-coated plastic tissue culture plates that were subsequently inverted. PBS was added to the bottom plate to prevent dehydration of droplets. Spheroid formation ability was assessed after 5-7 days of incubation at 37°C, 5% O_2, 5% CO_2, with spheroid formation of the cell lines being classified concordantly with previous research [11, 47].

Anchorage independent growth in soft agar

Cell lines were assayed for their ability to grow in anchorage independent conditions by culturing 2 x 10^4 cells in a semi-solid media containing noble agar. Cells suspended in 0.33% w/v agar in complete OSE medium were applied over a base layer comprised of 0.66% w/v agar in complete OSE medium [27, 76]. Cells were cultured in soft agar for three weeks, and colonies were stained with 0.1% crystal violet and 2% methanol solution (for 2h, RT), photographed and counted. Three independent experiments were performed in triplicate.

Wound-healing assay

Migration potential was evaluated using the scratch assay method as previously described [11, 27, 48]. Cells were grown to confluence in 12-well culture plate dishes. Using a 200µl pipette tip, a wound was produced in the middle of the monolayer. The adherent monolayer was washed with PBS to remove non-adherent cells and complete OSE media was then added. At each time point (0h, 6h, 12h, 24h, 30h, 36h, 48h), cells were stained with 0.5% methylene blue and 50% methanol solution for 5 minutes and images were taken using the Nikon Eclipse TE300 microscope (Nikon Instruments Inc., Melville, NY). The software NPS-

Elements BR (Nikon Instruments Inc.) was used to measure the residual scratch width at each time point and migration velocity was calculated as μm/h.

Clonogenic survival assays

Carboplatin sensitivity of cell lines was assessed using a clonogenic assay [27, 80]. Briefly, cells were seeded in a 6-well dish at a density of cells/well that allowed the formation of individual colonies (TOV3041G, 750 cells/well; OV866(2), TOV2978G and TOV3291G, 1500 cells/well; TOV3041G; OV4453 and OV4485, 2000 cells/well). Cells were seeded and allowed to adhere for 16 hours in a 37°C, 5% CO2, 5% O2 incubator after which the media was removed and replaced with OSE complete media containing carboplatin (0–100 μM) (Hospira Healthcare Corporation, Saint-Laurent, QC). Cells were incubated with the drug for 24 hours. The drug was then removed and OSE complete media was added. When colonies became visible at a 2X magnification plates were fixed with cold methanol and colored with a mix of 50% v/v methanol and 0,5% m/v blue methylene (Sigma–Aldrich Inc., St. Louis, MO). Colonies were counted under a stereomicroscope and reported as percent of control. IC_{50} values were determined using Graph Pad Prism 5 software (GraphPad Software Inc., San Diego, CA). Each individual experiment was performed in triplicate and repeated three times.

In vivo growth in SCID mice

All animal studies were approved by the Institutional Committee on Animal Protection (CIPA) protocol according to the Canadian Council on Animal Care. The tumorigenic potential of cell lines was assessed based on their ability to form tumors in 6-week old female SCID (severe combined immunodeficiency) mice (Charles River Laboratories, Saint-Constant, QC) at subcutaneous left gluteal injection (sc.) or intraperitoneal sites (ip.). A volume of 200 μl was injected in each mouse and consisted of 5 x 10^6 cells resuspended in 100 μl of cold D-PBS (Gibco®, Life Technologies Inc.) and 100 μl of either Matrigel (Becton-Dickinson, Franklin Lakes, NJ) for sc. injections or D-PBS for ip. injections. The animals were housed under sterile conditions in a laminar flow environment with *ad libitum* access to food and water. Tumor formationwas assessed twice a week for over 200 days. Animals were sacrificed before neoplastic masses reached limit points established by the CIPA according to the Canadian Council on Animal Care.

2.1.2.6 Acknowlegments

We acknowledge Kim Leclerc, Liliane Meunier, Isabelle Clément, Kathleen Klein Oros, Karine Bedard and Frédéric Ancot for technical assistance and helpful discussion. We would like to thank the gynecologic oncologists of CHUM for providing specimens. We thank friends and patients who fundraised for ovarian cancer research at the Institut du cancer de Montréal. A-M.M-M. and D.M.P. are Researchers of the Centre de recherche du Centre hospitalier de l'Université de Montréal (CRCHUM)/Institut du cancer de Montréal, and P.N.T. is a Medical Scientist at The Research Institute of the McGill University Health Centre, who receive support from the Fonds recherche Québec - Santé (FRQS). The ovarian tumor banking was supported by the Banque de tissus et de données of the Réseau de recherche sur le cancer of the FRQS affiliated with the Canadian Tumor Repository Network (CTRNet). L.C. is supported by an FRQS postdoctoral scholarship. H.F. was supported in part by studentship from the Canderel Fund of the Institut du Cancer de Montréal.

2.1.2.7 Disclosure of potential conflicts of interest

The authors have no conflict of interest to disclose.

2.1.2.8 Grant support

This work was supported by a grant (MOP #36056) from the Canadian Institutes of Health Research (CIHR) to A.-M.M.-M, P.N.T. and D.P. and by the Institut du cancer de Montréal (Rallye Défi Can-Am Spyder initiative).

Figure 1

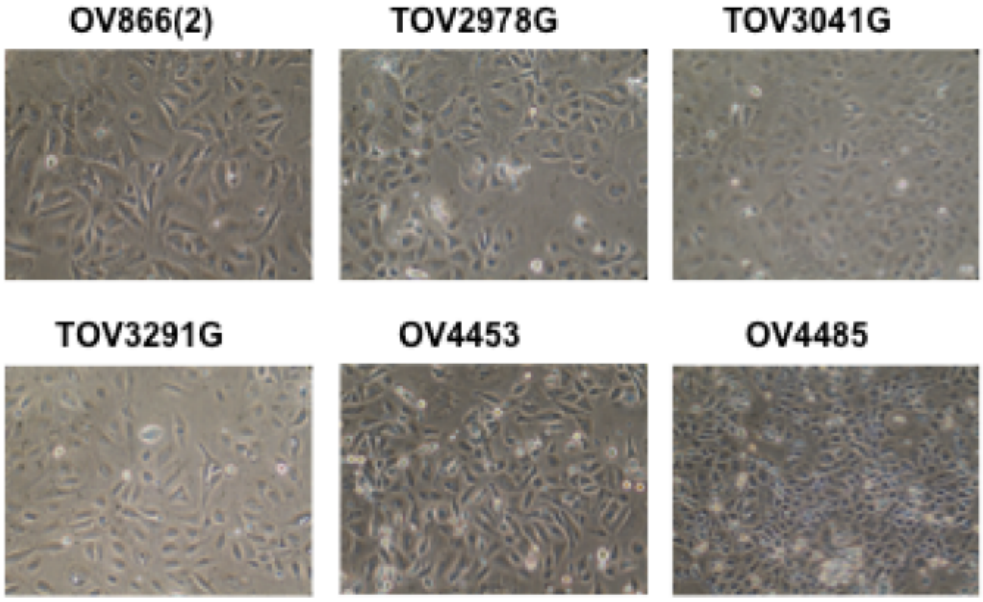

Figure 1 – Morphology of cell lines derived from patients 866, 2978, 3041, 3291, 4453 and 4485. Shown are light microscopy images of cell lines at 80% confluence at passages between 66 and 73. Cell lines had developed into predominantly small epithelial type cells, often aggregated, and fibroblast shaped cells were notably absent.

Figure 2

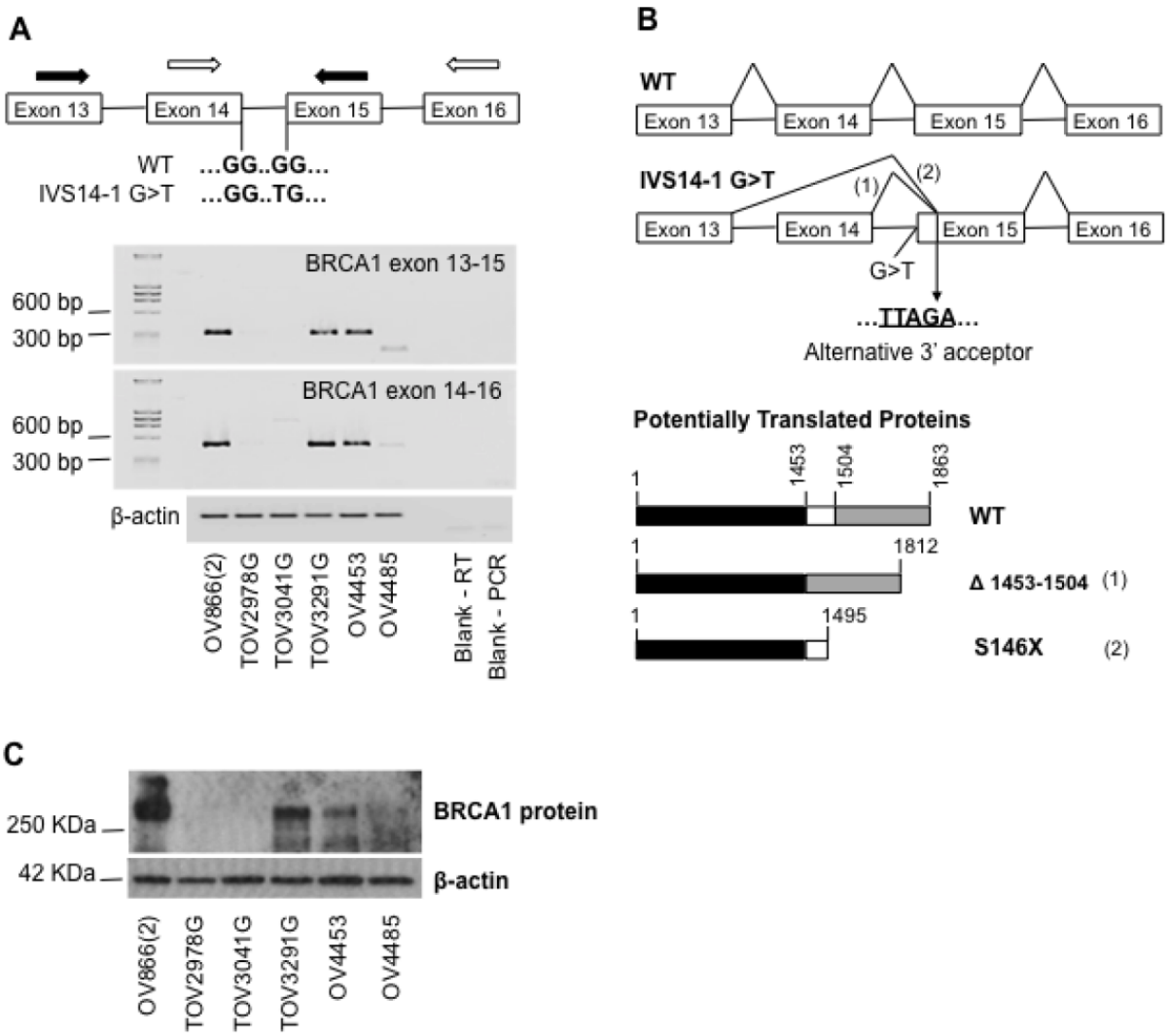

Figure 2 – Characterization of the new *BRCA1* intronic mutation identified in the OV4485 cell line. A) Primer design for amplification of *BRCA1* cDNA surrounding the intronic mutation (black arrows, exon 13-15; white arrows, exon 14-16), and agarose gel of obtained PCR products. PCR amplification of β–actin was used as a control. B) Schematic illustration of alternative *BRCA1* mRNA splicing, alternative 3'acceptor of exon 15, and predicted translated BRCA proteins obtained resultant from cDNA sequencing of the OV4485 PCR products. C) Detection of *BRCA1* protein in cell lysates of the different cell lines by Western blot. β–actin was used as loading control.

Figure 3

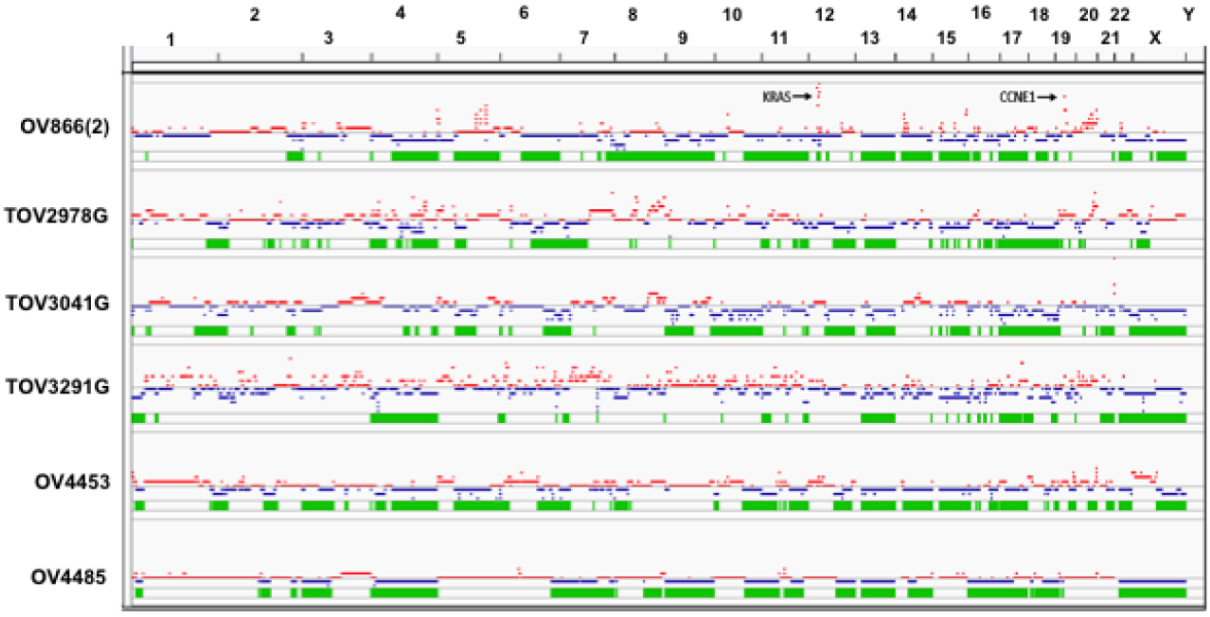

Figure 3 – Genomic landscape of the HGS cell lines. Total copy number of ASCAT derived segments was plotted for the genome on a scale of 0 to 15 copies using IGV. Segments with copy number above ploidy (see Table II for values) are indicated in red (CNV^{gain}), and those below ploidy are blue (CNV^{loss}). Regions of the genome with LOH are indicated in green and shown immediately below each CNA graph depicted for each cell line. Arrows indicategenomic locations containing amplification of *KRAS* and *CCNE1* loci in the genomic profile of the OV866(2) cell line.

Figure 4

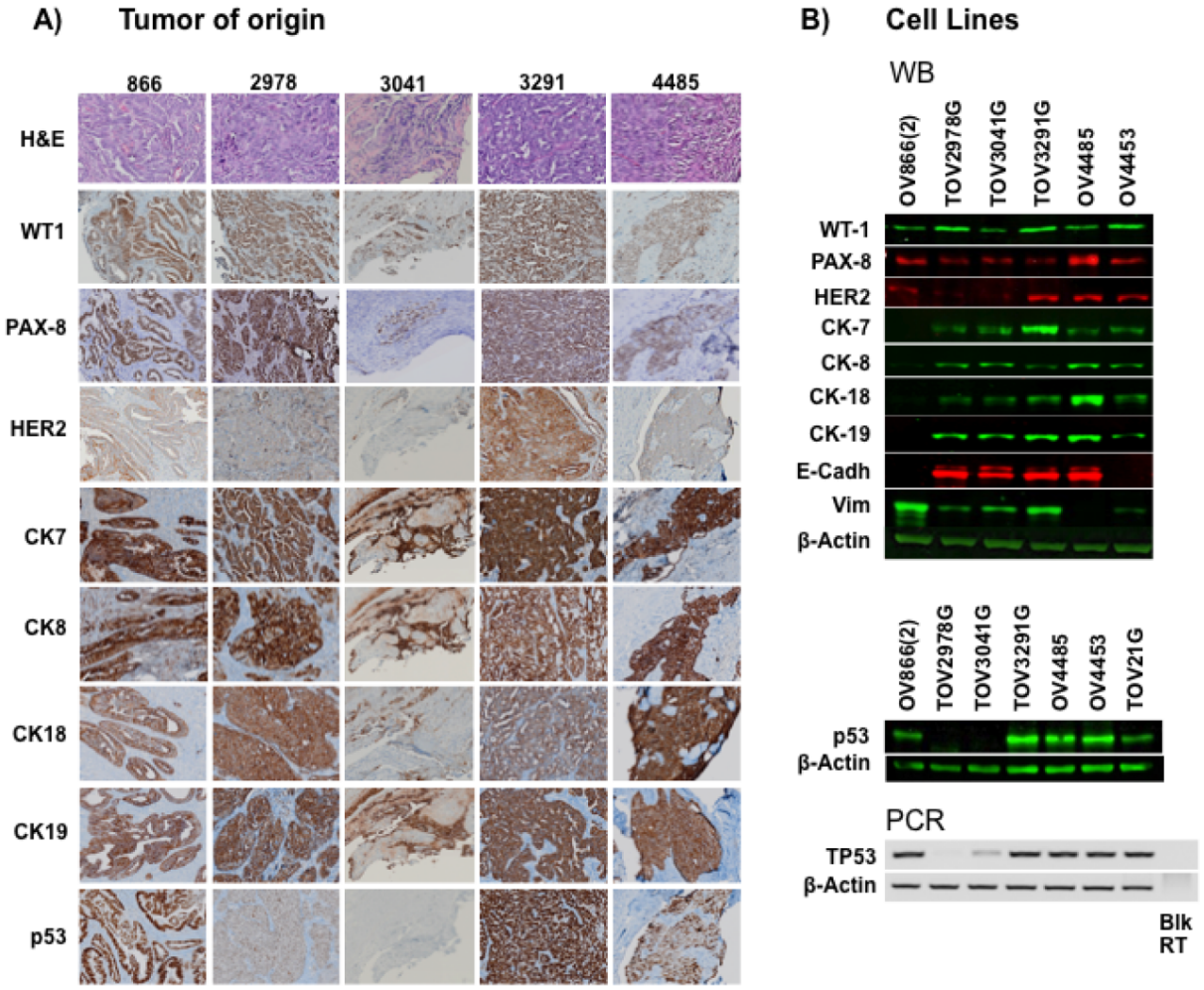

Figure 4 – Immunostaining of cell lines and corresponding solid tumors. A) Immunohistochemical analysis of formalin-fixed paraffin-embedded solid tumors from patients 866, 2978, 3041, 3291, 4453 and 4485 with cytokeratin (CK7, CK8, CK18 and CK19) markers, WT1, PAX8, p53 and HER2. Brown color indicates positive staining, nuclei are counterstained with hematoxylin, and images are at 400x magnification. Top most images are hematoxylin-eosin images of the corresponding tumor samples. B) Detection of CKs, WT1, PAX8, p53, HER2, E-cadherin and vimentin by Western blot of lysates of cell lines. Lower panel shows an agarose gel of *TP53* PCR products from reversed-transcribed cell line mRNAs. β–actin was used as control in both procedures. Blk = Blank, RT = Reverse transcription

Figure 5

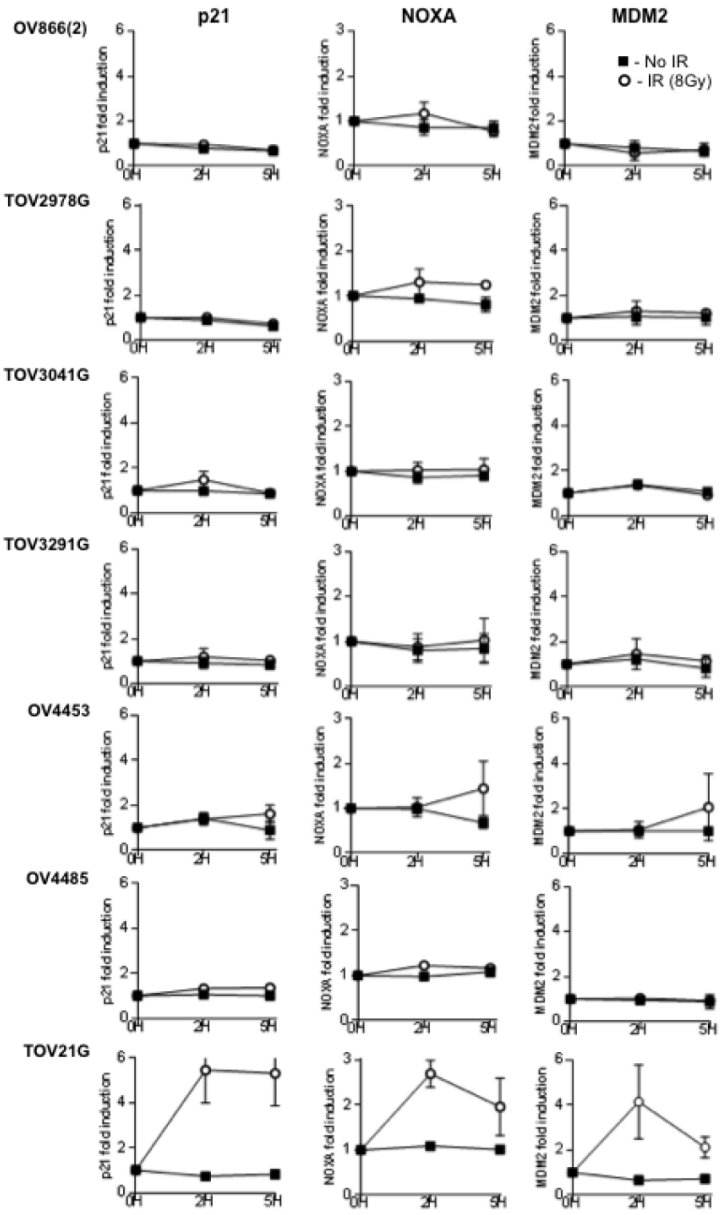

Figure 5 – Analysis of p53 function in the different cell lines by RT Q-PCR. Gene expression of p53 target genes (p21, NOXA and MDM2) were quantified by RT Q-PCR (see Methods for details) at times 0h, 2h and 5h after 8Gy gamma-irradiation (black square). Non-irradiated cells were used as controls (blank circle). Note the increased expression of p53 target genes after DNA damage induced by γ-irradiation in the control p53 proficient cell line TOV21G, and the absence of response for all the HGS EOC cell lines.

Figure 6

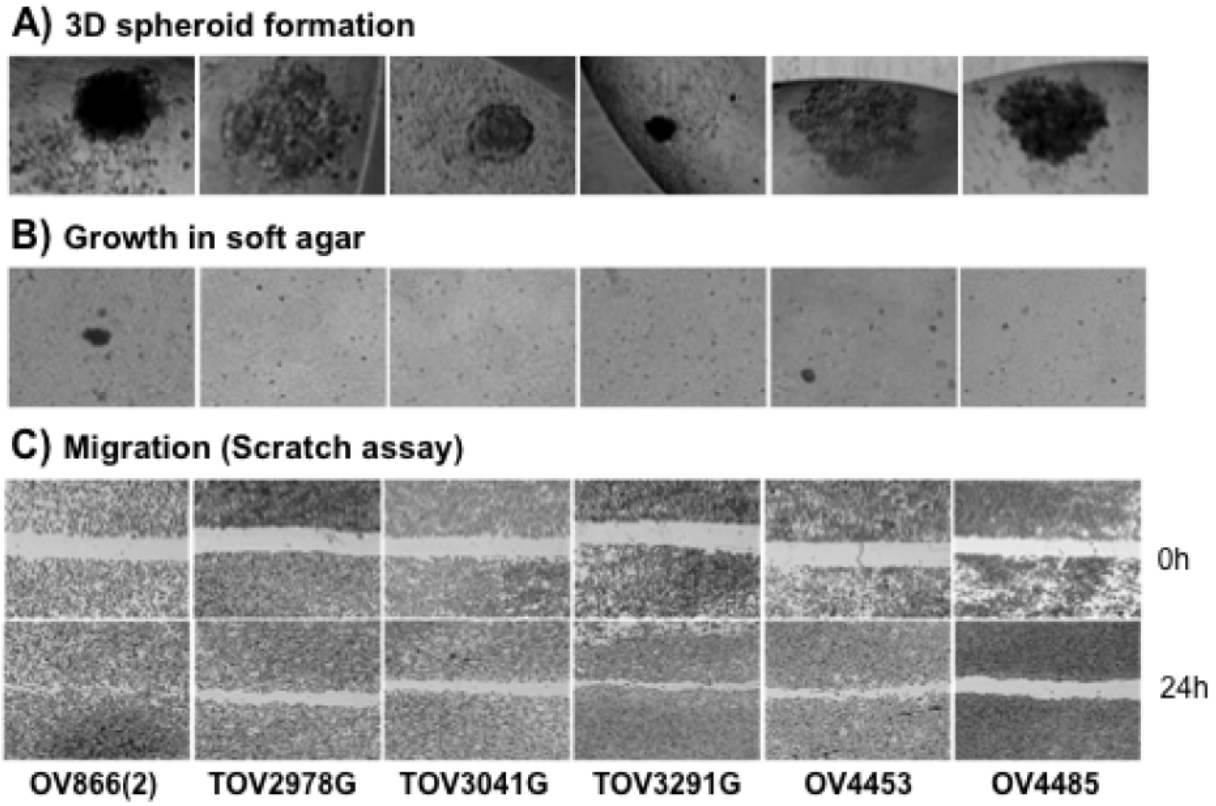

Figure 6 – *In vitro* characterization of cell lines using diverse oncogenic assays. A) Spheroid formation of cell lines after 5-7 days in OSE culture media using the inverted droplet technique. Photos are representative of observations from three independent experiments. B) Anchorage-independent growth in soft agar. Pictures show representative images of colonies formed in the agar after two-weeks of culture from three independent experiments performed in triplicate. C) Migration evaluation by the wound-healing scratch assay. Photos show representative images of monolayer cell cultures at 0h and 24h after the scratch was performed. Three independent experiments were performed in triplicate. In all experiments, pictures of different cell lines were taken at the same magnification.

Figure 7

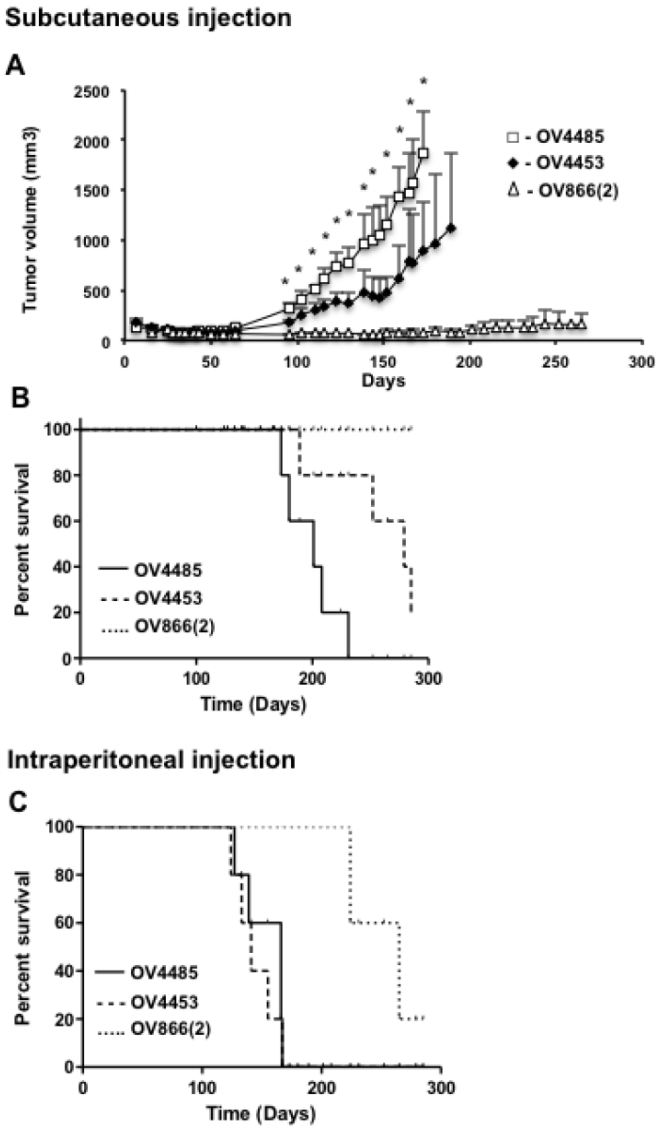

Figure 7 – *In vivo*SCID mouse xenograft tumor formation. A) Tumor volume of OV4485 (white square), OV4453 (black lozenge) and OV866(2) (white triangle) cell lines injected subcutaneously in SCID mice (n=5). Points represent average ± SEM and curves were plotted up until the first animal was sacrificed when end-point limits were attained. * denotes statistical differences ($p<0.05$, Student's t-test). B and C) Kaplan-Meyer survival curves of mice injected subcutaneously (n=5) or intraperitoneally (n=5) in SCID mice with OV4485 (solid line), OV4453 (dashed line) and OV866(2) (assured line) cell lines. Survival was followed over a period of approximately 10 months and each event was considered as the time of sacrifice at end-point limits.

Table I: Clinical features of patients and tumor characteristics of samples used to derive cell lines

Patient Identification	**866**	**2978**	**3041**	**3291**	**4453**	**4485**
Age of diagnosis (years)	60	63	61	59	70	55
Survival (months)	10	27	24	11	9	26
BRCA hereditary status	negative	negative	negative	negative	BRCA2(+)	BRCA1(+)
Histopathology sub-type	high-grade serous	high-grade serous	high-grade serous	high-grade serous	high-grade serous	high-grade serous
Disease stage	IIIC	IIIC	IVA	IIIC	IIIC	IIIC
CA125 (U/ml) at presentation	234	2397	2179	1631	2808	593
Cytoreduction	sub-optimal	sub-optimal	sub-optimal	optimal	complete	optimal
First-line treatment	1. surgery 2. carboplatin/ taxol (iv)	1. surgery 2. carboplatin/ taxol (iv)	1. carboplatin/ taxol (iv) 2. surgery 3. cisplatin/ taxol (ip,iv)	1. surgery 2. cisplatin/ taxol (ip,iv)	1. carboplatin/ taxol (iv) 2. interval surgery	1. carboplatin/ taxol (iv) 2. interval surgery 3. maintenance sorafenib *vs* placebo trial
Platinum response (6 months after first-line)	disease progression*	disease progression	progression-partial response	disease progression	disease progression	disease progression
Progression as cause of death	Yes	Yes	Yes	Yes + mesenteric ischemia	Yes	Yes
Previous personal history of cancer	No	No	No	No	breast cancer	No
Prior oncologic treatment	No	No	breast cancer prevention trial-tamoxifen	No	radiotherapy & hormono-therapy	No
Year of sampling	2000	2006	2007	2007	2009	2011
Cell line designation	OV866(2)	TOV2978G	TOV3041G	TOV3291G	OV4453	OV4485
Chemotherapy naïve at sample collection	No	Yes	No	Yes	Yes**	No

* Disease progression was defined as increased levels of blood CA125 and tumor size assessed by imaging.
** Note that this patient had received radiotherapy and hormonotherapy treatment for breast cancer five years prior to ovarian cancer diagnosis, but ovarian tumor samples were collected before any chemotherapy treatment for ovarian cancer.

Table II: Genetic and copy number alteration results of candidate loci in EOC cell lines

			Cell line					
Platform	Feature	Gene	**OV866(2)**	**TOV2978G**	**TOV3041G**	**TOV3291G**	**OV4453**	**OV4485**
Whole exome sequencing and targeted mutation analyses	Mutations in HGS	TP53	c.745 A>T (R249W)	c.920-2 A>G (splice)	N.I.	c.745 A>T (R249W)	c.376-1 G>A (splice)	c.818 G>A (R273H)
		BRCA1	N.I.	N.I.	N.I.	N.I.	N.I.	c.4485-1 G>T (splice)
		BRCA2	N.I.	N.I.	N.I.	N.I.	c.5857 G>T (E1953X)	N.I.
		CSMD3	N.I.	N.I.	N.I.	N.I.	c.1937 G>C (S646T)	N.I.
		NF1	N.I.	N.I.	N.I.	N.I.	N.I.	N.I.
		CDK12	N.I.	N.I.	N.I.	c.3095+1 G>A (splice)	N.I.	N.I.
		RB1	N.I.	N.I.	N.I.	N.I.	c.2490-5_ 2490-1 del5 (splice)	N.I.
	Mutations in Non-HGS	KRAS, BRAF, ARID1A, PIK3CA, CTNNB1	N.I.	N.I.	N.I.	N.I.	N.I.	N.I.
SNP array analyses	CNA^{gain} in HGS	MYC	5	7	6	6	4	2
		MECOM	5	4	6	9//8	3	3
		CCNE1	9	5	4	8	4	2
		KRAS	14	2	5	7	4	2
		ALG8	3	4	4	4	3	2
		SOX17	4	6	3	5	3	2
		TACC3	3	5	5	3	3	2
	CNA^{loss} in HGS	NF1	3//2	2	2	4	2	1
		RB1	3	2	2	3	2	1
		PTEN	3	3	3	5	2	1
	Ploidy		3.62	3.82	4.07	5.31	2.69	1.62
	Number of segments		535	541	470	637	502	128

Targeted mutation analyses were performed for BRCA1, BRCA2, TP53, BRAF and KRAS. No predicted deleterious mutation identified indicated by N.I. Copy number for overlapping ASCAT segment shown for each gene locus. Change in copy number in gene locus indicated by //. Copy number gain (dark gray highlighted) or loss (light gray highlighted) is shown relative to ploidy only for each category (CNA^{gain} or CNA^{loss}).

Table III: The in vitro and in vivo growth characteristics of the cell lines

Cell line		OV866(2)	TOV2978G	TOV3041G	TOV3291G	OV4453	OV4485
Growth characteristics in cell culture	Doubling time (days) AVG±SEM	1.77±0.32	1.87±0.11	1.33±0.02	2.28±0.19	2.44±0.03	1.85±0.29
	Saturation density ($1x10^6$ cells) AVG±SEM	3.31±0.02	2.04±0.12	8.10±0.87*	2.16±0.04	3.18±0.12	5.95±0.64*
	Number of passages to date	>P200	P100	P100	P100	P100	P90
Spheroid formation		semi compact	aggregate	compact	semi compact	aggregate	semi compact
Scratch assay migration velocity (μm/h) AVG±SEM		61.8±10.7*	17.2±0.75	15.2±2.9	21.7±2.7	17.4±1.3	3.9±0.6*
Growth efficiency in soft agar (colony count) AVG±SEM		34.4±7.3	N/D	N/D	N/D	21.1±5.0	N/D
Carboplatin IC_{50} (μM) AVG±SEM		32.1±7.1	0.76±0.24	0.81±0.64	2.7±0.9	0.23±0.07	6.1±0.27
Number of mice (n=5) with tumor xenograft	Subcutaneous injection site	2	0	0	0	5	5
	Intraperitoneal injection site	4	-	-	-	5	5
Mean time of tumor appearance (days)	Subcutaneous injection site	250	N/A	N/A	N/A	138	98
	Intraperitoneal injection site	150	-	-	-	70	50

N/D = non detectable, N/A = not applicable, - = experiement not conducted
* denotes statistical differences ($p<0.05$, Student's t-test) when compared to each of all the other cell lines

2.1.2.9 References

1. Siegel RL, Miller KD and Jemal A. Cancer statistics, 2015. CA Cancer J Clin. 2015; 65(1):5-29.
2. Gurung A, Hung T, Morin J and Gilks CB. Molecular abnormalities in ovarian carcinoma: clinical, morphological and therapeutic correlates. Histopathology. 2013; 62(1):59-70.
3. Le Page C, Provencher D, Maugard CM, Ouellet V and Mes-Masson AM. Signature of a silent killer: expression profiling in epithelial ovarian cancer. Expert Rev Mol Diagn. 2004; 4(2):157-167.
4. Bookman MA. First-line chemotherapy in epithelial ovarian cancer. Clin Obstet Gynecol. 2012; 55(1):96-113.
5. Stuart GC, Kitchener H, Bacon M, duBois A, Friedlander M, Ledermann J, Marth C, Thigpen T and Trimble E. 2010 Gynecologic Cancer InterGroup (GCIG) consensus statement on clinical trials in ovarian cancer: report from the Fourth Ovarian Cancer Consensus Conference. Int J Gynecol Cancer. 2011; 21(4):750-755.
6. Coleman MP, Forman D, Bryant H, Butler J, Rachet B, Maringe C, Nur U, Tracey E, Coory M, Hatcher J, McGahan CE, Turner D, Marrett L, Gjerstorff ML, Johannesen TB, Adolfsson J, et al. Cancer survival in Australia, Canada, Denmark, Norway, Sweden, and the UK, 1995-2007 (the International Cancer Benchmarking Partnership): an analysis of population-based cancer registry data. Lancet. 2011; 377(9760):127-138.
7. Cho KR and Shih Ie M. Ovarian cancer. Annu Rev Pathol. 2009; 4:287-313.
8. Prat J. New insights into ovarian cancer pathology. Ann Oncol. 2012; 23 Suppl 10:x111-117.
9. Wei W, Dizon D, Vathipadiekal V and Birrer MJ. Ovarian cancer: genomic analysis. Ann Oncol. 2013; 24 Suppl 10:x7-15.
10. Kuo KT, Guan B, Feng Y, Mao TL, Chen X, Jinawath N, Wang Y, Kurman RJ, Shih Ie M and Wang TL. Analysis of DNA copy number alterations in ovarian serous tumors identifies new molecular genetic changes in low-grade and high-grade carcinomas. Cancer Res. 2009; 69(9):4036-4042.
11. Ouellet V, Zietarska M, Portelance L, Lafontaine J, Madore J, Puiffe ML, Arcand SL, Shen Z, Hebert J, Tonin PN, Provencher DM and Mes-Masson AM. Characterization of three new serous epithelial ovarian cancer cell lines. BMC Cancer. 2008; 8:152.
12. Network TCGAR. Integrated genomic analyses of ovarian carcinoma. Nature. 2011; 474(7353):609-615.
13. Ahmed AA, Etemadmoghadam D, Temple J, Lynch AG, Riad M, Sharma R, Stewart C, Fereday S, Caldas C, Defazio A, Bowtell D and Brenton JD. Driver mutations in TP53 are ubiquitous in high grade serous carcinoma of the ovary. J Pathol. 2010; 221(1):49-56.
14. McAlpine JN, Porter H, Kobel M, Nelson BH, Prentice LM, Kalloger SE, Senz J, Milne K, Ding J, Shah SP, Huntsman DG and Gilks CB. *BRCA1* and *BRCA2* mutations

correlate with TP53 abnormalities and presence of immune cell infiltrates in ovarian high-grade serous carcinoma. Mod Pathol. 2012; 25(5):740-750.
15. Press JZ, De Luca A, Boyd N, Young S, Troussard A, Ridge Y, Kaurah P, Kalloger SE, Blood KA, Smith M, Spellman PT, Wang Y, Miller DM, Horsman D, Faham M, Gilks CB, et al. Ovarian carcinomas with genetic and epigenetic *BRCA1* loss have distinct molecular abnormalities. BMC Cancer. 2008; 8:17.
16. Bashashati A, Ha G, Tone A, Ding J, Prentice LM, Roth A, Rosner J, Shumansky K, Kalloger S, Senz J, Yang W, McConechy M, Melnyk N, Anglesio M, Luk MT, Tse K, et al. Distinct evolutionary trajectories of primary high-grade serous ovarian cancers revealed through spatial mutational profiling. J Pathol. 2013; 231(1):21-34.
17. Gorringe KL, George J, Anglesio MS, Ramakrishna M, Etemadmoghadam D, Cowin P, Sridhar A, Williams LH, Boyle SE, Yanaihara N, Okamoto A, Urashima M, Smyth GK, Campbell IG and Bowtell DD. Copy number analysis identifies novel interactions between genomic loci in ovarian cancer. PLoS One. 2010; 5(9).
18. Wojnarowicz PM, Oros KK, Quinn MC, Arcand SL, Gambaro K, Madore J, Birch AH, de Ladurantaye M, Rahimi K, Provencher DM, Mes-Masson AM, Greenwood CM and Tonin PN. The genomic landscape of TP53 and p53 annotated high grade ovarian serous carcinomas from a defined founder population associated with patient outcome. PLoS One. 2012; 7(9):e45484.
19. Alkema NG, Tomar T, van der Zee AG, Everts M, Meersma GJ, Hollema H, de Jong S, van Vugt MA and Wisman GB. Checkpoint kinase 2 (Chk2) supports sensitivity to platinum-based treatment in high grade serous ovarian cancer. Gynecol Oncol. 2014; 133(3):591-598.
20. Keita M, Bachvarova M, Morin C, Plante M, Gregoire J, Renaud MC, Sebastianelli A, Trinh XB and Bachvarov D. The RUNX1 transcription factor is expressed in serous epithelial ovarian carcinoma and contributes to cell proliferation, migration and invasion. Cell Cycle. 2013; 12(6):972-986.
21. Dong R, Liu X, Zhang Q, Jiang Z, Li Y, Wei Y, Li Y, Yang Q, Liu J, Wei JJ, Shao C, Liu Z and Kong B. miR-145 inhibits tumor growth and metastasis by targeting metadherin in high-grade serous ovarian carcinoma. Oncotarget. 2014; 5(21):10816-10829.
22. Chapman-Rothe N, Curry E, Zeller C, Liber D, Stronach E, Gabra H, Ghaem-Maghami S and Brown R. Chromatin H3K27me3/H3K4me3 histone marks define gene sets in high-grade serous ovarian cancer that distinguish malignant, tumour-sustaining and chemo-resistant ovarian tumour cells. Oncogene. 2013; 32(38):4586-4592.
23. Domcke S, Sinha R, Levine DA, Sander C and Schultz N. Evaluating cell lines as tumour models by comparison of genomic profiles. Nat Commun. 2013; 4:2126.
24. Jacob F, Nixdorf S, Hacker NF and Heinzelmann-Schwarz VA. Reliable in vitro studies require appropriate ovarian cancer cell lines. J Ovarian Res. 2014; 7:60.

25. DelloRusso C, Welcsh PL, Wang W, Garcia RL, King MC and Swisher EM. Functional characterization of a novel *BRCA1*-null ovarian cancer cell line in response to ionizing radiation. Mol Cancer Res. 2007; 5(1):35-45.
26. Sakai W, Swisher EM, Jacquemont C, Chandramohan KV, Couch FJ, Langdon SP, Wurz K, Higgins J, Villegas E and Taniguchi T. Functional restoration of *BRCA2* protein by secondary *BRCA2* mutations in *BRCA2*-mutated ovarian carcinoma. Cancer Res. 2009; 69(16):6381-6386.
27. Letourneau IJ, Quinn MC, Wang LL, Portelance L, Caceres KY, Cyr L, Delvoye N, Meunier L, de Ladurantaye M, Shen Z, Arcand SL, Tonin PN, Provencher DM and Mes-Masson AM. Derivation and characterization of matched cell lines from primary and recurrent serous ovarian cancer. BMC Cancer. 2012; 12:379.
28. Tonin PN, Mes-Masson AM, Futreal PA, Morgan K, Mahon M, Foulkes WD, Cole DE, Provencher D, Ghadirian P and Narod SA. Founder *BRCA1* and *BRCA2* mutations in French Canadian breast and ovarian cancer families. Am J Hum Genet. 1998; 63(5):1341-1351.
29. Oros KK, Ghadirian P, Greenwood CM, Perret C, Shen Z, Paredes Y, Arcand SL, Mes-Masson AM, Narod SA, Foulkes WD, Provencher D and Tonin PN. Significant proportion of breast and/or ovarian cancer families of French Canadian descent harbor 1 of 5 *BRCA1* and *BRCA2* mutations. Int J Cancer. 2004; 112(3):411-419.
30. Roy R, Chun J and Powell SN. *BRCA1* and *BRCA2*: different roles in a common pathway of genome protection. Nat Rev Cancer. 2012; 12(1):68-78.
31. Huen MS, Sy SM and Chen J. *BRCA1* and its toolbox for the maintenance of genome integrity. Nat Rev Mol Cell Biol. 2010; 11(2):138-148.
32. Kurman RJ. Origin and molecular pathogenesis of ovarian high-grade serous carcinoma. Ann Oncol. 2013; 24 Suppl 10:x16-21.
33. Payne DJ, Gwynn MN, Holmes DJ and Pompliano DL. Drugs for bad bugs: confronting the challenges of antibacterial discovery. Nat Rev Drug Discov. 2007; 6(1):29-40.
34. Singer G, Oldt R, 3rd, Cohen Y, Wang BG, Sidransky D, Kurman RJ and Shih Ie M. Mutations in BRAF and KRAS characterize the development of low-grade ovarian serous carcinoma. J Natl Cancer Inst. 2003; 95(6):484-486.
35. Wojnarowicz PM, Provencher DM, Mes-Masson AM and Tonin PN. Chromosome 17q25 genes, RHBDF2 and CYGB, in ovarian cancer. Int J Oncol. 2012; 40(6):1865-1880.
36. Kobel M, Kalloger SE, Lee S, Duggan MA, Kelemen LE, Prentice L, Kalli KR, Fridley BL, Visscher DW, Keeney GL, Vierkant RA, Cunningham JM, Chow C, Ness RB, Moysich K, Edwards R, et al. Biomarker-based ovarian carcinoma typing: a histologic investigation in the ovarian tumor tissue analysis consortium. Cancer Epidemiol Biomarkers Prev. 2013; 22(10):1677-1686.
37. Kommoss S, Gilks CB, Kommoss F, Chow C, Hilpert F, du Bois A, Kobel M, Huntsman DG, Anglesio M, Kalloger SE and Pfisterer J. Accelerating type-specific ovarian

carcinoma research: Calculator for Ovarian Subtype Prediction (COSP) is a reliable high-throughput tool for case review. Histopathology. 2013; 63(5):704-712.
38. Laury AR, Perets R, Piao H, Krane JF, Barletta JA, French C, Chirieac LR, Lis R, Loda M, Hornick JL, Drapkin R and Hirsch MS. A comprehensive analysis of PAX8 expression in human epithelial tumors. Am J Surg Pathol. 2011; 35(6):816-826.
39. Madore J, Ren F, Filali-Mouhim A, Sanchez L, Kobel M, Tonin PN, Huntsman D, Provencher DM and Mes-Masson AM. Characterization of the molecular differences between ovarian endometrioid carcinoma and ovarian serous carcinoma. J Pathol. 2010; 220(3):392-400.
40. Meden H and Kuhn W. Overexpression of the oncogene c-erbB-2 (HER2/neu) in ovarian cancer: a new prognostic factor. Eur J Obstet Gynecol Reprod Biol. 1997; 71(2):173-179.
41. Serrano-Olvera A, Duenas-Gonzalez A, Gallardo-Rincon D, Candelaria M and De la Garza-Salazar J. Prognostic, predictive and therapeutic implications of HER2 in invasive epithelial ovarian cancer. Cancer Treat Rev. 2006; 32(3):180-190.
42. Provencher DM, Lounis H, Champoux L, Tetrault M, Manderson EN, Wang JC, Eydoux P, Savoie R, Tonin PN and Mes-Masson AM. Characterization of four novel epithelial ovarian cancer cell lines. In Vitro Cell Dev Biol Anim. 2000; 36(6):357-361.
43. el-Deiry WS, Kern SE, Pietenpol JA, Kinzler KW and Vogelstein B. Definition of a consensus binding site for p53. Nat Genet. 1992; 1(1):45-49.
44. el-Deiry WS. Regulation of p53 downstream genes. Semin Cancer Biol. 1998; 8(5):345-357.
45. Kato S, Han SY, Liu W, Otsuka K, Shibata H, Kanamaru R and Ishioka C. Understanding the function-structure and function-mutation relationships of p53 tumor suppressor protein by high-resolution missense mutation analysis. Proc Natl Acad Sci U S A. 2003; 100(14):8424-8429.
46. Lee MK, Teoh WW, Phang BH, Tong WM, Wang ZQ and Sabapathy K. Cell-type, dose, and mutation-type specificity dictate mutant p53 functions in vivo. Cancer Cell. 2012; 22(6):751-764.
47. Zietarska M, Maugard CM, Filali-Mouhim A, Alam-Fahmy M, Tonin PN, Provencher DM and Mes-Masson AM. Molecular description of a 3D in vitro model for the study of epithelial ovarian cancer (EOC). Mol Carcinog. 2007; 46(10):872-885.
48. Meunier L, Puiffe ML, Le Page C, Filali-Mouhim A, Chevrette M, Tonin PN, Provencher DM and Mes-Masson AM. Effect of ovarian cancer ascites on cell migration and gene expression in an epithelial ovarian cancer in vitro model. Transl Oncol. 2010; 3(4):230-238.
49. Fujita M, Enomoto T and Murata Y. Genetic alterations in ovarian carcinoma: with specific reference to histological subtypes. Mol Cell Endocrinol. 2003; 202(1-2):97-99.
50. Kobel M, Huntsman D and Gilks CB. Critical molecular abnormalities in high-grade serous carcinoma of the ovary. Expert Rev Mol Med. 2008; 10:e22.

51. Do K and Chen AP. Molecular pathways: targeting PARP in cancer treatment. Clin Cancer Res. 2013; 19(5):977-984.
52. Gelmon KA, Tischkowitz M, Mackay H, Swenerton K, Robidoux A, Tonkin K, Hirte H, Huntsman D, Clemons M, Gilks B, Yerushalmi R, Macpherson E, Carmichael J and Oza A. Olaparib in patients with recurrent high-grade serous or poorly differentiated ovarian carcinoma or triple-negative breast cancer: a phase 2, multicentre, open-label, non-randomised study. Lancet Oncol. 2011; 12(9):852-861.
53. Ledermann J, Harter P, Gourley C, Friedlander M, Vergote I, Rustin G, Scott C, Meier W, Shapira-Frommer R, Safra T, Matei D, Macpherson E, Watkins C, Carmichael J and Matulonis U. Olaparib maintenance therapy in platinum-sensitive relapsed ovarian cancer. N Engl J Med. 2012; 366(15):1382-1392.
54. Liu JF, Konstantinopoulos PA and Matulonis UA. PARP inhibitors in ovarian cancer: current status and future promise. Gynecol Oncol. 2014; 133(2):362-369.
55. Olaparib Approved for Advanced Ovarian Cancer. Cancer Discov. 2015.
56. Cavallone L, Arcand SL, Maugard CM, Nolet S, Gaboury LA, Mes-Masson AM, Ghadirian P, Provencher D and Tonin PN. Comprehensive *BRCA1* and *BRCA2* mutation analyses and review of French Canadian families with at least three cases of breast cancer. Fam Cancer. 2010; 9(4):507-517.
57. Tonin PN, Maugard CM, Perret C, Mes-Masson AM and Provencher DM. A review of histopathological subtypes of ovarian cancer in BRCA-related French Canadian cancer families. Fam Cancer. 2007; 6(4):491-497.
58. Kreuzinger C, Gamperl M, Wolf A, Heinze G, Geroldinger A, Lambrechts D, Boeckx B, Smeets D, Horvat R, Aust S, Hamilton G, Zeillinger R and Cacsire Castillo-Tong D. Molecular characterization of 7 new established cell lines from high grade serous ovarian cancer. Cancer Lett. 2015; 362(2):218-228.
59. Langdon SP, Lawrie SS, Hay FG, Hawkes MM, McDonald A, Hayward IP, Schol DJ, Hilgers J, Leonard RC and Smyth JF. Characterization and properties of nine human ovarian adenocarcinoma cell lines. Cancer Res. 1988; 48(21):6166-6172.
60. Kalluri R and Weinberg RA. The basics of epithelial-mesenchymal transition. J Clin Invest. 2009; 119(6):1420-1428.
61. Stewart CJ and McCluggage WG. Epithelial-mesenchymal transition in carcinomas of the female genital tract. Histopathology. 2013; 62(1):31-43.
62. Auer K, Bachmayr-Heyda A, Aust S, Sukhbaatar N, Reiner AT, Grimm C, Horvat R, Zeillinger R and Pils D. Peritoneal tumor spread in serous ovarian cancer-epithelial mesenchymal status and outcome. Oncotarget. 2015.
63. Vousden KH and Prives C. Blinded by the Light: The Growing Complexity of p53. Cell. 2009; 137(3):413-431.
64. Brady CA and Attardi LD. p53 at a glance. J Cell Sci. 2010; 123(Pt 15):2527-2532.
65. Aylon Y and Oren M. New plays in the p53 theater. Curr Opin Genet Dev. 2011; 21(1):86-92.

66. Vousden KH and Lu X. Live or let die: the cell's response to p53. Nat Rev Cancer. 2002; 2(8):594-604.
67. Vousden KH and Ryan KM. p53 and metabolism. Nat Rev Cancer. 2009; 9(10):691-700.
68. Mahmoudi S, Henriksson S, Corcoran M, Mendez-Vidal C, Wiman KG and Farnebo M. Wrap53, a natural p53 antisense transcript required for p53 induction upon DNA damage. Mol Cell. 2009; 33(4):462-471.
69. Vilborg A, Wilhelm MT and Wiman KG. Regulation of tumor suppressor p53 at the RNA level. J Mol Med (Berl). 2010; 88(7):645-652.
70. Saldana-Meyer R and Recillas-Targa F. Transcriptional and epigenetic regulation of the p53 tumor suppressor gene. Epigenetics. 2011; 6(9):1068-1077.
71. Yemelyanova A, Vang R, Kshirsagar M, Lu D, Marks MA, Shih Ie M and Kurman RJ. Immunohistochemical staining patterns of p53 can serve as a surrogate marker for TP53 mutations in ovarian carcinoma: an immunohistochemical and nucleotide sequencing analysis. Mod Pathol. 2011; 24(9):1248-1253.
72. Birch AH, Arcand SL, Oros KK, Rahimi K, Watters AK, Provencher D, Greenwood CM, Mes-Masson AM and Tonin PN. Chromosome 3 anomalies investigated by genome wide SNP analysis of benign, low malignant potential and low grade ovarian serous tumours. PLoS One. 2011; 6(12):e28250.
73. Sereni MI, Baldelli E, Gambara G, Zanotti L, Bandiera E, Bignotti E, Ragnoli M, Tognon G, Ravaggi A, Meani F, Memo M, Angioli R, Liotta LA, Pecorelli SL, Petricoin E, 3rd and Pierobon M. Functional characterization of epithelial ovarian cancer histotypes by drug target-based protein signaling activation mapping: implications for personalized cancer therapy. Proteomics. 2014.
74. Zannoni GF, Morassi F, Prisco MG, De Stefano I, Vellone VG, Arena V, Scambia G and Gallo D. Clinicopathologic and immunohistochemical features of ovarian clear cell carcinomas in comparison with type I and type II tumors. Int J Gynecol Pathol. 2012; 31(6):507-516.
75. Heintz AP, Odicino F, Maisonneuve P, Quinn MA, Benedet JL, Creasman WT, Ngan HY, Pecorelli S and Beller U. Carcinoma of the ovary. FIGO 26th Annual Report on the Results of Treatment in Gynecological Cancer. Int J Gynaecol Obstet. 2006; 95 Suppl 1:S161-192.
76. Lounis H, Provencher D, Godbout C, Fink D, Milot MJ and Mes-Masson AM. Primary cultures of normal and tumoral human ovarian epithelium: a powerful tool for basic molecular studies. Exp Cell Res. 1994; 215(2):303-309.
77. Belanger MH, Dolman L, Arcand SL, Shen Z, Chong G, Mes-Masson AM, Provencher D and Tonin PN. A targeted analysis identifies a high frequency of *BRCA1* and *BRCA2* mutation carriers in women with ovarian cancer from a founder population. J Ovarian Res. 2015; 8(1):1.

78. Oros KK, Arcand SL, Bayani J, Squire JA, Mes-Masson AM, Tonin PN and Greenwood CM. Analysis of genomic abnormalities in tumors: a review of available methods for Illumina two-color SNP genotyping and evaluation of performance. Cancer Genet. 2013; 206(4):103-115.
79. Puiffe ML, Le Page C, Filali-Mouhim A, Zietarska M, Ouellet V, Tonin PN, Chevrette M, Provencher DM and Mes-Masson AM. Characterization of ovarian cancer ascites on cell invasion, proliferation, spheroid formation, and gene expression in an in vitro model of epithelial ovarian cancer. Neoplasia. 2007; 9(10):820-829.
80. Franken NA, Rodermond HM, Stap J, Haveman J and van Bree C. Clonogenic assay of cells in vitro. Nat Protoc. 2006; 1(5):2315-2319.

2.2 Chapitre 2 : Cumulative defects in DNA repair pathways drive the PARP inhibitor response in high-grade serous epithelial ovarian cancer cell lines

2.2.1 Article #2: Résumé en français

Titre en français : La cumulation des défauts dans les voies de réparation de l'ADN influence la réponse à l'inhibiteur de PARP dans les lignées cellulaires du cancer de l'ovaire épithélial séreux de haut grade.

Les inhibiteurs de PARP, tels que Olaparib, ont démontré des résultats prometteurs dans le traitement du cancer épithélial de l'ovaire (EOC) séreux de haut grade (HGS). La sensibilité aux inhibiteurs de PARP a été principalement associée à une déficience en recombinaison homologue (RH), mais les essais cliniques ont montré que la prédiction de la réponse du patient est complexe. Pour cette étude, nous avons étudié l'expression génique par puces à ADN, la fonctionnalité RH et la sensibilité à Olaparib au sein de 18 lignées cellulaires HGS EOC et démontré que la sensibilité aux inhibiteurs de PARP n'est pas seulement associée à des défauts de la RH. La validation en ciblant les gènes d'intérêts montre que la déficience de gènes dans les voies de réparation de l'excision des nucléotides (NER) et de la répartition des misappariements (MMR) (ERCC8 et MLH1, respectivement) augmente la sensibilité aux inhibiteurs de PARP. Cette réponse est encore plus significative lorsque les gènes à la fois de la RH et de la NER ou de la MMR sont dérégulés simultanément. À l'aide d'échantillons cliniques, on démontre que plus de 30% des patientes présentent ces caractéristiques. Sur la base de ces résultats, un nouveau modèle pour prédire la sensibilité aux inhibiteurs de PARP est proposé ici. Ce modèle implique que les très bons répondeurs identifiés dans les essais cliniques ont des déficiences en RH et NER ou MMR.

2.2.2 Article #2: Version originale soumise à Oncotarget (Appendice 2)

Oncotarget. 2016 Jun 27. doi: 10.18632/oncotarget.10308.

Cumulative defects in DNA repair pathways drive the PARP inhibitor response in high-grade serous epithelial ovarian cancer cell lines

Hubert Fleury[1,2], Euridice Carmona[1,2], Vincent G. Morin[1,2], Liliane Meunier[1,2], Jean-Yves Masson[3,4], Patricia N. Tonin[5,6,7], Diane Provencher[1,2,8], Anne-Marie Mes-Masson*[1,2,9]

[1]Centre de recherche du Centre hospitalier de l'Université de Montréal (CRCHUM), Montreal, Canada, [2]Institut du cancer de Montréal, Montreal, Canada, [3]Genome Stability Laboratory, CHU Research Center, Québec City, Canada, [4]Department of Molecular Biology, Medical Biochemistry and Pathology, Laval University Cancer Research Center, Québec City, Canada [5]Cancer Research Program (CRP), The Research Institute of the McGill University Health Centre, Montreal, Canada, [6]Department of Human Genetics, McGill University, Montreal, Canada, [7]Department of Medicine, McGill University, Montreal, Canada, [8]Division of Gynecologic Oncology, Université de Montréal, Montreal, Canada, [9]Department of Medicine, Université de Montréal, Montreal, Canada

***Correspondence:** Anne-Marie Mes-Masson, Department of Medicine, Université de Montréal, CRCHUM-Institut du cancer de Montréal, 900 rue St-Denis, Montreal, Quebec, Canada, H2X 0A9. Tel: (514) 890-8000 ext. 25496 Fax: (514) 412-7591 E-mail: anne-marie.mes-masson@umontreal.ca

Keywords: Olaparib, high-grade serous epithelial ovarian cancer, DNA repair pathways, NER, MMR

2.2.2.1 Abstract

PARP inhibitors (PARPi), such as Olaparib, have shown promising results in high-grade serous (HGS) epithelial ovarian cancer (EOC) treatment. PARPi sensitivity has been mainly associated with homologous recombination (HR) deficiency, but clinical trials have shown that predicting actual patient response is complex. Here, we investigated gene expression microarray, HR functionality and Olaparib sensitivity of 18 different HGS EOC cell lines and demonstrate that PARPi sensitivity is not only associated with HR defects. Gene target validation show that down regulation of genes in the nucleotide excision repair (NER) and mismatch repair (MMR) pathways (*ERCC8* and *MLH1*, respectively) increases PARPi response. The highest sensitivity was observed when genes in both the HR and either NER or MMR pathways were concomitantly down regulated. Using clinical samples, patients with these concurrent down regulations could be identified. Based on these results, a novel model to predict PARPi sensitivity is herein proposed. This model implies that the extreme responders identified in clinical trials have deficiencies in HR and either NER or MMR.

2.2.2.2 Introduction

Ovarian cancer is the most lethal of all gynecologic malignancies in North America [1]. This is attributed to the asymptomatic nature of the disease, resulting in a late stage diagnosis with a five-year survival rate of 45% [1]. The most common form is epithelial cancer of the ovary or fallopian tube (EOC), where approximately 70% of EOC patients present with a high-grade serous (HGS) histotype [2]. The etiology of EOC is unknown, although 15% are attributed to inherited genetic factors such as mutations in *BRCA1* and *BRCA2* which significantly increases risk [3]. Over the past 45 years, advances in surgery and chemotherapy have had little impact on overall patient survival [4, 5] underscoring the need for a greater understanding of the molecular basis of this disease and the development of new clinical tools for the detection and management of EOC patients.

Standard first line therapy of EOC consists of tumor cytoreductive surgery and treatment with platinum DNA alkylating agents such as carboplatin or cisplatin combined with the microtubule poison paclitaxel [5]. Although initial response rates are high (>70%), the disease eventually recurs in most patients who will develop chemoresistance [4, 5]. Several adjuvant drugs have been developed to improve EOC survival and decrease chemoresistance [6]. One area involves the poly (ADP-ribose) polymerase inhibitors (PARPi) such as Olaparib, Rucaparib, Veliparib, Niraparib, and BMN-673 [7-9]. PARPi were first introduced to treat breast cancer patients harboring germline *BRCA1*/*BRCA2* mutations based on the synthetic lethality context, where it has been proposed that a defect in one repair pathway is compatible with cell viability but results in cell death when combined with another repair pathway defect or inhibition [10]. *BRCA1/2* plays a role in DNA repair by homologous recombination (HR) [11] and defects in *BRCA1/2* contribute to loss or dysfunction of HR. Several models have been proposed to explain the synthetic lethality of HR-deficient cells to the PARPi, however due to the complex role of the PARP1 polymerase in repairing single and double strand DNA breaks, the complete mechanism is still not understood [8, 9].

In clinical trials, treatment with Olaparib as a single agent was promising in EOC patients as compared to triple negative breast cancer patients [12-14], and responses around 45% and 25% are observed in EOC patients with and without *BRCA1/2* mutations, respectively. The response observed in women with EOC lacking *BRCA1/2* mutations was

attributed to 'BRCA-ness', a molecular genetic signature in cancers equivalent to those with a *BRCA1/2* mutation [15] where other HR components were deficient by mutation or were epigenetically silenced [16, 17]. It was recently shown that ~40% of HGS EOCs exhibit HR abnormalities [18], and measurement of HR function in primary cultures of EOC ascites correlated with *in vitro* Rucaparib response [19, 20]. The recent approval by the US Food and Drug Administration of Olaparib as maintenance therapy for platinum-sensitive BRCA-mutated HGS EOC patients [21], further highlights the importance of this class of drugs in EOC clinical management. However, the molecular features that would predict the response to such drugs is still largely unknown, as not all patients with BRCA-ness HGS EOCs respond to these drugs [12-14]. We postulate that defects in DNA repair pathways other than the HR are also involved in PARPi sensitivity. Having a molecular gene signature linked to PARPi sensitivity would help the selection of patients that will undergo such treatment and increase effectiveness.

To identify DNA repair genes associated with the PARPi response, we applied gene expression microarray analysis to our unique repertoire of 18 spontaneously immortalized HGS EOC cell lines [22-25]. DNA repair genes that were associated with PARPi sensitivity were validated by small interference RNA (siRNA) and analyzed in clinical samples. Although previous reports have described DNA repair genes as potential biomarkers for PARPi response [26-28], the function of these genes were predominantly related to the HR system. Here we demonstrate that highest PARPi sensitivity is achieved when HR deficiency is combined with a defect in the DNA mismatch repair (MMR) or nucleotide excision repair (NER) pathway, and we propose a novel model to predict PARPi sensitivity based on these results.

2.2.2.3 Results

HGS EOC cell lines can be distinguished into three groups of Olaparib sensitivity

To better understand the PARPi response in HGS EOC, we used our unique collection of 18 HGS EOC cell lines derived from malignant tumors (TOV-) and ascites (OV-). These spontaneously immortalized cell lines have been extensively characterized [22-25]. Among the 18 cell lines, 17 harbor TP53 mutations, which is the most common somatically mutated gene found in HGS EOCs, while the remaining line fails to express TP53. The only two cell lines with a germline *BRCA1* (OV4485) or *BRCA2* (OV4453) mutation [22] were used as positive controls for HR deficiency. As a background work, we confirmed the inhibitory activity of Olaparib on PARP (Fig.1) in a carboplatin resistant [OV1369(R2)] and a sensitive (OV2295) cell line [23], based on the knowledge that carboplatin and PARPi sensitivities correlate [13, 29]. Formation of poly (ADP-ribose) (PAR) polymers, which results from PARP enzymatic action, was detected by Western blot (Fig.1A). Olaparib significantly diminished PARP catalytic activity in both of these cell lines, in comparison to an untreated control or an H_20_2-treated positive control where treatment of H_20_2 induces DNA damage that is known to be repaired by PARP [30]. To verify the known effect of PARPi on cell cycle arrest [31], we treated OV1369(R2) cells with Olaparib for 24 hours and performed flow cytometry. When compared to the untreated cells (control), Olaparib-treated cells had significantly increased proportion of cells in G2/M and S phase, indicating the expected cell cycle arrest in G2 (Fig.1B).

We then examined the IC_{50} of Olaparib in our cell lines by clonogenic assay (Fig.1C-D) and determined levels of sensitivity. Olaparib elicited a varied response with IC_{50} values that ranged from very low at 0.0003 μM (OV2295) to extremely high at 21.7μM [OV1369(R2)] (Fig.1C-D, Table 1). This range of IC_{50} concentrations has been observed by others in ovarian cancer cell lines treated with Olaparib [16, 26]. Based on statistical analysis of the IC_{50} values (Fig.S1A-B), the cell lines were classified into three distinct groups: sensitive (0.0003-0.074 μM), intermediate (0.4-3.0 μM) and resistant (7.0-21.7 μM). There were at least four cell lines within each grouping. Figure 1D shows examples of Olaparib dose-response curves for cell lines belonging to each group, and a log difference can be readily observed among them. As predicted, the *BRCA2* mutated cell line (OV4453) was

classified as sensitive with an IC_{50} of 0.01 μM. However, OV4485, the cell line harboring a *BRCA1* mutation, had an IC_{50} that was classified as intermediate (Fig 1C). This suggests that *BRCA* mutations, and therefore defects in HR, are not solely responsible for conferring PARPi sensitivity to cancer cells.

Defective HR is not the only predictor of Olaparib sensitivity in HGS EOC cell lines

Reports have described a direct association between the PARPi response and non-functional HR pathway [19, 32] such that deficiency in genes implicated in HR function (such as *BRCA1/2, RAD51C, PTEN*), has been shown to increase PARPi sensitivity [27, 33, 34]. Furthermore, deregulation of HR genes frequently occurs in HGS tumors [18]. Therefore, we examined the HR status of our cell lines by quantifying the increase in mean nuclear RAD51 foci after DNA damage induction by gamma-irradiation, as an indication of intact HR function (Fig.1E-F, Table 1). The results from cell lines representing each of our categories for resistant [OV1369(R2)], intermediate [TOV2295(R)] and sensitive (OV4453) response to Olaparib are shown in Figure 1E. Both OV1369(R2) and TOV2295(R) exhibited RAD51 foci with no radiation and the number of foci increased after radiation, indicating a functional HR response. In contrast, OV4453 displayed no foci, with or without irradiation, demonstrating a non-functional HR response. RAD51 foci response for all cell lines was ordered according to Olaparib sensitivity to infer any relationship between PARPi response (sensitive, intermediate, resistant) and HR functionality (Fig.1F). To ensure that a non-functional HR response was not due to lack of DNA double-strand break (DSB) induction after gamma-irradiation, γ-H2AX foci were evaluated as this protein is the first step in recruiting and localizing DSB repair proteins and can be used as a biomarker for this type of damage [35]. Our results (Fig.S2) show that more than three-fold increase in γ-H2AX foci was observed in all cell lines studied after gamma-irradiation, indicating effective DNA damage induction. Overall, our findings indicated that increasing the levels of Olaparib resistance were correlated with greater HR function such that resistant cells were more likely to have functional HR than intermediate and sensitive cells. As expected, both *BRCA1* and *BRCA2* mutated cell lines (OV4485 and OV4453, respectively) had impaired HR function. Therefore, our correlation between HR functionality and PARPi responsiveness supports the current literature [19, 27, 32-34]. However, not all cell lines followed this correlation, as there was no significant difference

between the Olaparib sensitive and intermediate cell lines based on RAD51 foci number (Fig.S1C). For example, some intermediate cell lines [such as OV485, OV3133(R) and TOV3133G] showed the same level of HR functionality as sensitive cell lines, while some intermediate cell lines showed little to no HR functionality. We also noted that although our control *BRCA1* mutated cell line had deficient HR function, this cell line did not demonstrate the highest sensitivity to Olaparib. Since HR works with sister chromatids, we verified whether the RAD51 foci staining was indeed localized to cells in the late S/G2 mitotic phases by co-staining with antibody against geminin as previously described [36]. Geminin is a nuclear protein that is absent during G1 phase and that accumulates through S, G2 and M phases of the cell cycle [37]. The number of cells with double positive RAD51 and geminin staining were counted before and after gamma-irradiation in six cell lines [two of each group, i.e. sensitive, OV1946, TOV3041G; intermediate, TOV2295, OV4485; and resistant, OV1369(R2), OV866(2)] (Fig.S3). Our results show the exact same profile as that shown in Fig.1F, indicating that our evaluation of HR function by counting RAD51 foci is accurate.

In all, our observations demonstrate that HR deficiency is not the only predictor of sensitivity to PARPi, and indicates that other DNA repair pathways, regardless of association with HR, may also contribute to PARPi responsiveness.

Olaparib sensitive cell lines have deregulated gene expression in multiple DNA repair pathways

To establish whether other DNA repair pathways could play a role in Olaparib sensitivity of HGS EOC cell lines, we analyzed gene expression of DNA repair genes and pathways using a microarray approach. Two types of analyses were performed (see methods for details), one where each sensitive cell line was individually compared to all the resistant cell lines (Table 2), which takes into consideration the particularity of each cell line, and another where genes commonly deregulated in all sensitive cell lines were examined (Fig.2). For the first approach, we used the total gene expression dataset to identify genes that were up- or down-regulated by two-fold when comparing each sensitive cell line to all the resistant cell lines, and differentially expressed genes were annotated using the IPA program to identify significantly affected DNA repair pathways ($p< 0.05$). Our results show that each sensitive cell line had one or more DNA repair pathways that were differentially regulated when

compared to the resistant cell lines (Table 2). Key genes of the MMR pathway such as *MLH1*, *MSH2* and *MSH6* were consistently down-regulated among the sensitive cell lines. However, less conclusive results were obtained for the NHEJ pathway since key genes of this pathway (*LIG4* and *DCLRE1C*) were both up- and down-regulated.

We next examined whether distinct DNA repair genes were commonly deregulated in all the sensitive cell lines. In this approach, mean expression values of specific DNA repair genes (155 genes, 240 probes) (see Table S1), selected based on previously published data [26, 38], were analyzed. Heat map visualization and clustering of genes with significant differences in expression ($p< 0.05$, Mann Whitney) between the two groups are shown in Figure 2. Our results showed that four genes (*ERCC1*, *FANCF*, *ATRIP*, and *OGG1*) were significantly up-regulated whereas six genes (*XRCC4*, *ERCC8*, *RAD51D*, *BRCA1*, *RAD51C*, and *MLH3*), were significantly down-regulated in the sensitive cell lines compared to resistant cell lines. As per our first approach, we observed de-regulation of multiple DNA repair pathways (HR, NER, MMR and NHEJ) in Olaparib sensitive cell lines when compared to resistant cells.

Increased Olaparib sensitivity upon down-regulation of MMR and NER genes in HGS cells

Although the BER and NHEJ pathways have been implicated in PARPi response [39, 40], our results did not reveal consistent gene alteration in these pathways when comparing sensitive to resistant HGS EOC cell lines. On the other hand, the relationship between PARPi and the MMR or NER pathways is still not clearly defined or well understood [41-44]. Therefore we explored these pathways as possible mechanisms, other than HR, that may contribute to the Olaparib sensitivity of HGS EOC cell lines. From our list of differentially expressed genes we focused on *MLH1* and *MLH3* from the MMR pathway and *ERCC8* from the NER pathway. *MRE11A*, shown to be an important in PARPi sensitivity [26, 43], was selected to represent the HR pathway to examine any association between the HR pathway and the MMR and NER pathways in Olaparib sensitivity.

Having selected target genes that are potentially associated with PARPi sensitivity, we performed validation experiments using siRNA knockdowns. Western blot analysis demonstrated that siRNAs against *MRE11A*, *MLH1*, *MLH3* and *ERCC8* efficiently down-

regulated their protein targets in the resistant OV1369(R2) cell line (Fig.3A and Fig.S4). Olaparib dose-response curves of this cell line were altered with the knockdown of all four genes (Fig.3B), indicating a decreased IC_{50} and increased sensitivity. Having validated the efficacy of our siRNAs, additional clonogenic assay experiments were performed in two resistant [OV1369(R2) and OV866(2)] and in two intermediate [TOV2295(R) and OV4485] cell lines to further verify whether these siRNAs could increase sensitivity to Olaparib. Figure 3C shows a significant decrease in the Olaparib IC_{50} of both resistant cell lines upon downregulation of each of the four selected genes. More precisely, down-regulation of *MLH1* (MMR pathway), *ERCC8* (NER pathway) or *MRE11A* (HR pathway) induced an approximate 10-fold decrease in the Olaparib IC_{50} (Table 3), which were closer to IC_{50} values observed for intermediate cell lines that were not subjected to siRNA knockdown. *MRE11A* knockdowns shifted the dose-response curves of the resistant cell lines closer to the intermediate but not to the sensitive group, which supports our initial hypothesis that defects in HR alone is insufficient for high sensitivity to PARPi. Although IC_{50} values of resistant cell lines were significantly decreased by all siRNA knockdowns, *MLH3* was the least effective of the four selected gene targets (Fig.3C, Table 3). The lack of efficacy with *MLH3* siRNA may be in part due to MLH3 having a minor role in the MMR pathway [45]. To ensure that our results were not due to off target effects of the chosen siRNAs, clonogenic assays were performed in these two resistant cell lines using a different siRNA sequence for each gene. Fig.S5 shows the same inhibition profile as that shown in Fig.3C, indicating the specificity of our siRNAs.

The two intermediate cell lines [TOV2295(R), OV4485] also demonstrated a decrease in Olaparib IC_{50} when target genes were down-regulated, with values shifting from the intermediate to the sensitive range (Fig.3C, Table 3). However, results were less striking than those obtained with the resistant cell lines, as not all gene knockdowns induced significant effects. The *BRCA1* mutated cell line, OV4485, is of special interest as these cells are compromised in HR function (Fig.1E). As expected, siMRE11A was unable to induce a significant decrease in Olaparib sensitivity since the HR pathway was already non-functional. However siRNAs against *MLH1*, *MLH3*, and *ERCC8* induced substantial decreases in the IC_{50} values (Fig.3C, Table 3). These extreme drops in IC_{50} values could indicate that deficiency of two DNA repair pathways may be necessary to achieve greater Olaparib sensitivity. In TOV2295(R) cells, siRNA against both *MRE11A* and *MLH1*, but not *MLH3* and *ERCC8*,

produced a significant decrease in Olaparib IC_{50}. The insignificant effect of *ERCC8* down-regulation in this cell line was not expected and we speculate that the NER pathway could be compromised. A recent study has described that 8% of HGS EOC exhibited mutations or homozygous deletions of NER genes [46]. Further investigation of the NER function in this cell line is warranted. Similar to the resistant cell lines, *MLH3* down-regulation was less effective than *MLH1* in increasing Olaparib sensitivity in both intermediate cell lines.

To further validate the siRNAs and their targets, siMLH1 and siMLH3 were tested in OV1946 a sensitive cell line that had lower expression for these two proteins based on gene expression microarray analyses relative to resistant cell lines (Table 2 and Fig.2). As expected, there was no change to PARPi sensitivity (Fig.3C). A similar result was observed with siERCC8 in TOV3041G cells (Fig.3C), which demonstrated lower ERCC8 expression by gene expression microarray analyses relative to resistant cell lines (Fig.2).

In order to demonstrate that silencing of MMR and NER genes do not affect the HR function, RAD51 foci were evaluated after MLH1, MLH3 and ERCC8 knockdown in HR proficient OV866(2) and OV1369(R2). As expected, knocking down these genes did not alter RAD51 foci number in total or geminin-positive cells (Fig.S6). On the other hand, MRE11 siRNA efficiently impaired HR function in both cell lines studied (Fig.S6).

Increased sensitivity to Olaparib involves defects in HR plus another DNA repair pathway

Our initial siRNA results indicate that more than one defective DNA repair pathway is necessary for cells to become highly sensitive to PARPi. This would explain the observation that some patients with *BRCA* mutations respond to PARPi while others do not. To this end we used siRNAs in combination to investigate their effect on the Olaparib response. Due to the less pronounced effects of *MLH3* down-regulation on Olaparib sensitivity, siRNA against this gene was not used for double knockdown assays. Therefore, siRNAs against *MRE11A*, *MLH1*, and *ERCC8* were used in combination. Efficacy of the siRNA combination was verified by Western blot and compared to each single siRNA treatment (Figs. 3A and 4A). All siRNA combinations showed efficient knockdowns of their targets except for siERCC8 combined with siMRE11A, which was not as effective as siERCC8 alone for *ERCC8* knockdown. Nevertheless, the double knockdown still induced diminished protein expression

compared to control scramble siRNA treated cells. When the representative resistant cell line OV1369(R2) was assayed for Olaparib sensitivity, single siRNA treatment against *MRE11A* or *MLH1* resulted in an increase in sensitivity, while a double knockdown of *MRE11A* and *MLH1* displayed an even greater enhancement when compared to the parental cell line (Fig.4B).

Two resistant and two intermediate cell lines were then used to test three different combinations of siRNAs (Fig.4C). The first combination was used to impair the HR and MMR pathways (siMRE11A/siMLH1) in resistant cell lines. As previously shown, each siRNA alone could modify resistant cells to respond as intermediate cells when exposed to Olaparib. However, IC_{50} values fell into the range of sensitive cells when the two siRNAs were used in combination (Fig.4C and Table 3). A similar effect was observed when both HR and NER pathways were impaired (siMRE11A/siERCC8). Interestingly, this was not the case for the double impairment of the MMR and NER pathways (siMLH1/siERCC8). In the resistant cell line OV1369(R2), a double knockdown further decreased the IC_{50} from levels achieved by a single knockdown, but still fell in the range of the intermediate IC_{50} values (Table 3). In the other resistant cell line OV866(2), the double knockdown did not drop the IC_{50} significantly from values that were obtained with single knockdowns (Fig.4C and Table 3).

When HR and MMR were targeted (siMRE11A/siMLH1) in intermediate cells, TOV2295(R) did not display a significant change in sensitivity between single and double knockdowns (Fig. 4C and Table 3). The same was observed for OV4485 when comparing double knockdown and siMLH1. However, siMLH1 alone or in combination with siMRE11A significantly enhanced Olaparib sensitivity compared to single *MRE11A* knockdown. As already stated, siMRE11A did not have a major effect, most likely because this cell line is a *BRCA1* mutant and already has non-functional HR. When both HR and NER were impaired (siMRE11A/siERCC8) the double knockdown was more effective than each single knockdown in both the TOV2295(R) and OV4485 cells (Fig. 4C and Table 3). In the combined impairment of MMR and NER (siMLH1/siERCC8), TOV2295(R) cells did not have a strong reaction to siERCC8 alone, while both siMLH1 and siMLH1/siERCC8 showed increased sensitivity that were of similar levels reflecting a possible inherent defect in NER in this cell line. OV4485 cells impaired in MMR and NER pathways showed equally strong response to Olaparib in reactions affected by both single and double knockdowns (Fig. 4C and

Table 3), indicating no enhanced sensitivity due to the impairment of both pathways, as observed in the resistant OV866(2) cell line.

These findings suggest that defective HR is vitally important for PARPi sensitivity, but insufficient on its own to render a cell fully sensitive to PARPi and that a second pathway must be deregulated (either MMR or NER) to achieve the highest sensitivity observed *in vitro*. However, based on results with OV4485, once HR and one other pathway are compromised, there is no added benefit to a third pathway being compromised.

Expression of targets in clinical samples

After observing that HR and another DNA pathway must be defective for optimal PARPi sensitivity, we sought to determine the co-occurrence of deficiencies in these pathways in clinical EOC specimens by examining the co-expression of MHL1 and MRE11A, or ERCC8 and MRE11A. The correlation analyses were performed on the gene expression microarray data from more than 400 HGS EOC patients available through the The Cancer Genome Atlas Research (TCGA) Network [18] (Fig.5A). Our results showed significant Pearson correlations between *MRE11A* and *MLH1* expression (p=0.013, R=0.113) and *MRE11A* and *ERCC8* expression (p=0.0001, R=0.122), indicating that defects in HR and MMR/NER pathways could co-occur in clinical specimens. Approximately 25% of the specimens exhibited concomitant low expression levels of these biomarkers pairs (Fig.5A), and according to our *in vitro* results (Fig.4C), patients with these cancers would potentially have a better response to Olaparib. At the protein level, we analyzed the expression of these by immunohistochemistry (IHC) using a tissue microarray (TMA) containing 213 HGS ovarian tumors. Specificity of antibodies against MLH1 and MRE11A are shown in Fig.S7. However, due to poor antibody specificity, ERCC8 was not assayed in the TMA. Our results showed a strong Pearson correlation between the expression of MRE11A and MLH1 proteins (p<0.0001, R=0.518) (Fig.5B), and we found 17.5% patients having low levels (scores≤1.5) of both of these proteins. Our findings suggest that the investigation of these genes as biomarkers in clinical specimens could help identify HGS EOC patients most likely to respond to PARPi treatment.

2.2.2.4 Discussion

PARP1 exerts significant effects on several biological functions that are critical for cell growth and survival [7-9]. In the context of DNA damage, PARP1 binds damaged DNA and undergoes a conformational change resulting in its activation. Once activated, PARP1 synthesizes PAR chains that covalently bind a variety of chromatin-associated proteins, although PARP1 itself is the major acceptor of the PAR chains. The resulting PARylation not only alters the function of covalently bound proteins but can also stimulate the recruitment of a wide variety of other DNA nuclear proteins. PAR levels reflect DNA damage that is present, but once DNA repair ensues, PAR is rapidly degraded by PAR glycohydrolases. Through PAR synthesis, PARP1 contributes to a number of DNA repair pathways [7-9]. PARP1 plays a role in the BER, is involved in the alternative end joining repair pathway, recruits MRE11A and NSB1 to initiate HR, PARylates *BRCA1* that further contributes to the HR pathway, and prevents NHEJ activation. Therefore, in the context of PARP1 inhibition, it is clear that response to PARPi extends beyond the *BRCA1/2* mutation- and HR-status.

Based on present research findings, we propose a new model to account for the spectrum of PARPi responsiveness that is dependent on the types of DNA pathways affected in EOC (Fig.6). Tumors with phenotypes that include either defective HR and NER, or defective HR and MMR pathways, should respond with the highest sensitivity to PARPi, in keeping with the concept of synthetic lethality. Tumor phenotypes with only one defective DNA repair pathway may show limited PARPi responsiveness, whereas patients with tumor phenotypes with functionally intact DNA repair pathways would not respond to PARPi treatment. Indeed, the ARPE19 normal epithelial retina cell line demonstrates an IC_{50} comparable to EOC Olaparib resistant cell lines (data not shown). Similar to the HR pathway, the MMR and NER pathways are involved in the repair of DSB [47], such that DSB repair is reduced when MMR or NER are deficient [44, 47, 48]. Also, it has been demonstrated that PARP1 acts directly on the activity of the NER and MMR [49, 50]. However, only few reports have described the role of the MMR and NER pathways in the response to PARPi [41-44, 51]. Our work has demonstrated that down-regulation of genes involved in the MMR or NER pathways increased Olaparib sensitivity of HGS EOC cell lines, even in *BRCA* mutated cell lines (Fig.3). In addition, our results suggest that the MMR and the NER pathways might

repair DSB when HR is defective in tumor cells, and may explain why some patients harboring a *BRCA* mutation do not respond to PARPi treatment. Alternatively, tumors cells having defects in HR and in either MMR or NER pathways are more sensitive. However, we did not observe a significant increase in Olaparib sensitivity when MMR and NER were both deficient in cells with intact HR, indicating that DSB are mainly repaired by the HR pathway when either one of these pathways are defective.

Although other studies have correlated NER deficiency with PARPi response [42, 51], this is the first report showing *ERCC8* as a potential target for PARPi sensitivity. NER deficiency has also been implicated in the response to platinum-based therapy in EOC patients [46, 52], which is consistent with the observation that platinum-sensitive patients also respond to PARPi treatment [13, 29]. Although a recent report showed that mutations in the NER genes *ERCC6* and *ERCC4* did not increase PARPi sensitivity to Rucaparib [46], our results showed that under-expression of *ERCC8* significantly increased Olaparib sensitivity in HGS cells that were either HR-deficient or -proficient. In the case of *MLH1*, reports have shown that MMR deficiency confers platinum resistance [53], whereas our results showed that down-regulation of *MLH1* resulted in a significant increase in Olaparib sensitivity. Therefore, our findings suggest that platinum-resistant patients with low *MLH1* expression may benefit from PARPi treatment. Indeed, the TOV1946 cell line exhibiting very low levels of *MLH1* (Fig.2) is very sensitive to Olaparib (IC_{50}=0.02 μM), and our previous work has shown that this cell line is not very sensitive to carboplatin (IC_{50}=4 μM) [23].

Analysis of gene (TCGA dataset) and protein (TMA) expression in HGS EOC patient samples showed a significant correlation between *MRE11A* (HR pathway) and *MLH1* (MMR pathway) or *ERCC8* (NER pathway) (Fig.5). Therefore, it may be possible to identify patients with tumors containing low levels of *MRE11A* and *MLH1* or *ERCC8*, and distinguish them as patients who may respond better to Olaparib. In the case of patients with *BRCA* mutations, low levels of either *MLH1* or *ERCC8* may predict a better response to Olaparib treatment, as demonstrated by our results with siRNA against either *MLH1* or *ERCC8* in a *BRCA1* mutated cell line (OV4485) (Fig.3). These findings could impact the clinical management of HGS EOC patients such that patients that have these molecular tumor characteristics, could be treated preferentially with Olaparib, and possibly at lower doses. Phase II clinical trials of Olaparib have been performed with 100, 200 or 400 mg twice daily where a 100 mg dose

resulted in a response rate of 12% and a 200 or 400 mg dose resulted in a response of around 30-40% [12, 29, 54]. However, only the dose of 400 mg twice daily was included in a clinical trial of Olaparib as maintenance therapy in a large cohort with platinum-sensitive *BRCA* mutated HGS EOC; although improved survival was observed for the Olaparib group, severe side effects were reported [13, 14]. Therefore, stratifying HGS patients may help to increase the quality of life for some patients by decreasing drug dosage. In our model, stratification of patients with "BRCAness" plus defective MMR or NER may identify those who could be treated with the lowest doses.

A microarray study characterizing Olaparib sensitivity in breast cancer cell lines have identified six DNA repair genes that were significantly down-regulated (MRE11A, NBS1, TNKS, TNKS2, XPA, XRCC5) and two that were significantly up-regulated (CHEK2, MK2) in sensitive cell lines relative to resistant cell lines [26]. MRE11A is the only gene in common between this study and our work (Table 2). However, the authors also identified a gene from the NER pathway (XPA gene) that was significantly down-regulated in sensitive cells, indicating that deregulation of this pathway affects PARPi response in both cancer types. Therefore, results from this study are consistent with our proposed model since they reported defects in HR and NER pathways in Olaparib-sensitive breast cancer cell lines. In contrast, MMR genes did not appear to be deregulated in breast cancer cells, highlighting the different roles of this pathway in breast and ovarian cancers. Although other potential biomarker genes in DNA repair have been described in association with Olaparib sensitivity [38, 55], our work is particularly noteworthy for the identification of defects in several DNA repair pathways that demonstrated a cumulative effect in our cell line models resulting in acute Olaparib sensitivity.

Furthermore, our findings provide evidence that proficiency in NER or MMR may account for mechanisms of PARPi resistance, other than mutation reversal or p-glycoprotein up-regulation [55], to explain why BRCA mutated EOC patients do not respond favorably to Olaparib.

2.2.2.5 Methods

Cell Lines and Cell Culture

The 18 human HGS EOC cell lines used (OV90, OV866(2), TOV1369, OV1369(R2), TOV1946, OV1946, TOV2223G, OV2295, OV2295(R2), TOV2295(R), TOV2978G, TOV3041G, TOV3291G, TOV3133G, TOV3133D, OV3133(R), OV4453, OV4485) were derived in our laboratory from patients' tumors (TOV) or ascites (OV) [22-25]. All cell lines were maintained in a low oxygen condition of 7% O_2 and 5% CO_2 and grown in complete OSE medium, which contains OSE medium (Wisent, Montreal, QC) with 10% FBS (Wisent), 0.5 μg/mL amphotericin B (Wisent) and 50 μg/mL gentamicin (Life Technologies Inc., Burlington, ON).

Antibodies

The following antibodies were used: beta-actin (AC-15) (ab6276; Abcam Inc., Toronto, ON, Canada); MLH1 (4C9C7) (3515; Cell Signaling Technology Inc., Danvers, MA); MLH3 (NBP1-00106; Novus Biologicals, Oakville, ON); ERCC8 (ABIN486848; Antibodies-online, Atlanta, GA); PAR (4335-MC-100; Trevigen®, Gaithersburg MD); PARP1 (H-250)(SC-7150, Santa Cruz Biotechnology Inc., Dallas, TX); MRE11A (4895, Cell Signaling Technology Inc.); RAD51 (14B4) (ab213; Abcam Inc.); phospho-histone γ-H2AX (Ser139) (JBW301) (05-636, Millipore, Temecula, CA); and Geminin (10802-1-AP, Proteintech, Rosemont, IL).

Western Blot

Thirty micrograms of total protein extracts were separated on 10% SDS-polyacrylamide gels and transferred onto nitrocellulose membrane. Membranes were blocked with 5% skim milk in PBS-Tween for 1 hour and probed with primary antibodies (diluted at 1:1000 for MLH1 or PARP1, 1:2000 for MLH3, 1:3000 for ERCC8 and 1:1000 for MRE11A) overnight at 4^{o}C. After the addition of HRP-conjugated secondary antibodies, proteins were detected using enhanced chemiluminescence (ECL). Loading control for the samples was determined with anti- ß-actin antibody (1:10000).

Analysis of PAR Levels

The analysis of PAR levels was performed as previously described [56]. Briefly, cells were seeded in 6-well plates, and incubated for 24 hours before they were treated with 1mM H_2O_2 for 20 minutes. Then, cells were treated with 10μM Olaparib for 24 hours, harvested and lysed to obtain protein extracts that were analyzed by Western blot using an anti-PAR antibody (1:1500).

Cell Cycle Flow Cytometry Analysis

Cells were seeded in 6-well plates and grown to 70% confluence. Media was then removed and replaced with complete OSE media containing 10 μM Olaparib. Cells were harvested 24 hours after, fixed in 70% ethanol and incubated (30 min, RT) with 100μg/ml RNAse A and 25μg/ml Propidium Iodide for cell cycle analysis. A maximum of 10,0000 events were counted per condition using the Fortessa flow cytometer (BD Biosciences, Mississauga, ON).

Clonogenic Survival Assay to Measure Drug Sensitivity

Olaparib (Selleckchem, Houston, TX) sensitivity of the cell lines was assessed using a concentration range of 0–50 μM on clonogenic assays as previously described [22, 23]. Colonies were counted under a stereo microscope and reported as percent of control. IC_{50} values were determined using Graph Pad Prism 5 software (GraphPad Software Inc., San Diego, CA). Each experiment was performed in triplicate and repeated three times. Cells were categorized as either sensitive, intermediate, or resistant to PARPi based on groupings of IC_{50}.

Analysis of Nuclear RAD51 and γ-H2AX Foci

Cells were seeded onto coverslips in 12-well plates, grown until 80% confluence, and gamma-irradiated at 8Gy for 2 hours for RAD51 or 2Gy for 1 hour for γ-H2AX foci analyses. These conditions were established to count an appropriate number of foci during the peak of recruitment of these proteins at the damaged DNA site after gamma-irradiation [57, 58]. Cells were then washed in ice-cold phosphate buffered saline (PBS), fixed in 4% paraformaldehyde and permeabilized with 0.25% Triton X-100 (Sigma–Aldrich Inc.). After blocking (5% BSA and 4% FBS in PBS), coverslips were incubated with the anti–RAD51 (1:500) or the anti-γ-

H2AX (1:1500) primary antibodies, and subsequently incubated with Alexa Fluor 488 (1:500) or Cy-5 (1:800) secondary antibodies (Life Technologies Inc.) for RAD51 or γ-H2AX staining, respectively. Coverslips were mounted onto slides using Prolong® Gold anti-fade reagent with DAPI (Life Technologies Inc.). Images were obtained using a Zeiss microscope (Zeiss observer Z1, Carl Zeiss, Jena, Germany). Automated analysis software from Zeiss (AxioVision™, Carl Zeiss) was used for foci counting. The average number of foci per nucleus was expressed as a percentage of the non-irradiated controls. Fold change was calculated as a ratio between percentages of Rad51 foci in treated over control non-treated cells. RAD51 foci were quantified in roughly 400 nuclei from three different fields of each coverslip. Reliability, reproducibility, and validity of our data were confirmed by repeated tests across different fields. For RAD51-geminin co-staining [36], coverslips were incubated with RAD51 (1:500) and Geminin (1:1000) primary antibodies and subsequently incubated with Cy-5 and Alexa Fluor 488 secondary antibodies, respectively.

RNA Preparation and Gene Expression Microarray Analyses

Four of the cell lines used in this study (OV90, TOV1946, OV1946, TOV2223G) had been previously subjected to gene microarray analyses using the Affymetrix Human Genome U133A [59, 60]. For the remaining 14 cell lines, RNA was extracted and purified as previously described [59, 60] and microarray experiments were performed at the McGill University and Genome Quebec Innovation Centre (genomequebec.mcgill.ca) using HG-U133 Plus 2.0 GeneChip arrays (Affymetrix®, Santa Clara, CA). Gene expression levels were calculated for each probe set from the scanned image by Affymetrix® GeneChip (MAS5) and prepared as previously described [61]. As reproducibility of expression values is highly variable at low values of expression [62], all normalized values below five were reassigned a threshold value of five based on the mean expression value of the lowest reliability scores. Probe sets having these threshold values in all the samples were not used for further the analysis. Further normalization across probe sets was performed in order to combine datasets from the previously analyzed HG-U133A (four cell lines) and the HG-U133 Plus 2.0 (14 cell lines). Altogether, there were more than 22,000 probe sets in common, covering 18,400 transcripts and variants, including 14,500 well-characterized human genes.

Microarray data were used to identify genes that were two fold up- or two fold down-regulated in expression for each sensitive cell line (OV2295, TOV3041G, OV4453, TOV1946 and OV1946) when compared to all resistant [OV90, OV886(2), TOV1369 and OV1369(R2)] cell lines. A list of genes was obtained for each sensitive cell line, following the strict criteria that genes must be differentially regulated when compared to all the other cell lines within the resistant group. Gene lists were uploaded onto the Ingenuity Pathway Analysis program (Qiagen Inc.) to obtain a list of canonical pathways affected in each cell line. Only significantly (p<0.05) affected DNA repair pathways were taken into account.

In another approach, probe sets of DNA repair genes were selected and mean expression values were analyzed to identify common differentially affected genes between Olaparib sensitive *versus* resistant cell lines using the non-parametric Mann-Whitney test. Significance was set at p value < 0.05. Visualization of gene expression values and gene clusters (heat maps) was performed using the MultiExperiment Viewer software (MeV_4_8_1 from TM4), a free, open-source tool for microarray analysis.

Small interference RNA (siRNA) Treatment

For each gene of interest, a collection of four different siRNAs (Dharmacon ON-TARGET plus siRNA, set of 4; Thermo Fisher Scientific Inc., Waltham, MA) (see Table S2 for sequences) was tested and the most effective were selected for further analysis (siRNA#2 for *MLH1* and *MLH3*; and siRNA#3 for *MRE11A* and *ERCC8*). To verify off target issues, a different siRNA for each gene was used in a subset of experiments (i.e., siRNA#4 for all genes). Scramble siRNA (Table S2) was used as control in all the experiments. Transfections were performed using the DharmaFECT® Transfection Reagents. Cells were transfected with 25 nM siRNA per well in a 6-well plate. For double siRNA treatment, 25 nM of each siRNA was added to the well at the same time. After 48 hours, cells were harvested and used for Western blot or clonogenic assays.

Immunohistochemistry

In the present work we used a HGS EOC tissue microarray (TMA) containing 213 cases (two cores per patient), which has been previously described [63]. The TMA blocks

were sectioned at 4μm thickness onto superfrost+ glass microscope slides (Fisher Scientific Limited, Nepean, ON, Canada), and stained using the BenchMark XT automated stainer (Ventana Medical System Inc., Tucson, AZ). Antigen retrieval for MLH1 and MRE11A was performed with Cell Conditioning Solution, CC1 (Ventana Medical System Inc.) for 30 minutes. Slides were incubated with anti-MLH1 (1:100) or anti-MRE11A (1:500) antibodies for 40 minutes, and developed with the iView DAB detection kit (Ventana Medical System Inc.). Hematoxylin and bluing reagent were used for counterstaining (Ventana Medical System Inc.). TMAs were observed by brightfield microscopy and digitally imaged (Aperio ScanScope, Vista, California, USA). Protein expression by IHC was scored according to the nuclear staining intensity in epithelial zones of the tumor cores. The staining intensity of DAB was defined as 0 (no staining), 1 (weak staining), 2 (moderate staining) and 3 (strong staining). All TMAs were analyzed in a blind study by two independent observers. Intra-class correlation (ICC) was greater than 75% for all assays. The average of all cores with cancer from the same patient was used for analysis. Graph Pad Prism 5 was used to perform Pearson correlation test (two-tailed) and significance was set at $p< 0.05$.

TCGA Dataset

The Unified Expression dataset of HGS EOC gene microarray from the TCGA was directly uploaded from The Cancer Genome Atlas (NCI/NIH) website (https://tcga-data.nci.nih.gov/docs/publications/ov_2011/) as a table format. This table contained normalized expression of 11864 genes from 489 HGS EOC samples as previously described [18]. Graph Pad Prism 5 was used to perform Pearson correlation test (two-tailed) and significance was set at $p< 0.05$.

2.2.2.6 Acknowlegements

We acknowledge Guillaume Chouinard for technical assistance. We thank Kishanda Vyboh and Jacqueline Chung for editing. A-M.M-M. and D.M.P. are Researchers of the Centre de recherche du Centre hospitalier de l'Université de Montréal (CRCHUM)/Institut du cancer de Montréal, J-Y.M. is a FRQS Chercheur National and FRQS Chair, and P.N.T. is a Medical Scientist at The Research Institute of the McGill University Health Centre, who receive support from the Fonds de recherche du Québec - Santé (FRQS). The ovarian tumor banking was supported by the Banque de tissus et de données of the Réseau de recherche sur le cancer of the FRQS affiliated with the Canadian Tumor Repository Network (CTRNet). H.F. was supported in part by studentship from the Canderel Fund of the Institut du Cancer de Montréal.

2.2.2.7 Competing financial interests

The authors declare no competing financial interests.

2.2.2.8 Grant support

This work was supported by a partnered Canadian Research Society and Ovarian Cancer Canada (#20087) grant, to A-M.M-M., D.P. and P.N.T., and by the Institut du cancer de Montréal (Rallye Défi Can-Am Spyder initiative).

2.2.2.9 Author contributions

H.F., E.C. conceived and designed the experiments. H.F., V.G.M., conducted the experiments. E.C., D.P., A-M.M-M. supervised the project. E.C. performed the microarray data analyses. H.F., L.M. performed the TMA analyses. H.F., E.C. wrote the manuscript. E.C., J.Y.M., P.N.T., D.P., A-M.M-M. reviewed and revised the manuscript.

FIGURE 1

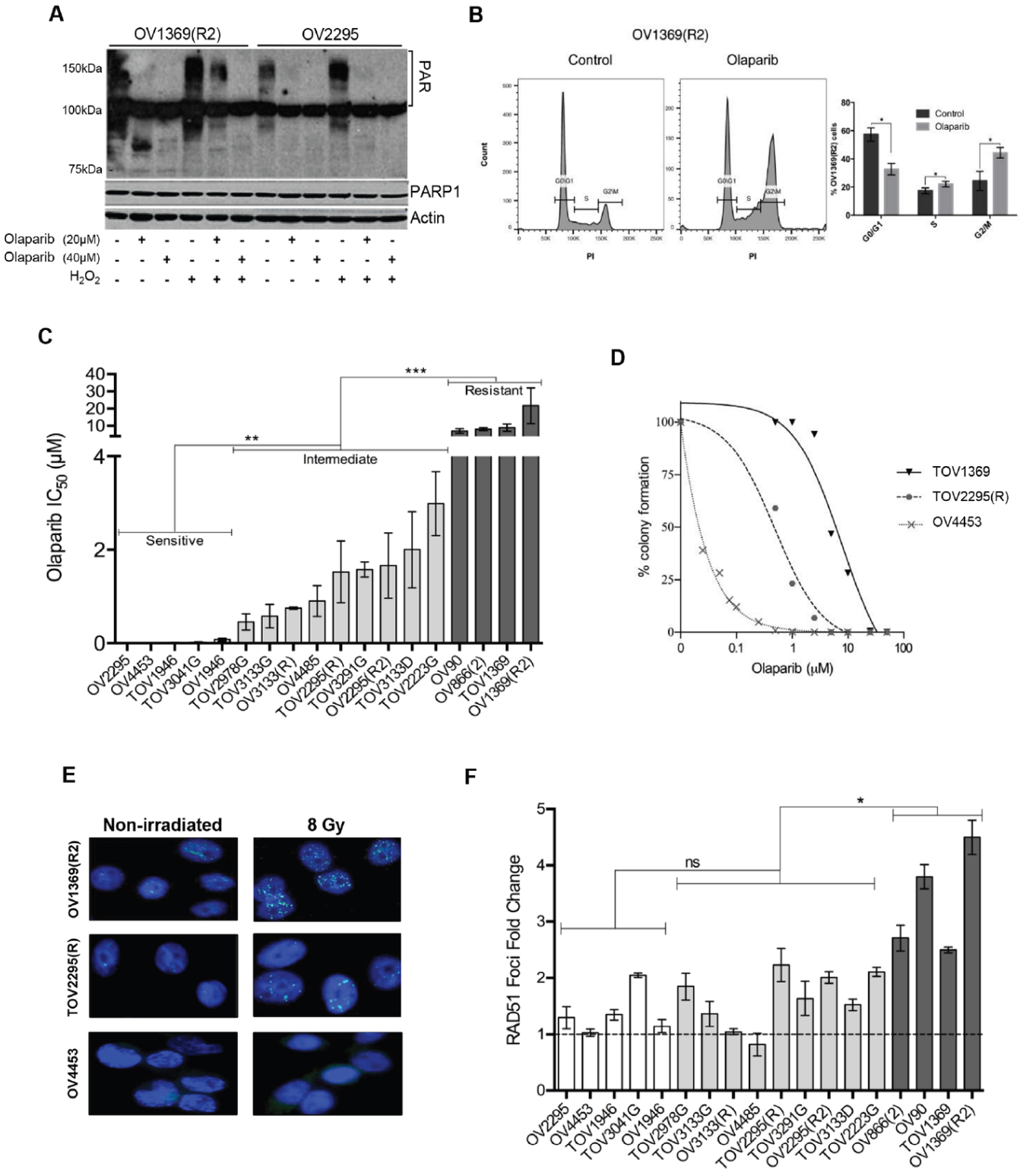
A
OV1369(R2)
OV2295
150kDa
100kDa
75kDa
PAR
PARP1
Actin
Olaparib (20μM)
Olaparib (40μM)
H2O2
B
OV1369(R2)
Control
Olaparib
Count
PI
G0/G1
S
G2/M
% OV1369(R2) cells
C
Olaparib IC50 (μM)
Sensitive
Intermediate
Resistant
OV2295
OV4453
TOV1946
TOV3041G
OV1946
TOV2978G
TOV3133G
OV3133(R)
OV4485
TOV2295(R)
TOV3291G
OV2295(R2)
TOV3133D
TOV2223G
OV90
OV866(2)
TOV1369
OV1369(R2)
D
% colony formation
Olaparib (μM)
TOV1369
TOV2295(R)
OV4453
E
Non-irradiated
8 Gy
OV1369(R2)
TOV2295(R)
OV4453
F
RAD51 Foci Fold Change
ns

FIGURE 1: Analysis of Olaparib sensitivity and HR functionality in HGS EOC cell lines. (A) Western blot detection of PAR polymer and PARP1 in OV1369(R2) and OV2295 after a 24 hour exposure to 20 or 40 μM of Olaparib, with or without H_2O_2 pre-treatment (1 mM). Actin was used as a loading control. (B) Flow cytometry analysis of cell cycle populations following exposure of OV1369(R2) cells to Olaparib (40 μM, 24 hours). Control = non-treated. Bars represent average ± SEM of percent cells in G0/G1, S, G2/M phases in control (dark grey) or Olaparib treated (light grey) cells obtained by three independent analyses. (C) Olaparib sensitivity evaluated by clonogenic assays using different drug concentrations. Cell lines were categorized as Olaparib sensitive (white bars), intermediate (light grey bars) or resistant (dark grey bars). Bars represent average ± SEM of IC_{50} values obtained by three independent clonogenic assays. (D) Olaparib sensitivity curves of cell lines representing each group: sensitive (OV4453), intermediate [TOV2295(R)] and resistant [OV1369(R2)]. (E) Representative images of RAD51 immunostaining after 8 Gy irradiation compared with non-irradiated controls of three selected cell line: sensitive (OV4453), intermediate [TOV2295(R2)] and resistant OV1369(R2). Images are at 400 X magnification. (F) HR response evaluation by RAD51 immunocytochemistry. Nuclear foci were counted 2 hours after exposure to 8 Gy gamma-radiation, and then compared and presented as percentage of the control group (non-irradiated). Fold change was calculated as a ratio between percentages of Rad51 foci in treated over control non-treated cells. Bars represent average ± SEM and bar colors are as in Figure 1C. * denotes $p< 0.05$, ** $p< 0.01$, *** $p< 0.001$, ns = non-significant.

FIGURE 2

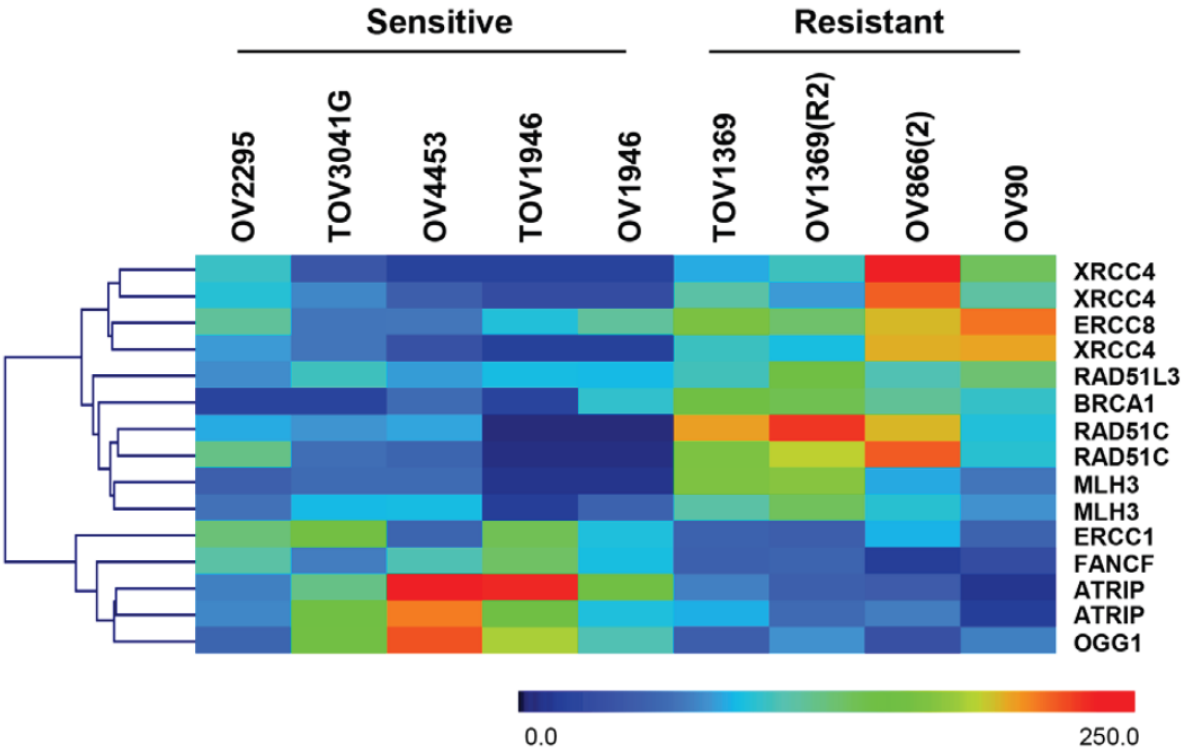

Figure 2: **Heat map representation and gene clustering of differentially expressed DNA repair genes in sensitive and resistant HGS EOC cell lines.** Scale 0 to 250 represents normalized expression values of the Affymetrix gene expression array.

FIGURE 3

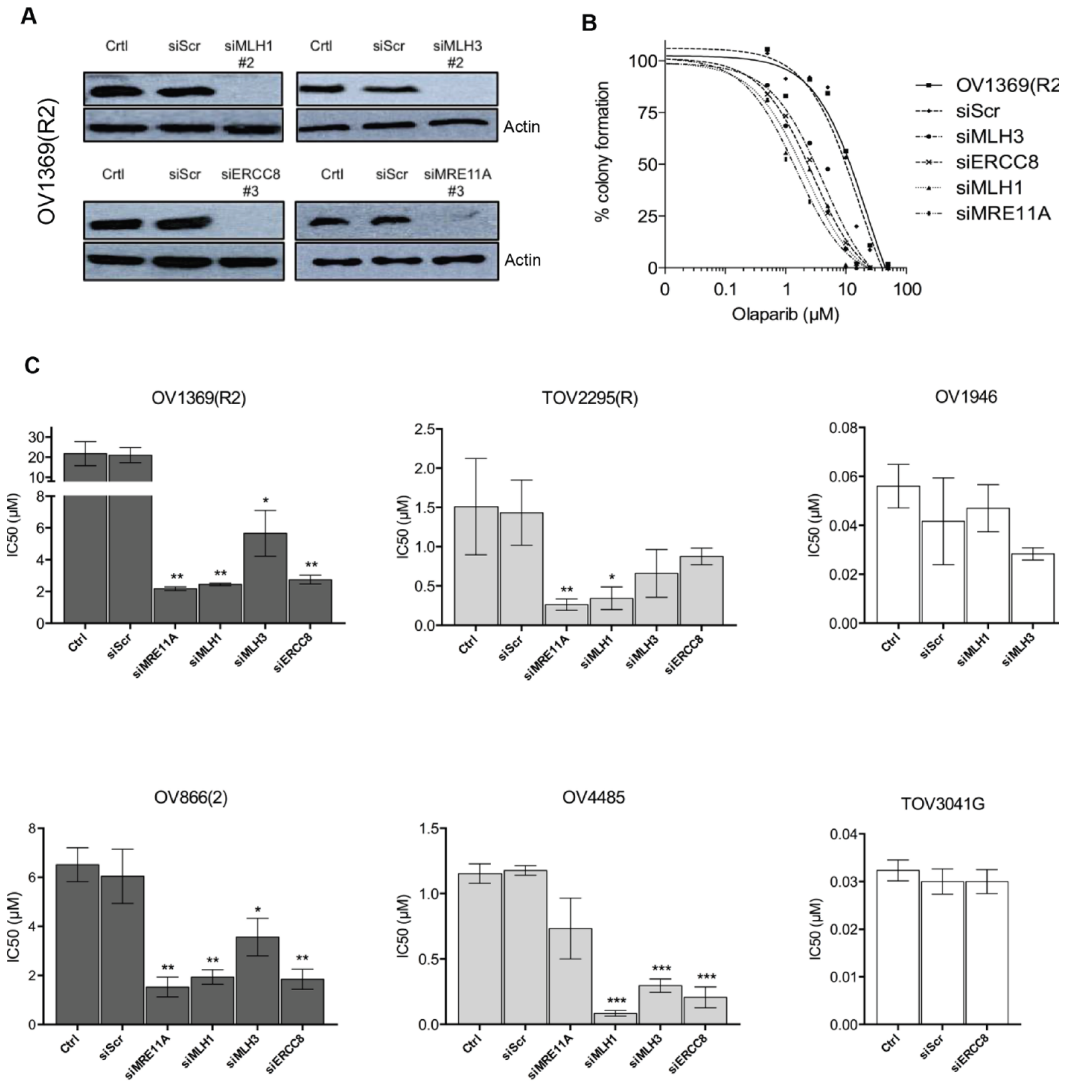

Figure 3: Validation by siRNA silencing of candidate genes contributing to Olaparib sensitivity. (A) Efficacy of siRNAs against *MLH1*, *MLH3*, *ERCC8* and *MRE11A* in OV1369(R2) was verified by Western blot. Control = non-treated cells, siScr = negative siRNA control using a scrambled sequence. (B) Increased Olaparib sensitivity of OV1369(R2) with siRNAs against *MRE11A*, *MLH1*, *MLH3* and *ERCC8*, assayed by clonogenic assay. (C) Verification of *MLH1*, *MLH3*, *ERCC8* and *MRE11* as candidate genes by siRNA knockdown in resistant [OV1369(R2) and OV866(2); dark grey bars], intermediate [TOV2295(R) and OV4485; light grey bars] and control sensitive (OV1946 and TOV3041G; white bars) cell lines. Bars represent average ± SEM of IC_{50} values obtained by clonogenic assay. * denotes $p< 0.05$, ** $p< 0.01$, *** $p< 0.001$.

FIGURE 4

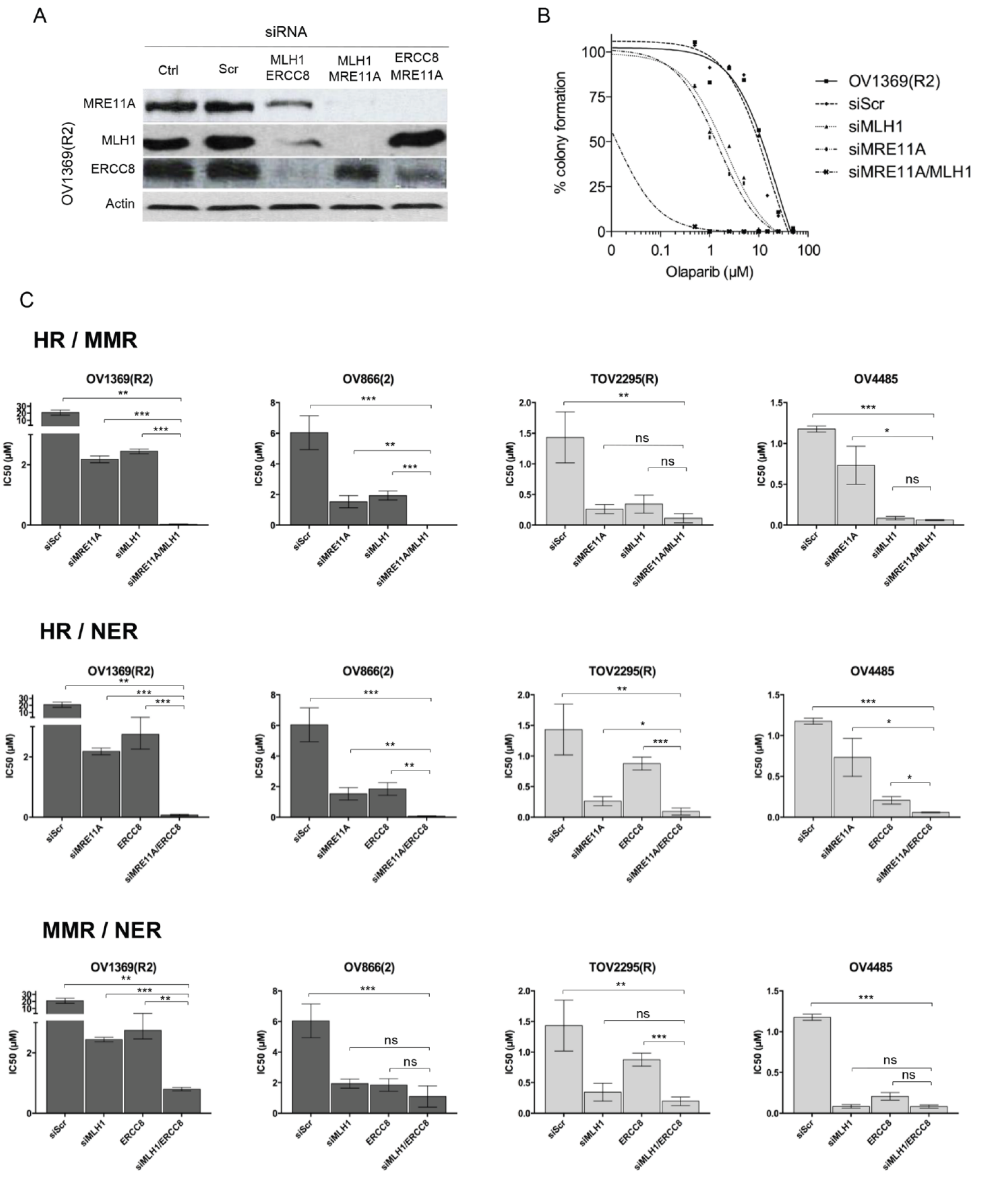

Figure 4: Olaparib sensitivity is enhanced by non-functional HR combined with defects in another DNA repair pathway. (A) siRNAs efficacy against MLH1, ERCC8, and MRE11A in combination, in OV1369(R2) cells was verified by Western blots. (B) Olaparib sensitivity curves of OV1369(R2) representing non-treated cells, control siRNA (siScr), and single and double siRNAs against MRE11A and MLH1 together. (C) IC50 representations of single and double siRNAs in resistant (dark grey bars), and intermediate (light grey bars) cells. Bars represent average ± SEM of IC50 values obtained by clonogenic assay. * denotes $p < 0.05$, ** $p < 0.01$, *** $p < 0.001$, ns = non-significant.

FIGURE 5

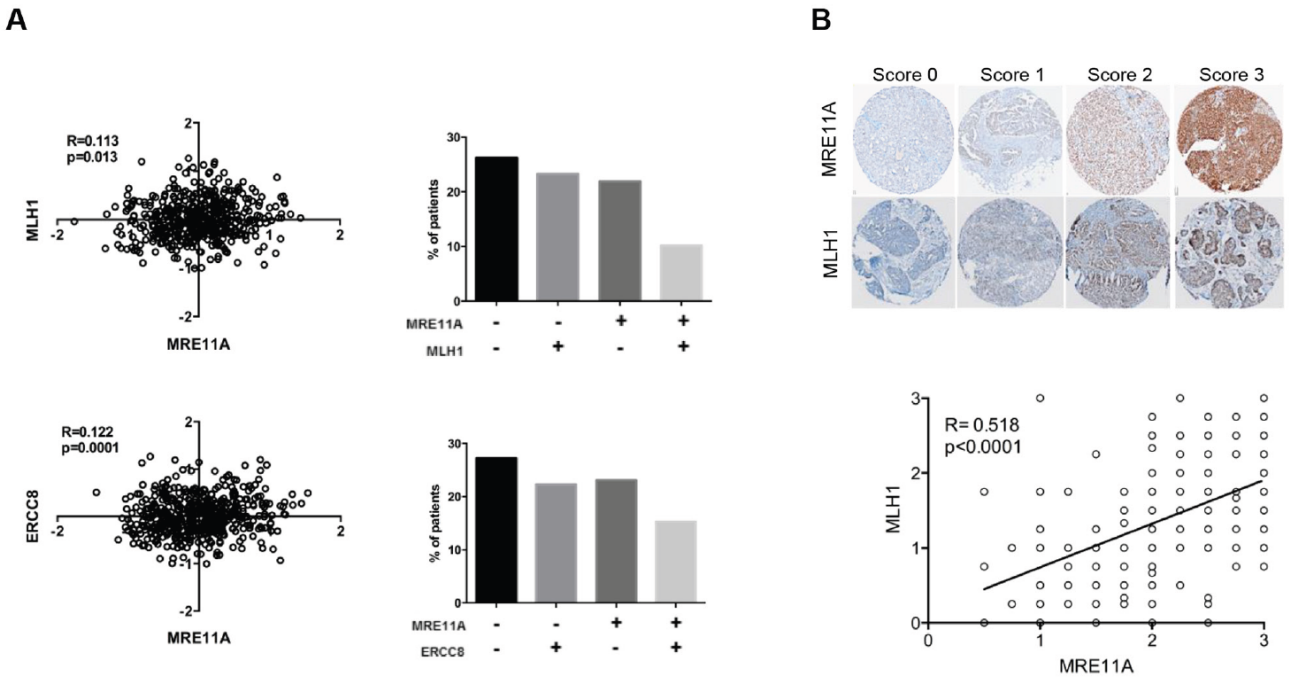

Figure 5: Correlations between expression levels of DNA repair genes in clinical samples. (A) Correlations between gene expression levels of MRE11A/MLH1 and MRE11A/ERCC8 using the TCGA dataset of HGS tumors. Bars represent percent of patients in each category: double negative, single positive or double positive biomarkers staining. (B) Upper panel shows representative images of IHC scores (0, 1, 2, 3) for MLH1 or MRE11A staining. Bottom panel shows correlation between expression levels of MLH1 and MRE11A proteins in a TMA containing patients' samples of HGS EOC.

FIGURE 6

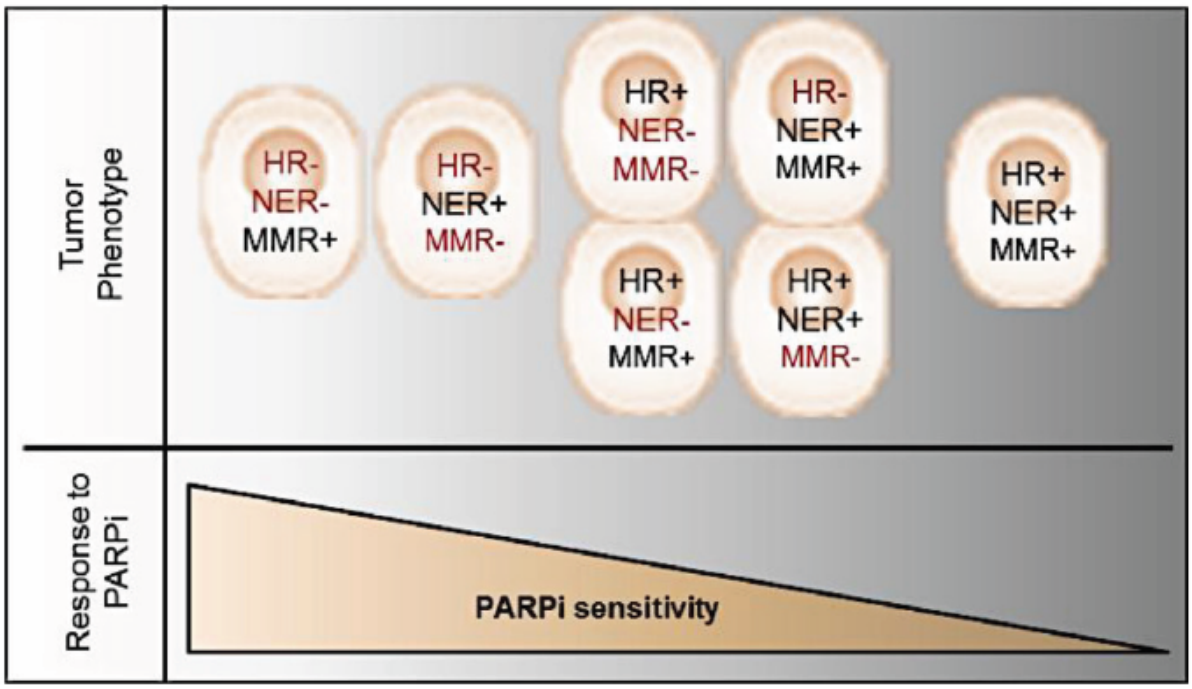

Figure 6: Schematic model representing tumor phenotype and corresponding PARPi response. The synthetic lethality resulting in PARPi sensitivity is presented if HR deregulation is concomitant with another DNA repair pathway deficiency.

Table I: Quantification of Olaparib sensitivities (IC_{50}) and Rad51 foci in EOC cell lines

		IC_{50} Olaparib (μM)	Rad51 Foci Fold change
Resistant	**OV1369 (R2)**	21.71 ± 10.33	4.5 ± 0.30
	TOV1369	9.02 ± 3.66	2.0 ± 0.05
	OV866(2)	8.11 ± 1.27	2.71 ± 0.21
	OV90	7.04 ± 2.33	3.80 ± 0.23
Intermediate	**TOV2223G**	2.99 ± 1.20	2.11 ± 0.08
	TOV3133D	2.00 ± 1.15	1.53 ± 0.1
	OV2295(R2)	1.66 ± 0.99	2.01 ± 0.1
	TOV3291G	1.58 ± 0.23	1.64 ± 0.3
	TOV2295(R)	1.52 ± 1.14	2.23 ± 0.29
	OV4485	0.90 ± 0.58	0.82 ± 0.2
	OV3133(R)	0.75 ± 0.04	1.05 ± 0.05
	TOV3133G	0.58 ± 0.44	1.37 ± 0.22
	TOV2978G	0.45 ± 0.30	1.85 ± 0.23
Sensitive	**OV1946**	0.07 ± 0.05	1.15 ± 0.11
	TOV3041G	0.02 ± 0.01	2.05 ± 0.04
	TOV1946	0.02 ± 0.007	1.35 ± 0.098
	OV4453	0.01 ± 0.0009	1.03 ± 0.067
	OV2295	0.0003 ± 0.0004	1.30 ± 0.2

Table II: Deregulated DNA repair pathways between Olaparib sensitive and resistant cell lines.

Cell Line	DNA Repair Ingenuity Canonical Pathways	p-value	Upregulated genes	Downregulated genes
OV2295	NHEJ	0.0035	DCLRE1C, LIG4	
OV4453	MMR	0.045	RPA1	EXO1
TOV1946	MMR	$5.25e^{-10}$		MLH1, FEN1, RFC3, EXO1, POLD1, PCNA, RFC1, RFC5, MSH6, RFC4, MSH2
	HR	$4.68e^{-07}$		*BRCA1*, POLA1, RAD50, ATM, RPA1, LIG1, RAD51, ATRX, MRE11A, NBN
	NHEJ	$6.92e^{-06}$		PARP1, RAD50, XRCC5, ATM, XRCC4, DCLRE1C, MRE11A, LIG4, NBN
TOV3041G	HR	$8.51e^{-06}$	LIG1, RAD51	*BRCA1*, RAD50, ATRX, MRE11A, NBN
	NHEJ	$1.15e^{-04}$		RAD50, XRCC4, DCLRE1C, MRE11A, LIG4, NBN
	MMR	0.015		RFC3, MSH6, MSH2
OV1946	MMR	$6.61e^{-10}$		MLH1, FEN1, RFC3, EXO1, MSH6, RFC5, POLD1, RFC4, PCNA, MSH2
	HR	0.0074		RPA1, RAD51, ATRX, MRE11A, NBN
	NHEJ	0.0074		PARP1, XRCC4, MRE11A, LIG4, NBN
	NER	0.044		POLR2B, RPA2, POLR2J, POLR2C, POLR2I, POLR2K

Table III: Quantification of Olaparib sensitivities (IC_{50}) in EOC cell lines upon gene downregulation of the selected genes by siRNA.

			Olaparib IC_{50} (μM)								
		siRNA	Control	Scr	MRE11A	MLH1	MLH3	ERCC8	MRE11A /MLH1	MRE11A /ERCC8	MLH1 /ERCC8
Resistant	OV1369(R2)		21.71 ±10.33	21.03 ±6.44	2.18 ±0.19	2.44 ±0.13	5.66 ±2.50	2.74 ±0.48	0.03 ±0.02	0.08 ±0.03	0.80 ±0.06
	OV866(2)		8.11 ±1.27	6.04 ±1.10	1.53 ±0.40	1.94 ±0.29	3.57 ±0.76	1.85 ±0.41	0.01 ±0.005	0.05 ±0.02	1.10 ±0.70
Intermediate	TOV2295(R)		1.52 ±1.14	1.43 ±0.42	0.26 ±0.07	0.34 ±0.15	0.66 ±0.30	0.88 ±0.11	0.11 ±0.08	0.09 ±0.06	0.20 ±0.07
	OV4485		0.90 ±0.58	1.18 ±0.07	0.73 ±0.40	0.08 ±0.04	0.30 ±0.05	0.21 ±0.08	0.06 ±0.01	0.06 ±0.004	0.08 ±0.02
Sensitive	OV1946		0.07 ±0.05	0.04 ±0.02	N/A	0.05 ±0.01	0.03 ±0.003	N/A	N/A	N/A	N/A
	TOV3041G		0.02 ±0.01	0.03 ±0.005	N/A	N/A	N/A	0.03 ±0.004	N/A	N/A	N/A

SUPPLEMENTAL DATA

A. Student's t-test analysis (p value) – Olaparib IC_{50}

	OV1369(R2)	TOV1369	OV866(2)	OV90	TOV2223G	OV3133D	OV2295(R2)	TOV3291G	TOV2295(R)	OV4485	OV3133(R)	TOV3133G	TOV2978G	OV1946	TOV3041G	TOV1946	OV4453	OV2295
OV1369(R2)		1,2E-01	8,9E-02	7,8E-02	2,9E-02	3,7E-02	3,1E-02	2,9E-02	2,9E-02	2,6E-02	2,5E-02	2,5E-02	2,4E-02	2,3E-02	2,3E-02	2,3E-02	2,3E-02	2,3E-02
TOV1369			6,9E-01	4,7E-01	2,6E-02	5,3E-02	3,2E-02	2,4E-02	2,8E-02	1,9E-02	1,7E-02	1,7E-02	1,6E-02	1,3E-02	1,3E-02	1,3E-02	1,3E-02	1,3E-02
OV866(2)				5,1E-01	6,1E-04	4,2E-03	9,8E-04	2,5E-04	1,5E-03	3,1E-04	1,5E-04	2,0E-04	1,6E-04	1,1E-04	1,0E-04	1,0E-04	1,0E-04	1,0E-04
OV90					1,8E-02	5,5E-02	2,4E-02	1,5E-02	2,1E-02	1,1E-02	9,4E-03	9,1E-03	8,2E-03	6,6E-03	6,4E-03	6,4E-03	6,3E-03	6,3E-03
TOV2223G						1,6E-01	5,6E-01	9,0E-01	9,2E-01	2,5E-01	1,0E-01	9,7E-02	5,9E-02	2,0E-02	1,7E-02	1,7E-02	1,7E-02	1,7E-02
OV3133D							3,0E-01	1,1E-01	2,0E-01	5,3E-02	3,1E-02	3,0E-02	2,3E-02	1,3E-02	1,3E-02	1,3E-02	1,2E-02	1,2E-02
OV2295(R2)								4,0E-01	5,9E-01	1,3E-01	5,6E-02	5,6E-02	3,6E-02	1,5E-02	1,4E-02	1,4E-02	1,3E-02	1,3E-02
TOV3291G									9,7E-01	1,3E-01	1,2E-03	2,2E-02	5,0E-03	1,2E-04	9,0E-05	8,9E-05	8,6E-05	8,4E-05
TOV2295(R)										4,5E-01	3,0E-01	2,5E-01	1,9E-01	9,3E-02	8,5E-02	8,5E-02	8,4E-02	8,2E-02
OV4485											6,7E-01	4,8E-01	2,9E-01	6,8E-02	5,7E-02	5,7E-02	5,5E-02	5,4E-02
OV3133(R)												5,4E-01	1,6E-01	4,2E-05	8,6E-06	6,3E-06	5,7E-06	5,4E-06
TOV3133G													7,0E-01	1,2E-01	9,1E-02	9,1E-02	8,8E-02	8,4E-02
TOV2978G														9,8E-02	6,8E-02	6,8E-02	6,4E-02	6,0E-02
OV1946															1,2E-01	1,1E-01	7,2E-02	4,8E-02
TOV3041G																9,7E-01	4,5E-01	1,4E-01
TOV1946																	1,2E-01	1,1E-02
OV4453																		5,1E-05
OV2295																		

B. Student's t-test analysis (p value) – Olaparib IC_{50}

Comparison	Difference	q	*p* value	Significance level
sensitive vs intermediate	-1,514	4,215	P<0.01	**
sensitive vs resistant	-11,446	7,637	P<0.001	***
Intermediate vs resistant	-9,932	7,398	P<0.001	***

C. Student's t-test analysis (p value) – RAD51 foci

Comparison	Difference	q	*p* value	Significance level
sensitive vs intermediate	-26.733	1.189	P>0.05	ns
sensitive vs resistant	-200.15	7.399	P<0.001	***
Intermediate vs resistant	-173.42	4.157	P<0.05	*

Figure S1: Statistical analysis for determining Olaparib sensitivity groups. (A) Student's t-test analysis of IC_{50} values comparing a cell line with each of the other ones. Red fonts indicate the shift of significant difference (p<0.05) that was used to define the three groups of Olaparib sensitivity. (B) Student's t-test comparison between the IC_{50} values of the three groups of sensitivity. (C) Student's t-test comparison of the increase in RAD51 foci in the three groups of sensitivity. For both tables (B and C), * denotes p< 0.05, ** p< 0.01, *** p< 0.001 and ns = non-significant.

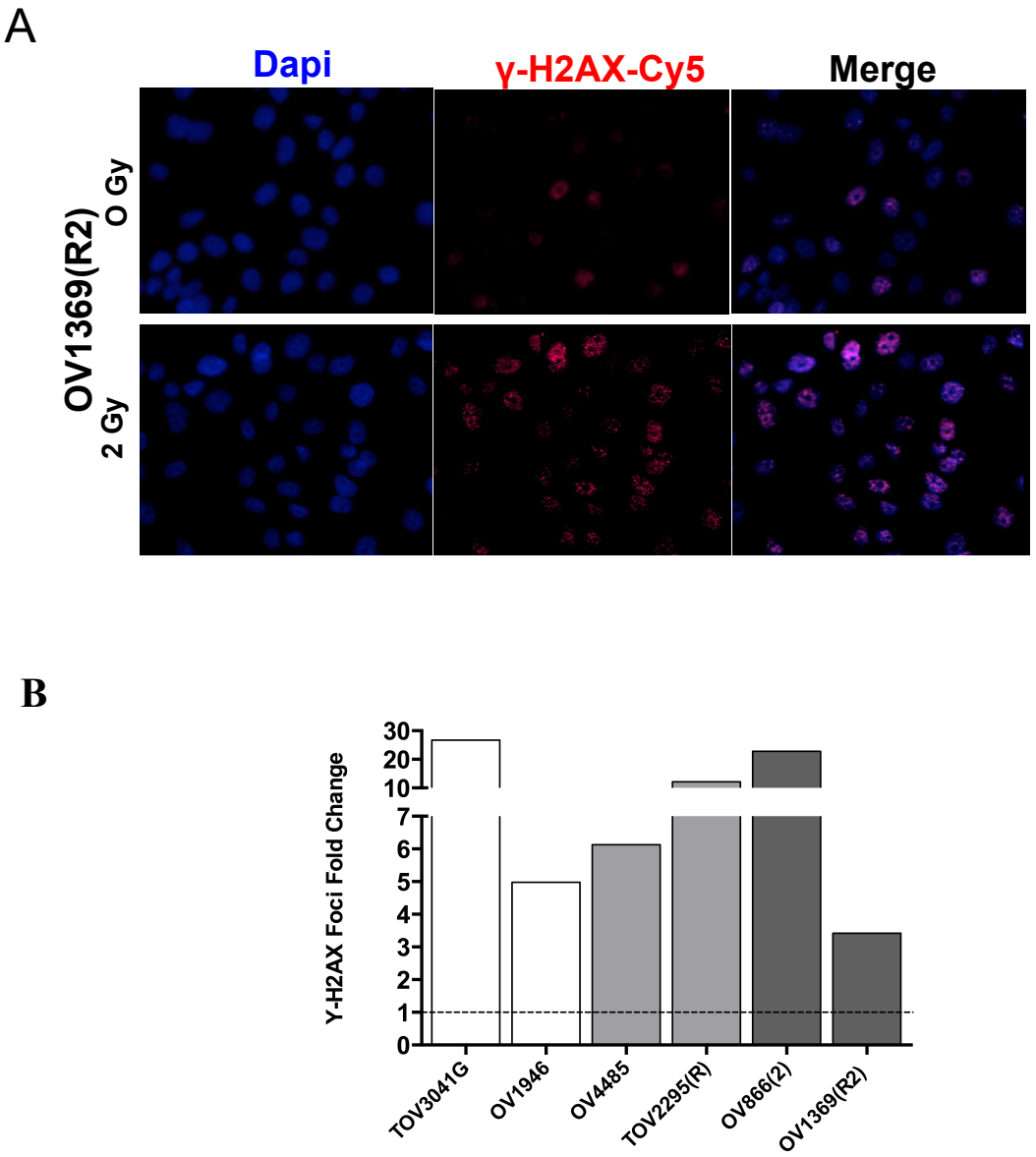

Figure S2: Evaluation of γ-H2AX foci formation after gamma-irradiation. (A) Representative images of γ-H2AX (red) and nuclear DAPI (blue) staining in resistant OV1369(R2) cell line after 2Gy irradiation. Images are at 400 X magnification. (B) Evaluation of DNA DSB induction by γ-H2AX immunocytochemistry. Nuclear foci were counted 1 hour after exposure to 2Gy gamma-irradiation in six cell lines of known HR status and Olaparib response. Fold change was calculated as a ratio between percentages of γ-H2AX foci in radiated cells over control non-irradiated cells from one experiment.

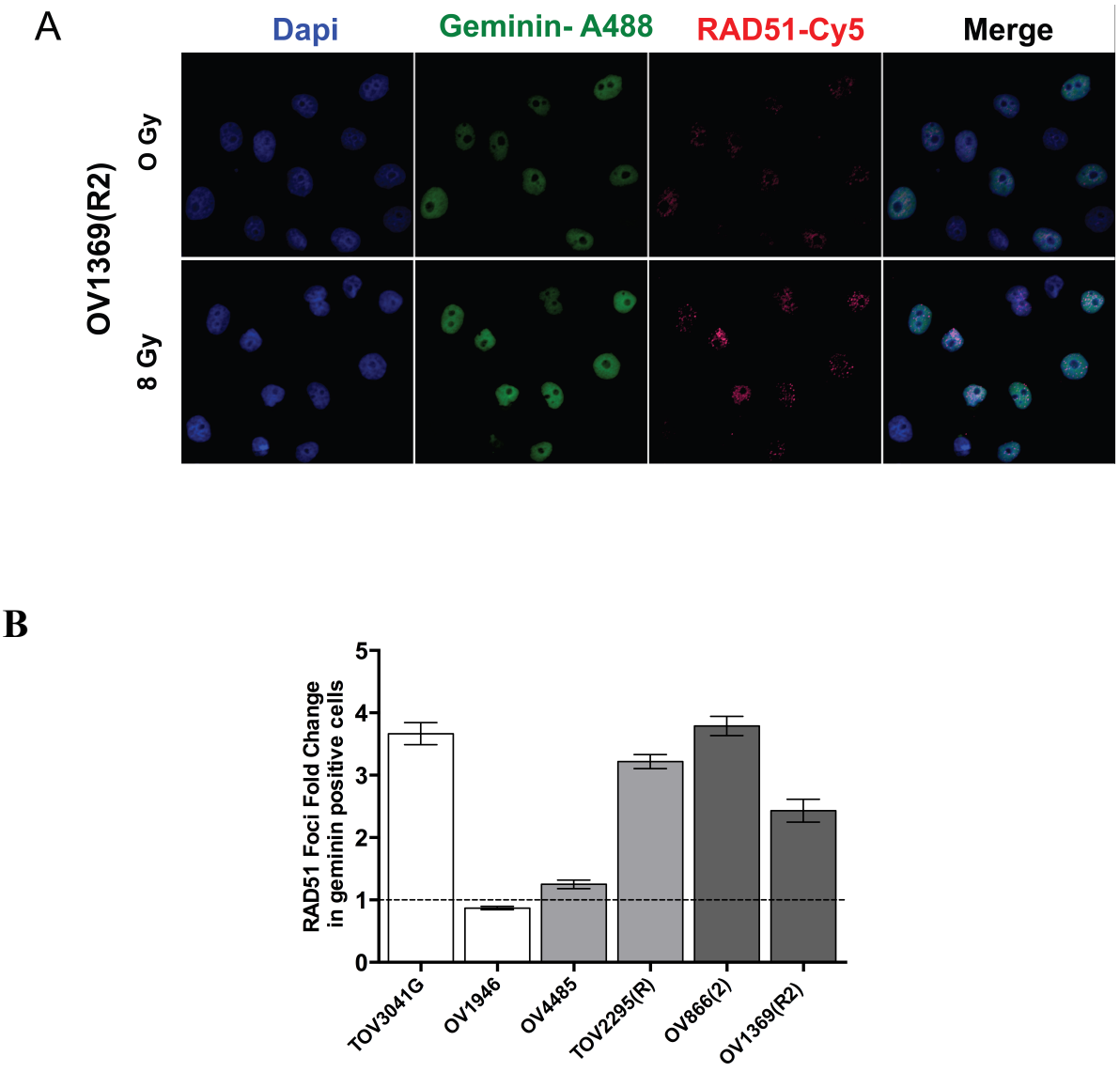

Figure S3: Evaluation of RAD51 foci in geminin positive cells. (A) Representative images of RAD51 (red) and geminin (green) co-immunostaining, and nuclear DAPI (blue) after 8 Gy irradiation in resistant OV1369(R2) cell line. Images are at 400 X magnification. (B) Evaluation of HR response by RAD51 immunocytochemistry. Nuclear foci were counted 2 hours after exposure to 8 Gy gamma-radiation, and then compared and presented as percentage of the control group (non-irradiated) in geminin positive cells. Fold change was calculated as a ratio between percentages of RAD51 foci in treated over control non-treated cells. Bars represent average ± SEM from two independent experiments (n=2).

Figure S4: Western blots demonstrating decreased protein expression by siRNA knockdowns in resistant cell line OV1369(R2). Wells 1, 2, 3 and 4 correspond to four different siRNA sequences used against each gene (*ERCC8*, *MLH3*, *MLH1* or *MRE11A*). Control = non-treated cells, siScr = negative siRNA control using a scrambled sequence.

A

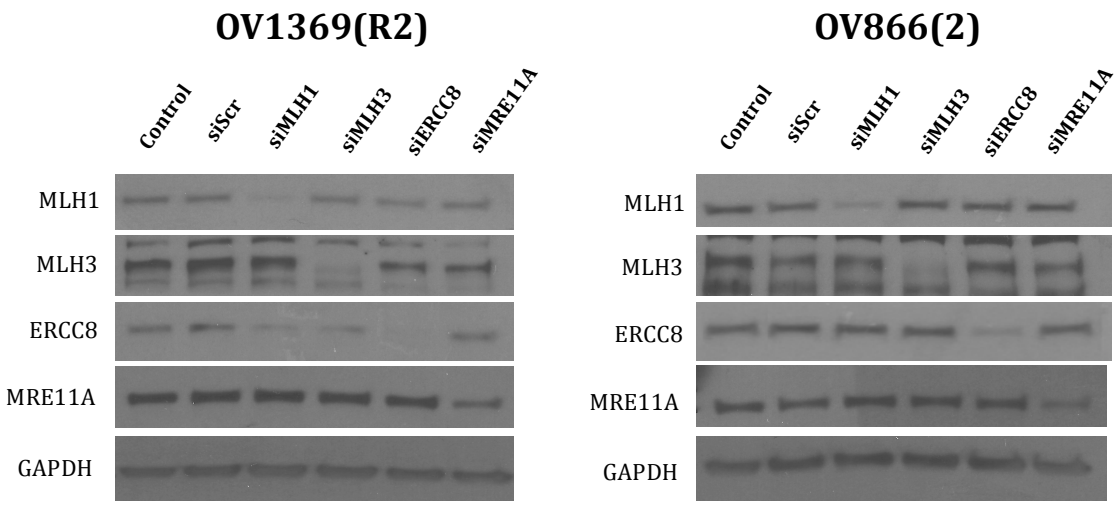

B

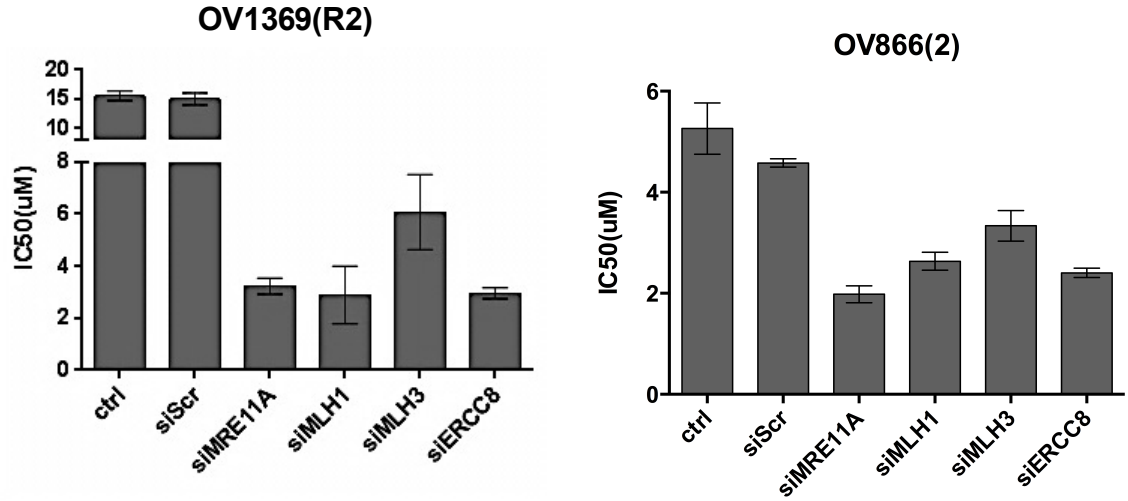

Figure S5: Gene knockdown validation using a different siRNA sequence for each target. (A) Efficacy of siRNAs against *MLH1*, *MLH3*, *ERCC8* and *MRE11A* in OV1369(R2) and OV866(2) was verified by Western blot. Control = non-treated cells, siScr = negative siRNA control using a scrambled sequence. (B) Increased Olaparib sensitivity of OV1369(R2) and OV866(2) with siRNAs against *MRE11A*, *MLH1*, *MLH3* and *ERCC8*, assayed by clonogenic assay. Bars represent average ± SEM of IC_{50} values obtained by clonogenic assay in two independent experiments (n=2).

A

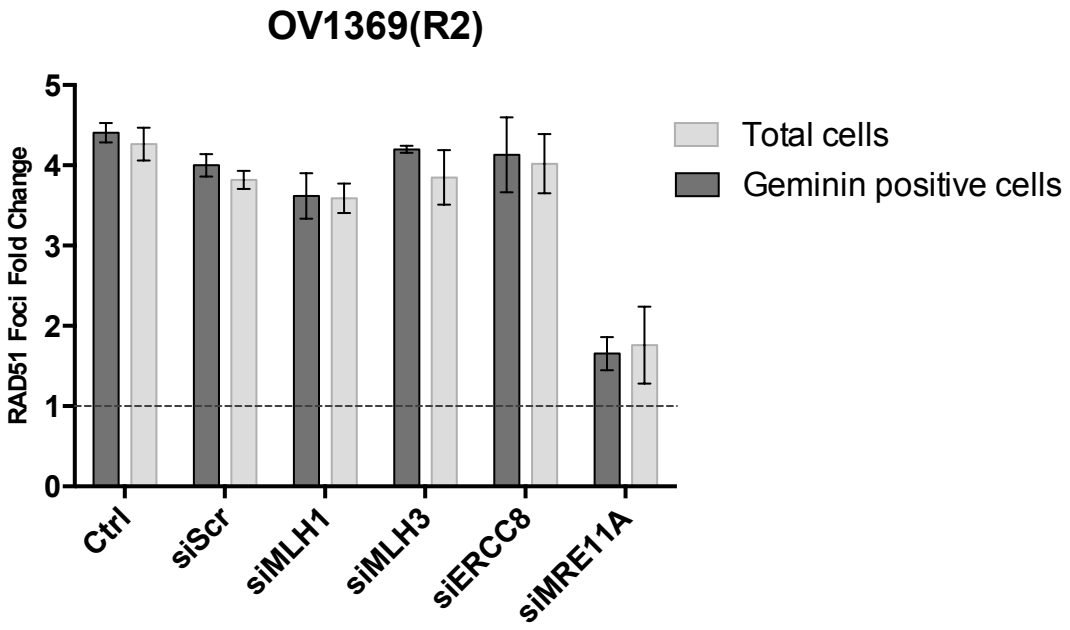

B

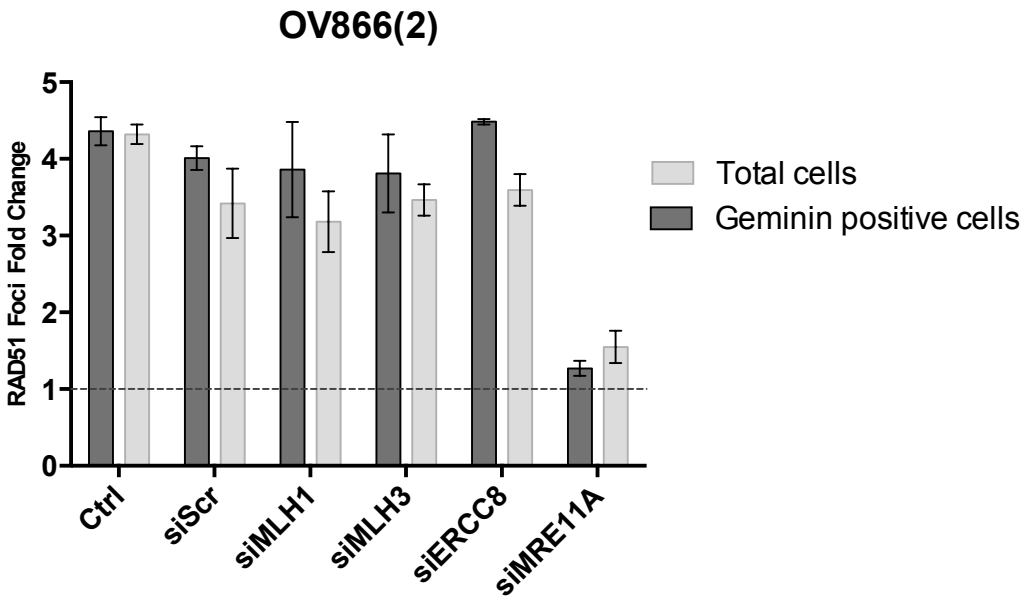

Figure S6: HR function after gene knockdown. HR response was evaluated by RAD51 foci analyses in OV1369(R2) (A) and OV866(2) (B) treated with the same siRNA sequences used in Figures 3 and 4. Nuclear foci were counted 2 hours after exposure to 8 Gy gamma-radiation, and then compared and presented as a percentage of the control group (non-irradiated) in geminin positive (G2/M phase) cells and total cells. Fold change was calculated as a ratio between percentages of RAD51 foci in treated cells over control non-treated cells. Bars represent average ± SEM from two independent experiments (n=2).

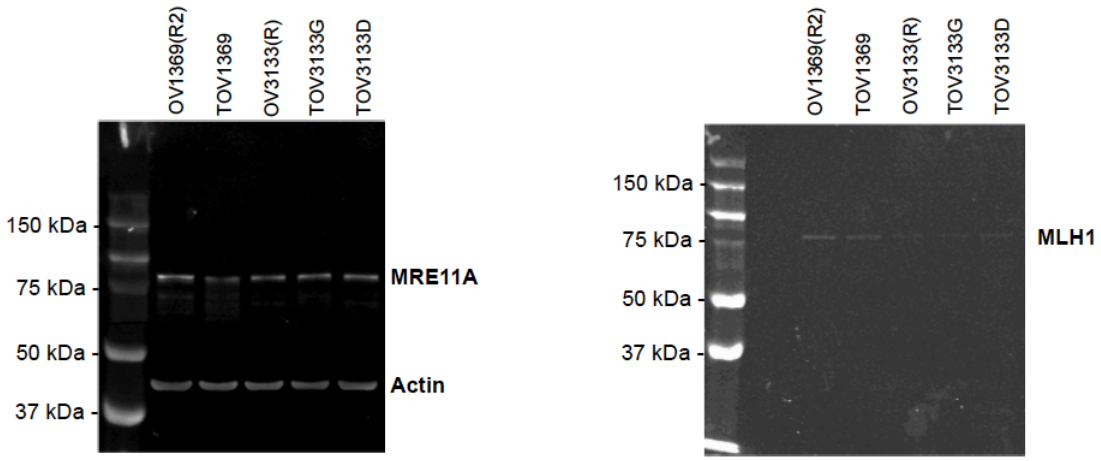

Figure S7: Western blot validation of antibodies against MRE11A and MLH1 used for immunohistochemistry analysis of HGS EOC in TMAs. Each well was loaded with 30 μg total cell lysate of HGS EOC cell lines. Actin represents protein loading control.

Table S I: List of DNA repair genes and Affymetrix probes used in our comparison analysis.

Gene	Probesets
APEX1	210027_s_at
APEX2	204408_at
APTX	218527_at
ATM	208442_s_at, 210858_x_at, 212672_at
ATR	209902_at, 209903_s_at
ATRIP	205875_s_at, 34689_at
BLM	205733_at
BRCA1	204531_s_at, 211851_x_at
BRCA2	208368_s_at, 214727_at
BRIP1	221703_at
C19orf40	214816_x_at
CCNH	204093_at
CDK7	211297_s_at
CETN2	209194_at
CHAF1A	203975_s_at, 203976_s_at, 214426_x_at
CHEK1	205393_s_at, 205394_at
CHEK2	210416_s_at
CLK2	203229_s_at
DCLRE1A	209804_at
DCLRE1B	219490_s_at
DCLRE1C	219678_x_at, 222233_s_at
DDB1	208619_at
DDB2	203409_at
DMC1	208382_s_at, 208386_x_at

Gene	Probesets
PALB2	219530_at
PARP1	208644_at
PARP2	204752_x_at, 214086_s_at, 215773_x_at
PARP3	209940_at
PCNA	201202_at
PER1	202861_at, 36829_at
PMS1	213677_s_at
PMS2	209805_at, 221206_at
PMS2L3	214473_x_at, 216111_x_at, 216525_x_at
PNKP	218961_s_at
POLB	203616_at
POLD1	203422_at
POLE	216026_s_at
POLG	203366_at, 217635_s_at
POLH	219380_x_at
POLI	219317_at
POLL	221049_s_at
POLM	222238_s_at
POLQ	207746_at, 219510_at
PRKDC	208694_at, 210543_s_at, 215757_at
PRPF19	203103_s_at
PTEN	204053_x_at, 204054_at, 211711_s_at
RAD1	204460_s_at, 204461_x_at, 210216_x_at
RAD17	207405_s_at, 210826_x_at, 211228_s_at

DUT	208955_at, 208956_x_at, 209932_s_at
ERCC1	203719_at, 203720_s_at
ERCC2	213468_at
ERCC3	202176_at
ERCC4	210158_at
ERCC5	202414_at
ERCC6	207347_at
ERCC8	205162_at
EXO1	204603_at
FANCA	203805_s_at, 203806_s_at, 215530_at
FANCC	205189_s_at
FANCE	220255_at
FANCF	218689_at
FANCG	203564_at
FANCI	213007_at, 213008_at
FANCL	218397_at
FEN1	204767_s_at, 204768_s_at
GIYD1	218317_x_at
GTF2H1	202451_at, 202453_s_at
GTF2H2	221540_x_at
GTF2H3	222104_x_at
GTF2H4	203577_at
GTF2H5	213357_at
H2AFX	205436_s_at, 212524_x_at, 212525_s_at, 213344_s_at
HLTF	202983_at
HUS1	204883_s_at, 204884_s_at, 217618_x_at
LIG1	202726_at
LIG3	204123_at, 207348_s_at
LIG4	206235_at

RAD23A	201039_s_at, 201046_s_at
RAD23B	214422_at
RAD23B	201222_s_at, 201223_s_at
RAD50	208393_s_at, 209349_at
RAD51	205023_at, 205024_s_at
RAD51C	206066_s_at, 209849_s_at
RAD51L1	210255_at, 216880_at
RAD51L3	209965_s_at, 37793_r_at
RAD52	205647_at, 210630_s_at, 211904_x_at
RAD54B	220549_at
RAD54B	219494_at
RAD54L	204558_at
RAD9A	204828_at
RBBP8	203344_s_at
RECQL	205091_x_at, 210568_s_at, 212917_x_at, 212918_at
RECQL4	213520_at
RECQL5	210309_at, 211468_s_at, 221686_s_at, 34063_at
REV1	218428_s_at
REV3L	208070_s_at
RFC1	208021_s_at
RNF4	212696_s_at
RNF8	203160_s_at, 203161_s_at
RPA1	201528_at, 201529_s_at
RPA2	201756_at
RPA3	209507_at
RPA4	221143_at
SETMAR	206554_x_at
SHFM1	202276_at
SMUG1	218685_s_at

MBD4	209579_s_at, 209580_s_at, 214047_s_at, 214048_at
MDC1	203061_s_at, 203062_s_at
MGMT	204880_at
MLH1	202520_s_at
MLH3	204838_s_at, 214525_x_at, 217216_x_at
MMS19	202167_s_at
MNAT1	203565_s_at
MPG	203686_at
MRE11A	205395_s_at, 211334_at
MSH2	209421_at
MSH3	205887_x_at, 210947_s_at
MSH4	210533_at
MSH5	210410_s_at, 212913_at
MSH6	202911_at, 211449_at, 211450_s_at
MTMR15	203678_at
MUS81	218463_s_at
MUTYH	207727_s_at
NBN	202905_x_at, 202906_s_at, 202907_s_at, 217299_s_at
NEIL1	219396_s_at
NEIL3	219502_at
NHEJ1	219418_at
NTHL1	209731_at
NUDT1	204766_s_at
OBFC2B	218903_s_at
OGG1	205301_s_at, 205760_s_at

TADA3L	215272_at
TDG	203742_s_at
TDG	203743_s_at
TDP1	219715_s_at
TOPBP1	202633_at
TP53	201746_at, 211300_s_at
TP53BP1	203050_at
TREX2	207891_s_at
TTRAP	202266_at
UBE2A	201898_s_at, 201899_s_at
UBE2B	202333_s_at, 202334_s_at, 202335_s_at, 211763_s_at
UBE2N	201523_x_at, 201524_x_at, 212751_at
UBE2V2	209096_at
UNG	202330_s_at
WRN	205667_at
XAB2	218110_at
XPA	205672_at
XPC	209375_at
XRCC1	203655_at
XRCC2	207598_x_at
XRCC3	216299_s_at
XRCC4	205071_x_at, 205072_s_at, 210812_at, 210813_s_at
XRCC5	208642_s_at, 208643_s_at
XRCC6	200792_at, 215308_at

Table S II: DNA sequences of siRNAs used in this study

siERCC8	1	GUAAAGCAGUGUGUUCCAU
	2	CAGACAAUCUUAUUACACA
	3	CAUCAUAUGUCUCCAGUCU
	4	GAUUGUACUUUAUGACCUU
siMLH1	1	GGAAGUUGUUGGAGGUAU
	2	CCAGAUGGUUCGUACAGAU
	3	GAAGUAGUGAUAAGGUCUA
	4	UAUCUUCAUUCUUCGACUA
siMLH3	1	CCAAACCAAUCGUCCGUAA
	2	GCUGAGAGCUUAGCAGUUA
	3	ACACAGAGUUCUAGGGAUU
	4	AGACAGGUUUCCAAUGAUA
siMRE11A	1	GGAGGUACGUCGUUUCAGA
	2	GGAAAUGAUACGUUUGUAA
	3	CGAAAUGUCACUACUAAGA
	4	GAAAGGCUCUAUCGAAUGU
siScramble	1	UCACAACCUCCUAGAAAGAGUAGA

2.2.2.10 References

1. Siegel RL, Miller KD and Jemal A. Cancer statistics, 2015. CA Cancer J Clin. 2015; 65(1):5-29.
2. R.R. B, M. M and M. R. (2009). Principles and Practice of Gynecologic Oncology: Wolters Kluwer).
3. Tan DS and Kaye SB. Chemotherapy for Patients with *BRCA1* and *BRCA2*-Mutated Ovarian Cancer: Same or Different? Am Soc Clin Oncol Educ Book. 2015:114-121.
4. Coleman MP, Forman D, Bryant H, Butler J, Rachet B, Maringe C, Nur U, Tracey E, Coory M, Hatcher J, McGahan CE, Turner D, Marrett L, Gjerstorff ML, Johannesen TB, Adolfsson J, et al. Cancer survival in Australia, Canada, Denmark, Norway, Sweden, and the UK, 1995-2007 (the International Cancer Benchmarking Partnership): an analysis of population-based cancer registry data. Lancet. 2011; 377(9760):127-138.
5. McGuire WP. Maintenance therapy for ovarian cancer: of Helsinki and Hippocrates. J Clin Oncol. 2009; 27(28):4633-4634.
6. Itamochi H and Kigawa J. Clinical trials and future potential of targeted therapy for ovarian cancer. Int J Clin Oncol. 2012; 17(5):430-440.
7. Feng FY, de Bono JS, Rubin MA and Knudsen KE. Chromatin to Clinic: The Molecular Rationale for PARP1 Inhibitor Function. Mol Cell. 2015; 58(6):925-934.
8. Konstantinopoulos PA, Ceccaldi R, Shapiro GI and D'Andrea AD. Homologous Recombination Deficiency: Exploiting the Fundamental Vulnerability of Ovarian Cancer. Cancer Discov. 2015; 5(11):1137-1154.
9. Scott CL, Swisher EM and Kaufmann SH. Poly (ADP-ribose) polymerase inhibitors: recent advances and future development. J Clin Oncol. 2015; 33(12):1397-1406.
10. Ashworth A. A synthetic lethal therapeutic approach: poly(ADP) ribose polymerase inhibitors for the treatment of cancers deficient in DNA double-strand break repair. J Clin Oncol. 2008; 26(22):3785-3790.
11. Tutt A and Ashworth A. The relationship between the roles of BRCA genes in DNA repair and cancer predisposition. Trends Mol Med. 2002; 8(12):571-576.
12. Gelmon KA, Tischkowitz M, Mackay H, Swenerton K, Robidoux A, Tonkin K, Hirte H, Huntsman D, Clemons M, Gilks B, Yerushalmi R, Macpherson E, Carmichael J and Oza A. Olaparib in patients with recurrent high-grade serous or poorly differentiated ovarian carcinoma or triple-negative breast cancer: a phase 2, multicentre, open-label, non-randomised study. Lancet Oncol. 2011; 12(9):852-861.
13. Ledermann J, Harter P, Gourley C, Friedlander M, Vergote I, Rustin G, Scott C, Meier W, Shapira-Frommer R, Safra T, Matei D, Macpherson E, Watkins C, Carmichael J and Matulonis U. Olaparib maintenance therapy in platinum-sensitive relapsed ovarian cancer. N Engl J Med. 2012; 366(15):1382-1392.
14. Ledermann J, Harter P, Gourley C, Friedlander M, Vergote I, Rustin G, Scott CL, Meier W, Shapira-Frommer R, Safra T, Matei D, Fielding A, Spencer S, Dougherty B, Orr M,

Hodgson D, et al. Olaparib maintenance therapy in patients with platinum-sensitive relapsed serous ovarian cancer: a preplanned retrospective analysis of outcomes by BRCA status in a randomised phase 2 trial. Lancet Oncol. 2014; 15(8):852-861.
15. Turner N, Tutt A and Ashworth A. Hallmarks of 'BRCAness' in sporadic cancers. Nat Rev Cancer. 2004; 4(10):814-819.
16. Loveday C, Turnbull C, Ramsay E, Hughes D, Ruark E, Frankum JR, Bowden G, Kalmyrzaev B, Warren-Perry M, Snape K, Adlard JW, Barwell J, Berg J, Brady AF, Brewer C, Brice G, et al. Germline mutations in RAD51D confer susceptibility to ovarian cancer. Nat Genet. 2011; 43(9):879-882.
17. Kalev P, Simicek M, Vazquez I, Munck S, Chen L, Soin T, Danda N, Chen W and Sablina A. Loss of PPP2R2A inhibits homologous recombination DNA repair and predicts tumor sensitivity to PARP inhibition. Cancer Res. 2012; 72(24):6414-6424.
18. Network TCGAR. Integrated genomic analyses of ovarian carcinoma. Nature. 2011; 474(7353):609-615.
19. Mukhopadhyay A, Elattar A, Cerbinskaite A, Wilkinson SJ, Drew Y, Kyle S, Los G, Hostomsky Z, Edmondson RJ and Curtin NJ. Development of a functional assay for homologous recombination status in primary cultures of epithelial ovarian tumor and correlation with sensitivity to poly(ADP-ribose) polymerase inhibitors. Clin Cancer Res. 2010; 16(8):2344-2351.
20. Mukhopadhyay A, Plummer ER, Elattar A, Soohoo S, Uzir B, Quinn JE, McCluggage WG, Maxwell P, Aneke H, Curtin NJ and Edmondson RJ. Clinicopathological features of homologous recombination-deficient epithelial ovarian cancers: sensitivity to PARP inhibitors, platinum, and survival. Cancer Res. 2012; 72(22):5675-5682.
21. Kim G, Ison G, McKee AE, Zhang H, Tang S, Gwise T, Sridhara R, Lee E, Tzou A, Philip R, Chiu HJ, Ricks TK, Palmby T, Russell AM, Ladouceur G, Pfuma E, et al. FDA Approval Summary: Olaparib Monotherapy in Patients with Deleterious Germline BRCA-Mutated Advanced Ovarian Cancer Treated with Three or More Lines of Chemotherapy. Clin Cancer Res. 2015; 21(19):4257-4261.
22. Fleury H, Communal L, Carmona E, Portelance L, Arcand SL, Rahimi K, Tonin PN, Provencher D and Mes-Masson AM. Novel high-grade serous epithelial ovarian cancer cell lines that reflect the molecular diversity of both the sporadic and hereditary disease. Genes Cancer. 2015; 6(9-10):378-398.
23. Letourneau IJ, Quinn MC, Wang LL, Portelance L, Caceres KY, Cyr L, Delvoye N, Meunier L, de Ladurantaye M, Shen Z, Arcand SL, Tonin PN, Provencher DM and Mes-Masson AM. Derivation and characterization of matched cell lines from primary and recurrent serous ovarian cancer. BMC Cancer. 2012; 12:379.
24. Ouellet V, Zietarska M, Portelance L, Lafontaine J, Madore J, Puiffe ML, Arcand SL, Shen Z, Hebert J, Tonin PN, Provencher DM and Mes-Masson AM. Characterization of three new serous epithelial ovarian cancer cell lines. BMC Cancer. 2008; 8:152.

25. Provencher DM, Lounis H, Champoux L, Tetrault M, Manderson EN, Wang JC, Eydoux P, Savoie R, Tonin PN and Mes-Masson AM. Characterization of four novel epithelial ovarian cancer cell lines. In Vitro Cell Dev Biol Anim. 2000; 36(6):357-361.
26. Daemen A, Wolf DM, Korkola JE, Griffith OL, Frankum JR, Brough R, Jakkula LR, Wang NJ, Natrajan R, Reis-Filho JS, Lord CJ, Ashworth A, Spellman PT, Gray JW and Van't Veer LJ. Cross-platform pathway-based analysis identifies markers of response to the PARP inhibitor Olaparib. Breast Cancer Res Treat. 2012; 135(2):505-517.
27. McCabe N, Turner NC, Lord CJ, Kluzek K, Bialkowska A, Swift S, Giavara S, O'Connor MJ, Tutt AN, Zdzienicka MZ, Smith GC and Ashworth A. Deficiency in the repair of DNA damage by homologous recombination and sensitivity to poly(ADP-ribose) polymerase inhibition. Cancer Res. 2006; 66(16):8109-8115.
28. Oplustilova L, Wolanin K, Mistrik M, Korinkova G, Simkova D, Bouchal J, Lenobel R, Bartkova J, Lau A, O'Connor MJ, Lukas J and Bartek J. Evaluation of candidate biomarkers to predict cancer cell sensitivity or resistance to PARP1 inhibitor treatment. Cell Cycle. 2012; 11(20):3837-3850.
29. Fong PC, Yap TA, Boss DS, Carden CP, Mergui-Roelvink M, Gourley C, De Greve J, Lubinski J, Shanley S, Messiou C, A'Hern R, Tutt A, Ashworth A, Stone J, Carmichael J, Schellens JH, et al. Poly(ADP)-ribose polymerase inhibition: frequent durable responses in BRCA carrier ovarian cancer correlating with platinum-free interval. J Clin Oncol. 2010; 28(15):2512-2519.
30. Driessens N, Versteyhe S, Ghaddhab C, Burniat A, De Deken X, Van Sande J, Dumont JE, Miot F and Corvilain B. Hydrogen peroxide induces DNA single- and double-strand breaks in thyroid cells and is therefore a potential mutagen for this organ. Endocr Relat Cancer. 2009; 16(3):845-856.
31. Al-Ejeh F, Kumar R, Wiegmans A, Lakhani SR, Brown MP and Khanna KK. Harnessing the complexity of DNA-damage response pathways to improve cancer treatment outcomes. Oncogene. 2010; 29(46):6085-6098.
32. Shah MM, Dobbin ZC, Nowsheen S, Wielgos M, Katre AA, Alvarez RD, Konstantinopoulos PA, Yang ES and Landen CN. An ex vivo assay of XRT-induced Rad51 foci formation predicts response to PARP-inhibition in ovarian cancer. Gynecol Oncol. 2014; 134(2):331-337.
33. Clague J, Wilhoite G, Adamson A, Bailis A, Weitzel JN and Neuhausen SL. RAD51C germline mutations in breast and ovarian cancer cases from high-risk families. PLoS One. 2011; 6(9):e25632.
34. Dedes KJ, Wetterskog D, Mendes-Pereira AM, Natrajan R, Lambros MB, Geyer FC, Vatcheva R, Savage K, Mackay A, Lord CJ, Ashworth A and Reis-Filho JS. PTEN deficiency in endometrioid endometrial adenocarcinomas predicts sensitivity to PARP inhibitors. Sci Transl Med. 2010; 2(53):53ra75.
35. Podhorecka M, Skladanowski A and Bozko P. H2AX Phosphorylation: Its Role in DNA Damage Response and Cancer Therapy. J Nucleic Acids. 2010; 2010.

36. Naipal KA, Verkaik NS, Ameziane N, van Deurzen CH, Ter Brugge P, Meijers M, Sieuwerts AM, Martens JW, O'Connor MJ, Vrieling H, Hoeijmakers JH, Jonkers J, Kanaar R, de Winter JP, Vreeswijk MP, Jager A, et al. Functional ex vivo assay to select homologous recombination-deficient breast tumors for PARP inhibitor treatment. Clin Cancer Res. 2014; 20(18):4816-4826.
37. Kroll KL. Geminin in embryonic development: coordinating transcription and the cell cycle during differentiation. Front Biosci. 2007; 12:1395-1409.
38. Wang X and Weaver DT. The ups and downs of DNA repair biomarkers for PARP inhibitor therapies. Am J Cancer Res. 2011; 1(3):301-327.
39. Horton JK, Stefanick DF, Prasad R, Gassman NR, Kedar PS and Wilson SH. Base excision repair defects invoke hypersensitivity to PARP inhibition. Mol Cancer Res. 2014; 12(8):1128-1139.
40. Patel AG, Sarkaria JN and Kaufmann SH. Nonhomologous end joining drives poly(ADP-ribose) polymerase (PARP) inhibitor lethality in homologous recombination-deficient cells. Proc Natl Acad Sci U S A. 2011; 108(8):3406-3411.
41. Curtin NJ, Wang LZ, Yiakouvaki A, Kyle S, Arris CA, Canan-Koch S, Webber SE, Durkacz BW, Calvert HA, Hostomsky Z and Newell DR. Novel poly(ADP-ribose) polymerase-1 inhibitor, AG14361, restores sensitivity to temozolomide in mismatch repair-deficient cells. Clin Cancer Res. 2004; 10(3):881-889.
42. Postel-Vinay S, Bajrami I, Friboulet L, Elliott R, Fontebasso Y, Dorvault N, Olaussen KA, Andre F, Soria JC, Lord CJ and Ashworth A. A high-throughput screen identifies PARP1/2 inhibitors as a potential therapy for ERCC1-deficient non-small cell lung cancer. Oncogene. 2013; 32(47):5377-5387.
43. Vilar E, Bartnik CM, Stenzel SL, Raskin L, Ahn J, Moreno V, Mukherjee B, Iniesta MD, Morgan MA, Rennert G and Gruber SB. MRE11 deficiency increases sensitivity to poly(ADP-ribose) polymerase inhibition in microsatellite unstable colorectal cancers. Cancer Res. 2011; 71(7):2632-2642.
44. Zhao H, Thienpont B, Yesilyurt BT, Moisse M, Reumers J, Coenegrachts L, Sagaert X, Schrauwen S, Smeets D, Matthijs G, Aerts S, Cools J, Metcalf A, Spurdle A, Amant F and Lambrechts D. Mismatch repair deficiency endows tumors with a unique mutation signature and sensitivity to DNA double-strand breaks. Elife. 2014; 3:e02725.
45. Sameer AS, Nissar S and Fatima K. Mismatch repair pathway: molecules, functions, and role in colorectal carcinogenesis. Eur J Cancer Prev. 2014; 23(4):246-257.
46. Ceccaldi R, O'Connor KW, Mouw KW, Li AY, Matulonis UA, D'Andrea AD and Konstantinopoulos PA. A unique subset of epithelial ovarian cancers with platinum sensitivity and PARP inhibitor resistance. Cancer Res. 2015; 75(4):628-634.
47. Zhang Y, Rohde LH and Wu H. Involvement of nucleotide excision and mismatch repair mechanisms in double strand break repair. Curr Genomics. 2009; 10(4):250-258.
48. Martin SA, Lord CJ and Ashworth A. Therapeutic targeting of the DNA mismatch repair pathway. Clin Cancer Res. 2010; 16(21):5107-5113.

49. Robu M, Shah RG, Petitclerc N, Brind'Amour J, Kandan-Kulangara F and Shah GM. Role of poly(ADP-ribose) polymerase-1 in the removal of UV-induced DNA lesions by nucleotide excision repair. Proc Natl Acad Sci U S A. 2013; 110(5):1658-1663.
50. Ko HL and Ren EC. Functional Aspects of PARP1 in DNA Repair and Transcription. Biomolecules. 2012; 2(4):524-548.
51. Lord CJ, McDonald S, Swift S, Turner NC and Ashworth A. A high-throughput RNA interference screen for DNA repair determinants of PARP inhibitor sensitivity. DNA Repair (Amst). 2008; 7(12):2010-2019.
52. Fleming ND, Agadjanian H, Nassanian H, Miller CW, Orsulic S, Karlan BY and Walsh CS. Xeroderma pigmentosum complementation group C single-nucleotide polymorphisms in the nucleotide excision repair pathway correlate with prolonged progression-free survival in advanced ovarian cancer. Cancer. 2012; 118(3):689-697.
53. Martin LP, Hamilton TC and Schilder RJ. Platinum resistance: the role of DNA repair pathways. Clin Cancer Res. 2008; 14(5):1291-1295.
54. Audeh MW, Carmichael J, Penson RT, Friedlander M, Powell B, Bell-McGuinn KM, Scott C, Weitzel JN, Oaknin A, Loman N, Lu K, Schmutzler RK, Matulonis U, Wickens M and Tutt A. Oral poly(ADP-ribose) polymerase inhibitor Olaparib in patients with *BRCA1* or *BRCA2* mutations and recurrent ovarian cancer: a proof-of-concept trial. Lancet. 2010; 376(9737):245-251.
55. Lord CJ, Tutt AN and Ashworth A. Synthetic lethality and cancer therapy: lessons learned from the development of PARP inhibitors. Annu Rev Med. 2015; 66:455-470.
56. Shah GM, Kandan-Kulangara F, Montoni A, Shah RG, Brind'amour J, Vodenicharov MD and Affar el B. Approaches to detect PARP1 activation in vivo, in situ, and in vitro. Methods Mol Biol. 2011; 780:3-34.
57. Beucher A, Birraux J, Tchouandong L, Barton O, Shibata A, Conrad S, Goodarzi AA, Krempler A, Jeggo PA and Lobrich M. ATM and Artemis promote homologous recombination of radiation-induced DNA double-strand breaks in G2. EMBO J. 2009; 28(21):3413-3427.
58. Redon CE, Dickey JS, Bonner WM and Sedelnikova OA. gamma-H2AX as a biomarker of DNA damage induced by ionizing radiation in human peripheral blood lymphocytes and artificial skin. Adv Space Res. 2009; 43(8):1171-1178.
59. Gambaro K, Quinn MC, Caceres-Gorriti KY, Shapiro RS, Provencher D, Rahimi K, Mes-Masson AM and Tonin PN. Low levels of IGFBP7 expression in high-grade serous ovarian carcinoma is associated with patient outcome. BMC Cancer. 2015; 15:135.
60. Zietarska M, Maugard CM, Filali-Mouhim A, Alam-Fahmy M, Tonin PN, Provencher DM and Mes-Masson AM. Molecular description of a 3D in vitro model for the study of epithelial ovarian cancer (EOC). Mol Carcinog. 2007; 46(10):872-885.
61. Cody NA, Ouellet V, Manderson EN, Quinn MC, Filali-Mouhim A, Tellis P, Zietarska M, Provencher DM, Mes-Masson AM, Chevrette M and Tonin PN. Transfer of chromosome 3

fragments suppresses tumorigenicity of an ovarian cancer cell line monoallelic for chromosome 3p. Oncogene. 2007; 26(4):618-632.
62. Arcand SL, Mes-Masson AM, Provencher D, Hudson TJ and Tonin PN. Gene expression microarray analysis and genome databases facilitate the characterization of a chromosome 22 derived homogeneously staining region. Mol Carcinog. 2004; 41(1):17-38.
63. Koti M, Siu A, Clement I, Bidarimath M, Turashvili G, Edwards A, Rahimi K, Masson AM and Squire JA. A distinct pre-existing inflammatory tumour microenvironment is associated with chemotherapy resistance in high-grade serous epithelial ovarian cancer. Br J Cancer. 2015; 112(7):1215-1222.

2.3 Chapitre 3 : PARP inhibitors elicit a reversible cancer senescence state targetable by senolytics

2.3.1 Article #3: Résumé en français

Titre en français : Les inhibiteurs de PARP induisent un état de sénescence-type réversible pouvant être ciblé par des sénolytiques.

La sénescence cellulaire est un mécanisme suppresseur de tumeur défini par un arrêt de prolifération stable. Cependant, particulièrement dans les cellules cancéreuses, l'idée selon laquelle cette sénescence est obligatoirement irréversible est de plsu en plus controversée, Ici, nous montrons que les inhibiteurs de poly (ADP-ribose) polymérase induisent une sénescence indépendante de p53 mais présentant la plupart des marqueurs phénotypiques spécifiques (SA-SCARS et SA-sécrétome). Le mécanisme implique l'activation de Chk2 et p21 induite par les dommages à l'ADN. Cependant, contrairement à la sénescence traditionnelle, les cellules cancéreuses de type senescent ne quittent jamais complètement le cycle cellulaire et conservent la capacité de ré-initier la prolifération lors du sevrage thérapeutique, ce qui pourrait expliquer la nécessité d'utuliser les inhibiteurs de PARP en maintenance. Fait important, cet état de type senescent induit par les inhibiteurs de PARP rend les cellules cancéreuses synergiquement sensibles à la plupart des sénolytiques. Dans l'ensemble, nous démontrons que les réponses au traitement du cancer mimant la sénescence peuvent être ciblées en utilisant des stratégies de létalité synthétique dirigées contre la sénescence permettant d'augmenter l'efficacité des médicaments anticancéreux utilisés en clinique.

2.3.2 Article #3: Version originale en préparation

PARP inhibitors elicit a reversible cancer senescence state targetable by senolytics.

Hubert Fleury[1,2]*, Nicolas Malaquin[1,2]*, Aurelie Martinez[1,2], Alexandre Sauriol[1,2], Euridice Carmona[1,2], Diane Provencher[1,2,3], Anne-Marie Mes-Masson[1,2,4#] and Francis Rodier[1,2,5#]

* These authors contributed equally

[1] Centre de recherche du Centre hospitalier de l'Université de Montréal (CRCHUM), Montreal, QC, Canada

[2] Institut du cancer de Montréal, Montreal, QC, Canada

[3] Division of Gynecologic Oncology, Université de Montréal, Montreal, QC, Canada

[4] Department of Medicine, Université de Montréal, Montreal, QC, Canada

[5] Department of Radiology, Radio-Oncology and Nuclear Medicine, Université de Montréal, Montreal, QC, Canada

Corresponding authors:

Francis Rodier, CRCHUM, R10-420, 900 Rue St-Denis, Montreal, Quebec, H2X 0A9,Canada. Phone: (514) 890-8000 ext 26939. Email: francis.rodier@umontreal.ca, rodierf@mac.com

Anne-Marie Mes-Masson, CRCHUM, R10-456, 900 rue St-Denis, Montreal, Quebec, Canada, H2X 0A9. Phone: (514) 890-8000 ext. 25496. E-mail: anne-marie.mes-masson@umontreal.ca

Keywords: Senescence, Olaparib, PARP1 inhibitors, cell growth arrest, combination therapy

2.3.2.1 Abstract

Cellular senescence is a tumor suppression mechanisms defined by stable proliferation arrest. Whether senescence, particularly when triggered in cancer cells, is irreversible, remains controversial. Here we show that Poly (ADP-ribose) polymerase1 inhibitors (PARPi) trigger p53-independent therapy-induced cancer senescence (TIS) displaying most senescence-associated (SA) phenotypic hallmarks including DNA-SCARS and SA-secretome. Mechanism involves Chk2 and p21 activation induced by DNA damage. However, unlike traditional senescence, TIS-like cancer cells never completely exit the cell cycle and retain the ability to re-initiate proliferation upon drug withdrawal, potentially explaining the requirement for sustained PARPi therapy in the clinic. Importantly, PARPi-induced TIS-like state renders cancer cells susceptible to synergistic killing using several senolytics. Indeed, combo treatments of PARPi/ABT-263 were effective in preclinical models of ovarian and breast cancer, two chronic human conditions currently treated using PARPi. Overall, we demonstrate that cancer treatment responses mimicking senescence can be targeted using senescence-directed synthetic lethal strategies that augment the efficacy of anti cancer drugs used in the clinic.

2.3.2.2 Introduction

Poly (ADP-ribose) polymerase 1 (PARP1) plays an important role in DNA damage repair [1]. A number of PARP inhibitors (PARPis) have been explored as anticancer agents based on the synthetic lethality induced by these drugs in the context of homologous recombination (HR) deficiency [2], such as that caused by BRCA1/2 mutation. Among these, Olaparib was the first to be approved by the FDA as maintenance therapy for treatment of high-grade serous epithelial ovarian cancer (HGSOC) [3-5]. However, results from several clinical trials have shown varied responses even in the context of HR deficiency [3-5], and several combination therapies have been proposed and are being tested in the clinic to improve response to this class of drugs [6-8]. The vast majority of combination studies and trials incorporating PARPi are exploring the synthetic lethality of these drugs in the context of HR deficiency. However, therapeutic effects of PARPis have shown efficacy in conditions of functional HR machinery in both clinical trials and in vitro studies [9]. Such anticancer activities of PARPis likely result from PARP1 functions unrelated to DNA repair or from some still unexplored pathway. Another clinical challenge is the maintenance therapy strategy that has been implicated in the appearance of resistance mechanisms, including additional mutations restoring BRCA functions [7,10].

To better understand the mechanism of action of PARPis, we focused on cell fate processes induced by PARPi treatment using *TP53* mutant HGSOC cell lines that are sensitive and resistant to Olaparib. Strikingly, we observed that Olaparib and other PARPis (Talazoparib and Niraparib) were able to induce a senescence-like phenotype in these cells. This included enlarged cell morphology, persistent DNA damage, cell growth arrest, expression of senescence-associated (SA) β-galactosidase and secretion of SA factors such as IL-6 and IL-8. Co-treatment of PARPi with a series of senolytic drugs [11-13], switched this senescence-like phenotype of HGSOC cells to apoptosis and induced a synergistic lethal effect. *To our knowledge, this is the first report showing that senescent cells induced by PARPi treatment are susceptible to elimination by senolytic drugs. Importantly, we showed that this senescence state induced by PARPis is reversible, where cells start to proliferate upon PARPi removal and are no longer sensitive to those senolytic drugs.* Using a xenograft-

based model, we also demonstrate a strong effect of the combination therapy on ovarian cancer growth. Our results suggest that the clinical application of PARPi as maintenance therapy may favor recurrence and resistance by inducing a reversible senescence-like phenotype, and combination therapy with PARPi and senolytic drugs may counter these undesired effects.

2.3.2.3 Material and methods

Cell lines and cell culture

The four human HGSOC cell lines used, OV1369(R2), OV90, OV4453 and OV1946, were derived from the ascites from patients diagnosed with HGSOC and have been extensively characterized [1-3]. All cell lines were maintained in a low oxygen condition (7% O_2 and 5% CO_2) and grown in OSE medium (Wisent, Montreal, QC) with 10% FBS (Wisent), 0.5 μg/mL amphotericin B (Wisent) and 50 μg/mL gentamicin (Life Technologies Inc., Burlington, ON). The MDA-MB-231 breast cancer cell line was a gift from the laboratory of Dr. John Stagg (CRCHUM, Canada). It was maintained in DMEM (Wisent) with 10% FBS (Wisent), 0.5 μg/mL amphotericin B (Wisent) and 50 μg/mL gentamicin (Life Technologies Inc.). The human retinal epithelial cell line ARPE-19 was purchased from American Type Culture Collection (ATCC, Manassas, VA) and maintained in DMEM-F12 (Wisent) with 10% FBS (Wisent), 0.5 μg/mL amphotericin B (Wisent) and 50 μg/mL gentamicin (Life Technologies Inc.).

Drugs

Olaparib (AZD2281) was purchased from Selleckchem (Houston, TX), ABT-263 (Navitoclax) from APExBIO (Houston, TX), Niraparib (M2215) from AbMole Bioscience (Houston, TX), Talazoparib (HY-16106) from MedChem Express (Monmouth Junction, NJ), ABT-199 (A8194) from ApexBio (Houston, TX), ABT115 (S7800) from Selleckchem (Houston, TX), ABT-133 (S7801) from Selleckchem (Houston, TX), Piperlongumine (1919) from BioVision (Milpitas, CA), Fisetin (15246) from Cayman chemical (Ann Arbor, MI), Dasatinib (S1021) from Selleckchem (Houston, TX), Quercetin (Q-4951) from Sigma Aldrich (St. Louis, MO).

Drugs were dissolved in 100% dimethyl sulfoxide (DMSO) and then further diluted in complete culture media for *in vitro* experiments. Drugs were added 24 hours after seeding.

Antibodies

The following antibodies were used: beta-actin (AC- 15) (ab6276; Abcam Inc., Toronto, ON, Canada); PAR (4335-MC-100; Trevigen®, Gaithersburg MD); phospho-histone γ-H2AX (JBW301, EMD Millipore, Temecula, CA); 53BP1 (clone 305, Novus Biologicals, Littleton, CO).

Cloning, viruses and infections

Viruses were produced as described previously [4] and titers were adjusted when necessary to achieve ~90% infectivity. Lentiviruses encoding H2B-GFP were produced by amplification of the H2B sequence from the pENTR1A-H2B-HcRed plasmid (a gift from the laboratory of Dr. Richard Bertrand, CRCHUM, Canada) using the following primers: ES-92 (5'-GGTACCCCACCATGCCAGAGCCAGCGAAGTCTGCT-3') and ES-93 (5'-GGATCCTAGCGCTGGTGTACTTGGTGATGG-3'). The amplified product was then inserted into the vector pENTR1A-GFP-N2 (FR1), after digestion with restriction enzymes Kpn1/BamH1, to obtain the final lentiviral vector pENTR1A-H2B-GFP. After infection and hygromycin selection, stable cells were either stored at -80°C or used for the IncuCyte cell proliferation assay. p21, CHk2 and RFP were subcloned into a lentiviral vector with puromycin selection. Lentiviruses encoding shRNAs against p21, CHk2 and RFP were purchased from Open Biosystems. Virus titres were adjusted to infect 95–99% of cells. For the sequence, shp21, RHS3979-200795840 target 5'-TTGGAGTGGTAGAAATCTGTC-3'; shCHK2-2, #TRCN0000039946 target 5'-GCCAATCTTGAATGTGTGAAT-3'; shRFP, TRCN0000231725 target 5'- ACTACACCATCGTGGAACAGT-3'.

IncuCyte cell proliferation phase-contrast imaging assay

For the cell proliferation assay, 1500 cells/well were seeded for OV1369(R2), OV90, OV1946, ARPE-19 and MDA-MB 231, and 2500 cells/well were seeded for OV4453 in 96-well plates (all H2B-GFP selected). Cells were incubated with PARPi and senolytics drugs at different concentrations and times in 0.75% DMSO. Cell number was imaged by phase

contrast and fluorescence using the IncuCyte™ Live-Cell Imaging System (IncuCyte HD). Frames were captured at 2-hour intervals from two separate regions/well using a 10X objective. Proliferation growth curves were constructed using IncuCyte™ Zoom software, where plates were imaged and growth curves were built from H2B-GFP cell number measurements acquired during round-the-clock kinetic imaging. IC_{50} values were determined by using Graph Pad Prism 6 software (GraphPad Software Inc., San Diego, CA). Each experiment was performed in triplicate and repeated three times.

Clonogenic Assay for release determination

Cells were seeded in a 6-well dish at a density of 1000 cells/well that allowed the formation of individual colonies. Cells were seeded and allowed to adhere for 16 hours in a 37°C, 5% CO2, 7% O2 incubator after which the media was removed and replaced with OSE complete media containing Olaparib. Cells were incubated until colonies became visible at a 2X magnification. Cells were fixed with cold methanol and coloured with a mix of 50% v/v methanol and 0,5% m/v blue methylene (Sigma– Aldrich Inc., St. Louis, MO). Colonies were counted under a stereomicroscope and reported as percent of control. Depending the condition, cells were treated for 6 days, for 12 days or for 6 days then release for 6 days. Each experiment was performed in triplicate and repeated three times.

Immunofluorescence

Cells were seeded onto coverslips in 12-well plates and grown for 3 and 6 days. Cells were fixed in formalin for 10 minutes at room temperature (RT) and permeabilized in 0.25% Triton in PBS for 10 minutes. Slides were blocked for 1 hour in PBS containing 1% BSA and 4% donkey serum. Primary antibodies diluted in blocking buffer were incubated overnight at 4°C. Cells were washed and incubated with secondary antibodies for 1 hour at RT, then washed again. Coverslips were mounted onto slides using Prolong® Gold anti-fade reagent with DAPI (Life Technologies Inc.). Images were obtained using a Zeiss microscope (Zeiss AxioObserver Z1, Carl Zeiss, Jena, Germany). Automated analysis software from Zeiss (AxioVision™, Carl Zeiss) was used to count foci to calculate the average number of foci per nucleus. The fold change was calculated as the ratio between percentages of γH2AX or 53BP1 nuclear foci in treated versus control (non-treated) cells. γH2AX and 53BP1 foci were quantified in > 150

nuclei from three different fields of each coverslip. Reliability, reproducibility, and validity of our data were confirmed by repeated tests across different fields.

EdU (5-ethynyl-2'-deoxyuridine) detection

To detect DNA synthesis, cells were seeded onto coverslips in 12-well plates. Drugs were added 24 hours after seeding. Ten micromolar of EdU (Invitrogen) was added to the medium and incubated for 8 or 24 hours before the end of drug treatment on days 3 or 6. Cells were washed three times with TBS and fixed with 10% formalin for 10 minutes. EdU staining was assessed using the Click-iT® EdU Alexa Fluor® 488 Imaging Kit (Invitrogen). Coverslips were mounted onto slides using Prolong® Gold anti-fade reagent with DAPI (Life Technologies Inc.). Images were obtained using a Zeiss microscope (Zeiss AxioObserver Z1, Carl Zeiss, Jena, Germany). Automated analysis software from Zeiss (AxioVision™, Carl Zeiss) was used for counting foci.

Protein preparation and western blot analysis

Whole cell lysates were prepared by scraping cells with mammalian protein extraction reagent (MPER, Thermo Fisher Scientific, Waltham, MA) containing protease and phosphatase inhibitor cocktail (Sigma-Aldrich Inc., St. Louis, MO). Protein concentration was measured using the bicinchoninic acid (BCA) protein assay (Thermo Fisher Scientific). Thirty micrograms of total protein extracts were separated in 7.5% or 4-15% gradient tris-glycine SDS-polyacrylamide gels (Bio-Rad Laboratories, Hercules, CA) and transferred onto PVDF membranes (Hybond-C Extra, GE Healthcare Life Sciences, Mississauga, ON, Canada). Membranes were blocked with 5% skim milk in PBS-Tween for 1 hour and probed with primary antibodies overnight at 4°C. Bound primary antibodies were detected with peroxidase-conjugated secondary antibodies (Santa Cruz Biotechnology Inc., Dallas, TX) and enhanced chemiluminescence (Thermo Fisher Scientific).

Analysis of PAR levels

The analysis of PAR levels was performed as previously described [5]. Briefly, cells were seeded in 6-well plates and incubated for 24 hours before they were treated with 1 mM H_2O_2 for 20 minutes. Then, cells were treated with 10 μM Olaparib for 1, 3 and 6 days, harvested and

lysed to obtain protein extracts that were then analyzed by Western blot using an anti-PAR antibody (1:1500).

Cell cycle and cell death by flow cytometry analysis

Cells were seeded in 6-well plates and treated 24 hours after seeding, then harvested 3 and 6 days after. For cell cycle analysis, live cells were fixed for 24 hours in 70% ethanol and incubated for 30 minutes at RT with 100 µg/ml RNAse A and 25 µg/ml propidium iodide (PI). For cell death analysis, all the cells were incubated 30 minutes at RT with BV421 Annexin V (563973, BD Biosciences, San Jose, CA) and 5 minutes at RT with DRAQ 7 (ab109202, Abcam Inc.). A maximum of 10,000 events were counted per condition using the Fortessa flow cytometer (BD Biosciences, Mississauga, ON) and analysed with FlowJo software.

Assessment of CDKi, Bcl2, Bcl-XL expression by real-time quantitative polymerase chain reaction (Q-PCR)

Cells were seeded in 6-well plates and treated with Olaparib 24 hours after seeding. For drug removal conditions, drugs were removed 3 days after. The cells were harvested at 3 and 6 days after drug treatment. Total RNA was extracted using the RNeasy kit (Qiagen Inc., Hilden, Germany). One microgram of total RNA was subjected to reverse transcription using the QuantiTect Reverse Transcription Kit (Qiagen Inc.). One microliter of the reverse-transcribed product was diluted (1:10) and subjected to Q-PCR using sequence specific primers (400 nM) and the SYBR Select Master Mix (Applied Biosystems®, Life Technologies Inc.). Sequence primers for target genes were as follows: p21, forward 5'- GGGACAGCAGAGGAAGAC -3' and reverse 5'- TGGAGTGGTAGAAATCTGTCA -3'; p27, forward 5'- TCCGGCTAACTCTGAGGACA-3' and reverse 5'- GTAGAAGAATCGTCGGTTGC -3'; p15, forward 5'- GAATGCGCGAGGAGAACAAG -3' and reverse 5'- CATCATCATGACCTGGATCGC -3'; p16, forward 5'- GGGAGCAGCATGGAGCCT -3' and reverse 5'- ATGACCTGGATCGGCCTCCGACCGT -3'; and p57, forward 5'- GCGGTGAGCCAATTTAGAGC -3' and reverse 5'- CGGTTGCTGCTACATGAACG -3'; IL8, forward 5'-GCCAACACAGAAATTATTGTAAAG-3'.and reverse 5'- TTATGAATTCTCAGCCCTCTTC-3'. The Q-PCR was achieved with the Applied BioSystems® Step One Plus apparatus. Thermocycling conditions were one UDG activation

cycle at 50°C for 2 minutes and one AmpliTaq activation plus denaturation cycle at 95°C for 2 minutes followed by 40 cycles at 95°C for 15 seconds, 60°C for 1 minute and 72°C for 30 seconds. Gene expression values were normalized to the TATA-binding protein (TBP) gene. Three independent experiments were performed in duplicate.

Senescence-associated β-galactosidase detection

Cells were washed once with 1X PBS and fixed with 10% formalin for 5 minutes, then washed again with PBS and finally incubated at 37°C for 6-24 hours (depending on the cell line) in a staining solution composed of 1 mg/mL 5-bromo-4-chloro-3-inolyl-β-galactosidase in dimethylformamide (20 mg/mL stock), 5 mM potassium ferricyanide, 150 mM NaCl, 40 mM citric acid/sodium phosphate and 2 mM $MgCl_2$, at pH 6.0. The following day, cells were washed twice with PBS and pictures were taken.

Cytokine secretion measurement in conditioned medium

Conditioned media (CM) was prepared by incubating cells with OSE medium without FBS for 24 hours. CM were collected and stored at −80°C until assayed for cytokine analysis. Levels of IL-6 and IL-8 in CM were assessed by ELISA using kits from R&D Systems (IL-6 #DY206; IL-8 #DY208). The data were normalized to cell number and reported as fold change of secreted protein compared to the control. CM of OV1369(R2), OV90 and OV1946 were also assayed using MSD V-PLEX Products: Proinflammatory Panel I, Chemokine Panel I, Angiogenesis Panel I, Cytokine Panel I and Vascular Injury Panel II (MSD, Gaithersburg, MD). These are highly sensitive multiplex ELISA for quantitatively measuring 40 secreted proteins from a single sample volume (25 µL) using an electrochemiluminescent detection method. The data were normalized to cell number and reported as log 2 - fold change of secreted protein compared to the control.

Drug combination analysis

Combinations synergisms were performed using the Chou-Talalay method using CompuSyn software (ComboSyn Inc., Paramus, NJ, USA) with constant ratios of drug combinations. The resulting combination index (CI) values defined synergistic (<0.9), additive (0.9-1.1), and antagonistic (>1.1) effects in drug combinations [6]. The Bliss independence model [7,8] was used

to assess combination activity, with negative integers indicating antagonism, a value of zero indicating additive activity, and positive integers indicating synergy. Bliss scores were calculated for each combination in the dose matrix (1X6, one dose of Olaparib and 6 doses of ABT-263 or ABT-199 or A-133 or A-115 or Piperlongumine or Fisetin or Dasatinib or Quercetin) and totalled to give a "Bliss sum" value. For each dose of senolytic, the senolytic index (SI) was calculated as follow. SI= $[(N_f/N_i)_{SX} / (N_f/N_i)_{S0}]_{Untreated} / [(N_f/N_i)_{SX} / (N_f/N_i)_{S0}]_{PARPi}$ (Nf= Final cell number; Ni= initial cell number; SX= X dose of the senolytic; S0= no senolytic).

Murine xenograft model

OV1946 cells in exponential phase were prepared at a concentration of 7.5 million cells/ml in 50% PBS - 50% matrigel. NRG mice (NOD-*Rag1*^{null} *IL2rg*^{null}, NOD rag gamma) were obtained from the Jackson laboratory (Bar Harbor, ME). All experiments were carried out with 6-week-old females. To initiate tumor xenografts, 0.5 mL of cell suspension was injected into the right and left flank of 40 animals. Tumor volumes and mice weights were measured two times per week. Fourty days post-injection mice with similar tumor size (400-500 mm^3) were randomized into four groups: untreated, treated with Olaparib, treated with ABT-263, or treated with both. Olaparib (50 mg/kg) was administered intraperitoneally and ABT-263 (50mg/kg) was administered orally by gavage every two days in a maximum of 3 times per week, skipping week-ends. Olaparib vehicle (DMSO 12%) and ABT-263 vehicle (PEG400) was administered to the control groups. All animal experiments were conducted in accordance with accepted standards of animal care and in accordance with our institutional committee on animal care (CIPA). Mice were sacrificed when tumor volumes increased two times from the day of injection (800-1000 mm^3). Tumor growth plots and survival curves were built using the Graph Pad Prism 5 software (GraphPad Software Inc.).

2.3.2.4 Results

Olaparib-treated HGSOC cells develop a senescence-like phenotype

In our previous work, we investigated the sensitivity of 18 HGSOC cell lines to Olaparib using the conventional clonogenic assay and were able to categorize these cell lines into groups of sensitive, intermediate and resistant to this drug [14]. However, this method takes into account only surviving clones and does not reveal the process by which the cells die. In the present study, we performed live-imaging proliferation assays to evaluate cell morphology and estimate cell viability. Work was conducted with two cell lines that we previously categorized as Olaparib resistant [OV1369(R2), OV90] and two that were sensitive (OV4453, OV1946) [14]. In accordance with the molecular characteristics of the HGSOC disease [15], all cell lines are *TP53* mutants, have high rates of copy number anomalies and in the case of OV4453, it carries a BRCA2 mutation [16-19]. Images were taken every 6 hours for up to six days using different Olaparib concentrations (Fig. 1A). As expected, we observed a dose-dependent inhibition of cell proliferation in all cell lines, and higher concentrations were required for the resistant cell lines. Using these results, we calculated the IC_{50}, which were consistent with those obtained by clonogenic assay (Fig. S1A). However, with the exception of the resistant OV1369(R2) cell line, this cell proliferation inhibition seems to be unstable, since EdU pulse-labeling assay revealed decreased proliferation at day 6 on a 8h-pulse that recovers on a 24h-pulse (Figs. 1B-C). We also observed that cell proliferation inhibition was not accompanied by a corresponding increase in cell death/apoptosis, as only 20-40% of cells were AnnexinV/PI positives 6 days post-treatment, even at the highest Olaparib concentrations used (Fig. 1D, Fig. S1B). In addition, detailed analysis of the cell imaging during the time course of Olaparib treatment revealed a change in cell morphology, where cells became bigger in size, starting at day 3 and that became more pronounced at day 6 post-treatment (Fig. S1C). Cell cycle analysis at days 3 and 6 showed an arrest at the S or G2/M phase of the cell cycle (Fig. 1E), which is in accordance with the described effect of Olaparib on the cell cycle [20,21].

Several of these features are consistent with a senescent phenotype [22-25]. Furthermore, senescence has been described as a cellular response to cancer therapy, including radiotherapy and chemotherapy [26]. Senescent cells are characterized by a series of senescence-associated (SA) phenotypes displayed *in vitro* as well as *in vivo* [27-29]. Following the initial SA growth

arrest, the nascent senescent cells undergo morphological changes, and increase lysosomal mass and autophagic activity to promote high levels of SA β-galactosidase activity. This is accompanied by alterations in metabolic activity, epigenetic state and chromatin structure, along with the development of apoptotic resistance, and expression of a SA secretory phenotype (SASP) [30-32]. We further investigated whether Olaparib-treated HGSOC cells presented a SA phenotype.

We first performed flow cytometry analysis of cell granularity (SSC) and cell size (FSC) and observed two distinct cell populations, R1 (normal size cells) and R2 (bigger size cells) (Fig. 1F, Fig.S2A), in which R2/R1 ratios were significantly higher in Olaparib-treated cells at day 6 (Fig. 1F). Thereafter we investigated the levels of SA β-galactosidase activity and observed a concentration and time-dependent increase in this enzyme's activity after Olaparib treatment in all four cells lines (Fig. 1G-H, Fig. S2B). In addition, higher levels of secreted interleukins IL-6 and IL-8 were also observed (Fig. 1I-J). Multiplex analysis of other SASP components revealed increased levels of several growth factors and chemokines in the conditioned medium of Olaparib-treated cells (Fig. 1K).

Olaparib-induced senescence is associated with p21 and Chk2 expression

Persistent DNA damage is considered one of the main causes of cellular senescence [23,33]. Consistently, we observed increased levels of γH2AX and 53BP1 nuclear foci at six days post Olaparib-treatment in HGSOC cells (Fig. 2A-B). To further elucidate the mechanisms involving the SA growth arrest induced by Olaparib in HGSOC cells, quantitative mRNA analysis of several cyclin-dependent kinase inhibitors (CDKi) were conducted six days after treatment. Reports have shown that SA growth arrest relies heavily on the p53/p21WAF1 and p16INK4a/Rb pathways [34,35]. Our results showed that p21 was the only CDKi tested with significant increased levels in all cell lines after Olaparib treatment (Fig. 2C). In contrast, p16 levels were either non-detected or did not increase, and the other CDKi studied had varied expression patterns depending on the cell line (Fig. 2C). Since the HGSOC cell lines studied here are all *TP53* mutants, the increase in p21 levels would appear unexpected. However, a p21 increase independent of p53 has already been reported in embryonic and oncogene-induced senescent cells [36]. Another possibility is that p21 induces a p53-independent senescence in response to Chk2 activation [37]. The kinase Chk2 has a central role in the DNA

damage response that is activated by DSBs [38], and it is well described that PARPis induce accumulation of SSBs that are subsequently converted into DSBs [1,7]. Therefore, the p53-independent senescence induced by PARPi may involve the activation of Chk2/p21 pathway induced by DNA damage. Validation experiments were performed using stable HGSOC cells expressing shRNA against p21 or Chk2. Our results show that knockdown of either p21 or Chk2 were effective and induced cell death only when treated with Olaparib (Fig. 2D-F, Fig.S3A), specifically we observed a cell cycle arrest, proliferation inhibition and senescence after Olaparib treatment (Fig.1) that when combined with p21 or Chk2 knockdown switches to a cell death/apoptosis state (Fig.2F). These findings indicate that p21 and Chk2 are important for the senescence phenotype, in their absence cells cannot bypass the persistent DNA damage (Fig.2G-H) and die by apoptosis (Fig.2F). These results accord with reports showing the p53-independent role of p21 in the senescent phenotype induced by DNA damage or Chk2 overexpression, where p21 knockdown/knockout resulted in increased DNA damage and apoptosis [37,39]. Our findings suggest that the Olaparib-induced senescence in HGSOC cells is associated with the intrinsic mechanism of action of this PARPi, causing DNA repair inhibition and persistent DNA damage. We confirmed that Olaparib inhibited PARP1 enzymatic activity as lower levels of PARylated proteins were detected by western blot using an anti-PAR antibody (Fig. S3B). This inhibitory activity was at its highest at 24 hours after treatment but still evident at days 3 and 6. Note that Olaparib is added to the culture medium only at the beginning of the experiment without media change, indicating a prolonged effect of this PARPi and mimicking the clinical use of this class of drugs as maintenance therapy.

The senescence-like phenotype induced by Olaparib in HGSOC cells is reversible

Although senescence is well recognized as a terminal arrest of cell division, reports have demonstrated that some types of senescence can be reversible. In particular, therapy induced senescence (TIS) by chemo or radiation treatments can escape irreversible arrest to resume proliferation [40-42], suggesting a mechanism of resistance. Therefore, we investigated whether the senescence-like phenotype induced by Olaparib in p53-mutant HGSOC cells was irreversible or not. Cell proliferation experiments were conducted so that ovarian cancer cells were treated with Olaparib for three or six days, and then media was changed to a drug-free medium and incubated for another three days. In these two time points we observed a

cumulative effect on senescence induction, i.e. on day three cells present a senescent-like phenotype that is evident but less intense than day 6, where the senescent-like phenotype is well established (Fig.1E,H and Fig.S4A-B). Results showed a clear recovery of cell proliferation in all cell lines tested (Fig. 3A-C, Fig. S4C). To further verify this cell growth recovery in isolated cells, additional clonogenic assays were conducted, where culture media was replaced six days after Olaparib treatment and colonies were allowed to grow for another six days. Our results confirmed cell growth recovery at a single cell level, since higher number of colonies was observed after drug removal compared to either 6 or 12 days of continuous Olaparib treatment (Fig. 3D). In addition, decreased levels of secreted IL-6 and IL-8 (Fig. 3E-F), as well as lower numbers of γH2AX and 53BP1 nuclear foci, were observed after recovery (Fig. 3G, Fig. S4D-E). These findings indicate that the senescent phenotype induced by Olapatrib in HGSOC is reversible. However, this process is more pronounced in Olaparib-resistant than sensitive cells. We postulate that recovery in Olaparib-sensitive cell lines is delayed due to their higher levels of DNA repair defects [14], resulting in more prolonged DNA damage. As with other TIS, the reversible senescence-like phenotype induced by Olaparib may contribute to therapy resistance and recurrence.

Senolytic Bcl2 family inhibitors synergize with Olaparib in HGSOC cells

Another feature of senescent cells is their resistance to apoptosis [43-45], which has been shown to involve an increased expression of anti-apoptotic proteins, such as Bcl2 and Bcl-XL [11,12]. In the present work we also observed higher levels of mRNA and/or protein of Bcl2/Bcl-XL in Olaparib-treated HGSOC cells (Fig.S5A-C), further confirming the senescence-like state. These anti-apoptotic proteins are targetable markers of senescence, in which small molecule inhibitors of Bcl2 or Bcl-XL have been used to eliminate senescent cells [11-13,46]. Therefore, we explored the possibility that a combination therapy of PARPi and inhibitors of the Bcl2 family would have synergistic effects in killing HGSOC. We first used the inhibitor ABT-263 because it has been extensively used in clinical trials [47-50] for targeting Bcl2 and Bcl-XL, and because it was recently shown to be senolytic [11,46]. Dose-response curves with this inhibitor showed that only OV1369(R2) (resistant to Olaparib) had decreased proliferation with increasing ABT-263 concentrations (Fig. S5D). This result was consistent with the higher basal levels of Bcl2 and Bcl-XL found in this cell line (Fig.4A). In subsequent experiments,

concentrations that had minimal effects (less than 20% inhibition of cell proliferation) in each cell line were used for the combination therapy, i.e. 0.25 μM for OV1369(R2) and 2.5 μM for the other three HGSOC cell lines. Using the Olaparib IC_{50} concentrations (Fig. S1A) in combination with the minimal ABT-263 dose for each cell line, we observed a significant potentiation of cell killing outcomes (Fig. 4B-C, Fig. S6A-B). To further investigate whether this effect was synergistic or additive, we performed cell proliferation assays using a range of ABT-263 and Olaparib concentrations in combination at same drug ratio (Fig. S6C), and calculated their potency and CI according to the Chou Talalay method [51]. In this method, a CI lower than 0.9 indicates synergism, whereas CI values between 0.9 and 1.1 denote additive effects, and those higher than 1.1 indicate antagonism. Interestingly, the combined treatment of Olaparib and ABT-263 resulted in CIs lower than 0.9 in all the concentration ranges used with all four cell lines (Fig. 4D-E). Importantly, we demonstrated this synergy *in vivo* using xenograft tumor growth of two different cell lines. Drugs were administered when tumors reached a volume of about 400-500 mm^3, and tumor progression was plotted as ratio in comparison to this initial volume (Fig. 4F). Our results showed a decrease in tumor growth when mice were treated with Olaparib alone, but that a further significant decrease was obtained when Olaparib and ABT-263 were administered simultaneously. Tumor volumes for mice treated with ABT alone were not different from those of controls for the OV1946 cell line, or same as Olaparib treated mice for the OV4453 cell line.

Because ABT-263 targets both Bcl2 and Bcl-XL proteins, we investigated the effects of other inhibitors that are more specific towards each of these proteins in order to dissect the contributions of Bcl2 and Bcl-XL to the senescent phenotype induced by Olaparib. We used specific inhibitors of Bcl2 (ABT-199, Venetoclax) or Bcl-XL (A-1155463 and A-1331852) recently described as senolytic agents [52], and verified the sensitivity of OV1369(R2) and OV1946 cell lines to these drugs in comparison to ABT-263 (Fig.4G). Our results show that the OV1369(R2) cell line was very sensitive to the Bcl-XL specific inhibitor A-1331852, and lesser to the Bcl2 specific ABT-199, suggesting that its sensitivity towards ABT-263 is probably related to Bcl-XL inhibition. In general OV1369(R2) was more sensitive to these inhibitors than the OV1946 cell line (Fig. 4G), probably due to its higher basal levels of Bcl2 and Bcl-XL (Fig.4A). According to the IC_{50} of each cell line to each inhibitor, combination treatments were performed using the IC_{50} concentration of Olaparib (Fig.S1A) and several

concentrations of the Bcl2 family inhibitors (Fig.S6D). To assess potential combination effects on cell killing, we used the Bliss independent model [53], in which negative values indicate antagonism, values around zero indicate additive effects and positive values indicate synergy. Our results show synergistic effects for the co-treatment of Olaparib with ABT-263 or Bcl-XL specific inhibitors in both cell lines studied, but not with the Bcl2 specific inhibitor (Fig.4H, Fig.S7). These findings indicate that the cell killing effects observed with ABT-263 in Olaparib-treated HGSOC cells comes from the Bcl-XL inhibition and not that of Bcl2.

Synergy between Olaparib and senolytic drugs occurs only in conditions when Olaparib induces senescence

To confirm that the Bcl2/Bcl-XL inhibitors were targeting senescent cells, we first performed cell proliferation assays where senolytic drugs were combined with Olaparib only for the first three days, in which the senescent phenotype is not yet present. Secondly, inhibitors were administered three or six days later than Olaparib, conditions of which senescence was already establish (Fig.1E,H; Fig.S4A-B and Fig.S5A-B). Our results showed similar levels of cell-proliferation inhibition and induction of apoptosis when ABT-263 was added 3 or 6 days later than Olaparib (Figs. 5A-B, Fig. S8A) and comparable to the simultaneous treatment for 6 days (Fig. 4C, Fig. S8B). In contrast, when both Olaparib and ABT-263 were incubated together only for three days, only a mild increase in cell death was observed (Fig. 5C-D), indicating the efficacy of this inhibitor towards senescent cells. The same selective effect of cell proliferation inhibition at days 3-6 compared to 0-3 was observed with the other Bcl2 family inhibitors (Fig. 5E). Furthermore, after senescence recovery, HGSOC cell lines were no longer sensitive to ABT-263 (Fig. 5F-G), particularly those in the Olaparib-resistant group.

Besides up-regulation of Bcl2 family members, reports have demonstrated that other anti-apoptotic pathways, such as PI3K/Akt, p53/p21/serpines, receptor tyrosine kinases, and HIF-1α, are also activated in senescent cells [54]. Therefore different classes of senolytic drugs targeting these networks have been described [55]. In order to further elucidate the senescence mechanism induced by Olaparib in HGSOC cells, we investigated the effect of other senolytic agents in combination with Olaparib. We tested: Dasatinib (D) (Src tyrosine kinase inhibitor), Quercetin (Q) (bioflavonoid with a broad spectrum of action targeting several pathways including PI3K/Akt, p53/p21/serpines and Bcl2/Bcl-XL), and two derivatives of Q, Fisetin (F)

(PI3K/Akt inhibitor) and Piperlongumine (PPL) (targeting p53/p21/serpines and PUMA) [55], and determined their IC_{50} for the OV1369(R2) and OV1946 cell lines. Our results show that both cell lines had low IC_{50} values for PPL, but higher for F and Q, and that OV1369(R2), but not OV1946, was very sensitive to D (Fig.6A). Bliss scores were calculated for combination treatments between Olaparib (IC_{50} concentration, Fig. S1A) and each of the senolytic drugs (several concentrations according to their IC_{50} values, Fig.S9A). Our results showed synergistic effects (positive bliss scores) between Olaparib and all these senolytic drugs in both cell lines that predominantly occurred when combination treatments were performed on days 3-6 but not on days 0-3 (Fig.6B, Fig.S9B), indicating selective targeting to senescent cells. For the OV1369(R2) cell line higher Bliss scores were obtained for ABT-263 and PPL, however for the OV1946 cell lines high Bliss score was observed for all drugs at different concentrations (Fig.6B). We also find the same results with the senolytic index (Fig.6C). These findings suggest that in addition to the Bcl-XL signaling, other anti-apoptotic pathways seemed to play a role in Olaparib TIS in HGSOC cells.

Reversible senescence is also induced by other PARPi and in breast cancer cells

Apart from Olaparib, other PARPis have been evaluated in clinical trials for the treatment of HGSOC patients [56-59]. Among them are Niraparib and Talazoparib, which have been shown to possess distinct PARP1-DNA trapping activity different from Olaparib [57,58]. Hence, we questioned whether these inhibitors would also induce a senescence-like phenotype in HGSOC cells. Dose-response curves for the OV1369(R2) cell line showed a concentration-dependent inhibition of cell proliferation for both Niraparib and Talazoparib (Fig. 7A), where the latter displayed higher cytotoxic effect due to its higher DNA-trapping activity, as previously described [60-62]. Interestingly, as with Olaparib, both inhibitors induced a senescence-like phenotype as evidenced by the increased levels of SA β-galactosidase positive cells and secreted IL-6 and IL-8 at days 3 and 6 post-treatment (Fig. 7B-C). Furthermore, increased levels of mRNA expression for IL-8, Bcl2 and Bcl-XL were also observed three days after these PARPis treatments (Fig. 7D). Similar to Olaparib, combination therapies of Niraparib or Talazoparib with the senolytic ABT-263 had synergistic cell-killing effects (Fig. 7E-F). Finally, we showed that the senescent-like phenotype observed at day 3 post-treatment was reversible when cells were no longer exposed to either of these PARP1 inhibitors (Fig.

7G). Taken together, all these findings suggest that TIS produced by PARPis is common to all three drugs studied, albeit with differences in cytoxicity and DNA-trapping.

PARPis have also been extensively studied in breast cancer, owing to the presence of BRCA mutations in this type of malignancy [63]. However, clinical trial results are less encouraging and the FDA has not yet approved this type of drug for breast cancer treatment [64]. Herein, we investigated whether combination therapy of Olaparib and ABT-263 could synergize in a triple-negative breast cancer cell line (MDA-MB-231), which also carries a *TP53* mutation. Olaparib dose-response curves for the MDA-MB-231 cell line showed a concentration-dependent inhibition of cell proliferation (Fig. S10A) with an IC_{50} of 2.92 ± 0.17 μM. This cell line was not as resistant as OV1369(R2) and OV90 but was less sensitive than OV4453 and OV1946. Interestingly, as with the ovarian cancer cell lines, Olaparib induced a senescence-like phenotype in MDA-MB-231 as evidenced by the increased cell size morphology and the elevated levels of secreted IL-8 at days 3 and 6 post-treatment (Fig. S10B-C). Also similar to the ovarian cancer cells, combination therapy of Olaparib with the senolytic ABT-263 had synergistic cell killing effects in MDA-MB-231 (Fig. S10D-F). Taken together, all these findings suggest that the senescence-like state induced by PARPi therapy is common to ovarian and breast cancer cell lines.

2.3.2.5 Discussion

Clinically, Olaparib is recommended as maintenance therapy for ovarian cancer patients with germline BRCA mutations who responded favorably to chemotherapy treatments (72), and for prostate cancer patients with BRCA or ATM mutations (73). Under this regimen, tumor cells are potentially in constant exposure to this PARPi. Based on our results, this approach may maintain these tumor cells in a reversible senescence-like state, which may trigger resistance or tumor re-growth upon drug withdrawal. Resistance to Olaparib and disease progression has been reported in cancer patients subjected to this maintenance therapy (74-76). The main mechanism of this resistance arises from the restoration of BRCA and/or HR function by secondary BRCA mutations or copy number alteration in HR genes (74-76). However, other resistance mechanisms, such as increase in drug efflux regulation, have been

described in pre-clinical models (3, 32), but have not yet been proven in patients. The constant release of SASP factors by HGSOC cells treated with PARPis might create a niche of chemo-resistant cells and support subsequent relapse. In line with this are reports showing that SASP can stimulate the proliferation of cancer cells through multiple factors, including growth-related oncogenes in breast cancer and melanomas, and amphiregulin in prostate cancer (51, 56, 77). Furthermore, secretion of matrix metalloproteinases by the SASP has been shown to promote migration of cancer cells while IL-6 and IL-8, in addition to promoting tumor growth, have been reported to induce an epithelial to mesenchymal transition, thereby stimulating invasion (51, 78, 79). Our observation that HGSOC cells re-grow almost immediately after PARPi removal suggests that the senescence induced by these drugs would have a pro-tumor effect. Cellular senescence has also been reported as a potential mechanism of chemoresistance in TNBC (80).

To avoid relapse and the emergence of chemoresistant cancer cells, we propose the removal of PARPi-induced senescent cells by senolytic drugs such as ABT-263 *(*Navitoclax), an inhibitor of Bcl2 and Bcl-XL (37-39). This drug has been extensively used in pre-clinical models and is the subject of past and ongoing clinical trials due to its pro-apoptotic effects (81-84). In these studies and trials, ABT-263 was administered alone or in combination with chemotherapeutic agents (carboplatin/paclitaxel) or targeted therapies (such as Erlotinib) with the goal to increase apoptosis and cell death (81-84). However, more recently these inhibitors have been described as agents to eliminate senescent cells (37-39). Our results show a synergistic effect of PARPis and ABT-263 for cell proliferation inhibition in all the four cell lines tested, along with the disappearance of senescence markers, induction of apoptosis, and extensive cell death. ABT-263 did not induce apoptosis and cell death when administered alone or after removal of PARPi, indicating that it was specifically targeting the senescent-like cells produced by the PARPis. Relevantly, this synergistic effect was observed in both PARPi sensitive and resistant cell lines, suggesting that this treatment strategy can be explored on patients who do not respond to PARPi alone. Furthermore, our combination treatment used lower doses of PARPi and Navitoclax suggesting that the undesirable side effects of these drugs may be decreased. A recent study has also reported a synergistic effect of Talazoparib and ABT-263 in ovarian cancer cells, however, the focus was solely on the pro-apoptotic role of Navitoclax (85), and not on its senolytic effect. To our knowledge, our results are the first

to demonstrate that senescent cells induced by PARPi treatment are targetable and can be eliminated by the Bcl2/Bcl-XL inhibitor ABT-263. Most importantly, we showed decreased xenograft tumor volume in mice treated with this combination therapy than with either drug alone.

Reports have described that PARPis can induce senescence in certain conditions, but that this phenomenon was strictly p53-dependent (21-23). In fact, in *TP53* wild-type prostate cancer cells, Olaparib induced senescence that was switched to apoptosis when p53 was silenced (23). It is well known that HGSOC has a very high frequency of *TP53* mutation (more than 95%) (46). Our *TP53*-mutated HGSOC cell lines are reflective of this cancer type and showed that distinct senescence process is induced by Olaparib in HGSOC, which is the main clinical indication for this class of drugs. Mechanistically, we demonstrated that PARPis induced a persistent DNA damage, with a G2/M cell cycle arrest due to increased levels of the CDKi p21. Although p21 is a known p53 target (86), p53-independent increased levels of p21 have already been reported in embryonic and oncogene-induced senescent cells (59). In addition, it has been shown that FOXO3A promotes p21/p27 transcription (independently of p53) (60, 62) and that PARP inhibition increases FOXO3A expression and activation (61, 63). Therefore, PARPi may enhance p21 levels through FOXO3A activation, and induce cell cycle arrest and senescence. Another possibility is that p21 induces a p53-independent senescence in response to Chk2 activation (87). The kinase Chk2 has a central role in the DNA damage response that is activated by DSBs (88), and it is well described that PARPis induce accumulation of SSBs that are subsequently converted into DSBs (2, 3). Therefore, the p53-independent senescence induced by PARPis may involve the Chek2/p21 pathway. Further knockdown experiments are needed to clarify the pathways that lead to p21 activiation in this context.

Finally, we demonstrated that this p53-independent senescence-like induced by Olaparib is not restricted to HGSOC since the same results were obtained with a *TP53* mutant breast cancer cell line (MDA-MB-231). Olaparib treatment induced enlarged cell morphology and increased levels of secreted IL-6 and IL-8, which were reverted upon drug removal. Similar to the ovarian cancer cells, combination therapy of Olaparib with the senolytic ABT-263 had synergistic cell killing effects in MDA-MB-231. Because this is a TNBC cell line, we

propose this combination therapy may be a promising alternative treatment for this hard to treat form of breast cancer.

Overall, the present work shows for the first time that PARPis can induce a reversible p53-independent senescence state that can be combined with senolytic agents to potentiate cancer cell death. Unlike the majority of combination therapies using PARPis, this strategy does not involve HR synthetic lethality but targets the resulting cell fate induced by these inhibitors.

2.3.2.6 Acknowledgements

We thank all laboratory members for valuable comments and discussions and Jackie Chung for manuscript editing. This work was supported by the Institut du cancer de Montréal (DP, AMMM, FR) and by grants from the Canadian Institute for Health Research (MOP114962 to FR), the Terry Fox Research Institute (1030 to FR) and the Cancer Research Society in partnership with Ovarian Cancer Canada (20087 to AMMM, DP). FR is supported by a Fonds de recherche du Québec - Santé (FRQS) junior I career award (22624). AMMM, DP, FR are researchers of the Centre de recherche du Centre hospitalier de l'Université de Montréal (CRCHUM), that receive support from the FRQS. The ovarian tumor banking was supported by the Banque de tissus et de données of the Réseau de recherche sur le cancer of the FRQS affiliated with the Canadian Tumor Repository Network (CTRNet). H.F. was supported in part by the Michèle St-Pierre Bursary of the Institut du cancer de Montréal.

Figure 1

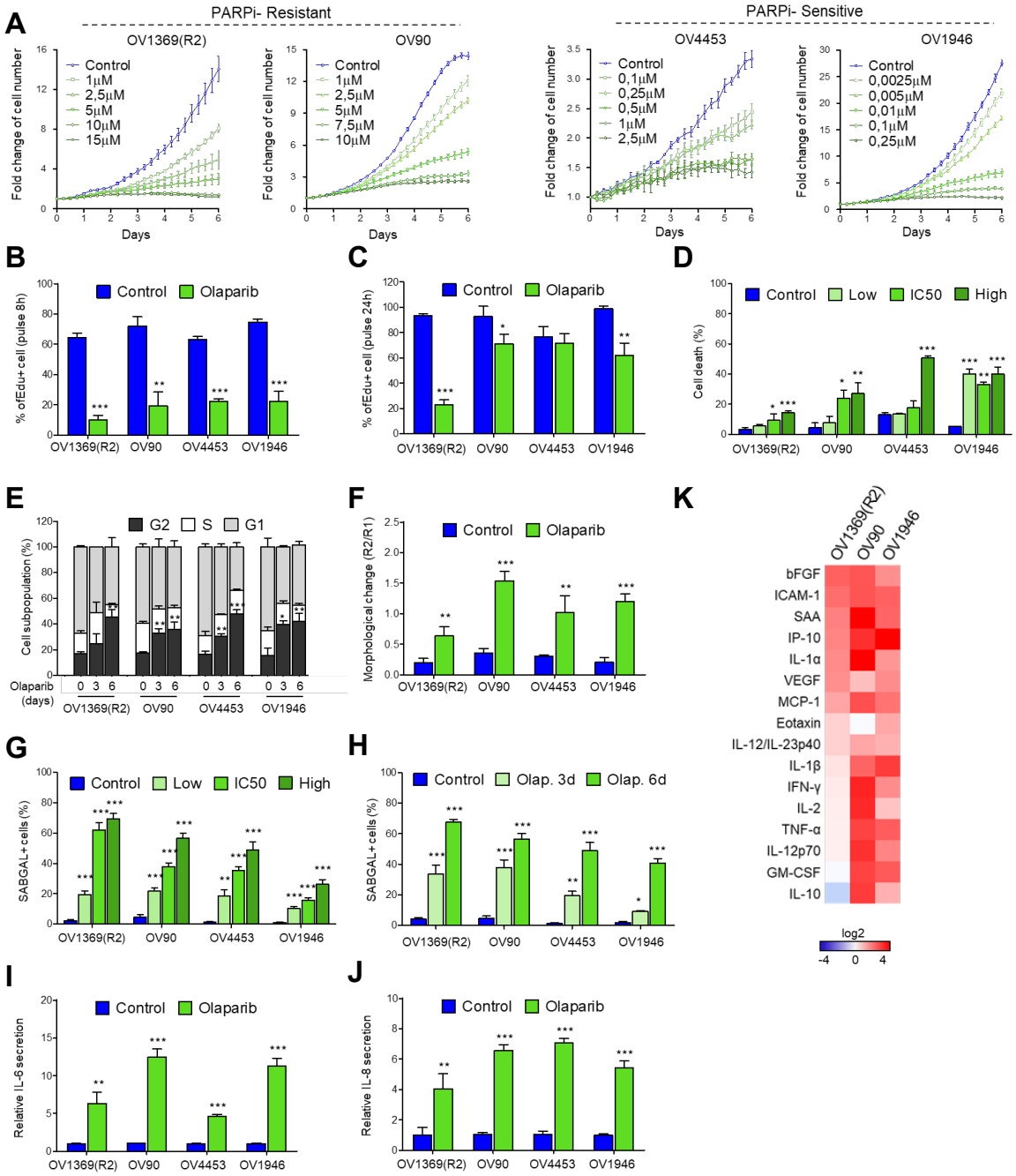
A
PARPi- Resistant
PARPi- Sensitive
OV1369(R2)
OV90
OV4453
OV1946
Control
1μM
2,5μM
5μM
10μM
15μM
7,5μM
0,1μM
0,25μM
0,5μM
0,0025μM
0,005μM
0,01μM
0,1μM
Fold change of cell number
Days
B
% ofEdu+ cell (pulse 8h)
Control
Olaparib
C
% ofEdu+ cell (pulse 24h)
D
Cell death (%)
Low
IC50
High
E
Cell subpopulation (%)
G2
S
G1
Olaparib (days)
F
Morphological change (R2/R1)
K
bFGF
ICAM-1
SAA
IP-10
IL-1α
VEGF
MCP-1
Eotaxin
IL-12/IL-23p40
IL-1β
IFN-γ
IL-2
TNF-α
IL-12p70
GM-CSF
IL-10
log2
G
SABGAL+cells (%)
H
Olap. 3d
Olap. 6d
I
Relative IL-6 secretion
J
Relative IL-8 secretion

Figure 1. Olaparib induces a senescence-like phenotype in *TP53* mutant HGSOC cell lines. A) Olaparib resistant [OV1369(R2), OV90] and sensitive (OV4453 and OV1946) HGSOC cell lines, stably expressing H2B-GFP, were exposed to different concentrations of Olaparib during 6 days with analysis of cell numbers every 6 hours. Cell proliferation curves were plotted and each point shows the mean ± SEM from three independent experiments. Control = non-treated. **B-C)** Analysis of 8h (**B)** or 24h (**C)** EdU pulse following 6 days exposure of HGSOC cells to IC_{50} Olaparib concentrations. Bars represent mean ± SEM of percentages of EdU positive cells obtained by three independent experiments. **D)** Flow cytometry analysis of Annexin-V and DRAQ-7 staining of HGSOC cells after 6 days exposure to low (light green), IC_{50} (green) and high (dark green) Olaparib concentrations. Bars represent mean ± SEM of percentages of Annexin-V/DRAQ-7 positive cells obtained by three independent experiments. **E)** Flow cytometry analysis of cell cycle populations following 3 and 6 days exposure of HGSOC cells to IC_{50} Olaparib concentrations and non-treated. Bars represent mean ± SEM of percent cells in G1 (grey), S (white), and G2 (black) phases obtained by three independent analyses. **F)** Cell morphology analysis by flow cytometry. Bars represent ratio of the number of cells in region R2 (high FSC and SSC) to the number of cells in region R1 (normal FSC and SSC) (see Fig. S2A) following 6 days exposure of HGSOC cells to IC_{50} Olaparib concentrations (green) or non-treated (control, blue). **G-H)** Quantification of SA-β-gal-positive (SABGL+) cells following exposure of HGSOC cells to low (light green), IC_{50} (green) and high (dark green) Olaparib concentrations **(G)**, or exposure to IC_{50} Olaparib concentrations for 3 or 6 days **(H)**. Bars represent mean ± SEM of percent positive cells obtained by three independent experiments. **I-K)** Supernatants of cell cultures were collected at 6 days for control and Olaparib treated. Medium was changed 24 hours before supernatant collection without FBS. Levels of IL-6 **(I)** and IL-8 (**G)** were measured by an ELISA assay. Bars represent mean ± SEM of fold change in comparison to control from three independent experiments. **(K)** Analysis of other secreted cytokines by the MSD serum based multiplex assay. Fold change in cytokines at 6 days post-Olaparib treatment versus baseline are depicted, with each column representing an individual cell line. * denotes $p < 0.05$, ** $p < 0.01$, *** $p < 0.001$.

Figure 2

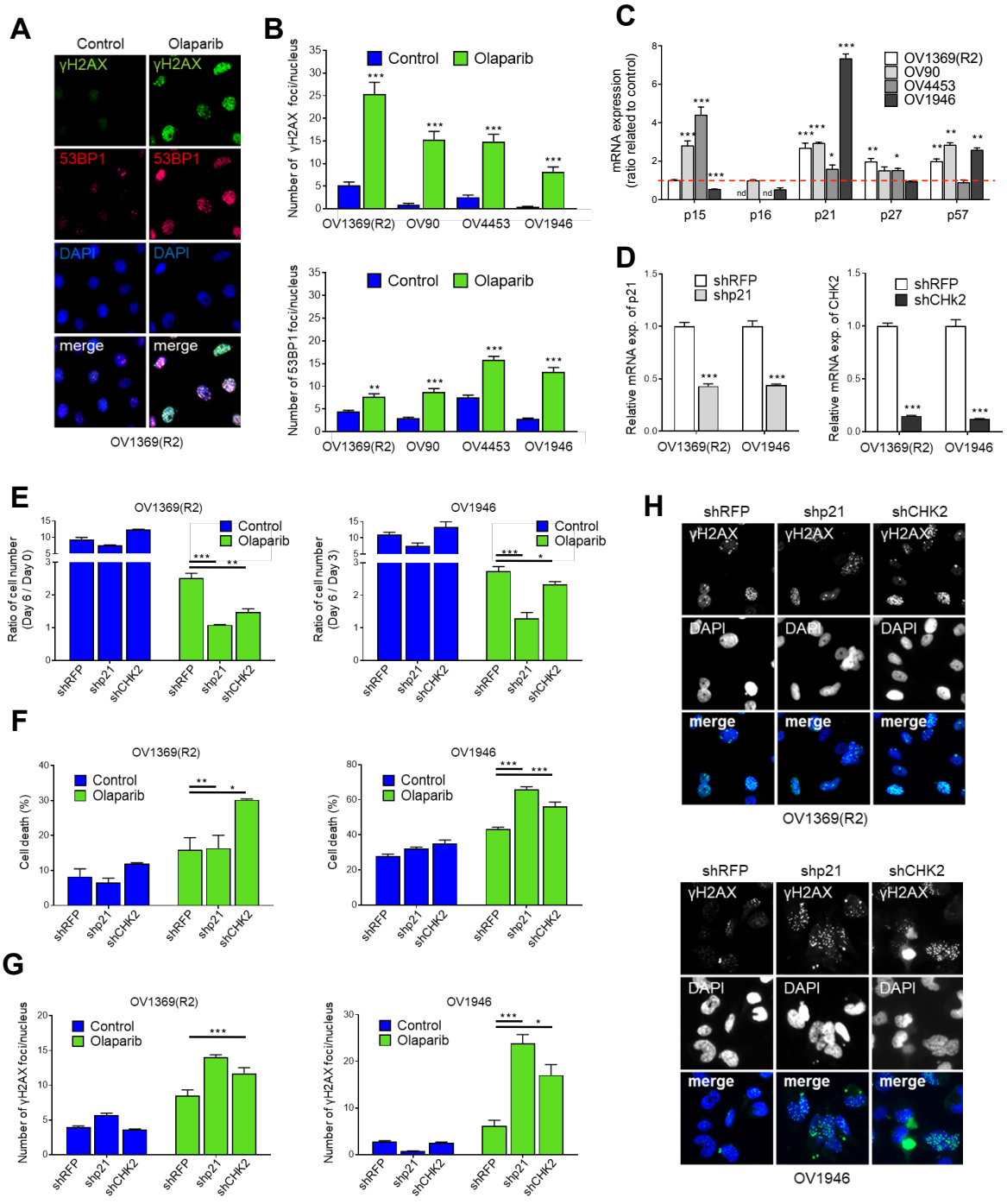
A
Control
Olaparib
γH2AX
53BP1
DAPI
merge
OV1369(R2)
B
Control
Olaparib
Number of γH2AX foci/nucleus
Number of 53BP1 foci/nucleus
OV1369(R2)
OV90
OV4453
OV1946
C
mRNA expression (ratio related to control)
OV1369(R2)
OV90
OV4453
OV1946
p15
p16
p21
p27
p57
nd
D
shRFP
shp21
shCHk2
Relative mRNA exp. of p21
Relative mRNA exp. of CHK2
E
OV1369(R2)
OV1946
Ratio of cell number (Day 6 / Day 0)
Ratio of cell number (Day 6 / Day 3)
shRFP
shp21
shCHK2
F
Cell death (%)
G
Number of γH2AX foci/nucleus
H
shRFP
shp21
shCHK2
γH2AX
DAPI
merge
OV1369(R2)
OV1946

Figure 2. Involvement of p21 and Chk2 in Olaparib-induced senescence. A-B) HGSOC cell lines were treated with the IC_{50} Olaparib concentrations for 6 days then stained for γ-H2AX and 53BP1. Non-treated cells were used as a control. **(A)** Representative images of γ-H2AX and 53BP1 immunostaining after 6 days of Olaparib treatment compared with non-treated controls of OV1369(R2) cells. Images are at 400X magnification. **(B)** The number of γ-H2AX and 53BP1 foci per nucleus were determined by analyzing >150 cells per condition and shown as the mean ± SEM of three independent experiments. **C)** Real-time qPCR was performed in Olaparib-treated cell lines to evaluate the relative mRNA levels of the cytokines p15, p16, p21, p27, and p57. The values represent the fold change expression related to control non-treated. The mean ± SEM of three independent experiments is shown. nd = not detectable **D)** p21 and Chk2 is effectively silenced by shRNA in OV1369(R2) and OV1946 cells. Real time qPCR of p21 and Chk2 mRNA in shp21 and shChk2 cells relative to the shRFP cells. Bar graph represents mean ± SEM of three independent experiments. **E)** Bar graph shows mean ± SEM of the fold change in cell number at day 6 related to day 0 for OV1369(R2) and OV1946 stably expressing shRFP, shp21 or shChk2 and treated with IC_{50} Olaparib concentrations for 6 days. **F.** Flow cytometry analysis of Annexin-V and DRAQ-7 staining following 6 days exposure of OV1369(R2) and OV1946 cells to IC_{50} Olaparib concentrations. Bars represent mean ± SEM of percentages of Annexin-V/DRAQ-7 positive cells obtained by three independent experiments **G-H)** OV1369(R2) and OV1946 stably expressing shRFP, shp21 or shChk2 were treated with IC_{50} Olaparib concentrations for 6 days then stained for γ-H2AX. Non-treated cells were used as a control. The number of γ-H2AX foci per nucleus were determined by analyzing >150 cells per condition and shown as the mean ± SEM of three independent experiments **(G)**. Representative images of γ-H2AX immunostaining **(H)** after 6 days of Olaparib treatment compared with non-treated controls. Images are at 400X magnification. * denotes $p < 0.05$, ** $p < 0.01$, *** $p < 0.001$.

Figure 3

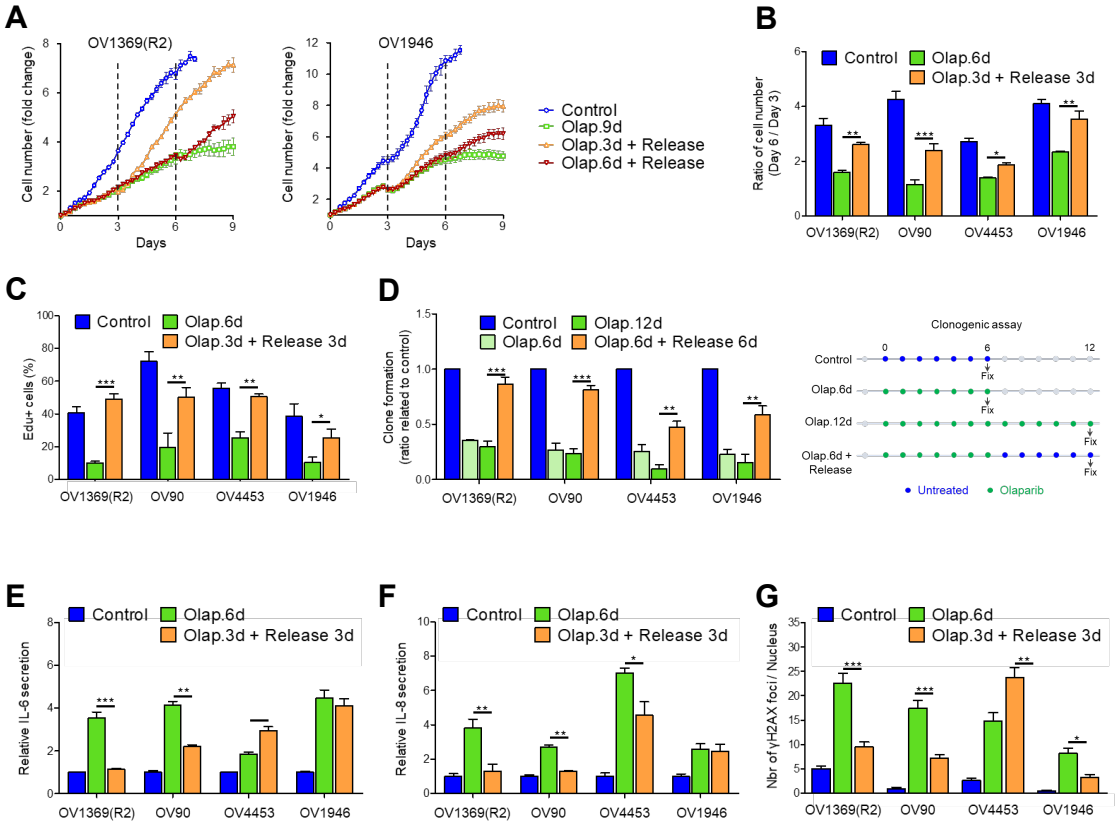
A
OV1369(R2)
OV1946
Cell number (fold change)
Days
Control
Olap.9d
Olap.3d + Release
Olap.6d + Release
B
Control
Olap.6d
Olap.3d + Release 3d
Ratio of cell number (Day 6 / Day 3)
OV1369(R2)
OV90
OV4453
OV1946
C
Control
Olap.6d
Olap.3d + Release 3d
Edu+ cells (%)
D
Control
Olap.12d
Olap.6d
Olap.6d + Release 6d
Clone formation (ratio related to control)
Clonogenic assay
Control
Olap.6d
Olap.12d
Olap.6d + Release
Fix
Untreated
Olaparib
E
Relative IL-6 secretion
F
Relative IL-8 secretion
G
Nbr of γH2AX foci / Nucleus

Figure 3. Senescent phenotype induced by Olaparib is reversible. A) Representative proliferation curves of OV1369(R2) and OV1946 treated with IC_{50} Olaparib concentrations for 9 days (green) or 6 days and then without for the next 3 days (orange, release 6d) or 3 days and then without for the next 6 days (red, release 6d) or with DMSO for 9 days (blue, control). Cell numbers were assessed every 6 hours. Cell proliferation curves were plotted and each point shows the mean ± SEM from three independent experiments. **B)** Bar graph shows mean ± SEM of the fold change in cell number at day 6 related to day 3. Cells were treated with IC_{50} Olaparib concentrations for 6 days (green) or 3 days and then without for the next 3 days (orange, release 3d) or DMSO (blue, control). **C)** Bar graph represents mean ± SEM of the percentage of 8h-EdU pulse positive-cells at day 6 after either untreated cells (blue, control), 6 days Olaparib treatment (green) or treated for 3 days then release for 3 days (orange). **D)** Clonogenic assays were performed on untreated HGSOC cells (blue, control), cells treated with Olaparib for 6 (light green) or 12 days (green), or treated for 6 days then without for the next 6 days (orange). Bars represent mean ± SEM of the relative colony number obtained by three independent clonogenic assays. **E-F)** Bar graph shows mean ± SEM of the fold change in IL-6 **(E)** and IL-8 **(F)** secretion in response to Olaparib and removal treatment in relation to control. Supernatants of cell cultures were collected at 6 days for control, Olaparib and removal conditions. Medium was changed 24 hours before supernatant collection without FBS. Levels of IL-6 and IL-8 were measured by an ELISA assay. **G)** Cells under Olaparib treatment, the removal protocol and controls were stained for γ-H2AX and analysed by immunofluorescence imaging. Non-treated was used as a control condition. The number of γ-H2AX foci per nucleus was determined by analysing >150 cells per condition and shown as the mean ± SEM of three independent experiments. * denotes $p < 0.05$, ** $p < 0.01$, *** $p < 0.001$.

Figure 4

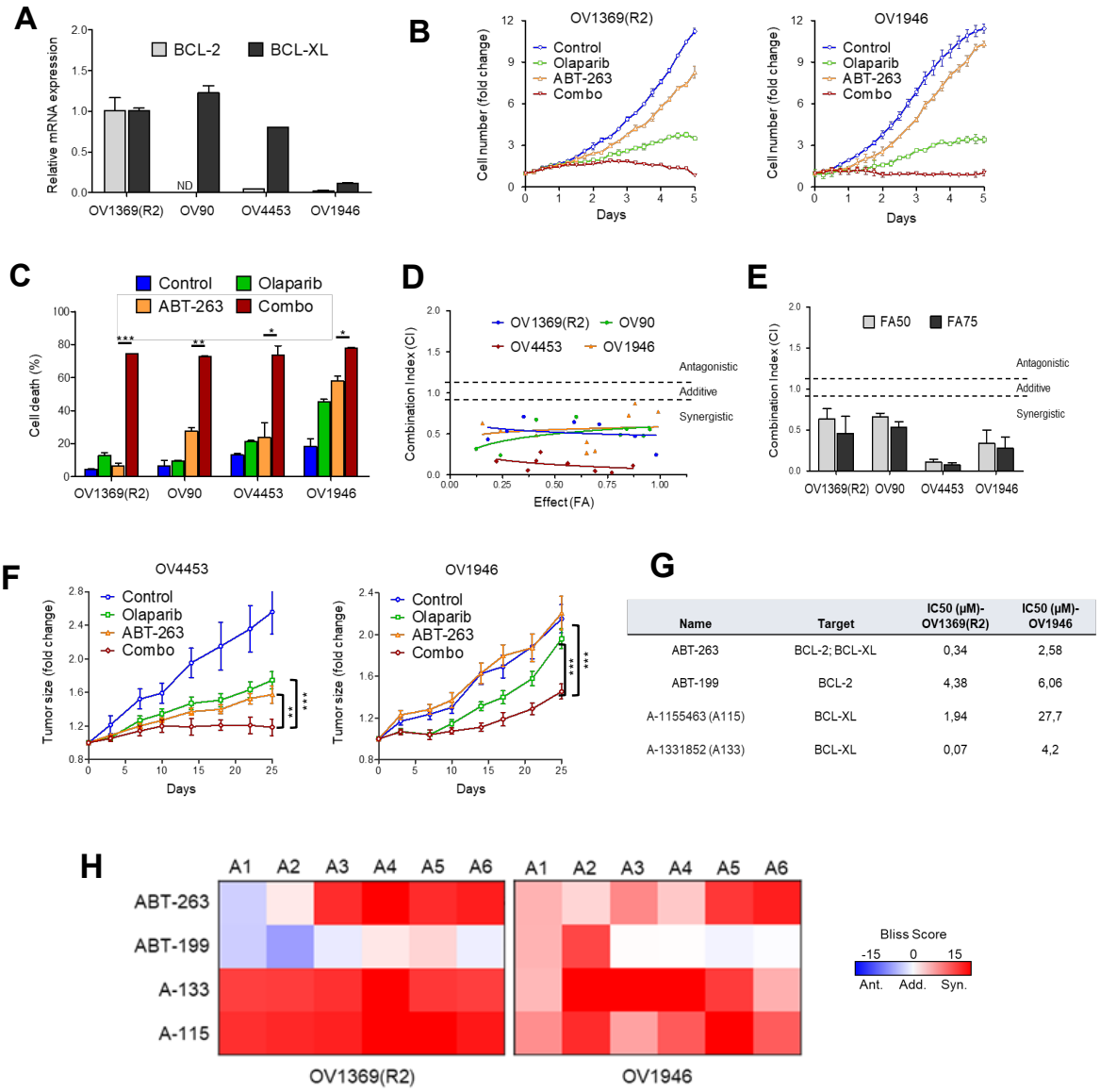

Name	Target	IC50 (μM)-OV1369(R2)	IC50 (μM)-OV1946
ABT-263	BCL-2; BCL-XL	0,34	2,58
ABT-199	BCL-2	4,38	6,06
A-1155463 (A115)	BCL-XL	1,94	27,7
A-1331852 (A133)	BCL-XL	0,07	4,2

Figure 4. Olaparib and Bcl2/Bcl-XL inhibitors are synergistic. A) Relative basal mRNA levels of Bcl2 and Bcl-XL were analysed in HGSOC cells by real-time qPCR. The values represent the fold change expression related to OV1369(R2). ND = not detectable. **B)** Dose-effect curves for the resistant OV1369(R2) and sensitive OV1946 cell lines treated with Olaparib (10 or 0.1 µM, respectively), ABT-263 (0.25 or 2.5 µM, respectively), or Olaparib/ABT-263 (10/0.25 or 0.1/2.5 µM, respectively) for 6 days. **C)** HGSOC cells were treated with DMSO as control (blue), Olaparib IC_{50} concentrations (green), ABT-263 (0.25 µM for OV1369(R2), 2.5 µM for all the others) (orange) or Olaparib/ABT-263 (combo, red) for 6 days and subjected to flow cytometry for apoptosis analysis. The percentage of Annexin-V/DRAQ-7-positive cells is shown as mean ± SEM of three independent experiments**. D-E)** CI values of Olaparib combined with ABT-263 treatment at the ratio of 75/1 for OV1369(R2), 8/1 for OV90, 0.1/1 for OV4453 and 0.1/1 for OV1946. Curve represents the CI for the entire fraction affected (Fa) of the four cell lines **(D)**. Bar graph represents mean ± SEM of the CI at Fa 0.50 and Fa 0.75 of the four cell lines **(E)**. **F)** Mice presenting OV4453 or OV1946 xenografts were injected every two days for a maximum of 3 times per week, intraperitoneally with Olaparib (50 mg/kg, green line, n=12), orally by gavage with ABT-263 (50 mg/kg, orange line, n=7), or the combination Olaparib + ABT-263 (red line, n=10). 12% DMSO was injected intraperitoneally in controls (blue line, n=8). Tumor volumes were measured with callipers every third day. **G)** Table of ABT-263, ABT-199, A-1155463 and A-1331852 IC_{50} (µM) displaying mean ± SEM data obtained after 6 days proliferation of OV1369(R2) and OV1946; these data determined the range concentrations used for this study. **H)** Heat map of Bliss scores for combination treatments between Olaparib and ABT-263, ABT-199, A-133 (A-1331852) or A-115 (A-1155463). Negative score values indicate antagonism (Ant.), values around zero indicate additive effects (Add.) and positive values indicate synergy (Syn.). * denotes $p < 0.05$, ** $p < 0.01$, *** $p < 0.001$.

Figure 5

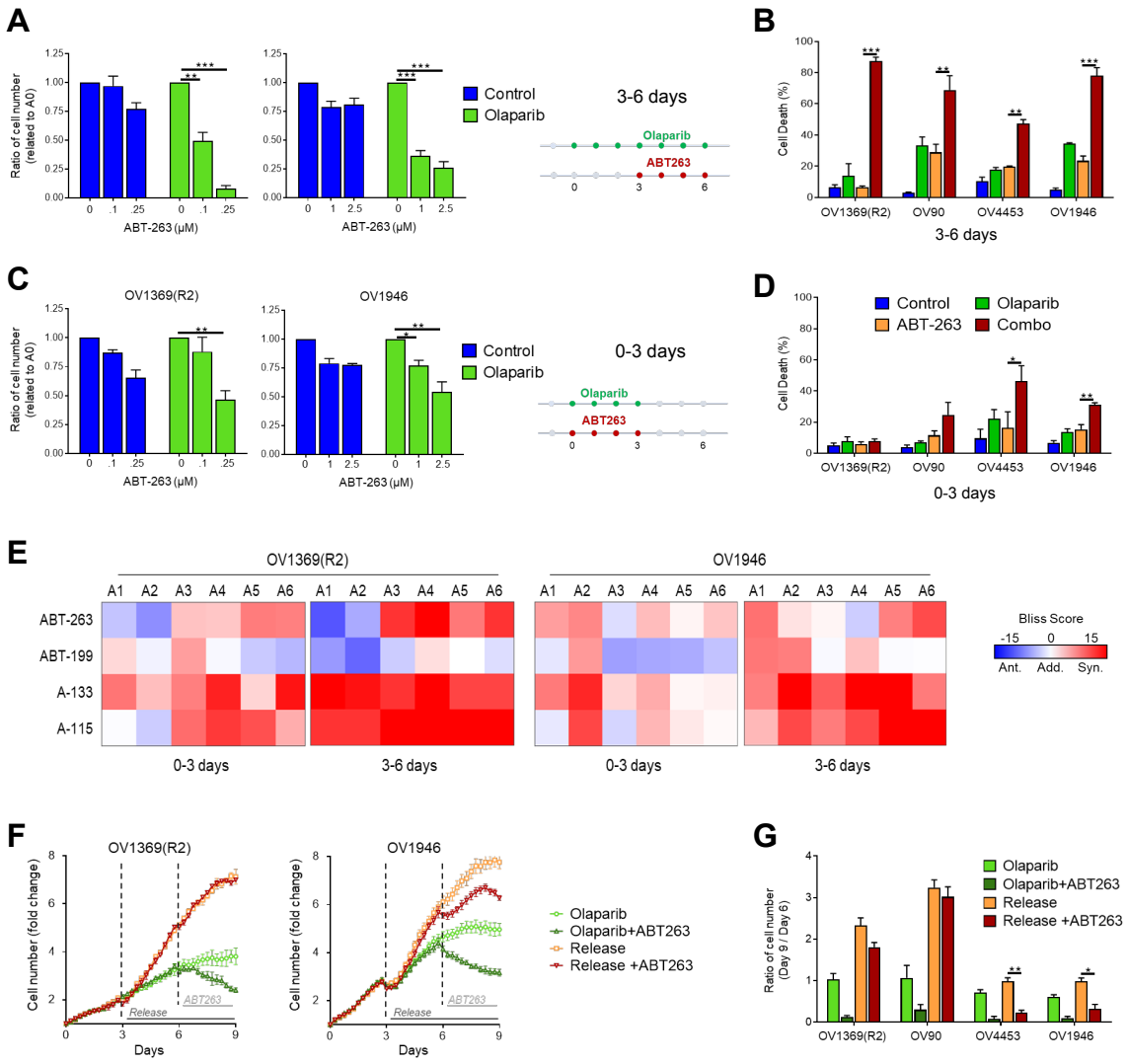
A
Ratio of cell number (related to A0)
ABT-263 (μM)
Control
Olaparib
3-6 days
Olaparib
ABT263
B
Cell Death (%)
OV1369(R2)
OV90
OV4453
OV1946
3-6 days
C
OV1369(R2)
OV1946
0-3 days
D
Control
Olaparib
ABT-263
Combo
0-3 days
E
ABT-263
ABT-199
A-133
A-115
Bliss Score
Ant. Add. Syn.
0-3 days
3-6 days
F
Cell number (fold change)
Days
Release
ABT263
Olaparib
Olaparib+ABT263
Release
Release +ABT263
G
Ratio of cell number (Day 9 / Day 6)

Figure 5. Bcl2/Bcl-XL inhibitors specifically target Olaparib-induced senescent cells. Cells were treated with Olaparib for 6 days and sequential addition of ABT-263 after 3 days of Olaparib **(A-B)** or co-treated with Olaparib and ABT-263 for 3 days **(C-D)**. Bar graph shows mean ± SEM of the fold change in cell numbers on day six related to A0 (control non-treated for blue bars; Olaparib-treated for green bars) at different concentrations of ABT-263 added on day 3 **(A, C)**. Flow cytometry for apoptosis analysis of HGSOC cells treated with Olaparib for 6 days and sequential addition of ABT-263 after 3 days of Olaparib **(B)**, or co-treated with Olaparib and ABT-263 for 3 days **(D)**. The percentage of Annexin-V/DRAQ-7-positive cells is shown as mean ± SEM of three independent experiments. **E)** Heat map of Bliss scores for combination treatments between Olaparib and ABT-263, ABT-199, A-133 (A-1331852) or A-115 (A-1155463) in OV1369(R2) (right) and OV1946 (left) cell lines. Cells were co-treated with Olaparib and Bcl2/Bcl-XL inhibitors for 3 days (0-3 days) or treated with Olaparib for 6 days and sequential addition of inhibitors after 3 days of Olaparib (3-6 days). **F)** Representative proliferation curves of OV1369(R2) and OV1946 treated with Olaparib for 9 days (light green), or treated with Olaparib for 6 days and sequential addition of ABT-263 for the next 3 days (dark green), or treated with Olaparib for 3 days and then without for the next 6 days (orange), or treated with Olaparib for 3 days and sequential addition of ABT-263 for the next 6 days (red). **G)** Bar graph represents mean ± SEM of the fold change in cell number between first day of ABT-263 (day 6) and last day of treatment (day 9) in the four cell lines. * denotes $p < 0.05$, ** $p < 0.01$, *** $p < 0.001$.

Figure 6

A

Name	IC50 (μM)-OV1369(R2)	IC50 (μM)-OV1946
Piperlongumine (PPL)	0,58	1,48
Fisetin (F)	72,8	32,09
Dasatinib (D)	0,04	14,26
Quercitin (Q)	192,1	58,02

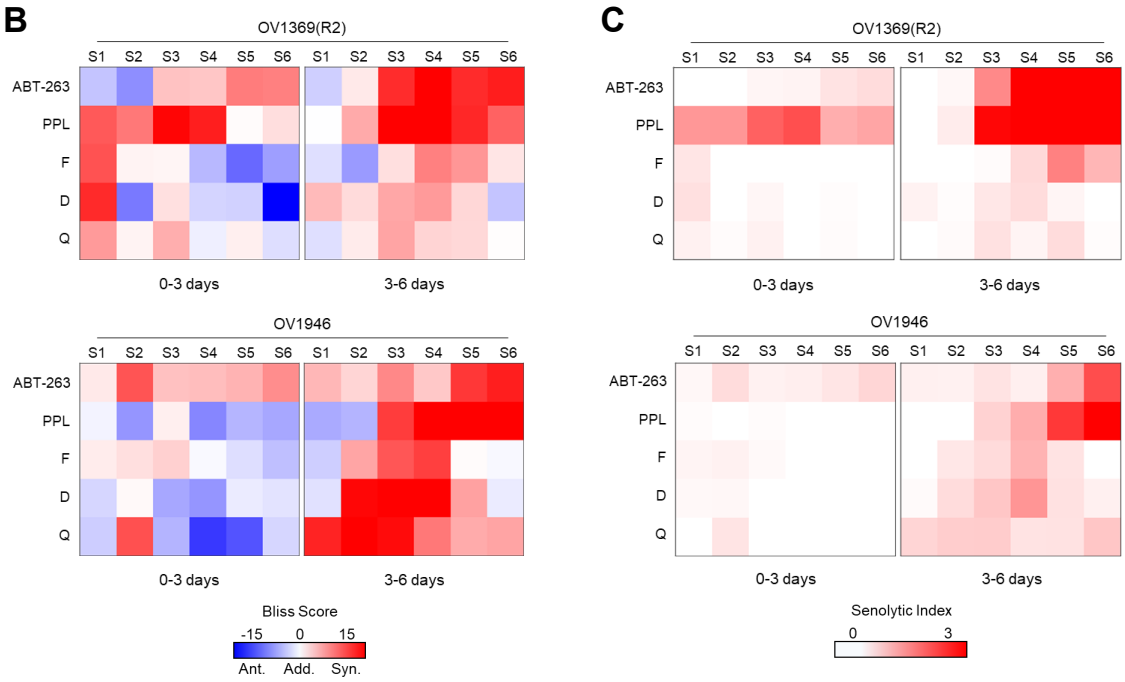

Figure 6. Effects of other senolytic drugs on Olaparib-treated HGSOC cells. A) Table of Piperlongumine (PPL), Fisetin (F), Dasatinib (D) and Quercetin (Q) IC_{50} (μM) displaying mean ± SEM data obtained after 6 days proliferation of OV1369(R2) and OV1946 cells; these data determined the range concentrations used for this study. **B)** Heat map of Bliss scores for combination treatments between Olaparib and ABT-263, PPL, F, D and Q in OV1369(R2) (top) and OV1946 (bottom) cell lines. Cells were co-treated with Olaparib and senolytics for 3 days (0-3 days) or treated with Olaparib for 6 days and sequential addition of senolytics after 3 days of Olaparib (3-6 days). **C)** Senolytic index for each dose combination on OV1369(R2) and OV1946 after 3 days Olaparib and senolytics co-treatment or after treatment of Olaparib for 6 days and sequential addition of senolytrics after 3 days of Olaparib.

Figure 7

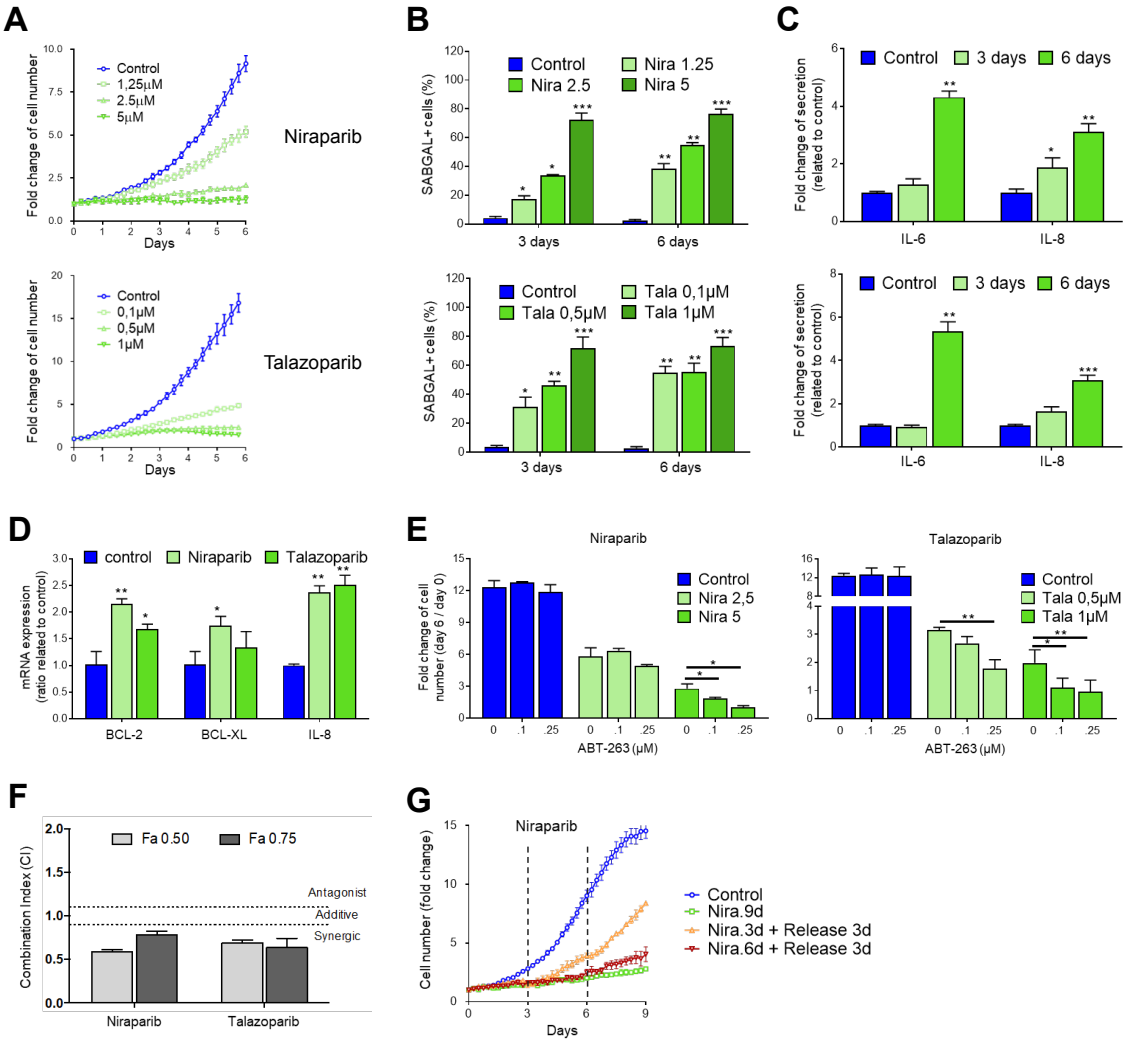
A
Fold change of cell number
Control
1,25µM
2.5µM
5µM
Days
Niraparib
Control
0,1µM
0,5µM
1µM
Talazoparib
B
SABGAL+ cells (%)
Control
Nira 1.25
Nira 2.5
Nira 5
3 days
6 days
Control
Tala 0,1µM
Tala 0,5µM
Tala 1µM
C
Fold change of secretion (related to control)
Control
3 days
6 days
IL-6
IL-8
D
mRNA expression (ratio related to control)
control
Niraparib
Talazoparib
BCL-2
BCL-XL
IL-8
E
Niraparib
Talazoparib
Fold change of cell number (day 6 / day 0)
Control
Nira 2,5
Nira 5
Tala 0,5µM
Tala 1µM
ABT-263 (µM)
F
Combination Index (CI)
Fa 0.50
Fa 0.75
Antagonist
Additive
Synergic
Niraparib
Talazoparib
G
Niraparib
Cell number (fold change)
Control
Nira.9d
Nira.3d + Release 3d
Nira.6d + Release 3d
Days

Figure 7. Other PARP inhibitors also induce the senescence-like phenotype in HGSOC cells. OV1369(R2) was treated with different concentrations of Niraparib or Talazoparib. **A)** Proliferation response throughout 6 days of treatment with analysis of cell numbers every 6 hours. Control = non-treated. **B)** Quantification of SA-β-gal (SABGAL)-positive cells based on microscopic analysis performed on day 3 and 6 after treatment with Niraparib (top) or Talazoparib (botttom). **C)** Secretion of IL-6 or IL-8 in response to Niraparib or Talazoparib treatment monitored by ELISA analysis. OV1369(R2) was treated with 2.5 μM Niraparib or 0.5 μM Talazoparib, and supernatants of cell cultures were collected at the indicated time points (3 and 6 days). Medium was changed 24 hours before supernatant collection without FBS. **D)** Relative mRNA levels of Bcl2, Bcl-XL, IL-6 and IL-8 presented as fold change expression related to control. Total RNA was extracted from OV1369(R2) treated with 2.5μM Niraparib (Nira) or 0.5μM Talazoparib (Talazo) for 6 days and real-time qPCR was then performed. The mean ± SEM of three independent experiments is shown. **E)** Bar graph represents the fold change of cell number at day 0 and day 6 of OV1369(R2) co-treated with Niraparib and ABT-263 or Talazoparib and ABT-263 for 6 days. **F)** Bar graph represents the CI at Fa 0.50 and Fa 0.75 of OV1369(R2) treated with the combination therapy of Niraparib/ABT263 at a ratio of 10/1 or Talazoparib/ABT-263 at the ratio of 2/1. **G)** Representative proliferation curve in response to different Niraparib conditions for 6 days. OV1369(R2) was treated with 2.5μM of Niraparib at day 1 and at day 3 the medium was removed and replaced by fresh medium for the next 3 days. * denotes $p < 0.05$, ** $p < 0.01$, *** $p < 0.001$.

SUPPLEMENTAL DATA

Supplementary Figure S1

A

Cell lines	Olaparib clonogenic IC_{50} (µM)	Olaparib proliferation IC_{50}(µM)	Selected concentrations (µM)		
			Low	IC50	High
OV1369(2)	21.71 ± 10.33	9.45 ± 1.05	2.5	10	15
OV90	7.04 ± 2,33	5.9 ± 0.4	2.5	7.5	10
OV4453	0.01 ± 0.0009	0.95 ± 0.05	0.1	0.5	2.5
OV1946	0,07 ± 0.05	0.195 ± 0.0045	0.01	0.1	0.25

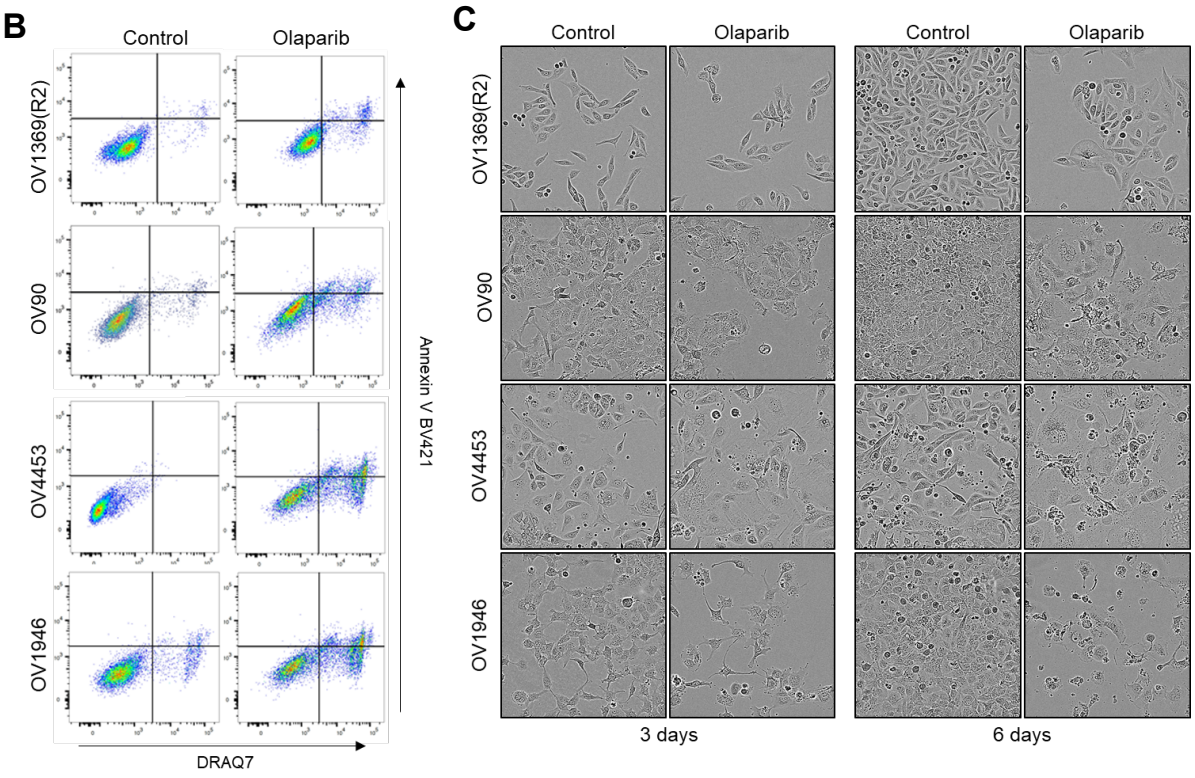

Supplementary Figure S1. Evaluation of Olaparib sensitivity in HGSOC cell lines. A) Table of Olaparib IC_{50} (μM) displaying mean ± SEM data obtained by previous clonogenic assays [14] or after 6 days proliferation; these data determined the Low, IC_{50} and High concentrations used for this study. **B)** Representative flow cytometry analysis of apoptosis showing DRAQ-7 positive cell population (X-axis) and Annexin-V positive cells (Y-axis) at day 6. **C.** Images represent control and Olaparib-treated HGSOC cells at day 3 and 6.

Supplementary Figure S2

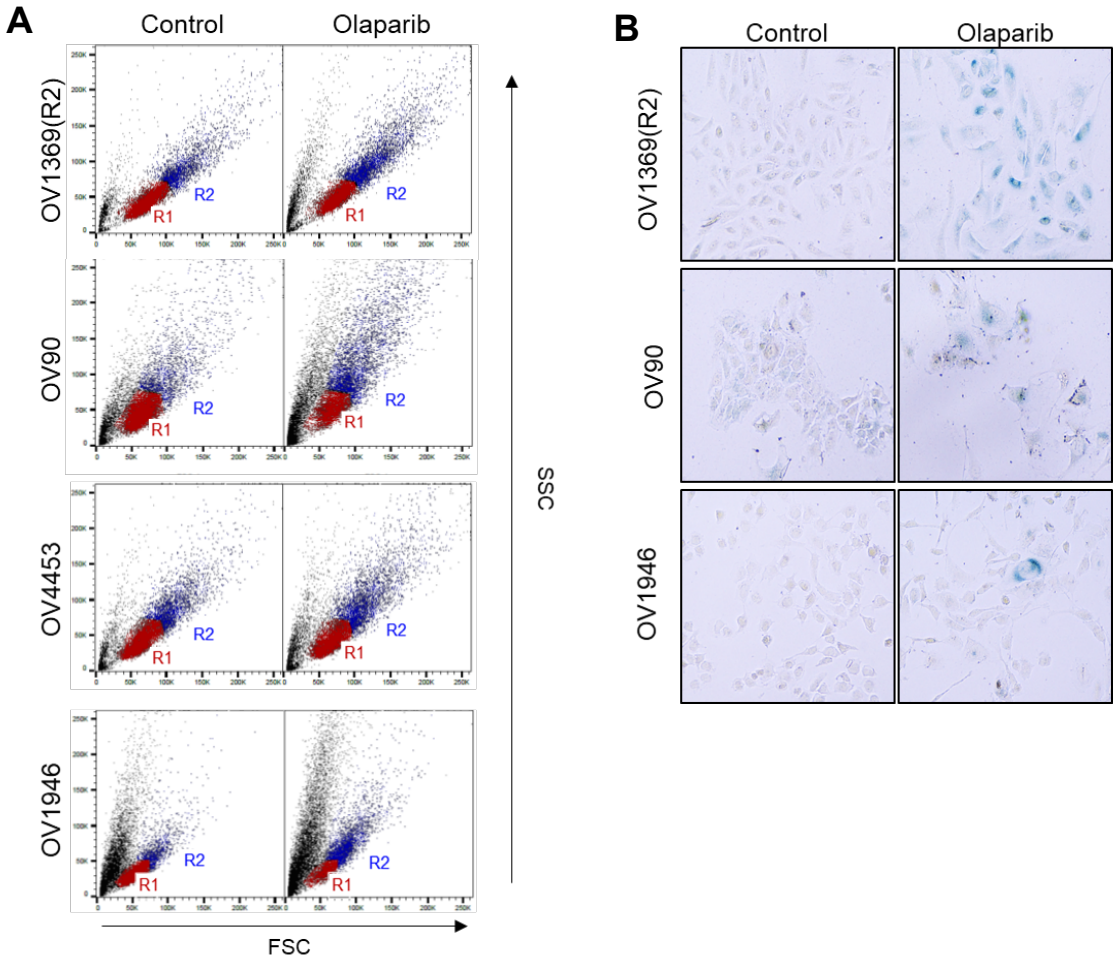

Supplementary Figure S2. Olaparib induces a senescent phenotype in HGSOC cell lines. A) Representative flow cytometry analysis of the cell population plot for forward scatter factor (FSC, indicative of size, X-axis) and side scatter factor (SSC, indicative of granularity, Y-axis). **B)** Representative morphology and SA-B-Gal staining image of OV1369(R2), OV90 and OV1946 after 6 days of Olaparib treatment.

Supplementary Figure S3

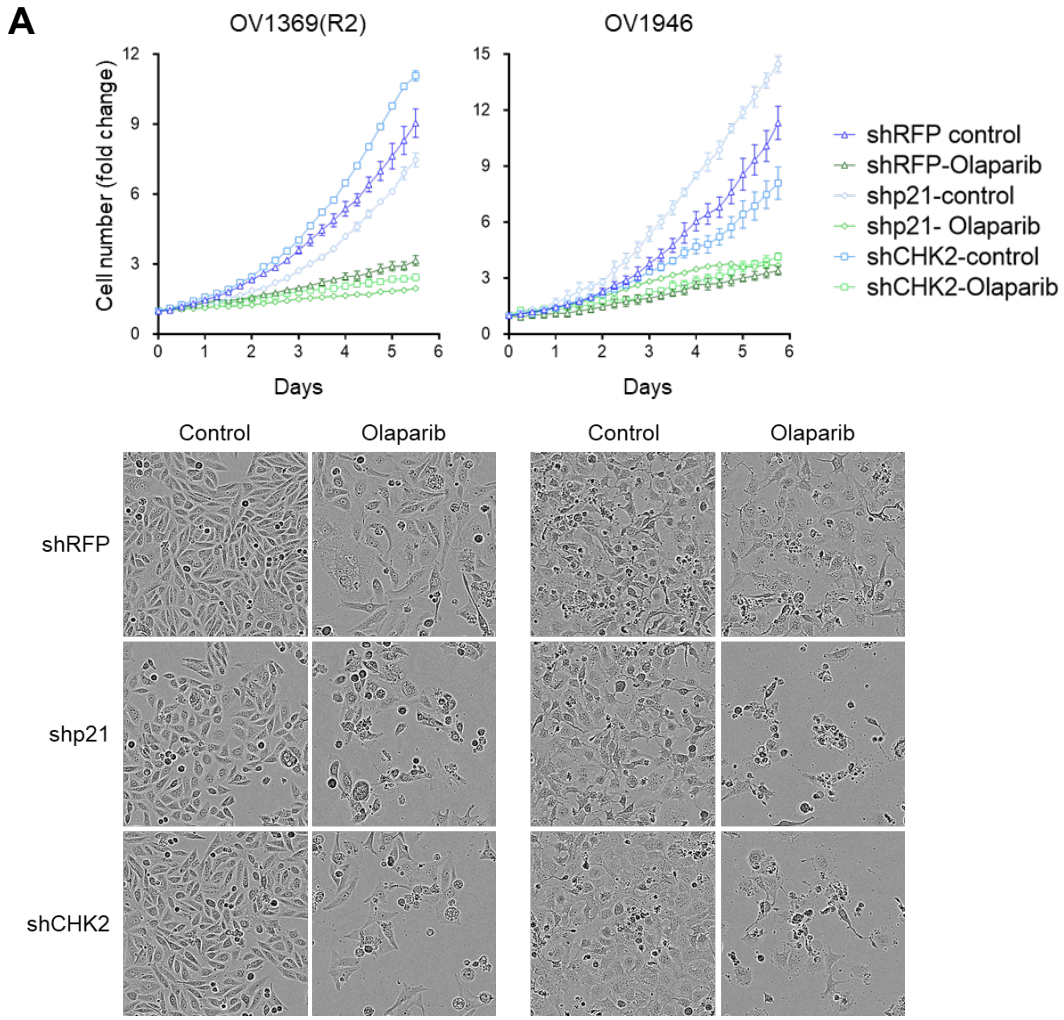

Supplementary Figure S3. Cell viability of HGSOC cells after p21 or Chk2 knockdown, and analysis of Olaparib efficacy. A) Olaparib resistant OV1369(R2) and sensitive OV1946 HGSOC cell lines, stably expressing shRFP, shp21 or shChk2, were exposed to different concentrations of Olaparib during 6 days with analysis of cell numbers every 6 hours. Cell proliferation curves were plotted and each point shows the mean ± SEM from three independent experiments. Control = non-treated. Pictures are corresponding images taken at day 6. **B)** Western blot detection of PAR polymers in OV1369(R2) after 1, 3 or 6 days exposure to 10 μM of Olaparib, with or without H_2O_2 pre-treatment (1 mM). Actin was used as a loading control.

Supplementary Figure S4

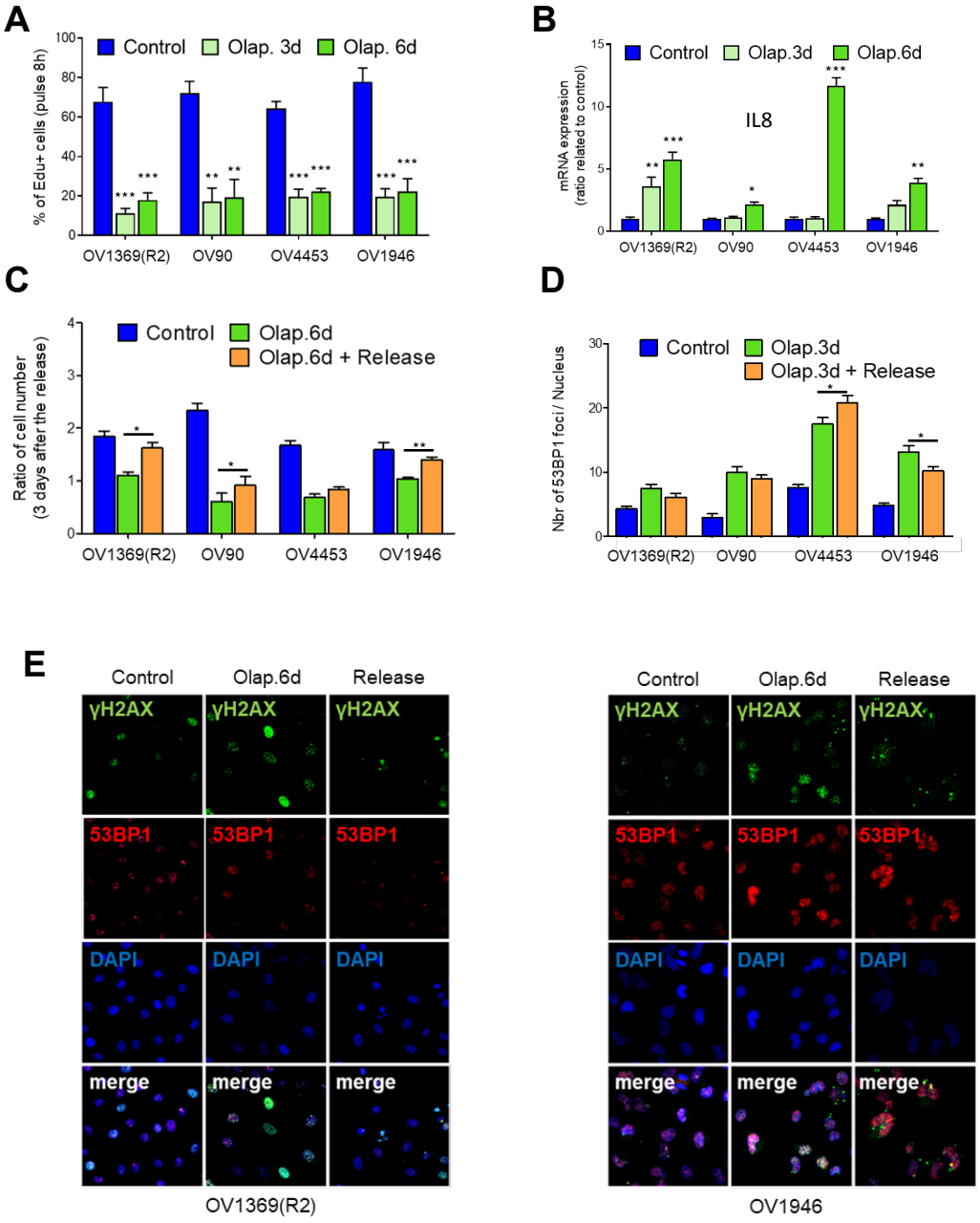

Supplementary Figure S4. Evaluation of the reversible senescent phenotype induced by Olaparib. A) 8h-EdU pulse following 3 and 6 days exposure of HGSOC cells to IC_{50} Olaparib concentrations. The percentages of EdU positive cells are shown as the mean ± SEM of three independent experiments. **B)** Real-time qPCR to evaluate the relative mRNA levels of IL-8. Bars represent mean ± SEM of the fold change expression related to control obtained by three independent experiments. **C)** Bar graph shows mean ± SEM of the fold change in cell number at day 9 related to day 6. Cells were treated with IC_{50} Olaparib doses for 9 days (green) or 6 days and then without for the next 3 days (orange, release 6d) or DMSO (blue, control). **D)** Cells under Olaparib treatment, the removal protocol and controls were stained for 53BP1 and analysed by immunofluorescence imaging. Non-treated was used as a control condition. The number of 53BP1 foci per nucleus was determined by analysing >150 cells per condition and shown as the mean ± SEM of three independent experiments. **E)** Representative images of γ-H2AX and 53BP1 immunostaining after 6 days Olaparib or 3 days Olaparib and then release of two selected cell lines OV1369(R2) and OV1946. Images are at 400 X magnifications. * denotes $p < 0.05$, ** $p < 0.01$, *** $p < 0.001$.

Supplementary Figure S5

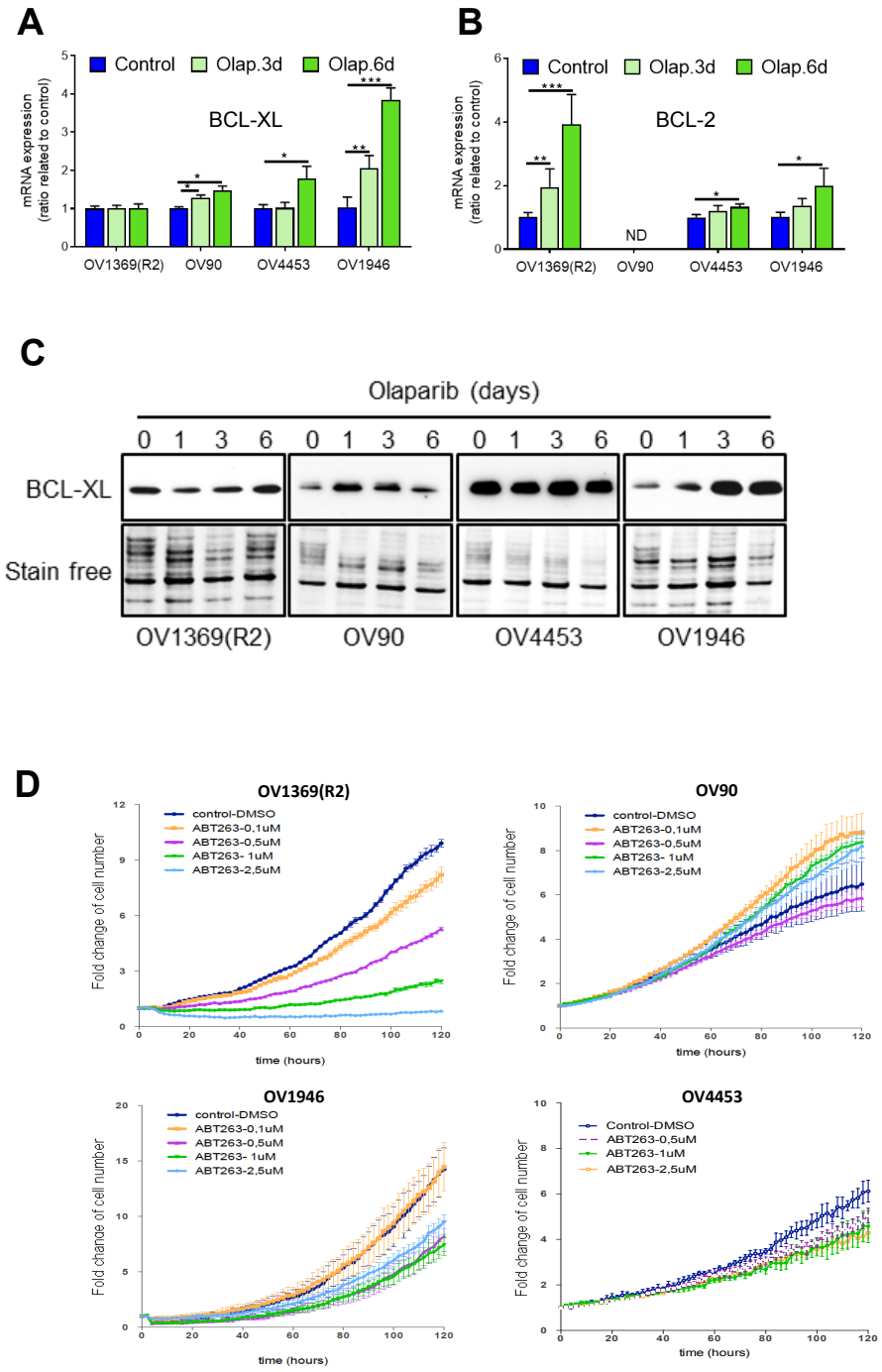

Supplementary Figure S5. Analysis of Bcl2 and Bcl-XL expression, and effects of Bcl2/Bcl-XL inhibitors in HGSOC cell lines. A-C) HGSOC cells were treated with IC_{50} Olaparib concentrations for 3 and 6 days. Relative mRNA levels of Bcl-XL **(A)** and Bcl-2 **(B)** were analysed by real-time qPCR. The values represent the fold change expression related to control. **C)** Western blot detection of Bcl-XL. Total protein stain was used as a loading control. **D)** Cell proliferation response of HGSOC cells to different concentrations of ABT-263 for 6 days with analysis of cell numbers every 6 hours. Control = non-treated. * denotes $p < 0.05$, ** $p < 0.01$, *** $p < 0.001$.

Supplementary Figure S6

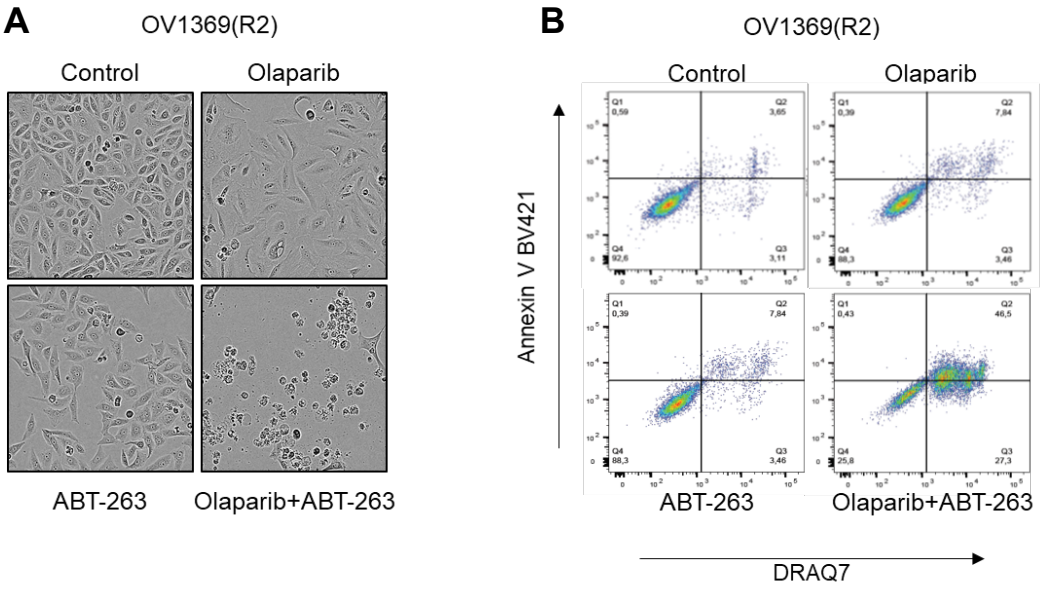

C

	OV1369(R2)		OV90		OV1946		OV4453	
	Olaparib	ABT-263	Olaparib	ABT-263	Olaparib	ABT-263	Olaparib	ABT-263
Ratio	75	1	7.5	1	0.1	1	0.1	1
D1	1	0.013	1	0.13	0.001	0.01	0.001	0.01
D2	2.5	0.03	2.5	0.33	0.01	0.1	0.01	0.01
D3	5	0.07	5	0.66	0.05	0.5	0.05	0.05
D4	7.5	0.1	7.5	1	0.1	1	0.1	1
D5	10	0.13	10	1.33	0.2	2	0.2	2
D6	15	0.2	15	2	0.3	3	0.3	3
D7	25	0.33	25	3.33	0.5	5	0.5	5

Concentration (μM)

D

OV1369(R2)

	ABT-263	ABT-199	A133	A115
A1	0,05	0,5	0,01	0,025
A2	0,1	1	0,025	0,05
A3	0,25	2,5	0,05	0,1
A4	0,5	5	0,075	0,5
A5	0,75	10	0,1	1
A6	1	20	0,5	2,5

Concentration (μM)

OV1946

	ABT-263	ABT-199	A133	A115
A1	0,25	0,5	0,5	0,5
A2	0,5	1	1	1
A3	0,75	2,5	2,5	2,5
A4	1	5	5	5
A5	2,5	10	10	10
A6	5	20	20	20

Concentration (μM)

Supplementary Figure S6. Bcl2/Bcl-XL inhibitors synergize with Olaparib in HGSOC cells. A) Representative images at day 6 of OV1369(R2) treated with 10 μM Olaparib or with 0.25 μM ABT-263 or the combination of Olaparib/ABT-263 (10/0.25 μM). **B)** Representative flow cytometry analysis of apoptosis showing DRAQ-7 positive cell population (X-axis) and Annexin-V positive cells (Y-axis) at day 6. **C)** Table of Olaparib and ABT-263 doses (μM) used for the CI model study (constant ratio) for OV1369(R2), OV90, OV1946 and OV4453 cells. **D)** Table of ABT-263, ABT-199, A-1155463 and A-1331852 doses (μM) used for the Bliss model study for the OV1369(R2) and OV1946 cell lines.

Supplementary Figure S7

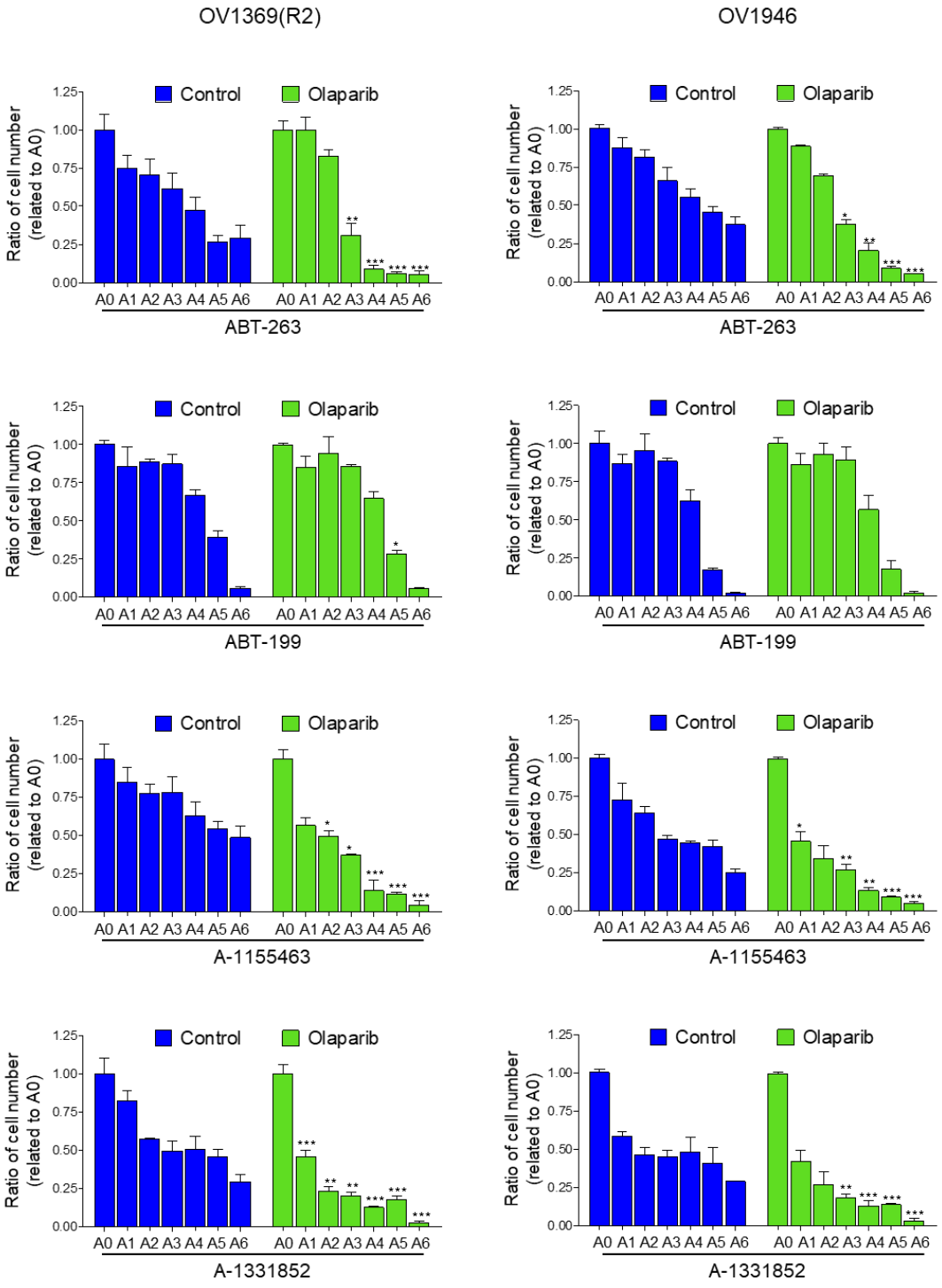

Supplementary Figure S7. Cell viability analysis for the co-treatment of Olaparib with distinct Bcl2/Bcl-XL inhibitors. Cells were co-treated with IC_{50} Olaparib concentrations and a range of ABT-263, ABT199, A-1155463 or A-1331852 concentrations (see Fig. S6D) for 6 days. Bar graph shows mean ± SEM of the fold change in cell numbers on day 6 related to A0 (control non-treated for blue bars; Olaparib-treated for green bars) at different concentrations of Bcl2/Bcl-XL inhibitors added on day 3. * denotes $p < 0.05$, ** $p < 0.01$, *** $p < 0.001$.

Supplementary Figure S8

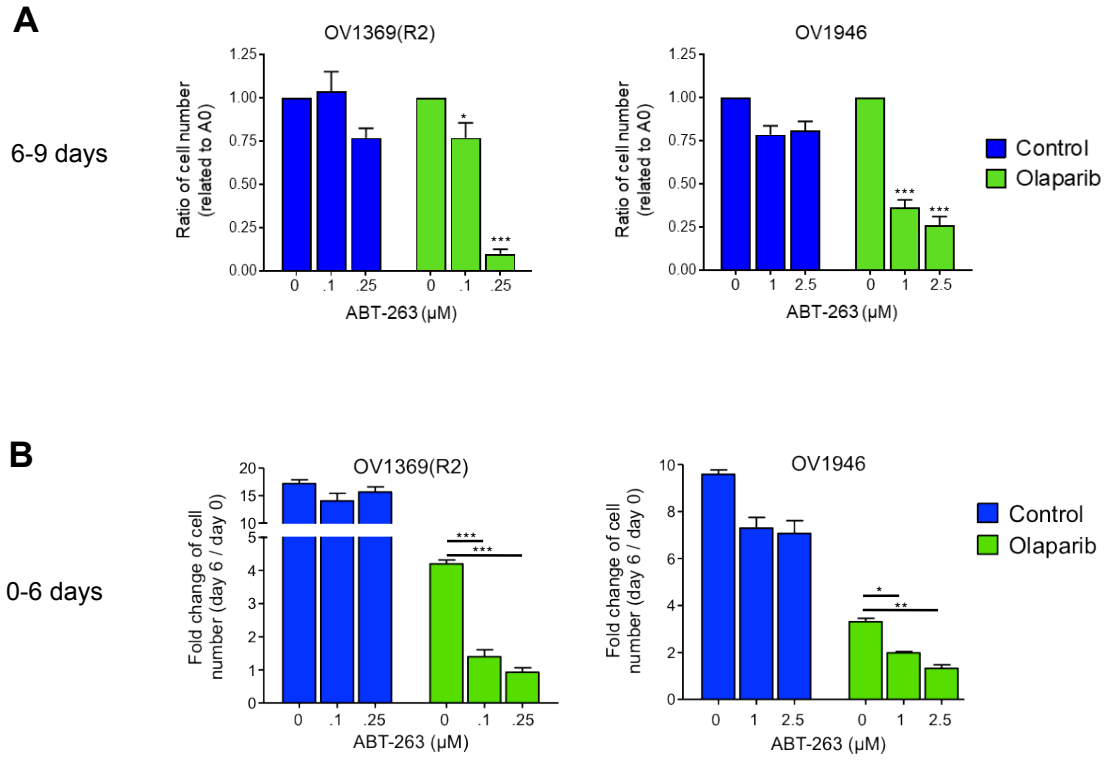

Supplementary Figure S8. Cell viability analysis for different time interval co-cultures of Olaparib with ABT-263. A) OV1369(R2) and OV1946 cells were treated with Olaparib for 9 days and sequential addition of ABT-263 after 6 days of Olaparib. Bar graph shows mean ± SEM of the fold change in cell number related to A0 (control non-treated for blue bars; Olaparib-treated for green bars) at different ABT-263 concentrations. **B)** Cells were co-treated with Olaparib and ABT-263 for 6 days. Bar graph represents the fold change of cell number at day 0 and day 6 for each cell line. * denotes $p < 0.05$, ** $p < 0.01$, *** $p < 0.001$.

Supplementary Figure S9

A

OV1369(R2)

Concentration (μM)	PPL	Fisetin	Dasatinib	Quercetin
S1	0,1	1	0,0001	10
S2	0,25	5	0,0025	25
S3	0,5	10	0,005	50
S4	0,65	25	0,01	100
S5	0,75	75	0,1	200
S6	0,85	100	0,5	300

OV1946

	PPL	Fisetin	Dasatinib	Quercetin
S1	0,1	1	1	5
S2	0,25	5	2,5	10
S3	0,5	10	4	25
S4	0,65	25	7	50
S5	0,75	75	10	75
S6	0,85	100	15	100

B

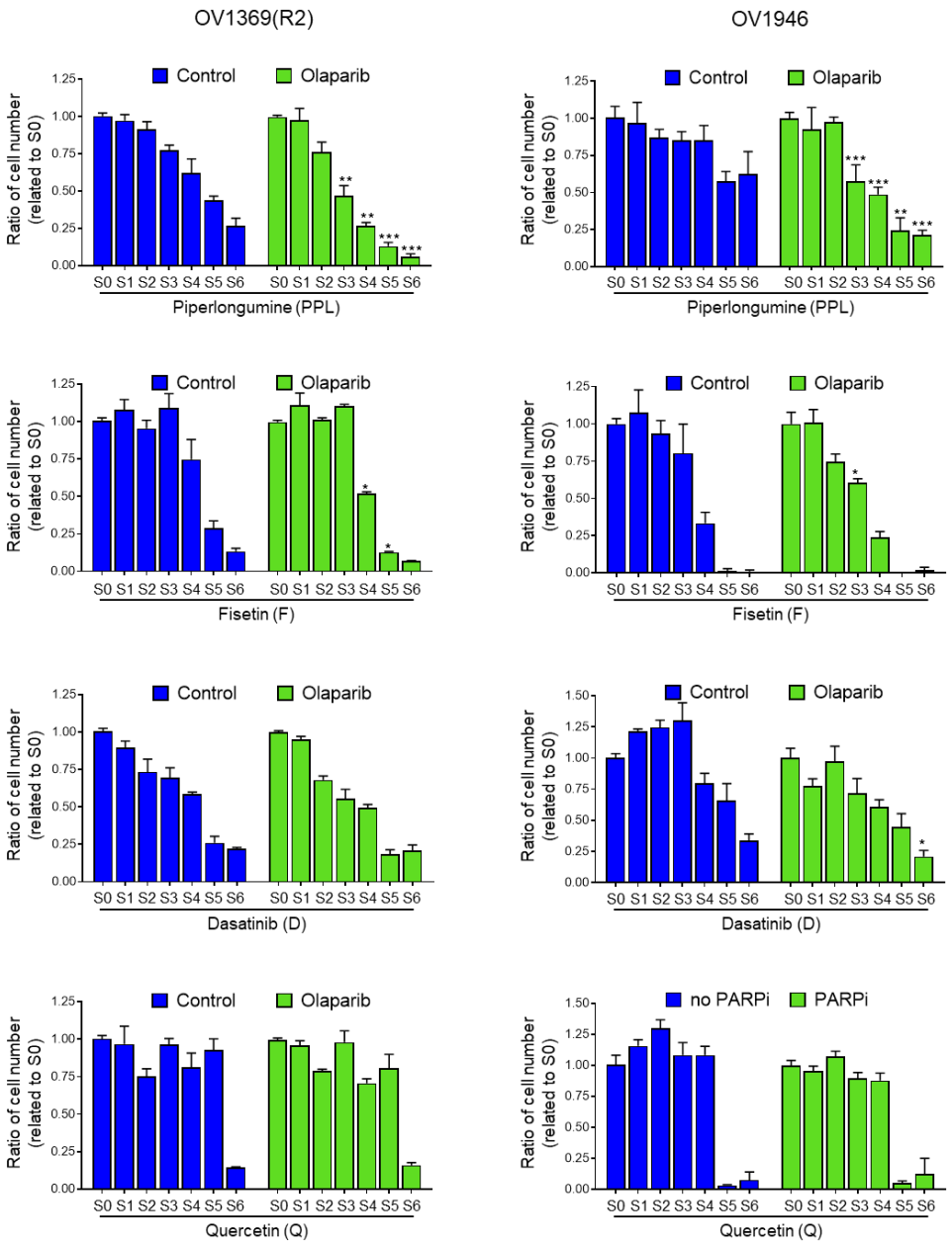

Supplementary Figure S9. Distinct senolytic drugs synergize with Olaparib in HGSOC cells.

A) Table of Piperlongumine (PPL), Fisetin (F), Dasatinib (D) and Quercetin (Q) doses (μM) used for this study for OV1369(R2) and OV1946 cell lines. **B)** Cells were co-treated with IC_{50} Olaparib concentrations and a range of PPL or F or D or Q concentrations for 6 days. Bar graph shows mean ± SEM of the fold change in cell number related to S0 (control non-treated for blue bars; Olaparib-treated for green bars) at different concentrations of the senolytic drugs. * denotes $p < 0.05$, ** $p < 0.01$, *** $p < 0.001$.

Supplementary Figure S10

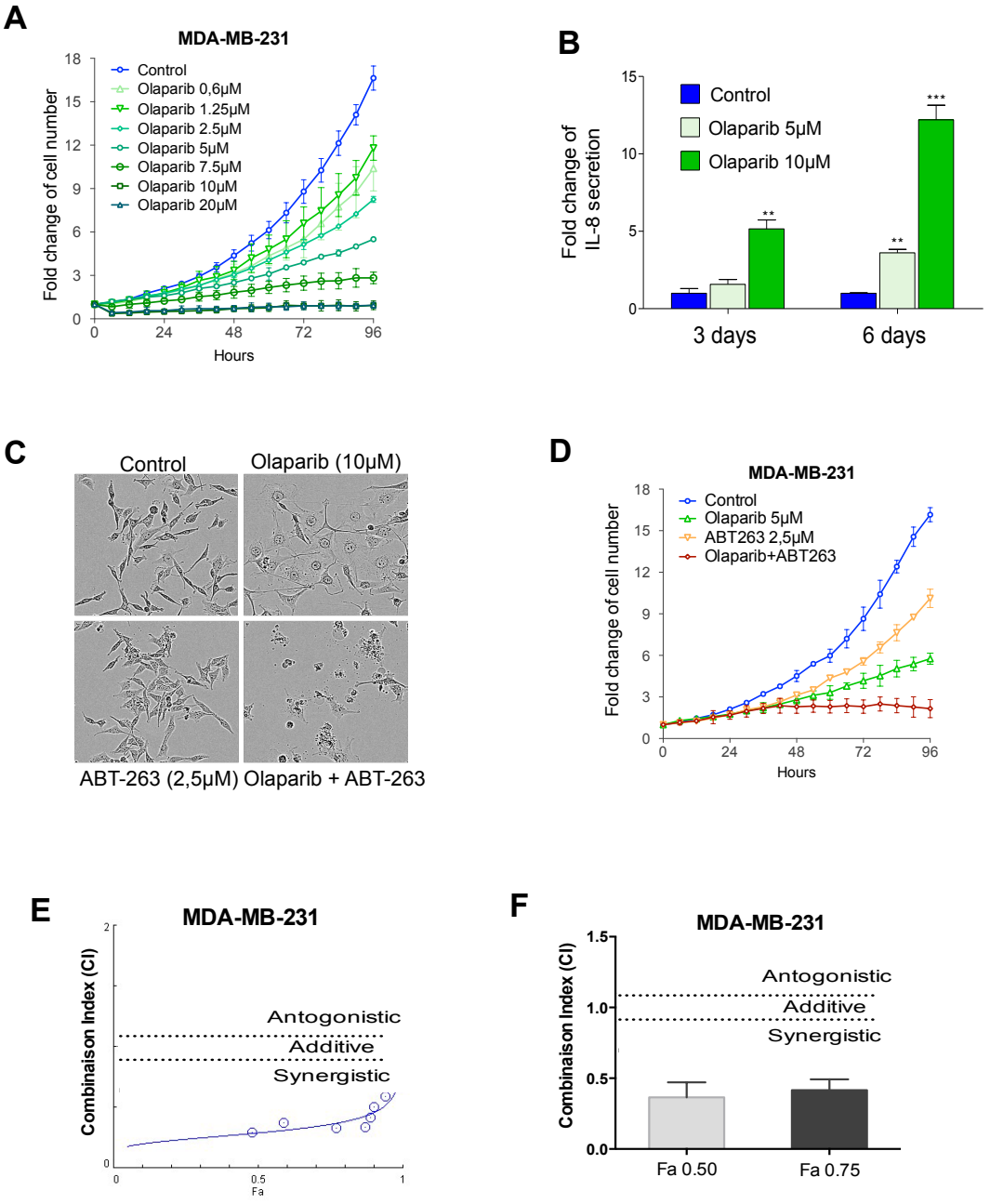

Supplementary Figure S10. Olaparib induces senescenc-like phenotype in a TN breast cancer cell line. A) Proliferation response of MDA-MB-231 treated with different concentrations of Olaparib for 6 days with analysis of cell numbers every 6 hours. Control = non-treated. **B)** Secretion of IL-8 in response to Olaparib treatment monitored by ELISA analysis. MDA-MB-231 was treated with 5 or 10 μM Olaparib, and supernatants of cell cultures were collected at the indicated time points (3 and 6 days). Medium was changed 24 hours before supernatant collection without FBS. **C-D)** MDA-MB-231 was treated with 5 μM of Olaparib or 2.5μM of ABT-263 or combination Olaparib/ABT-263 (5/2.5 μM) for 4 days. Images of cell morphology represent the different conditions at day 4 **(C)**. Dose-effect curve of the combination or of each agent alone are presented for comparison **(D)**. **E-F)** CI values of the combination therapy of Olaparib/ABT-263 at a ratio of 2/1. Curve represents the CI for all the fractions affected (Fa) **(E)**. Bar graph represents the CI at Fa 0.50 and Fa 0.75 **(F)**. * denotes $p < 0.05$, ** $p < 0.01$, *** $p < 0.001$.

2.3.2.7 References

1 Rodriguez, M. I. *et al.* Deciphering the insights of poly(ADP-ribosylation) in tumor progression. *Medicinal research reviews* **35**, 678-697, doi:10.1002/med.21339 (2015).

2 Wang, Y. Q. *et al.* An Update on Poly(ADP-ribose)polymerase-1 (PARP-1) Inhibitors: Opportunities and Challenges in Cancer Therapy. *Journal of medicinal chemistry* **59**, 9575-9598, doi:10.1021/acs.jmedchem.6b00055 (2016).

3 Fong, P. C. *et al.* Inhibition of poly(ADP-ribose) polymerase in tumors from BRCA mutation carriers. *The New England journal of medicine* **361**, 123-134, doi:10.1056/NEJMoa0900212 (2009).

4 Ledermann, J. *et al.* Olaparib maintenance therapy in platinum-sensitive relapsed ovarian cancer. *The New England journal of medicine* **366**, 1382-1392, doi:10.1056/NEJMoa1105535 (2012).

5 Ledermann, J. *et al.* Olaparib maintenance therapy in patients with platinum-sensitive relapsed serous ovarian cancer: a preplanned retrospective analysis of outcomes by BRCA status in a randomised phase 2 trial. *The Lancet. Oncology* **15**, 852-861, doi:10.1016/S1470-2045(14)70228-1 (2014).

6 Drean, A., Lord, C. J. & Ashworth, A. PARP inhibitor combination therapy. *Critical reviews in oncology/hematology* **108**, 73-85, doi:10.1016/j.critrevonc.2016.10.010 (2016).

7 Dulaney, C., Marcrom, S., Stanley, J. & Yang, E. S. Poly(ADP-ribose) polymerase activity and inhibition in cancer. *Seminars in cell & developmental biology* **63**, 144-153, doi:10.1016/j.semcdb.2017.01.007 (2017).

8 O'Sullivan Coyne, G., Chen, A. P., Meehan, R. & Doroshow, J. H. PARP Inhibitors in Reproductive System Cancers: Current Use and Developments. *Drugs* **77**, 113-130, doi:10.1007/s40265-016-0688-7 (2017).

9 Kraus, W. L. & Hottiger, M. O. PARP-1 and gene regulation: progress and puzzles. *Molecular aspects of medicine* **34**, 1109-1123, doi:10.1016/j.mam.2013.01.005 (2013).

10 Lord, C. J., Tutt, A. N. & Ashworth, A. Synthetic lethality and cancer therapy: lessons learned from the development of PARP inhibitors. *Annual review of medicine* **66**, 455-470, doi:10.1146/annurev-med-050913-022545 (2015).

11 Chang, J. *et al.* Clearance of senescent cells by ABT263 rejuvenates aged hematopoietic stem cells in mice. *Nature medicine* **22**, 78-83, doi:10.1038/nm.4010 (2016).

12 Yosef, R. *et al.* Directed elimination of senescent cells by inhibition of BCL-W and BCL-XL. *Nature communications* **7**, 11190, doi:10.1038/ncomms11190 (2016).

13 Zhu, Y. *et al.* Identification of a novel senolytic agent, navitoclax, targeting the Bcl-2 family of anti-apoptotic factors. *Aging cell* **15**, 428-435, doi:10.1111/acel.12445 (2016).

14 Fleury, H. *et al.* Cumulative defects in DNA repair pathways drive the PARP inhibitor response in high-grade serous epithelial ovarian cancer cell lines. *Oncotarget* **8**, 40152-40168, doi:10.18632/oncotarget.10308 (2017).

15 Integrated genomic analyses of ovarian carcinoma. *Nature* **474**, 609-615, doi:10.1038/nature10166 (2011).

16 Fleury, H. *et al.* Novel high-grade serous epithelial ovarian cancer cell lines that reflect the molecular diversity of both the sporadic and hereditary disease. *Genes & cancer* **6**, 378-398, doi:10.18632/genesandcancer.76 (2015).
17 Letourneau, I. J. *et al.* Derivation and characterization of matched cell lines from primary and recurrent serous ovarian cancer. *BMC cancer* **12**, 379, doi:10.1186/1471-2407-12-379 (2012).
18 Ouellet, V. *et al.* Characterization of three new serous epithelial ovarian cancer cell lines. *BMC cancer* **8**, 152, doi:10.1186/1471-2407-8-152 (2008).
19 Provencher, D. M. *et al.* Characterization of four novel epithelial ovarian cancer cell lines. *In vitro cellular & developmental biology. Animal* **36**, 357-361, doi:10.1290/1071-2690(2000)036<0357:COFNEO>2.0.CO;2 (2000).
20 Chuang, H. C., Kapuriya, N., Kulp, S. K., Chen, C. S. & Shapiro, C. L. Differential anti-proliferative activities of poly(ADP-ribose) polymerase (PARP) inhibitors in triple-negative breast cancer cells. *Breast cancer research and treatment* **134**, 649-659, doi:10.1007/s10549-012-2106-5 (2012).
21 Jelinic, P. & Levine, D. A. New insights into PARP inhibitors' effect on cell cycle and homology-directed DNA damage repair. *Molecular cancer therapeutics* **13**, 1645-1654, doi:10.1158/1535-7163.MCT-13-0906-T (2014).
22 Malaquin, N., Martinez, A. & Rodier, F. Keeping the senescence secretome under control: Molecular reins on the senescence-associated secretory phenotype. *Experimental gerontology* **82**, 39-49, doi:10.1016/j.exger.2016.05.010 (2016).
23 Malaquin, N., Carrier-Leclerc, A., Dessureault, M. & Rodier, F. DDR-mediated crosstalk between DNA-damaged cells and their microenvironment. *Frontiers in genetics* **6**, 94, doi:10.3389/fgene.2015.00094 (2015).
24 Baker, D. J. & Sedivy, J. M. Probing the depths of cellular senescence. *The Journal of cell biology* **202**, 11-13, doi:10.1083/jcb.201305155 (2013).
25 van Deursen, J. M. The role of senescent cells in ageing. *Nature* **509**, 439-446, doi:10.1038/nature13193 (2014).
26 Gonzalez, L. C., Ghadaouia, S., Martinez, A. & Rodier, F. Premature aging/senescence in cancer cells facing therapy: good or bad? *Biogerontology* **17**, 71-87, doi:10.1007/s10522-015-9593-9 (2016).
27 Kuilman, T., Michaloglou, C., Mooi, W. J. & Peeper, D. S. The essence of senescence. *Genes & development* **24**, 2463-2479, doi:10.1101/gad.1971610 (2010).
28 Lopez-Otin, C., Blasco, M. A., Partridge, L., Serrano, M. & Kroemer, G. The hallmarks of aging. *Cell* **153**, 1194-1217, doi:10.1016/j.cell.2013.05.039 (2013).
29 Rodier, F. & Campisi, J. Four faces of cellular senescence. *The Journal of cell biology* **192**, 547-556, doi:10.1083/jcb.201009094 (2011).
30 Acosta, J. C. *et al.* Chemokine signaling via the CXCR2 receptor reinforces senescence. *Cell* **133**, 1006-1018, doi:10.1016/j.cell.2008.03.038 (2008).
31 Coppe, J. P., Desprez, P. Y., Krtolica, A. & Campisi, J. The senescence-associated secretory phenotype: the dark side of tumor suppression. *Annual review of pathology* **5**, 99-118, doi:10.1146/annurev-pathol-121808-102144 (2010).
32 Kuilman, T. & Peeper, D. S. Senescence-messaging secretome: SMS-ing cellular stress. *Nature reviews. Cancer* **9**, 81-94, doi:10.1038/nrc2560 (2009).

33 Campisi, J. & d'Adda di Fagagna, F. Cellular senescence: when bad things happen to good cells. *Nature reviews. Molecular cell biology* **8**, 729-740, doi:10.1038/nrm2233 (2007).
34 Beausejour, C. M. *et al.* Reversal of human cellular senescence: roles of the p53 and p16 pathways. *The EMBO journal* **22**, 4212-4222, doi:10.1093/emboj/cdg417 (2003).
35 Narita, M. *et al.* Rb-mediated heterochromatin formation and silencing of E2F target genes during cellular senescence. *Cell* **113**, 703-716 (2003).
36 Storer, M. *et al.* Senescence is a developmental mechanism that contributes to embryonic growth and patterning. *Cell* **155**, 1119-1130, doi:10.1016/j.cell.2013.10.041 (2013).
37 Aliouat-Denis, C. M. *et al.* p53-independent regulation of p21Waf1/Cip1 expression and senescence by Chk2. *Molecular cancer research : MCR* **3**, 627-634, doi:10.1158/1541-7786.MCR-05-0121 (2005).
38 Zannini, L., Delia, D. & Buscemi, G. CHK2 kinase in the DNA damage response and beyond. *Journal of molecular cell biology* **6**, 442-457, doi:10.1093/jmcb/mju045 (2014).
39 Yosef, R. *et al.* p21 maintains senescent cell viability under persistent DNA damage response by restraining JNK and caspase signaling. *The EMBO journal* **36**, 2280-2295, doi:10.15252/embj.201695553 (2017).
40 Alotaibi, M. *et al.* Radiosensitization by PARP Inhibition in DNA Repair Proficient and Deficient Tumor Cells: Proliferative Recovery in Senescent Cells. *Radiation research* **185**, 229-245, doi:10.1667/RR14202.1 (2016).
41 Chitikova, Z. V. *et al.* Sustained activation of DNA damage response in irradiated apoptosis-resistant cells induces reversible senescence associated with mTOR downregulation and expression of stem cell markers. *Cell Cycle* **13**, 1424-1439, doi:10.4161/cc.28402 (2014).
42 Wang, Q. *et al.* Polyploidy road to therapy-induced cellular senescence and escape. *International journal of cancer* **132**, 1505-1515, doi:10.1002/ijc.27810 (2013).
43 Sagiv, A. *et al.* Granule exocytosis mediates immune surveillance of senescent cells. *Oncogene* **32**, 1971-1977, doi:10.1038/onc.2012.206 (2013).
44 Sasaki, M., Kumazaki, T., Takano, H., Nishiyama, M. & Mitsui, Y. Senescent cells are resistant to death despite low Bcl-2 level. *Mechanisms of ageing and development* **122**, 1695-1706 (2001).
45 Wang, E. Senescent human fibroblasts resist programmed cell death, and failure to suppress bcl2 is involved. *Cancer research* **55**, 2284-2292 (1995).
46 Merino, D. *et al.* Bcl-2, Bcl-x(L), and Bcl-w are not equivalent targets of ABT-737 and navitoclax (ABT-263) in lymphoid and leukemic cells. *Blood* **119**, 5807-5816, doi:10.1182/blood-2011-12-400929 (2012).
47 Ashkenazi, A., Fairbrother, W. J., Leverson, J. D. & Souers, A. J. From basic apoptosis discoveries to advanced selective BCL-2 family inhibitors. *Nature reviews. Drug discovery* **16**, 273-284, doi:10.1038/nrd.2016.253 (2017).
48 Rudin, C. M. *et al.* Phase II study of single-agent navitoclax (ABT-263) and biomarker correlates in patients with relapsed small cell lung cancer. *Clinical cancer research : an official journal of the American Association for Cancer Research* **18**, 3163-3169, doi:10.1158/1078-0432.CCR-11-3090 (2012).

49 Tolcher, A. W. *et al.* Safety, efficacy, and pharmacokinetics of navitoclax (ABT-263) in combination with erlotinib in patients with advanced solid tumors. *Cancer chemotherapy and pharmacology* **76**, 1025-1032, doi:10.1007/s00280-015-2883-8 (2015).

50 Vlahovic, G. *et al.* A phase I safety and pharmacokinetic study of ABT-263 in combination with carboplatin/paclitaxel in the treatment of patients with solid tumors. *Investigational new drugs* **32**, 976-984, doi:10.1007/s10637-014-0116-3 (2014).

51 Chou, T. C. Drug combination studies and their synergy quantification using the Chou-Talalay method. *Cancer research* **70**, 440-446, doi:10.1158/0008-5472.CAN-09-1947 (2010).

52 Zhu, Y. *et al.* New agents that target senescent cells: the flavone, fisetin, and the BCL-XL inhibitors, A1331852 and A1155463. *Aging* **9**, 955-963, doi:10.18632/aging.101202 (2017).

53 Bansal, M. *et al.* A community computational challenge to predict the activity of pairs of compounds. *Nature biotechnology* **32**, 1213-1222, doi:10.1038/nbt.3052 (2014).

54 Zhu, Y. *et al.* The Achilles' heel of senescent cells: from transcriptome to senolytic drugs. *Aging cell* **14**, 644-658, doi:10.1111/acel.12344 (2015).

55 Kirkland, J. L. & Tchkonia, T. Cellular Senescence: A Translational Perspective. *EBioMedicine* **21**, 21-28, doi:10.1016/j.ebiom.2017.04.013 (2017).

56 Coleman, R. L. *et al.* A phase II evaluation of the potent, highly selective PARP inhibitor veliparib in the treatment of persistent or recurrent epithelial ovarian, fallopian tube, or primary peritoneal cancer in patients who carry a germline BRCA1 or BRCA2 mutation - An NRG Oncology/Gynecologic Oncology Group study. *Gynecologic oncology* **137**, 386-391, doi:10.1016/j.ygyno.2015.03.042 (2015).

57 de Bono, J. *et al.* Phase I, Dose-Escalation, 2-Part Trial of Poly(ADP-Ribose) Polymerase Inhibitor Talazoparib in Patients with Advanced Germline BRCA1/2 Mutations and Selected Sporadic Cancers. *Cancer discovery*, doi:10.1158/2159-8290.CD-16-1250 (2017).

58 Mirza, M. R. *et al.* Niraparib Maintenance Therapy in Platinum-Sensitive, Recurrent Ovarian Cancer. *The New England journal of medicine* **375**, 2154-2164, doi:10.1056/NEJMoa1611310 (2016).

59 Swisher, E. M. *et al.* Rucaparib in relapsed, platinum-sensitive high-grade ovarian carcinoma (ARIEL2 Part 1): an international, multicentre, open-label, phase 2 trial. *The Lancet. Oncology* **18**, 75-87, doi:10.1016/S1470-2045(16)30559-9 (2017).

60 Murai, J. *et al.* Trapping of PARP1 and PARP2 by Clinical PARP Inhibitors. *Cancer research* **72**, 5588-5599, doi:10.1158/0008-5472.CAN-12-2753 (2012).

61 Murai, J. *et al.* Stereospecific PARP trapping by BMN 673 and comparison with olaparib and rucaparib. *Molecular cancer therapeutics* **13**, 433-443, doi:10.1158/1535-7163.MCT-13-0803 (2014).

62 Pommier, Y., O'Connor, M. J. & de Bono, J. Laying a trap to kill cancer cells: PARP inhibitors and their mechanisms of action. *Science translational medicine* **8**, 362ps317, doi:10.1126/scitranslmed.aaf9246 (2016).

63 Szekely, B., Silber, A. L. & Pusztai, L. New Therapeutic Strategies for Triple-Negative Breast Cancer. *Oncology (Williston Park)* **31**, 130-137 (2017).

64 Livraghi, L. & Garber, J. E. PARP inhibitors in the management of breast cancer: current data and future prospects. *BMC medicine* **13**, 188, doi:10.1186/s12916-015-0425-1 (2015).
65 Kim, G. *et al.* FDA Approval Summary: Olaparib Monotherapy in Patients with Deleterious Germline BRCA-Mutated Advanced Ovarian Cancer Treated with Three or More Lines of Chemotherapy. *Clinical cancer research : an official journal of the American Association for Cancer Research* **21**, 4257-4261, doi:10.1158/1078-0432.CCR-15-0887 (2015).
66 Helleday, T. PARP inhibitor receives FDA breakthrough therapy designation in castration resistant prostate cancer: beyond germline BRCA mutations. *Annals of oncology : official journal of the European Society for Medical Oncology* **27**, 755-757, doi:10.1093/annonc/mdw048 (2016).
67 Norquist, B. *et al.* Secondary somatic mutations restoring BRCA1/2 predict chemotherapy resistance in hereditary ovarian carcinomas. *Journal of clinical oncology : official journal of the American Society of Clinical Oncology* **29**, 3008-3015, doi:10.1200/JCO.2010.34.2980 (2011).
68 Pishvaian, M. J. *et al.* BRCA2 secondary mutation-mediated resistance to platinum and PARP inhibitor-based therapy in pancreatic cancer. *British journal of cancer* **116**, 1021-1026, doi:10.1038/bjc.2017.40 (2017).
69 Quigley, D. *et al.* Analysis of Circulating Cell-free DNA Identifies Multi-clonal Heterogeneity of BRCA2 Reversion Mutations Associated with Resistance to PARP Inhibitors. *Cancer discovery*, doi:10.1158/2159-8290.CD-17-0146 (2017).
70 Bavik, C. *et al.* The gene expression program of prostate fibroblast senescence modulates neoplastic epithelial cell proliferation through paracrine mechanisms. *Cancer research* **66**, 794-802, doi:10.1158/0008-5472.CAN-05-1716 (2006).
71 Coppe, J. P. *et al.* Senescence-associated secretory phenotypes reveal cell-nonautonomous functions of oncogenic RAS and the p53 tumor suppressor. *PLoS biology* **6**, 2853-2868, doi:10.1371/journal.pbio.0060301 (2008).
72 Laberge, R. M., Awad, P., Campisi, J. & Desprez, P. Y. Epithelial-mesenchymal transition induced by senescent fibroblasts. *Cancer microenvironment : official journal of the International Cancer Microenvironment Society* **5**, 39-44, doi:10.1007/s12307-011-0069-4 (2012).
73 O'Reilly, E. A. *et al.* The fate of chemoresistance in triple negative breast cancer (TNBC). *BBA clinical* **3**, 257-275, doi:10.1016/j.bbacli.2015.03.003 (2015).
74 Yokoyama, T., Kohn, E. C., Brill, E. & Lee, J. M. Apoptosis is augmented in high-grade serous ovarian cancer by the combined inhibition of Bcl-2/Bcl-xL and PARP. *International journal of oncology*, doi:10.3892/ijo.2017.3914 (2017).
75 Efimova, E. V. *et al.* Poly(ADP-ribose) polymerase inhibitor induces accelerated senescence in irradiated breast cancer cells and tumors. *Cancer research* **70**, 6277-6282, doi:10.1158/0008-5472.CAN-09-4224 (2010).
76 Gonzalez-Billalabeitia, E. *et al.* Vulnerabilities of PTEN-TP53-deficient prostate cancers to compound PARP-PI3K inhibition. *Cancer discovery* **4**, 896-904, doi:10.1158/2159-8290.CD-13-0230 (2014).
77 Fischer, M. Census and evaluation of p53 target genes. *Oncogene*, doi:10.1038/onc.2016.502 (2017).

78 Dijkers, P. F. *et al.* Forkhead transcription factor FKHR-L1 modulates cytokine-dependent transcriptional regulation of p27(KIP1). *Molecular and cellular biology* **20**, 9138-9148 (2000).
79 Seoane, J., Le, H. V., Shen, L., Anderson, S. A. & Massague, J. Integration of Smad and forkhead pathways in the control of neuroepithelial and glioblastoma cell proliferation. *Cell* **117**, 211-223 (2004).
80 Park, S. H. *et al.* Tumor suppressive effect of PARP1 and FOXO3A in gastric cancers and its clinical implications. *Oncotarget* **6**, 44819-44831, doi:10.18632/oncotarget.6264 (2015).
81 Wang, S. *et al.* PARP1 inhibitors attenuate AKT phosphorylation via the upregulation of PHLPP1. *Biochemical and biophysical research communications* **412**, 379-384, doi:10.1016/j.bbrc.2011.07.107 (2011).

Material and Methods REFERENCES

1 Letourneau, I. J. *et al.* Derivation and characterization of matched cell lines from primary and recurrent serous ovarian cancer. *BMC cancer* **12**, 379, doi:10.1186/1471-2407-12-379 (2012).
2 Ouellet, V. *et al.* Characterization of three new serous epithelial ovarian cancer cell lines. *BMC cancer* **8**, 152, doi:10.1186/1471-2407-8-152 (2008).
3 Provencher, D. M. *et al.* Characterization of four novel epithelial ovarian cancer cell lines. *In vitro cellular & developmental biology. Animal* **36**, 357-361, doi:10.1290/1071-2690(2000)036<0357:COFNEO>2.0.CO;2 (2000).
4 Beausejour, C. M. *et al.* Reversal of human cellular senescence: roles of the p53 and p16 pathways. *The EMBO journal* **22**, 4212-4222, doi:10.1093/emboj/cdg417 (2003).
5 Shah, G. M. *et al.* Approaches to detect PARP-1 activation in vivo, in situ, and in vitro. *Methods Mol Biol* **780**, 3-34, doi:10.1007/978-1-61779-270-0_1 (2011).
6 Chou, T. C. Drug combination studies and their synergy quantification using the Chou-Talalay method. *Cancer research* **70**, 440-446, doi:10.1158/0008-5472.CAN-09-1947 (2010).
7 Bansal, M. *et al.* A community computational challenge to predict the activity of pairs of compounds. *Nature biotechnology* **32**, 1213-1222, doi:10.1038/nbt.3052 (2014).
8 Leverson, J. D. *et al.* Exploiting selective BCL-2 family inhibitors to dissect cell survival dependencies and define improved strategies for cancer therapy. *Science translational medicine* **7**, 279ra240, doi:10.1126/scitranslmed.aaa4642 (2015).

3 DISCUSSION

3.1 Modèle de lignée cellulaire pour l'étude des inhibiteurs de PARP

La littérature entourant les caractéristiques moléculaires montre une importante différence entre les différents types et sous-types du cancer de l'ovaire. Entre autres, la publication TCGA a mis en évidence l'instabilité génomique procurant une grande hétérogénéité moléculaire au sein des HGS. Ces travaux associés à d'autres recherches ont permis de définir des profils de mutations aidant à différencier les types et sous-types du cancer de l'ovaire (40, 109, 168). En relation avec les résultats démontrés dans ces recherches, nos travaux ont utilisé les mutations *CSDM3*, *NF1*, *CDK12*, *RB1*, *BRCA* et *Tp53* mais aussi les altérations du nombre de copies comme critères pour définir les lignées comme des HGS. De plus, ces résultats ont été mis en relation avec des mutations non présentes dans les gènes *PIK3CA*, *KRAS*, *BRAF*, *CTNNB1* et *ARID1A* qui sont spécifiques d'autres sous-types des EOC (168). Nous avons donc démontré que les six lignées cellulaires nouvellement dérivées présentent des caractéristiques génétiques et génomiques spécifiques des échantillons de HGS, suggérant donc une forte probabilité d'être d'origine tumorale de EOC HGS bien que chacune de nos lignées cellulaires EOC présente un profil génétique et moléculaire unique.

Parmi les six lignées que nous avons caractérisées, les OV4485 et OV4453 ont des spécificités particulièrement intéressantes notamment pour étudier de nouvelles thérapies, telles que les inhibiteurs de poly (ADP-ribose) polymérase. Sachant qu'environ 12% des EOC HGS présentent des mutations *BRCA1/2*, notre modèle de 6 lignées s'ajoutant aux 12 autres lignées dérivées et déjà caractérisées au laboratoire représentent très bien la maladie avec un total de 2 lignées cellulaires mutées *BRCA1/2* (2 lignées sur 18 donc environ 11% présentent des mutations *BRCA1/2*) (169-171). Ces lignées mutées *BRCA1* et 2 sont les seules des 6 lignées nouvellement caractérisées à avoir un potentiel tumoral chez les souris SCID. Dans la littérature, jusqu'à récemment, seulement cinq lignées cellulaires de EOC HGS présentant des mutations *BRCA1/2* à partir d'échantillons EOC ont été décrites (172) (173), dont seulement

une (la PEO1 mutée *BRCA2*) est capable de former des tumeurs chez les souris (174). La ligne cellulaire OV4485 est donc, à notre connaissance, la seule lignée cellulaire CEO SHG mutée *BRCA1* avec un potentiel tumoral chez les souris SCID. De plus, la OV4485 a également démontré une résistance à la carboplatine. De plus, étant peu sensible aux inhibiteurs de PARP, elle s'est avéré être un bon modèle pour étudier de nouvelles thérapies dans les cas de mutation BRCA résistant au platine et aux inhibiteurs de PARP. Sur un plan fonctionnel, nos travaux ont décrit une nouvelle mutation *BRCA1* située à la limite intron/exon de l'exon 15 (IVS14-1 G> T) induisant un épissage alternatif ainsi qu'une instabilité de l'ARNm *BRCA1*. La mutation non-sens *BRCA2*, G6085T (E1953X), trouvée chez la patiente OV4453 est celle déterminée dans la lignée cellulaire correspondante ; elle est connue dans la population canadienne française (175, 176). Les deux lignées cellulaires TOV2978G et TOV3041G ne présentent aucune mutation *BRCA1*, par contre, elles n'expriment ni l'ARNm ni la protéine *BRCA1*. Ces lignées cellulaires représenteraient alors un gène BRCA silencieux, éventuellement par des mécanismes épigénétiques, ce qui est une autre caractéristique très commune des HGS. D'après l'étude de TCGA, la fréquence d'hyperméthylation du promoteur *BRCA1*, est estimée à 12% des tumeurs EOC HGS (40). Ceci confirme que nos lignées dérivées au laboratoire représentent bien la maladie avec toutes ses caractéristiques moléculaires. La réponse à la carboplatine est différente entre les cas mutés, le type sauvage et les cas silencieux *BRCA1*, ce qui laisse penser que la réponse aux traitements (carboplatine) n'est pas le même selon le statut *BRCA1/2* muté ou silencieux des lignées cellulaires (40).

Notre étude démontre une fonction altérée de p53 pour les six lignées cellulaires mais seulement cinq d'entre elles présentent une mutation somatique de *TP53* détectée par le séquençage effectué au cours de cette étude. La lignée TOV3041G, elle, ne présente pas de mutation mais une absence de l'ARNm et de la protéine p53, montrant les caractéristiques d'une mutation p53 connue. La protéine p53 fonctionne comme un facteur de transcription avec un rôle crucial dans la réponse au stress cellulaire, c'est pour cela que son expression et son activité sont sévèrement régulées (177). Par exemple, MDM2 dégrade l'expression protéique de p53 par son ubiquitinisation. De plus BCL6, PAX2, PAX8, Wrap53 contrôlent la stabilité de l'ARNm et la transcription *TP53* (178). Nos résultats de PCR nous suggèrent que dans la TOV3041G, l'inactivation de *TP53* se produit au niveau de l'ARNm plutôt qu'au niveau de la protéine. Il faudrait effectuer des recherches plus poussées pour comprendre les

modifications post-transcriptionnelles sous-jacentes de cette inactivation. Parmi nos 6 lignées, la TOV2978G ne présente, elle non plus, ni d'ARNm ni de protéine ; cela provient certainement de la mutation intronique (c.920-2 A>G) déterminée par séquençage. Parmi les 18 lignées EOC HGS que l'on a au laboratoire et qui constitueront notre modèle final, deux (TOV3041G et TOV2978G) présentent des mutations avec une perte d'expression de p53 et les 16 autres des mutations dominantes négatives. Par conséquent, notre modèle reflète les multiples facettes de la maladie EOC HGS dans laquelle le gène *TP53* est soit muté (70% des cas) soit silencieux (30% des cas) (179, 180). La perte de p53 est très clairement associée à un mauvais pronostic alors que ce n'est pas aussi significatif pour les patientes présentant des mutations dominantes négatives (181).

Parmi les 6 lignées cellulaires décrites dans notre étude, la OV866 (2) est la seule exprimant les marqueurs de la TEM. Cela se reflète par des caractéristiques conjointes d'absence de cytokeratines (CK7, CK8, CK18, CK19), de E-cadhérine et de forte expression de vimentine. Des publications ont montré que des niveaux opposés d'E-Cadhérine et de vimentine se produisent dans des cellules qui ont subi une TEM (182). La OV866 (2) est dérivée de l'ascite post-chimiothérapie suite à une rechute de la patiente qui n'a pas démontré de sensibilité aux traitements. Comparativement aux cinq autres, cette lignée cellulaire présente des caractéristiques phénotypiques spécifiques de la TEM comme une faible sensibilité à la carboplatine, une importante croissance indépendante de l'ancrage et une forte vitesse de migration cellulaire. D'autres marqueurs associés à la TEM, comme l'augmentation de Snail, Slug, Twist, Zeb1 et la diminution de ZO-1, claudins, occludin, laminin-1, seraient à étudier pour confirmer ce résultat (183, 184). Les autres cinq lignées cellulaires ont toutes un profil épithélial comme le suggère la présence de cytokeratines et / ou l'expression de la E-Cadhérine. La OV866 (2) est intéressante pour étudier les processus de EOC liés à la métastase péritonéale et à l'invasion dans la réponse à la chimiothérapie (185). Mais le profil de réponse aux traitements ne peut pas être seulement associée à la TEM. La réparation de l'ADN reste donc une voie importante pour l'influencer (186). La dérégulation des principaux acteurs, et donc des voies de réparation de l'ADN, présente une importante hétérogénéité entre les sous-types du EOC et est corrélée avec l'hétérogénéité retrouvée dans la réponse aux traitements (6). D'ailleurs, nos travaux démontrent une réponse à la carboplatine variable

parmi nos 6 lignées. Cette réponse corrèle avec la capacité d'ancrage, de migration et, comme expliqué dans le paragraphe précédent, avec le phénotype de TEM.

3.2 Réponse aux inhibiteurs de Poly (ADP-ribose) polymérase

La protéine PARP1 a un rôle significatif dans plusieurs fonctions essentielles de la croissance cellulaire et de la survie (187) (49) (134). Dans le contexte de la réparation de l'ADN, PARP1 subit un changement conformationel entraînant son activation une fois liée à l'ADN endommagé. Une fois activée, PARP1 synthétise des chaînes de PAR qui lient de manière covalente une variété de protéines associées à la chromatine dont PARP1 elle-même. Par la fonction des PAR de recruter une importante quantité de protéines et de les modifier structuralement, PARP1 joue un rôle dans plusieurs voies de signalisation dont celles de la réparation de l'ADN comme la BER, la NHEJ et la MMR (134) (187, 188). En relation avec l'idée que la RH joue un rôle dans la réponse aux inhibiteurs de PARP, le laboratoire du Dr Jean-Yves Masson a publié un article (5), dans lequel le laboratoire et moi-même avons collaboré en tant que co-auteurs, démontrant pour la première fois l'implication de APRIN comme que médiateur de la RH. APRIN améliore fortement le recrutement de l'ADN complémentaire et stimule ce processus en synergie avec *BRCA2*. De plus, l'inhibition d'APRIN induit une déficience en RH et donc une sensibilité aux inhibiteurs de PARP. APRIN pourrait servir de biomarqueur pour les inhibiteurs de PARP. Enfin, ces recherches montrent que les faibles niveaux d'expression d'APRIN corrèlent avec une meilleure survie chez les patientes atteintes de cancer de l'ovaire.

Afin de démontrer que la réponse aux inhibiteurs de PARP s'étend au-delà de l'état de déficience de la RH, nos travaux proposent un nouveau modèle de réponse prenant en compte l'ensemble des voies de la réparation de l'ADN. Notre modèle se base sur l'idée que les tumeurs présentant une RH associée à une NER ou une MMR défectueux, conformément au concept de létalité synthétique, seraient extrêmement sensibles aux inhibiteurs de PARP. Les tumeurs avec une seule voie de réparation de l'ADN défectueuse peuvent présenter une réactivité limitée aux inhibiteurs de PARP, tandis que les tumeurs avec des voies de réparation

de l'ADN fonctionnellement intactes ne répondraient pas au traitement des inhibiteurs de PARP. Nous avons démontré que la régulation négative des gènes impliqués dans les voies MMR ou NER a augmenté la sensibilité à Olaparib des lignées cellulaires EOC HGS, même dans celles mutées BRCA. Nos résultats suggèrent que le MMR et la NER pourraient réparer les cassures double-brins de l'ADN lorsque la RH est défectueuse. Ceci peut expliquer pourquoi certaines patientes avec une mutation BRCA ne répondent pas à ce traitement. Les cellules tumorales présentant des défauts à la fois au niveau de la RH et dans l'une des deux voies MMR ou NER sont plus sensibles. Cependant, nous n'avons pas observé d'augmentation significative de la sensibilité à l'Olaparib lorsque le MMR et le NER sont tous deux déficients mais que la RH est fonctionnelle. Cela indique que les cassures double-brins sont principalement réparées par la voie RH. Bien que d'autres études montrent une corrélation entre la carence en NER et la réponse aux inhibiteurs de PARP (158, 189), c'est la première publication montrant que ERCC8 est une cible potentielle pour la sensibilité aux inhibiteurs de PARP. La déficience en NER a également été impliquée dans la réponse aux thérapies à base de platine (105, 106), ce qui correspond aux observations montrant que la majorité des patientes sensibles au traitement de platine est également sensible aux inhibiteurs de PARP (147, 190). Bien qu'une publication récente démontre que les mutations des gènes impliqués dans la NER (*ERCC6* et *ERCC4*) n'augmentent pas la sensibilité au Rucaparib (105), nos résultats ont montré que la sous-expression de ERCC8 augmente de manière significative la sensibilité à l'Olaparib dans les cellules HGS présentant une déficience en RH.

Dans le cas de MLH1, gène primordial de la voie du MMR, de précédentes recherches soutiennent que la déficience en MMR confère une résistance au traitement à base de platine (107), alors que nos résultats montrent que l'inhibition de MLH1 a entraîné une augmentation significative de la sensibilité à l'Olaparib. Par conséquent, nos résultats suggèrent que les patientes résistantes au platine avec une faible expression de MLH1 peuvent bénéficier des inhibiteurs de PARP. En effet, la lignée cellulaire TOV1946 présentant des niveaux très bas de MLH1 est très sensible à Olaparib (IC_{50} = 0,02 μM), et les travaux du laboratoire précédent ont démontré que cette lignée cellulaire n'est pas sensible à la carboplatine (171).

Les mécanismes mettant le MMR et le NER en relation avec la RH dans la réponse aux inhibiteurs de PARP, restent peu étudiés. Plusieurs publications montrent qu'à l'instar de la voie de la RH, les voies du MMR et de la NER jouent eux aussi un rôle dans la réparation des

cassures double-brins de l'ADN (191) : la déficience en MMR et en NER réduit la capacité de la cellule à les réparer (192) (191, 193). Il a été démontré dans d'autres publications que PARP1 agit directement sur l'activité du NER et du MMR (194, 195). Cependant, seuls quelques rapports ont décrit le rôle des voies MMR et NER dans la réponse aux inhibiteurs de PARP (192, 196).

L'implication du NER et plus spécifiquement de ERCC8, appelé aussi CSA (Cockayne syndrome A), dans le principe de la létalité synthétique avec les inhibiteurs de PARP, peut s'expliquer par son rôle avec Cockayne syndrome B (CSB) dans la RH. L'assemblage de RPA1, RAD51C, RAD51 et RAD52 sur le site de dommage est strictement régi par une transcription active, nécessitant donc la fonction ATPase de CSA et CSB et la présence d'ARN dans la phase G0/G1 (197). Cela peut expliquer que la diminution ou la perte de ERCC8 sensibilise les cellules EOC HGS aux inhibiteurs de PARP. De plus, il a été démontré que la déficience en NER par la perte ou l'inhibition de CSA et/ou CSB rend la lésion accessible à d'autres systèmes de réparation comme la réparation par BER. Si la BER est inhibé par les inhibiteurs de PARP, ces cassures s'accumuleront, ce qui aura l'effet d'augmenter l'instabilité génomique et l'entrée en apoptose. Ce phénomène amène une sensibilité aux inhibiteurs de PARP. Il est encore plus fort si ces cassures ne sont pas prises en charge par la RH dans les cas de *BRCA1/2* mutée, expliquant ainsi l'augmentation de la sensibilité aux inhibiteurs de PARP suite à une déficience de CSA donc du NER couplé à celle de la RH.

Concernant l'implication de MMR dans la réponse aux inhibiteurs de PARP, plusieurs protéines dans la voie de l'anémie BRCA-Fanconi (FA), telles que FANCJ, *BRCA1* et FANCD2, interagissent avec les facteurs de la répartition des correspondances (MMR), mais la signification de ce lien reste inconnue (198). Cependant il a été prouvé que la MMR permet, en collaboration de la voie BRCA-Fanconi Anemia, la poursuite de la fourche de réplication suite à un stress de réplication provoquant une structure secondaire sur l'ADN. C'est une interaction de FANCJ-MLH1 coordonnée avec la voie MMR qui permet le redémarrage de la fourche de réplication. MSH2 se fixe sur cette structure secondaire bloquant la réplication et recrute MLH1. L'activité ADN hélicase et translocase de FANCJ déplace le complexe MSH2/MLH1 et déroule la structure secondaire permettant ainsi le redémarrage de la fourche de réplication. Si BRCA-Fanconi Anemia seul est déficient, FANCJ ne permet plus d'enlever le complexe MSH2/MLH1, laissant la place à l'activité nucléolitique de décrocher la structure

secondaire et ainsi produire un dommage pris en charge par DNA-PK donc par le NHEJ. La déficience de BRCA-Fanconi Anemia dans un blocage de la fourche ne pose pas de problème à la cellule pour continuer à proliférer. Par contre, dans le cas d'une déficience de BRCA-Fanconi Anemia (FANCJ) et de MMR (MLH1), le complexe FANCJ reste bloqué au niveau de la structure secondaire, bloquant ainsi la fourche de réplication. Ce mécanisme peut se comprendre par l'activité de piégeage des inhibiteurs de PARP bloquant la fourche de réplication à cause d'une structure secondaire, ici le PARP. On comprend alors qu'une déficience en MMR couplé à une déficience en BRCA-Fanconi Anemia provoquerait une mort cellulaire suite à un blocage persistant de la fourche. Ainsi, la régulation de la réponse aux dommages à l'ADN dépendante de MSH2 sous-entend l'importance des interactions entre les voies BRCA-FA et MMR (188, 198).

L'ensemble des mécanismes décrits laisse imaginer comment il serait possible que nos résultats sur le MMR et le NER jouent un rôle sur la réponse aux inhibiteurs de PARP. Ils pourraient aussi expliquer une résistance aux inhibiteurs de PARP, surtout dans les cas de cellules déficientes en *BRCA1/2* n'y répondant pas.

D'autres mécanismes comme le NHEJ ont été mis en évidence pour jouer un rôle dans la réponse aux inhibiteurs de PARP. En plus des cibles déterminées dans la RH, le NER et le MMR, nos travaux ont déterminé d'autres cibles impliquées dans ces mêmes voies mais aussi dans d'autres voies de la réparation comme celle du NHEJ. On a pu démontrer une dérégulation de l'expression des gènes *LIG4* et *DCLRE1C* dans les lignées sensibles à l'Olaparib. Cependant, ces résultats sont moins concluants car ces gènes sont surexprimés dans la OV2295 mais inhibés dans les lignées TOV3041G et OV1946 et pourtant ces 3 lignées sont sensibles à l'Olaparib. Malgré l'intérêt du NHEJ dans la létalité synthétique des inhibiteurs de PARP (122, 199), nos travaux n'ont pas poursuivi cette piste. Cela aurait pourtant été intéressant car, dans des résultats non publiés, nous montrons que des gènes du NHEJ dont LIG4 sont principalement surexprimés dans les lignées résistantes aux inhibiteurs de PARP. Cette constatation a désormais été publiée par d'autres laboratoires qui démontrent que le NHEJ joue un rôle important dans la résistance aux inhibiteurs de PARP (137) (199). Les résultats obtenus dans ces recherches prouvent que les défauts dans la NHEJ, contribuant à l'instabilité génomique et associés au développement de la chimiorésistance, sont présents

dans 40% des EOC et pourraient être, indépendamment de la RH, associés à la résistance aux inhibiteurs de PARP dans des cultures primaires *ex vivo* (199).

Le niveau protéique de PARP a été démontré comme jouant un rôle important dans la réponse aux inhibiteurs de PARP (200). Les laboratoires du Dr. Walter H Gotlieb et Dr. Michael Witcher (2) ont démontré, dans un article auquel le laboratoire et moi-même avons contribué en tant que co-auteurs, une réduction de l'expression de PARP1 intratumoral chez les patientes traitées préalablement à la chimiothérapie. Ceci laisse penser que le traitement aux inhibiteurs de PARP devrait se faire soit avant un traitement à la chimiothérapie, soit de façon simultanée. Les résultats suggèrent que les patientes recevant des inhibiteurs de PARP pourraient être sélectionnées non seulement en fonction de leur statut *BRCA1*, mais aussi pour l'expression de la protéine PARP1. Un tel dépistage est courant pour d'autres thérapies ciblées, telles que les inhibiteurs d'aromatase (Anastrozole) dans le cancer du sein ou le Vemurafenib, un inhibiteur de RAF (201, 202), et pourrait être intégré aux procédures d'exploitation standard pour les pathologistes et les oncologues (2). Ces mécanismes ont principalement été étudiés avec l'Olaparib, mais désormais l'intérêt se tourne sur des nouveaux inhibiteurs de PARP à l'efficacité plus prometteuse.

Nos travaux ont démontré qu'à des doses spécifiques d'inhibiteurs de PARP dépendant de leur sensibilité, les lignées cellulaires du EOC HGS présentent un état sénescent. La plupart des marqueurs de sénescence est retrouvée dans nos lignées cellulaires traitées aux inhibiteurs de PARP avec une activité SA-β-Gal, un grossissement caractéristique des cellules, un phénotype sécrétoire activé (activation caractéristique de IL-6 et IL8) et un arrêt du cycle en G2/M. Par contre, l'état irréversible et l'augmentation des CDKi, sauf p21, caractéristiques de la sénescence ne se retrouvent pas dans nos cellules. Le relâchement des inhibiteurs de PARP permet aux cellules en état sénescent de reprendre leur croissance. On appelle donc ce phénotype «pseudo-sénescence» car c'est une sénescence réversible caractéristique soit des inhibiteurs de PARP, soit des cellules tumorales. Cette caractéristique nous laisse penser que ces cellules, en passant par cet état sénescent avant de reprendre leur croissance, acquièrent un phénotype résistant aux inhibiteurs de PARP comme le montrent une publication sur le cancer du sein (203) et des résultats préliminaires non publiés que nous avons effectués en essais clonogénique.

Il existe plusieurs publications qui démontrent que les inhibiteurs de PARP induisent un état sénescent, mais toujours dépendant de p53 (204) (155) (154, 205). Cependant, nos résultats sont les premiers à démontrer la mise en place d'un état apparenté à la sénescence dans les cellules traitées aux inhibiteurs de PARP malgré la présence de mutation *TP53*. Nous observons une augmentation de p21 après traitement aux inhibiteurs de PARP, ce qui nous laisse penser que cet arrêt de prolifération amenant à l'état sénescent indépendant de *TP53* passe par l'activation de p21. De plus, des recherches précédentes démontraient une régulation Chk2/p21 indépendante de p53 pour l'entrée en sénescence (206). Des résultats supplémentaires non présentés dans ce manuscrit démontrent que l'inhibition de p21 ou chk2 par shRNA empêche les cellules d'entrer en sénescence après traitement aux inhibiteurs de PARP. Ces cellules tentent de proliférer malgré leurs nombreuses cassures de l'ADN qui les rendent instables et les amènent à finalement mourir par crise mitotique. Cet état sénescent protège la cellule tumorale en l'empêchant de se diviser lorsqu'elle présente trop d'instabilité génomique. Le lien entre Chk2 et PARP se fait par l'accumulation de cassures double-brins créées par les inhibiteurs de PARP et induisant une surexpression de Chk2 (207). Il a d'ailleurs déjà été démontré l'importance d'une déficience en Chk2 pour une meilleure réponse aux inhibiteurs de PARP (208) mais aussi l'intérêt d'une combinaison de Chk2 avec les inhibiteurs de PARP (209). Le gène *''AKT-associated phosphorylation of forkhead box O''* (FOXO3A) fait le lien entre l'inhibition de PARP et p21. Il joue un rôle dans plusieurs mécanismes cellulaires comme l'arrêt du cycle, l'induction de l'autophagie, la sensibilisation à la chimiothérapie, l'inhibition de métastase, la différenciation cellulaire et l'apoptose. FOXO3A a été montré comme surexprimé après l'inhibition de PARP1 dans les cellules cancéreuses gastriques : il serait une cible de PARP (210). FOXO3A est connu pour déréguler p21 et ainsi bloquer la prolifération des cellules tumorales après le traitement aux inhibiteurs de PARP de façon indépendante de *TP53* (211-213).

Des expériences supplémentaires sont nécessaires pour comprendre les mécanismes qu'utilisent les inhibiteurs de PARP pour induire cet arrêt de prolifération indépendant de p53. On cherchera à vérifier si cela passe par l'inhibition d'une ou plusieurs protéines fixées à la chaîne de PAR ou par le mécanisme de piégeage provoquant un arrêt et blocage de la fourche de réplication. Des expériences pour déterminer quelles sont les protéines impliquées dans

l'inhibition de la PARylation et pouvant jouer un rôle dans l'arrêt du cycle et la sénescence sont en cours.

Nos résultats indiquent que l'utilisation clinique de l'Olaparib comme thérapie en maintenance pourrait favoriser la reprise et la résistance dues à un passage par un état sénescent induit par les inhibiteurs de PARP. L'Olaparib en monothérapie de maintenance prolonge de manière significative la survie des patientes atteintes du EOC HGS (147). On retrouve le même phénomène pour le traitement des patientes avec l'inhibiteur de PARP, Rucaparib (214), Niraparib (136) et Talazoparib (215). Cependant, malgré une meilleure efficacité, il reste obligatoire de l'utiliser en maintenance pour obtenir une réponse cliniquement significative. Nos résultats nous laissent penser, qu'en clinique, un état apparenté à la sénescence est induit au sein de la tumeur provoquant sa diminution et son arrêt de prolifération mais que l'arrêt de traitement permettrait aux cellules tumorales de reprendre leur prolifération d'où l'obligation d'utiliser les inhibiteurs de PARP en maintenance. Une publication a démontré dans le cancer du sein que les cellules entrant en sénescence après un traitement d'irradiation apportaient à la tumeur un environnement favorable à la mise en place d'une population de cellules plus résistantes (216). De plus, dans le cancer de l'ovaire, il a été démontré que les patientes présentant une mutation *BRCA2* développaient de la résistance aux inhibiteurs de PARP par un phénomène de réversibilité de la mutation BRCA (217-220). Ces publications en plus de nos résultats nous amènent à penser que le traitement des inhibiteurs de PARP en maintenance rendrait la tumeur résistante à cause des cellules sénescentes qui, soient se transformeraient elles-mêmes, soient créeraient un microenvironnement favorable à la mise en place de cellules tumorales résistantes aux inhibiteurs de PARP.

Plusieurs résultats non publiés au laboratoire montrent un changement de morphologie des cellules après induction de la sénescence par l'Olaparib. De plus, le développement de lignées résistantes aux inhibiteurs de PARP montre clairement un passage de nos cellules par un stade sénescent (test B-Gal) avant l'obtention de lignées résistantes. On pense qu'il est donc primordial d'éliminer la totalité de la tumeur pour ne pas laisser le temps aux cellules restantes ou environnantes de se transformer en cellules résistantes. C'est la stratégie utilisée en combinant les inhibiteurs de PARP avec l'ABT 263.

Pour améliorer la réponse aux inhibiteurs de PARP, éviter la rechute et l'apparition de cellules cancéreuses résistantes, nous proposons d'éliminer les cellules sénescentes induites

par les inhibiteurs de PARP par des drogues sénolytiques telles que l'ABT-263 (Navitoclax), un inhibiteur de Bcl2 et Bcl-XL (221, 222). Ce médicament a été largement utilisé dans les modèles précliniques ; il fait l'objet d'essais cliniques passés et en cours en raison de ses effets pro-apoptotiques (222). Les essais cliniques montrent une faible réponse des patientes traitées à l'ABT263 en monothérapie (10%), ce qui est trop faible pour l'utiliser en monothérapie (223, 224). Dans ces études cliniques, l'ABT-263 a été administré seul mais aussi en association avec d'autres chimiothérapies (comme la carboplatine ou le docétaxel) dans le but d'augmenter l'apoptose et la mort cellulaire (225). Cependant, très récemment, il a été décrit pour ses capacités à éliminer spécifiquement les cellules sénescentes (221, 226, 227). Nos résultats ont montré un effet synergique des inhibiteurs de PARP avec l'ABT-263 dans quatre lignées cellulaires, avec la disparition des marqueurs de sénescence et l'induction de l'apoptose. De plus, ils démontrent la spécificité de cette sénescence car l'ABT-263 ne cause aucune apoptose lorsqu'il a été administré seul ou après le relâchement du traitement aux inhibiteurs de PARP. Une étude récente a également signalé un effet synergique de Talazoparib et ABT-263 dans les cellules cancéreuses ovariennes, mais dans ce cas, l'accent a été uniquement mis sur le rôle pro-apoptotique de l'ABT263 sans décrire la sénescence (228). C'est pour cela que nous souhaiterions tester notre hypothèse en combinant les inhibiteurs de PARP avec d'autres sénolytiques comme le Dasatinib, le Quercetin et d'autres qui sont connus pour éliminer spécifiquement les cellules sénescentes (226). Point important, nous avons montré une diminution du volume de la tumeur chez les souris traitées avec cette thérapie combinée ce qui suggère qu'aux doses d'inhibiteurs de PARP utilisées en *in vivo*, un état sénescent se développe.

3.3 Perspectives

Les travaux publiés par l'équipe du Dr Sohrab Shah (6), auxquels le laboratoire et moi-même avons contribué en tant que co-auteurs, étudient les mutations ponctuelles dans l'ensemble du génome et les variations structurelles génomiques de 133 tumeurs (59 SHG, 35 cellules claires, 29 endométrioïdes et 10 tumeurs adultes de cellules granulosa). Les résultats ont permis de déterminer un nouveau classement composé de sept sous-groupes. Dans cette nouvelle classification, les HGS sont divisés en deux sous-groupes : un groupe présentant une

déficience en HR (HRD) et un autre présentant des segments d'ADN inversés en double tandem (Foldback Inversion, FBI). De plus, ils ont démontré que ces critères de classement permettraient de regrouper de façon pronostique les patientes, remplaçant ainsi les mutations et l'expression génique de *BRCA1/2* comme biomarqueurs. Dans l'ensemble, ces résultats présentent une nouvelle façon de regrouper les différentes maladies du cancer de l'ovaire, en divisant les histotypes classiques et en identifiant de nouvelles strates biologiques susceptibles d'informer les opportunités thérapeutiques actuelles et futures comme les inhibiteurs de PARP. Il serait donc intéressant de caractériser les 18 lignées présentes au laboratoire en fonction de ces nouveaux critères pour savoir si elles se retrouvent dans le nouveau sous-groupe FBI ou HRD. Cela pourra peut-être nous expliquer les réponses variées à la chimiothérapie et aux inhibiteurs de PARP mais aussi nous donner un modèle pour étudier les facteurs moléculaires permettant de discriminer ces deux sous-groupes.

Plus de 60 ans se sont écoulés depuis la création de la première lignée cellulaire cancéreuse humaine, HeLa, en 1951. Depuis, les lignées cellulaires tumorales humaines ont eu un impact extrêmement important sur la recherche sur le cancer et ont grandement facilité le développement d'une variété de traitements contre le cancer qui profitent aux patients. Il serait donc important pour la suite, de dériver de nouvelles lignées cellulaires de EOC HGS mais aussi et surtout d'autres sous-types comme les cellules claires. Au laboratoire, nous avons dans notre collection deux lignées cellulaires de sous-type cellule claire dont une décrite dans la littérature (TOV21G). Avoir un grand nombre de lignées cellulaires permet de mieux refléter l'hétérogénéité de la maladie, d'où l'intérêt de dériver et caractériser d'autres lignées cellulaires de sous–type cellule claire. De plus, ces cellules ne répondent que très peu aux thérapies actuelles et même si ce sous-type est peu présent en Amérique du nord, on le retrouve beaucoup plus fréquemment au Japon. Aussi, il serait pertinent de contrôler que les lignées dérivées reflètent bien la tumeur par la comparaison du profil génomique par CNV, des marqueurs spécifiques de HGS par immunohistochimie et par la réponse à la chimiothérapie. De nouveaux modèles de lignées cellulaires robustes et efficaces permettraient de prédire la réponse du patient à divers médicaments et amélioreraient considérablement le développement et la mise en place de nouveaux médicaments pour un traitement personnalisé des patients atteints de cancer.

Plusieurs autres inhibiteurs de PARP ont été créés. Le Niraparib, le Talazoparib et le Rucaparib semblent, actuellement, les plus prometteurs pour remplacer l'Olaparib en clinique dû à leur efficacité à faible dose et leurs faibles effets secondaires. Il reste cependant à analyser leurs caractéristiques moléculaires, à déterminer les biomarqueurs associés et à étudier leur résistance. Ceci permettra de vérifier si ces nouveaux inhibiteurs pourraient cibler d'autres patientes que celles sensibles à Olaparib et être combinés à d'autres thérapies. Il a déjà été démontré que tous ces inhibiteurs bloquent la PARylation de PARP1 mais qu'ils présentent une activité piégeage différente de PARP sur l'ADN (Talazoparib >> Niraparib ~ Olaparib > Rucaparib) ce qui va déterminer l'activité anticancéreuse des inhibiteurs de PARP en tant qu'agents uniques (141). La synergie avec les agents alkylants ou d'autres agents est différente si l'action est le trapping, la diminution de la parylation ou le manque de réparation des cassures simple brins. De plus, une étude a démontré que l'efficacité du Talazoparib et du Rucaparib est nulle lorsqu'il n'y avait aucune expression de PARP dans les cellules alors que l'efficacité est dose dépendante avec des cellules présentant une expression normale de PARP (148). Ces résultats ont conduit à la conclusion que les mécanismes cytotoxiques des inhibiteurs de PARP sont médiés par la fréquence de la protéine PARP mais pas par leur efficacité d'inhibition catalytique. Au laboratoire, la suite des recherches s'intéressera à comprendre les différentes voies de la réparation de l'ADN impliquées dans la réponse à ces nouveaux inhibiteurs de PARP. L'objectif est de voir si leur activité de piégeage change les voies impliquées mais aussi de comprendre quelles sont les patientes qui pourraient en bénéficier, et cela toujours dans l'optique que la RH ne soit pas le seul impliquée dans cette réponse.

En plus de la compréhension des mécanismes de réponse aux inhibiteurs de PARP, il manque toujours une méthode clinique permettant de discriminer les patientes qui peuvent bénéficier des inhibiteurs de PARP de celles qui ne peuvent pas.

Il a été largement démontré dans la plupart des recherches dont les nôtres qu'il est primordial de définir le statut de la RH et des autres voies de la réparation de l'ADN et pas seulement celui des mutations de *BRCA1/2* pour définir la réponse aux inhibiteurs de PARP (122, 137, 138). Il est donc important de développer des tests fonctionnels pouvant être utilisés en clinique pour permettre de détecter les défauts des voies de réparation de l'ADN dont principalement la RH. Des travaux récents (229) ont analysé 54 échantillons de tumeurs

mammaires primaires provenant de patientes soumises à une intervention chirurgicale. Ils ont déterminé leur fonctionnalité de RH en étudiant la formation de foyers RAD51 induits par rayonnement après irradiation *ex vivo* de ces échantillons de tumeurs organotypiques. Les tumeurs présentant une formation altérée de foyers RAD51 ont été soumises à une analyse génétique et épigénétique afin de vérifier les résultats. Ceux-ci démontrent que 5 tumeurs sur 45 présentaient une déficience en RH dont 2 qui n'étaient pas causée par une mutation des gènes *BRCA1/2*. Les auteurs affirment qu'il s'agit d'une expérience relativement simple qui peut être réalisée avec du matériel de biopsie, ce qui en fait un outil puissant pour sélectionner les patientes déficientes en RH qui pourraient bénéficier d'un traitement aux inhibiteurs de PARP. De plus d'autres méthodes pour analyser la déficience en RH sont actuellement en essais, voire même déjà proposés pour la clinique. C'est le cas du test Myriad Mychoice HDR qui se base sur trois mesures indépendantes de l'instabilité génomique, la perte d'hétérozygotie (LOH), du déséquilibre allélique téléférique (TAI) et des transitions d'état à grande échelle (LST). Ils démontrent que le score de ce test corrèle avec la réponse au cisplatin (230). Au laboratoire, suite à nos résultats prouvant l'implication de toutes les voies de la réparation de l'ADN pour la réponse aux inhibiteurs de PARP, nous analyserons la déficience en RH et en NER au sein des morceaux de biopsies de patientes en comptabilisant, par FACS, les foyers Rad51 et les produits 6-4 photoproton après respectivement irradiations et ultraviolets (231, 232). De plus, afin de confirmer nos résultats, nous associerons l'analyse de fonctionnalité de RH et NER, à la réponse aux inhibiteurs de PARP des biopsies. Pour ce faire, on utilisera des systèmes microfluidiques, mis au point au laboratoire (233), dans lesquels un morceau de cette même biopsie sera déposé et exposé à des doses croissantes d'inhibiteur de PARP.

Comme expliqué dans les paragraphes ci-dessus, la diminution d'expression de PARP ou la déficience de NER ou MMR en plus de celle de la RH pourraient justifier la résistance aux inhibiteurs de PARP. Beaucoup études décrivant d'autres mécanismes ont été publiées, comme par exemple la surexpression de p-glycoprotéine (234), la réversion de la mutation BRCA (220) ou encore une dérégulation de NHEJ (105), mais beaucoup de travail reste encore à faire pour comprendre et empêcher cette résistance. Pour cela, la mise en place de lignées EOC HGS devenant résistantes après plusieurs doses croissantes de traitement aux inhibiteurs de PARP permettrait de déterminer leurs différences et caractéristiques moléculaires et ainsi apporter de nouvelles connaissances sur la résistance acquise des

différents inhibiteurs de PARP. La suite de nos travaux au laboratoire s'oriente dans cette direction en utilisant l'Olaparib mais aussi le Niraparib et le Talazoparib. Afin de contrer cette résistance mais aussi d'améliorer le traitement, beaucoup de combinaisons ont déjà été testées et publiées. Cependant la plupart a été faite dans l'idée qu'il fallait cibler en priorité la RH avec des inhibiteurs la touchant directement (235) ou indirectement (236) (237). Notre but sera de déterminer si les facteurs jouant un rôle dans la totalité des voies de la réparation de l'ADN sont impliqués dans la résistance acquise aux inhibiteurs de PARP. Ces résultats nous permettront de déterminer de nouvelles combinaisons permettant d'améliorer la sensibilité aux inhibiteurs de PARP mais aussi d'éviter ou de combattre la résistance acquise.

Plusieurs projets de recherche portent sur la combinaison des inhibiteurs de PARP avec une chimiothérapie conventionnelle ou avec un autre médicament inhibant la RH. Sur la base de nos résultats publiés, nous analysons l'effet combiné d'Olaparib et d'un inhibiteur de l'interaction de ERCC1 et XPF (NSC130813) (238). Cet inhibiteur démontre une capacité à inhiber le NER et d'une manière différente la HR. Nos résultats préliminaires montrent un effet synergique de la combinaison dans deux lignées cellulaires résistantes à l'Olaparib (TOV11D et OV90). Ces résultats prometteurs suggèrent qu'une thérapie combinée d'Olaparib et NSC130813 pourrait être efficace pour traiter les patients résistants aux EOC. De plus, ces résultats coïncident bien avec notre modèle de réponse à l'Olaparib. Dans le même principe, l'utilisation de nouveaux inhibiteurs ciblant la réparation par RH et NHEJ ou par NER est actuellement essayée au laboratoire en les combinant avec les inhibiteurs de PARP. Cet inhibiteur, le Dbait, décrit par le laboratoire du Dre Marie Dutreix, est une molécule recréant des cassures simple ou double brins exogènes, induisant ainsi une déficience dans ces voies de réparation de l'ADN (239).

Les inhibiteurs de PARP ont largement démontré leur efficacité chez les patientes présentant des mutations *BRCA1/2* ou présentant une déficience dans la RH (BRCAness). De plus, d'autres études dont les nôtres montrent que d'autres voies de la réparation de l'ADN entrent en jeu pour sensibiliser les inhibiteurs de PARP. Cela amène la plupart des recherches à combiner les inhibiteurs de PARP avec des drogues ciblant la réparation de l'ADN. Nous montrons ici une synergie en combinant les inhibiteurs de PARP avec une autre drogue ne touchant pas la réparation de l'ADN dans des lignées résistantes et sensibles aux inhibiteurs de PARP, ce qui laisse penser que cette stratégie de combinaison, indépendante de la

fonctionnalité des voies de la réparation, serait efficace pour l'ensemble des patientes présentant des tumeurs EOC HGS. Sachant que la sénescence a été observée à la suite d'autres traitements que les inhibiteurs de PARP, phénomène de sénescence induite par le stress (*treatment induced senescence,* TIS), l'utilisation de l'ABT-263 comme sénolytique pourrait certainement s'appliquer à d'autres drogues comme l'irradiation ou encore les traitements communs de chimiothérapie. De plus, cela permettrait d'amener ce principe à d'autres types cancéreux comme la prostate utilisant l'irradiation comme traitement. Ici, nous démontrons que la combinaison des inhibiteurs de PARP avec l'ABT263 fonctionne dans les cancers du sein triple négatif (MDA-MB231), un cancer dans lequel les inhibiteurs de PARP sont testés car la mutation *BRCA1/2* et les déficiences dans les voies de la réparation de l'ADN sont souvent retrouvées. Nous avons aussi démontré la mise en place de la sénescence avec de nouveaux inhibiteurs de PARP comme le Niraparib et le Talazoparib et prouvé l'effet synergique de la combinaison avec l'ABT263. Par la suite, nous pensons déterminer d'autres traitements sénolytiques plus performants en faisant un screening de CRISPR ciblant les différents acteurs spécifiques de la sénescence après traitement aux inhibiteurs de PARP. Un second criblage de traitements sénolytiques déjà connus sera effectué sur différentes drogues largement utilisées en clinique et sur différents types de cancer, pour déterminer les meilleures combinaisons à utiliser. Cela permettra d'améliorer les traitements et d'éliminer soit les cellules sénescentes susceptibles de reprendre leur croissance en développant une résistance, soit la mise en place de cellules résistantes induites par la sécrétion des cellules sénescentes dans le microenvironnement. Cela diminuerait la rechute, la résistance acquise et permettrait de ne pas utiliser les traitements en maintenance.

4 CONCLUSION ET PERSPECTIVES

Notre modèle de nouvelles lignées cellulaires EOC HGS et leur caractérisation détaillée fournissent de nouveaux outils de recherche pour étudier la forme la plus commune et la plus létale d'EOC. Aussi, pour l'étude des inhibiteurs de PARP, ce modèle représentatif de la maladie permet une étude efficace par la présence de deux lignées *BRCA1* et BRCA 2 mutées. De plus, notre modèle peut être distingué efficacement des autres sous-types EOC, soulignant l'importance de ces lignes cellulaires pour l'étude des EOC HGS. Il resterait à contrôler les lignées dérivées et nouvelles en vérifiant qu'elles reflètent bien la tumeur par la comparaison du profil génomique par CNV, des marqueurs spécifiques de HGS par immunohistochimie et par la réponse à la chimiothérapie. Aussi, suite aux résultats du papier de Dr. Sohrab Shah (6), il serait intéressant de vérifier si les déficiences de la réparation de l'ADN spécifiques aux EOC HGS se retrouvent au sein de notre modèle et si cela confirme l'importance de la réparation de l'ADN dans la réponse aux inhibiteurs de PARP. De plus, il faudra caractériser et dériver d'autres lignées capables de former des tumeurs en xénogreffe mais aussi d'autres sous-types d'EOC comme celui des cellules claires peu représentées en Amérique du nord mais très létales dû au manque de traitements. Peu de thérapies fonctionnent bien pour l'instant donc la caractérisation d'un bon modèle d'étude présenterait un grand intérêt.

Dans un deuxième volet de nos travaux, nous avons développé un nouveau modèle permettant de prédire la sensibilité à l'Olaparib. Ce modèle implique que les patientes répondant aux inhibiteurs de PARP ne présentent pas seulement des mutations de *BRCA1/2* ou un profil BRCAness mais qu'il doit être associé à des déficiences des autres voies de la réparation de l'ADN comme le NER ou le MMR. Bien que d'autres gènes de la réparation de l'ADN aient été décrits en association avec la sensibilité d'Olaparib, notre travail identifie des défauts dans plusieurs voies de réparation de l'ADN démontrant un effet cumulatif dans les cellules sensibles à l'Olaparib. Nos travaux aident à repérer les patientes susceptibles de répondre aux inhibiteurs de PARP mais cela nécessite une méthode clinique permettant de déterminer un profil de réparation de l'ADN chez les patientes. Pour cela, au laboratoire, nous pensons tester dans le futur la fonctionnalité des voies RH, NER et MMR en induisant des

dommages spécifiques dans les biopsies de patientes. On analysera ensuite la fonctionnalité de ces voies en regardant, par exemple les foci Rad 51 et les formations de 6-4 photoproton, au FACS. On associera ces résultats à la réponse aux inhibiteurs de PARP par l'utilisation de système microfluidique dans lequel un morceau de cette même biopsie sera déposé et exposé à des doses croissantes d'inhibiteur de PARP. La combinaison de ces deux résultats nous donnera une information fiable sur la capacité des patientes à répondre aux inhibiteurs de PARP. Une suite logique à notre projet sera de tenter de sensibiliser les patientes ne répondant pas aux inhibiteurs de PARP en utilisant des combinaisons de traitements : soit avec un inhibiteur du NER ciblant l'interaction de ERCC1 et XPF (NSC130813), soit avec un nouvel inhibiteur de la réparation de la RH et du NHEJ ou du NER. Cet inhibiteur, le Dbait, est une molécule recréant des cassures simple ou double brins exogènes entrant en compétition avec les cassures de l'ADN endogènes et induisant ainsi une déficience dans ces voies de réparation de l'ADN. De plus, on s'intéressera à la résistance acquise des différents inhibiteurs de PARP en créant des cellules à la base sensibles aux inhibiteurs de PARP, puis résistantes en les exposant chroniquement à des doses croissantes d'inhibiteurs de PARP. On regardera le profil moléculaire de ces cellules pour les comparer avec le profil des cellules de base. Finalement pour valider notre modèle, on utilisera un TMA de patientes traitées à l'Olaparib pour lesquelles on connaîtra les données cliniques.

Dans un troisième volet, nous nous sommes concentrés sur les processus du devenir cellulaire induits par le traitement PARPi et avons exploré ces mécanismes dans des thérapies combinées. Il est important à noter que l'interruption du traitement d'inhibiteurs de PARP a entraîné une reprise de la croissance des cellules tumorales, ce qui nous laisse penser que l'application clinique de l'Olaparib comme thérapie de maintenance favorise la rechute et la résistance en induisant un phénotype réversible de type sénescent. Nous suggérons donc que la thérapie combinée des inhibiteurs de PARP avec l'ABT-263 peut contrer ces effets indésirables. Par la suite, nous aimerions, au laboratoire, comprendre plus le mécanisme par lequel les inhibiteurs de PARP induisent un arrêt de cycle puis une sénescence. Nous pensons que cela passe par une augmentation de p21 régulée par FOXO3A qui lui est surexprimé lorsque PARP est inhibé ou Chk2 surexprimé par l'accumulation des cassures double brins. Au laboratoire, des résultats préliminaires non publiés montrent que les cellules infectées par des shRNA de p21 ou Chk2 traitées aux inhibiteurs de PARP ne rentrent plus en sénescence

mais en crise mitotique et mourir. Tout ce mécanisme reste encore à étudier plus en profondeur. Il reste encore à comprendre si c'est l'inhibition de la chaine de poly(ADP-ribose) ou le piégeage par arrêt de la fourche qui amène la modulation de FOXO3A ou d'autres protéines responsables de l'arrêt de prolifération. De plus, on voudrait consolider l'idée que le traitement de maintenance fait entrer les cellules en sénescence puis amène au développement de cellules résistantes aux inhibiteurs de PARP soit par la reprise de la cellule sénescente elle-même, soit par le microenvironnement activé par le SASP. De plus, un screening de CRISPR, dans les cellules EOC HGS présentant un état de pseudo-sénescence lorsqu'elles sont traitées aux inhibiteurs de PARP, permettra de déterminer les cibles primordiales pour la mise en place de cette sénescence et ainsi permettre le développement de nouveaux sénolytiques. Un deuxième screening de drogues pouvant induire de la sénescence serait utile et permettrait d'utiliser ce concept à d'autres traitements et donc aussi à d'autres types de cancers. De plus, une TMA de patientes traitées aux inhibiteurs de PARP permettrait de valider la sénescence acquise après traitement aux initiateurs de PARP.

Pour conclure, nous avons établi un nouveau modèle de lignées cellulaires EOC HGS représentant bien l'hétérogénéité et les caractéristiques de la maladie. Cela nous a permis de proposer un nouveau modèle de réponse aux inhibiteurs de PARP. Celui-ci distingue les patientes pouvant bénéficier des inhibiteurs de PARP de celles pour lesquelles il faudra se tourner vers d'autres thérapies ou, comme on le propose, vers des combinaisons de drogues. Ceci a comme but d'éviter les traitements en maintenance et donc de diminuer les effets secondaires et la résistance acquise. Les inhibiteurs de PARP constituent une découverte majeure qui améliore la survie des patientes, cependant il reste à déterminer une méthode clinique efficace pour tester la fonctionnalité des voies de la réparation de l'ADN et à découvrir une combinaison efficace permettant de traiter l'ensemble des patientes, éviter la rechute et empêcher la résistance.

C'est dans cette optique que nos résultats, en contribuant à mieux comprendre le mécanisme de réponse aux inhibiteurs de PARP et le destin cellulaire qui en résulte, ouvrent de nouvelles et encourageantes approches dans l'amélioration de la prise en charge des patients par un traitement aux inhibiteurs de PARP seuls ou combinés à d'autres traitements.

5 Bibliographie

1. Fleury H, Communal L, Carmona E, Portelance L, Arcand SL, Rahimi K, et al. Novel high-grade serous epithelial ovarian cancer cell lines that reflect the molecular diversity of both the sporadic and hereditary disease. Genes Cancer. 2015;6(9-10):378-98.
2. Marques M, Beauchamp MC, Fleury H, Laskov I, Qiang S, Pelmus M, et al. Chemotherapy reduces PARP1 in cancers of the ovary: implications for future clinical trials involving PARP inhibitors. BMC Med. 2015;13:217.
3. Fleury H, Carmona E, Morin VG, Meunier L, Masson JY, Tonin PN, et al. Cumulative defects in DNA repair pathways drive the PARP inhibitor response in high-grade serous epithelial ovarian cancer cell lines. Oncotarget. 2016;8(25):40152.
4. Edjekouane L, Benhadjeba S, Jangal M, Fleury H, Gevry N, Carmona E, et al. Proximal and distal regulation of the HYAL1 gene cluster by the estrogen receptor alpha in breast cancer cells. Oncotarget. 2016;7(47):77276-90.
5. Couturier AM, Fleury H, Patenaude AM, Bentley VL, Rodrigue A, Coulombe Y, et al. Roles for APRIN (PDS5B) in homologous recombination and in ovarian cancer prediction. Nucleic Acids Res. 2016;44(22):10879-97.
6. Wang YK, Bashashati A, Anglesio MS, Cochrane DR, Grewal DS, Ha G, et al. Genomic consequences of aberrant DNA repair mechanisms stratify ovarian cancer histotypes. Nat Genet. 2017;49(6):856-65.
7. Siegel RL, Miller KD, Jemal A. Cancer statistics, 2016. CA Cancer J Clin. 2016;66(1):7-30.
8. Oktem O, Oktay K. The ovary: anatomy and function throughout human life. Ann N Y Acad Sci. 2008;1127:1-9.
9. Partridge EE, Barnes MN. Epithelial ovarian cancer: prevention, diagnosis, and treatment. CA Cancer J Clin. 1999;49(5):297-320.
10. Martin VR. Ovarian cancer. Semin Oncol Nurs. 2002;18(3):174-83.
11. Argento M, Hoffman P, Gauchez AS. Ovarian cancer detection and treatment: current situation and future prospects. Anticancer Res. 2008;28(5B):3135-8.
12. Henderson JT, Harper CC, Gutin S, Saraiya M, Chapman J, Sawaya GF. Routine bimanual pelvic examinations: practices and beliefs of US obstetrician-gynecologists. Am J Obstet Gynecol. 2013;208(2):109 e1-7.
13. Babic A, Cramer DW, Kelemen LE, Kobel M, Steed H, Webb PM, et al. Predictors of pretreatment CA125 at ovarian cancer diagnosis: a pooled analysis in the Ovarian Cancer Association Consortium. Cancer Causes Control. 2017;28(5):459-68.
14. Mircea R, Frincu DL, Dumitrache F. [Expression of CA-125 in ovarian cancer]. Rev Med Chir Soc Med Nat Iasi. 2009;113(4):1191-4.
15. Colombo N, Peiretti M, Garbi A, Carinelli S, Marini C, Sessa C, et al. Non-epithelial ovarian cancer: ESMO Clinical Practice Guidelines for diagnosis, treatment and follow-up. Ann Oncol. 2012;23 Suppl 7:vii20-6.
16. Reed N, Millan D, Verheijen R, Castiglione M, Group EGW. Non-epithelial ovarian cancer: ESMO Clinical Practice Guidelines for diagnosis, treatment and follow-up. Ann Oncol. 2010;21 Suppl 5:v31-6.

17. Chen VW, Ruiz B, Killeen JL, Cote TR, Wu XC, Correa CN. Pathology and classification of ovarian tumors. Cancer. 2003;97(10 Suppl):2631-42.
18. Piek JM, van Diest PJ, Zweemer RP, Jansen JW, Poort-Keesom RJ, Menko FH, et al. Dysplastic changes in prophylactically removed Fallopian tubes of women predisposed to developing ovarian cancer. J Pathol. 2001;195(4):451-6.
19. Salvador S, Gilks B, Kobel M, Huntsman D, Rosen B, Miller D. The fallopian tube: primary site of most pelvic high-grade serous carcinomas. Int J Gynecol Cancer. 2009;19(1):58-64.
20. Chene G, Ouellet V, Rahimi K, Barres V, Meunier L, De Ladurantaye M, et al. Expression of Stem Cell Markers in Preinvasive Tubal Lesions of Ovarian Carcinoma. Biomed Res Int. 2015;2015:808531.
21. Bjorkholm E, Pettersson F, Einhorn N, Krebs I, Nilsson B, Tjernberg B. Long-term follow-up and prognostic factors in ovarian carcinoma. The radiumhemmet series 1958 to 1973. Acta Radiol Oncol. 1982;21(6):413-9.
22. Hogberg T, Carstensen J, Simonsen E. Treatment results and prognostic factors in a population-based study of epithelial ovarian cancer. Gynecol Oncol. 1993;48(1):38-49.
23. Scully RE. Classification of human ovarian tumors. Environ Health Perspect. 1987;73:15-25.
24. McCluggage WG. My approach to and thoughts on the typing of ovarian carcinomas. J Clin Pathol. 2008;61(2):152-63.
25. Shih Ie M, Kurman RJ. Ovarian tumorigenesis: a proposed model based on morphological and molecular genetic analysis. Am J Pathol. 2004;164(5):1511-8.
26. Crum CP, Drapkin R, Kindelberger D, Medeiros F, Miron A, Lee Y. Lessons from BRCA: the tubal fimbria emerges as an origin for pelvic serous cancer. Clin Med Res. 2007;5(1):35-44.
27. Kaku T, Ogawa S, Kawano Y, Ohishi Y, Kobayashi H, Hirakawa T, et al. Histological classification of ovarian cancer. Med Electron Microsc. 2003;36(1):9-17.
28. Jordan S, Green A, Webb P. Benign epithelial ovarian tumours-cancer precursors or markers for ovarian cancer risk? Cancer Causes Control. 2006;17(5):623-32.
29. Merritt MA, Cramer DW. Molecular pathogenesis of endometrial and ovarian cancer. Cancer Biomark. 2010;9(1-6):287-305.
30. Prat J. Pathology of borderline and invasive cancers. Best Pract Res Clin Obstet Gynaecol. 2016.
31. Mabuchi S, Sugiyama T, Kimura T. Clear cell carcinoma of the ovary: molecular insights and future therapeutic perspectives. J Gynecol Oncol. 2016;27(3):e31.
32. Hennessy BT, Coleman RL, Markman M. Ovarian cancer. Lancet. 2009;374(9698):1371-82.
33. Andrews L, Mutch DG. Hereditary Ovarian Cancer and Risk Reduction. Best Pract Res Clin Obstet Gynaecol. 2017.
34. Tonin PN, Maugard CM, Perret C, Mes-Masson AM, Provencher DM. A review of histopathological subtypes of ovarian cancer in BRCA-related French Canadian cancer families. Fam Cancer. 2007;6(4):491-7.
35. Risch HA, McLaughlin JR, Cole DE, Rosen B, Bradley L, Fan I, et al. Population BRCA1 and BRCA2 mutation frequencies and cancer penetrances: a kin-cohort study in Ontario, Canada. J Natl Cancer Inst. 2006;98(23):1694-706.

36. Pennington KP, Walsh T, Harrell MI, Lee MK, Pennil CC, Rendi MH, et al. Germline and somatic mutations in homologous recombination genes predict platinum response and survival in ovarian, fallopian tube, and peritoneal carcinomas. Clin Cancer Res. 2014;20(3):764-75.
37. Toss A, Tomasello C, Razzaboni E, Contu G, Grandi G, Cagnacci A, et al. Hereditary ovarian cancer: not only BRCA 1 and 2 genes. Biomed Res Int. 2015;2015:341723.
38. Lynch HT, Casey MJ, Snyder CL, Bewtra C, Lynch JF, Butts M, et al. Hereditary ovarian carcinoma: heterogeneity, molecular genetics, pathology, and management. Mol Oncol. 2009;3(2):97-137.
39. Wiegand KC, Shah SP, Al-Agha OM, Zhao Y, Tse K, Zeng T, et al. ARID1A mutations in endometriosis-associated ovarian carcinomas. N Engl J Med. 2010;363(16):1532-43.
40. Cancer Genome Atlas Research N. Integrated genomic analyses of ovarian carcinoma. Nature. 2011;474(7353):609-15.
41. Perren TJ. Mucinous epithelial ovarian carcinoma. Ann Oncol. 2016;27 Suppl 1:i53-i7.
42. Malpica A, Deavers MT, Lu K, Bodurka DC, Atkinson EN, Gershenson DM, et al. Grading ovarian serous carcinoma using a two-tier system. Am J Surg Pathol. 2004;28(4):496-504.
43. Pejovic T. Genetic changes in ovarian cancer. Ann Med. 1995;27(1):73-8.
44. Gilks CB. Subclassification of ovarian surface epithelial tumors based on correlation of histologic and molecular pathologic data. Int J Gynecol Pathol. 2004;23(3):200-5.
45. Singer G, Kurman RJ, Chang HW, Cho SK, Shih Ie M. Diverse tumorigenic pathways in ovarian serous carcinoma. Am J Pathol. 2002;160(4):1223-8.
46. Rosen DG, Yang G, Liu G, Mercado-Uribe I, Chang B, Xiao XS, et al. Ovarian cancer: pathology, biology, and disease models. Front Biosci (Landmark Ed). 2009;14:2089-102.
47. Sieben NL, Macropoulos P, Roemen GM, Kolkman-Uljee SM, Jan Fleuren G, Houmadi R, et al. In ovarian neoplasms, BRAF, but not KRAS, mutations are restricted to low-grade serous tumours. J Pathol. 2004;202(3):336-40.
48. Bowtell DD. The genesis and evolution of high-grade serous ovarian cancer. Nat Rev Cancer. 2010;10(11):803-8.
49. Konstantinopoulos PA, Ceccaldi R, Shapiro GI, D'Andrea AD. Homologous Recombination Deficiency: Exploiting the Fundamental Vulnerability of Ovarian Cancer. Cancer Discov. 2015;5(11):1137-54.
50. Mittempergher L. Genomic Characterization of High-Grade Serous Ovarian Cancer: Dissecting Its Molecular Heterogeneity as a Road Towards Effective Therapeutic Strategies. Curr Oncol Rep. 2016;18(7):44.
51. Walsh T, Lee MK, Casadei S, Thornton AM, Stray SM, Pennil C, et al. Detection of inherited mutations for breast and ovarian cancer using genomic capture and massively parallel sequencing. Proc Natl Acad Sci U S A. 2010;107(28):12629-33.
52. Wilkerson PM, Dedes KJ, Wetterskog D, Mackay A, Lambros MB, Mansour M, et al. Functional characterization of EMSY gene amplification in human cancers. J Pathol. 2011;225(1):29-42.
53. O'Hara AJ, Bell DW. The genomics and genetics of endometrial cancer. Adv Genomics Genet. 2012;2012(2):33-47.
54. Moreno-Bueno G, Gamallo C, Perez-Gallego L, de Mora JC, Suarez A, Palacios J. beta-Catenin expression pattern, beta-catenin gene mutations, and microsatellite instability in

endometrioid ovarian carcinomas and synchronous endometrial carcinomas. Diagn Mol Pathol. 2001;10(2):116-22.
55. Cai KQ, Albarracin C, Rosen D, Zhong R, Zheng W, Luthra R, et al. Microsatellite instability and alteration of the expression of hMLH1 and hMSH2 in ovarian clear cell carcinoma. Hum Pathol. 2004;35(5):552-9.
56. Leary AF, Quinn M, Fujiwara K, Coleman RL, Kohn E, Sugiyama T, et al. Fifth Ovarian Cancer Consensus Conference of the Gynecologic Cancer InterGroup (GCIG): clinical trial design for rare ovarian tumours. Ann Oncol. 2017;28(4):718-26.
57. Lawrie TA, Winter-Roach BA, Heus P, Kitchener HC. Adjuvant (post-surgery) chemotherapy for early stage epithelial ovarian cancer. Cochrane Database Syst Rev. 2015(12):CD004706.
58. Berek JS, Crum C, Friedlander M. Cancer of the ovary, fallopian tube, and peritoneum. Int J Gynaecol Obstet. 2012;119 Suppl 2:S118-29.
59. Gubbels JA, Claussen N, Kapur AK, Connor JP, Patankar MS. The detection, treatment, and biology of epithelial ovarian cancer. J Ovarian Res. 2010;3:8.
60. Poklar N, Pilch DS, Lippard SJ, Redding EA, Dunham SU, Breslauer KJ. Influence of cisplatin intrastrand crosslinking on the conformation, thermal stability, and energetics of a 20-mer DNA duplex. Proc Natl Acad Sci U S A. 1996;93(15):7606-11.
61. Jordan MA, Wilson L. Microtubules as a target for anticancer drugs. Nat Rev Cancer. 2004;4(4):253-65.
62. Helleday T, Petermann E, Lundin C, Hodgson B, Sharma RA. DNA repair pathways as targets for cancer therapy. Nat Rev Cancer. 2008;8(3):193-204.
63. Liu C, Srihari S, Lal S, Gautier B, Simpson PT, Khanna KK, et al. Personalised pathway analysis reveals association between DNA repair pathway dysregulation and chromosomal instability in sporadic breast cancer. Mol Oncol. 2016;10(1):179-93.
64. Curtin NJ. DNA repair dysregulation from cancer driver to therapeutic target. Nat Rev Cancer. 2012;12(12):801-17.
65. Bunting SF, Nussenzweig A. End-joining, translocations and cancer. Nat Rev Cancer. 2013;13(7):443-54.
66. Mavaddat N, Antoniou AC, Easton DF, Garcia-Closas M. Genetic susceptibility to breast cancer. Mol Oncol. 2010;4(3):174-91.
67. Cerbinskaite A, Mukhopadhyay A, Plummer ER, Curtin NJ, Edmondson RJ. Defective homologous recombination in human cancers. Cancer Treat Rev. 2012;38(2):89-100.
68. Moynahan ME, Jasin M. Mitotic homologous recombination maintains genomic stability and suppresses tumorigenesis. Nat Rev Mol Cell Biol. 2010;11(3):196-207.
69. Leibeling D, Laspe P, Emmert S. Nucleotide excision repair and cancer. J Mol Histol. 2006;37(5-7):225-38.
70. Sertic S, Pizzi S, Lazzaro F, Plevani P, Muzi-Falconi M. NER and DDR: classical music with new instruments. Cell Cycle. 2012;11(4):668-74.
71. Dianov GL. Base excision repair targets for cancer therapy. Am J Cancer Res. 2011;1(7):845-51.
72. Fu D, Calvo JA, Samson LD. Balancing repair and tolerance of DNA damage caused by alkylating agents. Nat Rev Cancer. 2012;12(2):104-20.
73. Martin LM, Marples B, Coffey M, Lawler M, Lynch TH, Hollywood D, et al. DNA mismatch repair and the DNA damage response to ionizing radiation: making sense of apparently conflicting data. Cancer Treat Rev. 2010;36(7):518-27.

74. Rivera A, Rojas JJ, Salazar-Barrios J, Maldonado M, Rios-Motta J. Synthesis of a new series of N,N'-dimethyltetrahydrosalen (H2[H2Me]salen) ligands by the reductive ring-opening of 3,3'-ethylene-bis(3,4-dihydro-6-substituted-2H-1,3-benzoxazines). Molecules. 2010;15(6):4102-10.
75. Roos WP, Kaina B. DNA damage-induced cell death: from specific DNA lesions to the DNA damage response and apoptosis. Cancer Lett. 2013;332(2):237-48.
76. Hanahan D, Weinberg RA. Hallmarks of cancer: the next generation. Cell. 2011;144(5):646-74.
77. Surova O, Zhivotovsky B. Various modes of cell death induced by DNA damage. Oncogene. 2013;32(33):3789-97.
78. Luong KV, Wang L, Roberts BJ, Wahl JK, 3rd, Peng A. Cell fate determination in cisplatin resistance and chemosensitization. Oncotarget. 2016;7(17):23383-94.
79. Adams JM, Cory S. Bcl-2-regulated apoptosis: mechanism and therapeutic potential. Curr Opin Immunol. 2007;19(5):488-96.
80. Chaitanya GV, Steven AJ, Babu PP. PARP-1 cleavage fragments: signatures of cell-death proteases in neurodegeneration. Cell Commun Signal. 2010;8:31.
81. Hanahan D, Weinberg RA. The hallmarks of cancer. Cell. 2000;100(1):57-70.
82. Adams JM, Cory S. The Bcl-2 apoptotic switch in cancer development and therapy. Oncogene. 2007;26(9):1324-37.
83. Letai AG. Diagnosing and exploiting cancer's addiction to blocks in apoptosis. Nat Rev Cancer. 2008;8(2):121-32.
84. Vazquez A, Bond EE, Levine AJ, Bond GL. The genetics of the p53 pathway, apoptosis and cancer therapy. Nat Rev Drug Discov. 2008;7(12):979-87.
85. Yip KW, Reed JC. Bcl-2 family proteins and cancer. Oncogene. 2008;27(50):6398-406.
86. Youle RJ, Strasser A. The BCL-2 protein family: opposing activities that mediate cell death. Nat Rev Mol Cell Biol. 2008;9(1):47-59.
87. Cragg MS, Harris C, Strasser A, Scott CL. Unleashing the power of inhibitors of oncogenic kinases through BH3 mimetics. Nat Rev Cancer. 2009;9(5):321-6.
88. Labi V, Erlacher M. How cell death shapes cancer. Cell Death Dis. 2015;6:e1675.
89. Luke CJ, Pak SC, Askew YS, Naviglia TL, Askew DJ, Nobar SM, et al. An intracellular serpin regulates necrosis by inhibiting the induction and sequelae of lysosomal injury. Cell. 2007;130(6):1108-19.
90. Hotchkiss RS, Strasser A, McDunn JE, Swanson PE. Cell death. N Engl J Med. 2009;361(16):1570-83.
91. Klionsky DJ. Autophagy: from phenomenology to molecular understanding in less than a decade. Nat Rev Mol Cell Biol. 2007;8(11):931-7.
92. Maiuri MC, Tasdemir E, Criollo A, Morselli E, Vicencio JM, Carnuccio R, et al. Control of autophagy by oncogenes and tumor suppressor genes. Cell Death Differ. 2009;16(1):87-93.
93. Vitale I, Galluzzi L, Castedo M, Kroemer G. Mitotic catastrophe: a mechanism for avoiding genomic instability. Nat Rev Mol Cell Biol. 2011;12(6):385-92.
94. Hayflick L, Moorhead PS. The serial cultivation of human diploid cell strains. Exp Cell Res. 1961;25:585-621.
95. Ewald JA, Desotelle JA, Wilding G, Jarrard DF. Therapy-induced senescence in cancer. J Natl Cancer Inst. 2010;102(20):1536-46.

96. Gonzalez LC, Ghadaouia S, Martinez A, Rodier F. Premature aging/senescence in cancer cells facing therapy: good or bad? Biogerontology. 2016;17(1):71-87.
97. Rodier F, Munoz DP, Teachenor R, Chu V, Le O, Bhaumik D, et al. DNA-SCARS: distinct nuclear structures that sustain damage-induced senescence growth arrest and inflammatory cytokine secretion. J Cell Sci. 2011;124(Pt 1):68-81.
98. Storer M, Mas A, Robert-Moreno A, Pecoraro M, Ortells MC, Di Giacomo V, et al. Senescence is a developmental mechanism that contributes to embryonic growth and patterning. Cell. 2013;155(5):1119-30.
99. Gilbert LA, Hemann MT. DNA damage-mediated induction of a chemoresistant niche. Cell. 2010;143(3):355-66.
100. Pare R, Yang T, Shin JS, Lee CS. The significance of the senescence pathway in breast cancer progression. J Clin Pathol. 2013;66(6):491-5.
101. Kelland L. The resurgence of platinum-based cancer chemotherapy. Nat Rev Cancer. 2007;7(8):573-84.
102. Kilari D, Guancial E, Kim ES. Role of copper transporters in platinum resistance. World J Clin Oncol. 2016;7(1):106-13.
103. Yamasaki M, Makino T, Masuzawa T, Kurokawa Y, Miyata H, Takiguchi S, et al. Role of multidrug resistance protein 2 (MRP2) in chemoresistance and clinical outcome in oesophageal squamous cell carcinoma. Br J Cancer. 2011;104(4):707-13.
104. Williams J, Lucas PC, Griffith KA, Choi M, Fogoros S, Hu YY, et al. Expression of Bcl-xL in ovarian carcinoma is associated with chemoresistance and recurrent disease. Gynecol Oncol. 2005;96(2):287-95.
105. Ceccaldi R, O'Connor KW, Mouw KW, Li AY, Matulonis UA, D'Andrea AD, et al. A unique subset of epithelial ovarian cancers with platinum sensitivity and PARP inhibitor resistance. Cancer Res. 2015;75(4):628-34.
106. Fleming ND, Agadjanian H, Nassanian H, Miller CW, Orsulic S, Karlan BY, et al. Xeroderma pigmentosum complementation group C single-nucleotide polymorphisms in the nucleotide excision repair pathway correlate with prolonged progression-free survival in advanced ovarian cancer. Cancer. 2012;118(3):689-97.
107. Martin LP, Hamilton TC, Schilder RJ. Platinum resistance: the role of DNA repair pathways. Clin Cancer Res. 2008;14(5):1291-5.
108. Ali AY, Farrand L, Kim JY, Byun S, Suh JY, Lee HJ, et al. Molecular determinants of ovarian cancer chemoresistance: new insights into an old conundrum. Ann N Y Acad Sci. 2012;1271:58-67.
109. Patch AM, Christie EL, Etemadmoghadam D, Garsed DW, George J, Fereday S, et al. Whole-genome characterization of chemoresistant ovarian cancer. Nature. 2015;521(7553):489-94.
110. Syrios J, Banerjee S, Kaye SB. Advanced epithelial ovarian cancer: from standard chemotherapy to promising molecular pathway targets--where are we now? Anticancer Res. 2014;34(5):2069-77.
111. Tan DS, Miller RE, Kaye SB. New perspectives on molecular targeted therapy in ovarian clear cell carcinoma. Br J Cancer. 2013;108(8):1553-9.
112. Colombo PE, Fabbro M, Theillet C, Bibeau F, Rouanet P, Ray-Coquard I. Sensitivity and resistance to treatment in the primary management of epithelial ovarian cancer. Crit Rev Oncol Hematol. 2014;89(2):207-16.

113. Lokadasan R, James FV, Narayanan G, Prabhakaran PK. Targeted agents in epithelial ovarian cancer: review on emerging therapies and future developments. Ecancermedicalscience. 2016;10:626.
114. Cheaib B, Auguste A, Leary A. The PI3K/Akt/mTOR pathway in ovarian cancer: therapeutic opportunities and challenges. Chin J Cancer. 2015;34(1):4-16.
115. Jackson SP, Bartek J. The DNA-damage response in human biology and disease. Nature. 2009;461(7267):1071-8.
116. Ba X, Garg NJ. Signaling mechanism of poly(ADP-ribose) polymerase-1 (PARP-1) in inflammatory diseases. Am J Pathol. 2011;178(3):946-55.
117. O'Sullivan Coyne G, Chen AP, Meehan R, Doroshow JH. PARP Inhibitors in Reproductive System Cancers: Current Use and Developments. Drugs. 2017;77(2):113-30.
118. Beck C, Robert I, Reina-San-Martin B, Schreiber V, Dantzer F. Poly(ADP-ribose) polymerases in double-strand break repair: focus on PARP1, PARP2 and PARP3. Exp Cell Res. 2014;329(1):18-25.
119. Karlberg T, Langelier MF, Pascal JM, Schuler H. Structural biology of the writers, readers, and erasers in mono- and poly(ADP-ribose) mediated signaling. Mol Aspects Med. 2013;34(6):1088-108.
120. Rodriguez MI, Majuelos-Melguizo J, Marti Martin-Consuegra JM, Ruiz de Almodovar M, Lopez-Rivas A, Javier Oliver F. Deciphering the insights of poly(ADP-ribosylation) in tumor progression. Med Res Rev. 2015;35(4):678-97.
121. Benafif S, Hall M. An update on PARP inhibitors for the treatment of cancer. Onco Targets Ther. 2015;8:519-28.
122. Patel AG, Sarkaria JN, Kaufmann SH. Nonhomologous end joining drives poly(ADP-ribose) polymerase (PARP) inhibitor lethality in homologous recombination-deficient cells. Proc Natl Acad Sci U S A. 2011;108(8):3406-11.
123. Dulaney C, Marcrom S, Stanley J, Yang ES. Poly(ADP-ribose) polymerase activity and inhibition in cancer. Semin Cell Dev Biol. 2017;63:144-53.
124. Robert I, Karicheva O, Reina San Martin B, Schreiber V, Dantzer F. Functional aspects of PARylation in induced and programmed DNA repair processes: preserving genome integrity and modulating physiological events. Mol Aspects Med. 2013;34(6):1138-52.
125. Ossovskaya V, Koo IC, Kaldjian EP, Alvares C, Sherman BM. Upregulation of Poly (ADP-Ribose) Polymerase-1 (PARP1) in Triple-Negative Breast Cancer and Other Primary Human Tumor Types. Genes Cancer. 2010;1(8):812-21.
126. Godoy H, Mhawech-Fauceglia P, Beck A, Miller A, Lele S, Odunsi K. Expression of poly (adenosine diphosphate-ribose) polymerase and p53 in epithelial ovarian cancer and their role in prognosis and disease outcome. Int J Gynecol Pathol. 2011;30(2):139-44.
127. Veskimae K, Staff S, Gronholm A, Pesu M, Laaksonen M, Nykter M, et al. Assessment of PARP protein expression in epithelial ovarian cancer by ELISA pharmacodynamic assay and immunohistochemistry. Tumour Biol. 2016;37(9):11991-9.
128. Ferraris DV. Evolution of poly(ADP-ribose) polymerase-1 (PARP-1) inhibitors. From concept to clinic. J Med Chem. 2010;53(12):4561-84.
129. Wang YQ, Wang PY, Wang YT, Yang GF, Zhang A, Miao ZH. An Update on Poly(ADP-ribose)polymerase-1 (PARP-1) Inhibitors: Opportunities and Challenges in Cancer Therapy. J Med Chem. 2016;59(21):9575-98.

130. Bryant HE, Schultz N, Thomas HD, Parker KM, Flower D, Lopez E, et al. Specific killing of BRCA2-deficient tumours with inhibitors of poly(ADP-ribose) polymerase. Nature. 2005;434(7035):913-7.
131. McCabe N, Lord CJ, Tutt AN, Martin NM, Smith GC, Ashworth A. BRCA2-deficient CAPAN-1 cells are extremely sensitive to the inhibition of Poly (ADP-Ribose) polymerase: an issue of potency. Cancer Biol Ther. 2005;4(9):934-6.
132. Brown JS, Kaye SB, Yap TA. PARP inhibitors: the race is on. Br J Cancer. 2016;114(7):713-5.
133. Polyak K, Garber J. Targeting the missing links for cancer therapy. Nat Med. 2011;17(3):283-4.
134. Scott CL, Swisher EM, Kaufmann SH. Poly (ADP-ribose) polymerase inhibitors: recent advances and future development. J Clin Oncol. 2015;33(12):1397-406.
135. McCabe N, Turner NC, Lord CJ, Kluzek K, Bialkowska A, Swift S, et al. Deficiency in the repair of DNA damage by homologous recombination and sensitivity to poly(ADP-ribose) polymerase inhibition. Cancer Res. 2006;66(16):8109-15.
136. Mirza MR, Monk BJ, Herrstedt J, Oza AM, Mahner S, Redondo A, et al. Niraparib Maintenance Therapy in Platinum-Sensitive, Recurrent Ovarian Cancer. N Engl J Med. 2016;375(22):2154-64.
137. Ceccaldi R, Liu JC, Amunugama R, Hajdu I, Primack B, Petalcorin MI, et al. Homologous-recombination-deficient tumours are dependent on Poltheta-mediated repair. Nature. 2015;518(7538):258-62.
138. Mateos-Gomez PA, Gong F, Nair N, Miller KM, Lazzerini-Denchi E, Sfeir A. Mammalian polymerase theta promotes alternative NHEJ and suppresses recombination. Nature. 2015;518(7538):254-7.
139. Wang M, Wu W, Wu W, Rosidi B, Zhang L, Wang H, et al. PARP-1 and Ku compete for repair of DNA double strand breaks by distinct NHEJ pathways. Nucleic Acids Res. 2006;34(21):6170-82.
140. Paddock MN, Bauman AT, Higdon R, Kolker E, Takeda S, Scharenberg AM. Competition between PARP-1 and Ku70 control the decision between high-fidelity and mutagenic DNA repair. DNA Repair (Amst). 2011;10(3):338-43.
141. Murai J, Huang SY, Das BB, Renaud A, Zhang Y, Doroshow JH, et al. Trapping of PARP1 and PARP2 by Clinical PARP Inhibitors. Cancer Res. 2012;72(21):5588-99.
142. Shen Y, Aoyagi-Scharber M, Wang B. Trapping Poly(ADP-Ribose) Polymerase. J Pharmacol Exp Ther. 2015;353(3):446-57.
143. Pal T, Permuth-Wey J, Betts JA, Krischer JP, Fiorica J, Arango H, et al. BRCA1 and BRCA2 mutations account for a large proportion of ovarian carcinoma cases. Cancer. 2005;104(12):2807-16.
144. Gelmon KA, Tischkowitz M, Mackay H, Swenerton K, Robidoux A, Tonkin K, et al. Olaparib in patients with recurrent high-grade serous or poorly differentiated ovarian carcinoma or triple-negative breast cancer: a phase 2, multicentre, open-label, non-randomised study. Lancet Oncol. 2011;12(9):852-61.
145. Audeh MW, Carmichael J, Penson RT, Friedlander M, Powell B, Bell-McGuinn KM, et al. Oral poly(ADP-ribose) polymerase inhibitor olaparib in patients with BRCA1 or BRCA2 mutations and recurrent ovarian cancer: a proof-of-concept trial. Lancet. 2010;376(9737):245-51.

146. Kaufman B, Shapira-Frommer R, Schmutzler RK, Audeh MW, Friedlander M, Balmana J, et al. Olaparib monotherapy in patients with advanced cancer and a germline BRCA1/2 mutation. J Clin Oncol. 2015;33(3):244-50.
147. Ledermann J, Harter P, Gourley C, Friedlander M, Vergote I, Rustin G, et al. Olaparib maintenance therapy in platinum-sensitive relapsed ovarian cancer. N Engl J Med. 2012;366(15):1382-92.
148. Murai J, Huang SY, Renaud A, Zhang Y, Ji J, Takeda S, et al. Stereospecific PARP trapping by BMN 673 and comparison with olaparib and rucaparib. Mol Cancer Ther. 2014;13(2):433-43.
149. Hopkins TA, Shi Y, Rodriguez LE, Solomon LR, Donawho CK, DiGiammarino EL, et al. Mechanistic Dissection of PARP1 Trapping and the Impact on In Vivo Tolerability and Efficacy of PARP Inhibitors. Mol Cancer Res. 2015;13(11):1465-77.
150. Yuan B, Ye N, Song SS, Wang YT, Song Z, Chen HD, et al. Poly(ADP-ribose)polymerase (PARP) inhibition and anticancer activity of simmiparib, a new inhibitor undergoing clinical trials. Cancer Lett. 2017;386:47-56.
151. Papeo G, Posteri H, Borghi D, Busel AA, Caprera F, Casale E, et al. Discovery of 2-[1-(4,4-Difluorocyclohexyl)piperidin-4-yl]-6-fluoro-3-oxo-2,3-dihydro-1H-isoind ole-4-carboxamide (NMS-P118): A Potent, Orally Available, and Highly Selective PARP-1 Inhibitor for Cancer Therapy. J Med Chem. 2015;58(17):6875-98.
152. Meng XW, Koh BD, Zhang JS, Flatten KS, Schneider PA, Billadeau DD, et al. Poly(ADP-ribose) polymerase inhibitors sensitize cancer cells to death receptor-mediated apoptosis by enhancing death receptor expression. J Biol Chem. 2014;289(30):20543-58.
153. Xu K, Chen Z, Cui Y, Qin C, He Y, Song X. Combined olaparib and oxaliplatin inhibits tumor proliferation and induces G2/M arrest and gamma-H2AX foci formation in colorectal cancer. Onco Targets Ther. 2015;8:3047-54.
154. Efimova EV, Mauceri HJ, Golden DW, Labay E, Bindokas VP, Darga TE, et al. Poly(ADP-ribose) polymerase inhibitor induces accelerated senescence in irradiated breast cancer cells and tumors. Cancer Res. 2010;70(15):6277-82.
155. Gonzalez-Billalabeitia E, Seitzer N, Song SJ, Song MS, Patnaik A, Liu XS, et al. Vulnerabilities of PTEN-TP53-deficient prostate cancers to compound PARP-PI3K inhibition. Cancer Discov. 2014;4(8):896-904.
156. Jenner ZB, Sood AK, Coleman RL. Evaluation of rucaparib and companion diagnostics in the PARP inhibitor landscape for recurrent ovarian cancer therapy. Future Oncol. 2016;12(12):1439-56.
157. Meehan RS, Chen AP. New treatment option for ovarian cancer: PARP inhibitors. Gynecol Oncol Res Pract. 2016;3:3.
158. Lord CJ, Ashworth A. Mechanisms of resistance to therapies targeting BRCA-mutant cancers. Nat Med. 2013;19(11):1381-8.
159. Nakada S, Yonamine RM, Matsuo K. RNF8 regulates assembly of RAD51 at DNA double-strand breaks in the absence of BRCA1 and 53BP1. Cancer Res. 2012;72(19):4974-83.
160. Liu X, Han EK, Anderson M, Shi Y, Semizarov D, Wang G, et al. Acquired resistance to combination treatment with temozolomide and ABT-888 is mediated by both base excision repair and homologous recombination DNA repair pathways. Mol Cancer Res. 2009;7(10):1686-92.
161. Bouwman P, Jonkers J. Molecular pathways: how can BRCA-mutated tumors become resistant to PARP inhibitors? Clin Cancer Res. 2014;20(3):540-7.

162. Gill SJ, Travers J, Pshenichnaya I, Kogera FA, Barthorpe S, Mironenko T, et al. Combinations of PARP Inhibitors with Temozolomide Drive PARP1 Trapping and Apoptosis in Ewing's Sarcoma. PLoS One. 2015;10(10):e0140988.
163. Sui H, Shi C, Yan Z, Li H. Combination of erlotinib and a PARP inhibitor inhibits growth of A2780 tumor xenografts due to increased autophagy. Drug Des Devel Ther. 2015;9:3183-90.
164. Pfaffle HN, Wang M, Gheorghiu L, Ferraiolo N, Greninger P, Borgmann K, et al. EGFR-activating mutations correlate with a Fanconi anemia-like cellular phenotype that includes PARP inhibitor sensitivity. Cancer Res. 2013;73(20):6254-63.
165. Chan N, Bristow RG. "Contextual" synthetic lethality and/or loss of heterozygosity: tumor hypoxia and modification of DNA repair. Clin Cancer Res. 2010;16(18):4553-60.
166. Kraus WL, Hottiger MO. PARP-1 and gene regulation: progress and puzzles. Mol Aspects Med. 2013;34(6):1109-23.
167. Booth L, Cruickshanks N, Ridder T, Dai Y, Grant S, Dent P. PARP and CHK inhibitors interact to cause DNA damage and cell death in mammary carcinoma cells. Cancer Biol Ther. 2013;14(5):458-65.
168. McConechy MK, Ding J, Senz J, Yang W, Melnyk N, Tone AA, et al. Ovarian and endometrial endometrioid carcinomas have distinct CTNNB1 and PTEN mutation profiles. Mod Pathol. 2014;27(1):128-34.
169. Provencher DM, Lounis H, Champoux L, Tetrault M, Manderson EN, Wang JC, et al. Characterization of four novel epithelial ovarian cancer cell lines. In Vitro Cell Dev Biol Anim. 2000;36(6):357-61.
170. Ouellet V, Zietarska M, Portelance L, Lafontaine J, Madore J, Puiffe ML, et al. Characterization of three new serous epithelial ovarian cancer cell lines. BMC Cancer. 2008;8:152.
171. Letourneau IJ, Quinn MC, Wang LL, Portelance L, Caceres KY, Cyr L, et al. Derivation and characterization of matched cell lines from primary and recurrent serous ovarian cancer. BMC Cancer. 2012;12:379.
172. Domcke S, Sinha R, Levine DA, Sander C, Schultz N. Evaluating cell lines as tumour models by comparison of genomic profiles. Nat Commun. 2013;4:2126.
173. DelloRusso C, Welcsh PL, Wang W, Garcia RL, King MC, Swisher EM. Functional characterization of a novel BRCA1-null ovarian cancer cell line in response to ionizing radiation. Mol Cancer Res. 2007;5(1):35-45.
174. Langdon SP, Lawrie SS, Hay FG, Hawkes MM, McDonald A, Hayward IP, et al. Characterization and properties of nine human ovarian adenocarcinoma cell lines. Cancer Res. 1988;48(21):6166-72.
175. Tonin PN, Mes-Masson AM, Futreal PA, Morgan K, Mahon M, Foulkes WD, et al. Founder BRCA1 and BRCA2 mutations in French Canadian breast and ovarian cancer families. Am J Hum Genet. 1998;63(5):1341-51.
176. Cavallone L, Arcand SL, Maugard CM, Nolet S, Gaboury LA, Mes-Masson AM, et al. Comprehensive BRCA1 and BRCA2 mutation analyses and review of French Canadian families with at least three cases of breast cancer. Fam Cancer. 2010;9(4):507-17.
177. Aylon Y, Oren M. New plays in the p53 theater. Curr Opin Genet Dev. 2011;21(1):86-92.
178. Saldana-Meyer R, Recillas-Targa F. Transcriptional and epigenetic regulation of the p53 tumor suppressor gene. Epigenetics. 2011;6(9):1068-77.

179. Wojnarowicz PM, Oros KK, Quinn MC, Arcand SL, Gambaro K, Madore J, et al. The genomic landscape of TP53 and p53 annotated high grade ovarian serous carcinomas from a defined founder population associated with patient outcome. PLoS One. 2012;7(9):e45484.
180. Oros Klein K, Oualkacha K, Lafond MH, Bhatnagar S, Tonin PN, Greenwood CM. Gene Coexpression Analyses Differentiate Networks Associated with Diverse Cancers Harboring TP53 Missense or Null Mutations. Front Genet. 2016;7:137.
181. Kurman RJ. Origin and molecular pathogenesis of ovarian high-grade serous carcinoma. Ann Oncol. 2013;24 Suppl 10:x16-21.
182. Stewart CJ, McCluggage WG. Epithelial-mesenchymal transition in carcinomas of the female genital tract. Histopathology. 2013;62(1):31-43.
183. Yi BR, Kim TH, Kim YS, Choi KC. Alteration of epithelial-mesenchymal transition markers in human normal ovaries and neoplastic ovarian cancers. Int J Oncol. 2015;46(1):272-80.
184. Davidson B, Trope CG, Reich R. Epithelial-mesenchymal transition in ovarian carcinoma. Front Oncol. 2012;2:33.
185. Auer K, Bachmayr-Heyda A, Aust S, Sukhbaatar N, Reiner AT, Grimm C, et al. Peritoneal tumor spread in serous ovarian cancer-epithelial mesenchymal status and outcome. Oncotarget. 2015;6(19):17261-75.
186. Bouwman P, Jonkers J. The effects of deregulated DNA damage signalling on cancer chemotherapy response and resistance. Nat Rev Cancer. 2012;12(9):587-98.
187. Feng FY, de Bono JS, Rubin MA, Knudsen KE. Chromatin to Clinic: The Molecular Rationale for PARP1 Inhibitor Function. Mol Cell. 2015;58(6):925-34.
188. Liu Y, Kadyrov FA, Modrich P. PARP-1 enhances the mismatch-dependence of 5'-directed excision in human mismatch repair in vitro. DNA Repair (Amst). 2011;10(11):1145-53.
189. Postel-Vinay S, Bajrami I, Friboulet L, Elliott R, Fontebasso Y, Dorvault N, et al. A high-throughput screen identifies PARP1/2 inhibitors as a potential therapy for ERCC1-deficient non-small cell lung cancer. Oncogene. 2013;32(47):5377-87.
190. Fong PC, Yap TA, Boss DS, Carden CP, Mergui-Roelvink M, Gourley C, et al. Poly(ADP)-ribose polymerase inhibition: frequent durable responses in BRCA carrier ovarian cancer correlating with platinum-free interval. J Clin Oncol. 2010;28(15):2512-9.
191. Zhang Y, Rohde LH, Wu H. Involvement of nucleotide excision and mismatch repair mechanisms in double strand break repair. Curr Genomics. 2009;10(4):250-8.
192. Zhao H, Thienpont B, Yesilyurt BT, Moisse M, Reumers J, Coenegrachts L, et al. Mismatch repair deficiency endows tumors with a unique mutation signature and sensitivity to DNA double-strand breaks. Elife. 2014;3:e02725.
193. Martin SA, Lord CJ, Ashworth A. Therapeutic targeting of the DNA mismatch repair pathway. Clin Cancer Res. 2010;16(21):5107-13.
194. Robu M, Shah RG, Petitclerc N, Brind'Amour J, Kandan-Kulangara F, Shah GM. Role of poly(ADP-ribose) polymerase-1 in the removal of UV-induced DNA lesions by nucleotide excision repair. Proc Natl Acad Sci U S A. 2013;110(5):1658-63.
195. Ko HL, Ren EC. Functional Aspects of PARP1 in DNA Repair and Transcription. Biomolecules. 2012;2(4):524-48.
196. Sameer AS, Nissar S, Fatima K. Mismatch repair pathway: molecules, functions, and role in colorectal carcinogenesis. Eur J Cancer Prev. 2014;23(4):246-57.

197. Marteijn JA, Lans H, Vermeulen W, Hoeijmakers JH. Understanding nucleotide excision repair and its roles in cancer and ageing. Nat Rev Mol Cell Biol. 2014;15(7):465-81.
198. Peng M, Xie J, Ucher A, Stavnezer J, Cantor SB. Crosstalk between BRCA-Fanconi anemia and mismatch repair pathways prevents MSH2-dependent aberrant DNA damage responses. EMBO J. 2014;33(15):1698-712.
199. McCormick A, Donoghue P, Dixon M, O'Sullivan R, O'Donnell RL, Murray J, et al. Ovarian Cancers Harbor Defects in Nonhomologous End Joining Resulting in Resistance to Rucaparib. Clin Cancer Res. 2017;23(8):2050-60.
200. Sander Effron S, Makvandi M, Lin L, Xu K, Li S, Lee H, et al. PARP-1 Expression Quantified by [18F]FluorThanatrace: A Biomarker of Response to PARP Inhibition Adjuvant to Radiation Therapy. Cancer Biother Radiopharm. 2017;32(1):9-15.
201. Baum M, Budzar AU, Cuzick J, Forbes J, Houghton JH, Klijn JG, et al. Anastrozole alone or in combination with tamoxifen versus tamoxifen alone for adjuvant treatment of postmenopausal women with early breast cancer: first results of the ATAC randomised trial. Lancet. 2002;359(9324):2131-9.
202. Bollag G, Hirth P, Tsai J, Zhang J, Ibrahim PN, Cho H, et al. Clinical efficacy of a RAF inhibitor needs broad target blockade in BRAF-mutant melanoma. Nature. 2010;467(7315):596-9.
203. O'Reilly EA, Gubbins L, Sharma S, Tully R, Guang MH, Weiner-Gorzel K, et al. The fate of chemoresistance in triple negative breast cancer (TNBC). BBA Clin. 2015;3:257-75.
204. Dale Rein I, Solberg Landsverk K, Micci F, Patzke S, Stokke T. Replication-induced DNA damage after PARP inhibition causes G2 delay, and cell line-dependent apoptosis, necrosis and multinucleation. Cell Cycle. 2015;14(20):3248-60.
205. Alotaibi M, Sharma K, Saleh T, Povirk LF, Hendrickson EA, Gewirtz DA. Radiosensitization by PARP Inhibition in DNA Repair Proficient and Deficient Tumor Cells: Proliferative Recovery in Senescent Cells. Radiat Res. 2016;185(3):229-45.
206. Aliouat-Denis CM, Dendouga N, Van den Wyngaert I, Goehlmann H, Steller U, van de Weyer I, et al. p53-independent regulation of p21Waf1/Cip1 expression and senescence by Chk2. Mol Cancer Res. 2005;3(11):627-34.
207. Zannini L, Delia D, Buscemi G. CHK2 kinase in the DNA damage response and beyond. J Mol Cell Biol. 2014;6(6):442-57.
208. Ganguly B, Dolfi SC, Rodriguez-Rodriguez L, Ganesan S, Hirshfield KM. Role of Biomarkers in the Development of PARP Inhibitors. Biomark Cancer. 2016;8(Suppl 1):15-25.
209. Duong HQ, Hong YB, Kim JS, Lee HS, Yi YW, Kim YJ, et al. Inhibition of checkpoint kinase 2 (CHK2) enhances sensitivity of pancreatic adenocarcinoma cells to gemcitabine. J Cell Mol Med. 2013;17(10):1261-70.
210. Park SH, Jang KY, Kim MJ, Yoon S, Jo Y, Kwon SM, et al. Tumor suppressive effect of PARP1 and FOXO3A in gastric cancers and its clinical implications. Oncotarget. 2015;6(42):44819-31.
211. Buontempo F, Chiarini F, Bressanin D, Tabellini G, Melchionda F, Pession A, et al. Activity of the selective IkappaB kinase inhibitor BMS-345541 against T-cell acute lymphoblastic leukemia: involvement of FOXO3a. Cell Cycle. 2012;11(13):2467-75.
212. Seoane J, Le HV, Shen L, Anderson SA, Massague J. Integration of Smad and forkhead pathways in the control of neuroepithelial and glioblastoma cell proliferation. Cell. 2004;117(2):211-23.

213. Dijkers PF, Medema RH, Pals C, Banerji L, Thomas NS, Lam EW, et al. Forkhead transcription factor FKHR-L1 modulates cytokine-dependent transcriptional regulation of p27(KIP1). Mol Cell Biol. 2000;20(24):9138-48.
214. Rucaparib Approved for Ovarian Cancer. Cancer Discov. 2017;7(2):120-1.
215. de Bono J, Ramanathan RK, Mina L, Chugh R, Glaspy J, Rafii S, et al. Phase I, Dose-Escalation, Two-Part Trial of the PARP Inhibitor Talazoparib in Patients with Advanced Germline BRCA1/2 Mutations and Selected Sporadic Cancers. Cancer Discov. 2017.
216. Gordon RR, Nelson PS. Cellular senescence and cancer chemotherapy resistance. Drug Resist Updat. 2012;15(1-2):123-31.
217. Norquist B, Wurz KA, Pennil CC, Garcia R, Gross J, Sakai W, et al. Secondary somatic mutations restoring BRCA1/2 predict chemotherapy resistance in hereditary ovarian carcinomas. J Clin Oncol. 2011;29(22):3008-15.
218. Pishvaian MJ, Biankin AV, Bailey P, Chang DK, Laheru D, Wolfgang CL, et al. BRCA2 secondary mutation-mediated resistance to platinum and PARP inhibitor-based therapy in pancreatic cancer. Br J Cancer. 2017;116(8):1021-6.
219. Quigley D, Alumkal JJ, Wyatt AW, Kothari V, Foye A, Lloyd P, et al. Analysis of Circulating Cell-free DNA Identifies Multi-clonal Heterogeneity of BRCA2 Reversion Mutations Associated with Resistance to PARP Inhibitors. Cancer Discov. 2017.
220. Lheureux S, Bruce JP, Burnier JV, Karakasis K, Shaw PA, Clarke BA, et al. Somatic BRCA1/2 Recovery as a Resistance Mechanism After Exceptional Response to Poly (ADP-ribose) Polymerase Inhibition. J Clin Oncol. 2017;35(11):1240-9.
221. Chang J, Wang Y, Shao L, Laberge RM, Demaria M, Campisi J, et al. Clearance of senescent cells by ABT263 rejuvenates aged hematopoietic stem cells in mice. Nat Med. 2016;22(1):78-83.
222. Tse C, Shoemaker AR, Adickes J, Anderson MG, Chen J, Jin S, et al. ABT-263: a potent and orally bioavailable Bcl-2 family inhibitor. Cancer Res. 2008;68(9):3421-8.
223. Rudin CM, Hann CL, Garon EB, Ribeiro de Oliveira M, Bonomi PD, Camidge DR, et al. Phase II study of single-agent navitoclax (ABT-263) and biomarker correlates in patients with relapsed small cell lung cancer. Clin Cancer Res. 2012;18(11):3163-9.
224. Gandhi L, Camidge DR, Ribeiro de Oliveira M, Bonomi P, Gandara D, Khaira D, et al. Phase I study of Navitoclax (ABT-263), a novel Bcl-2 family inhibitor, in patients with small-cell lung cancer and other solid tumors. J Clin Oncol. 2011;29(7):909-16.
225. Vlahovic G, Karantza V, Wang D, Cosgrove D, Rudersdorf N, Yang J, et al. A phase I safety and pharmacokinetic study of ABT-263 in combination with carboplatin/paclitaxel in the treatment of patients with solid tumors. Invest New Drugs. 2014;32(5):976-84.
226. Zhu Y, Tchkonia T, Fuhrmann-Stroissnigg H, Dai HM, Ling YY, Stout MB, et al. Identification of a novel senolytic agent, navitoclax, targeting the Bcl-2 family of anti-apoptotic factors. Aging Cell. 2016;15(3):428-35.
227. Yosef R, Pilpel N, Tokarsky-Amiel R, Biran A, Ovadya Y, Cohen S, et al. Directed elimination of senescent cells by inhibition of BCL-W and BCL-XL. Nat Commun. 2016;7:11190.
228. Yokoyama T, Kohn EC, Brill E, Lee JM. Apoptosis is augmented in high-grade serous ovarian cancer by the combined inhibition of Bcl-2/Bcl-xL and PARP. Int J Oncol. 2017.
229. Naipal KA, Verkaik NS, Ameziane N, van Deurzen CH, Ter Brugge P, Meijers M, et al. Functional ex vivo assay to select homologous recombination-deficient breast tumors for PARP inhibitor treatment. Clin Cancer Res. 2014;20(18):4816-26.

230. Telli ML, Timms KM, Reid J, Hennessy B, Mills GB, Jensen KC, et al. Homologous Recombination Deficiency (HRD) Score Predicts Response to Platinum-Containing Neoadjuvant Chemotherapy in Patients with Triple-Negative Breast Cancer. Clin Cancer Res. 2016;22(15):3764-73.
231. Auclair Y, Rouget R, Affar el B, Drobetsky EA. ATR kinase is required for global genomic nucleotide excision repair exclusively during S phase in human cells. Proc Natl Acad Sci U S A. 2008;105(46):17896-901.
232. Lee JM, Gordon N, Trepel JB, Lee MJ, Yu M, Kohn EC. Development of a multiparameter flow cytometric assay as a potential biomarker for homologous recombination deficiency in women with high-grade serous ovarian cancer. J Transl Med. 2015;13:239.
233. Astolfi M, Peant B, Lateef MA, Rousset N, Kendall-Dupont J, Carmona E, et al. Micro-dissected tumor tissues on chip: an ex vivo method for drug testing and personalized therapy. Lab Chip. 2016;16(2):312-25.
234. Montoni A, Robu M, Pouliot E, Shah GM. Resistance to PARP-Inhibitors in Cancer Therapy. Front Pharmacol. 2013;4:18.
235. Wang D, Du R, Liu S. Rad51 inhibition sensitizes breast cancer stem cells to PARP inhibitor in triple-negative breast cancer. Chin J Cancer. 2017;36(1):37.
236. Mo W, Liu Q, Lin CC, Dai H, Peng Y, Liang Y, et al. mTOR Inhibitors Suppress Homologous Recombination Repair and Synergize with PARP Inhibitors via Regulating SUV39H1 in BRCA-Proficient Triple-Negative Breast Cancer. Clin Cancer Res. 2016;22(7):1699-712.
237. Liu JF, Tolaney SM, Birrer M, Fleming GF, Buss MK, Dahlberg SE, et al. A Phase 1 trial of the poly(ADP-ribose) polymerase inhibitor olaparib (AZD2281) in combination with the anti-angiogenic cediranib (AZD2171) in recurrent epithelial ovarian or triple-negative breast cancer. Eur J Cancer. 2013;49(14):2972-8.
238. Jordheim LP, Barakat KH, Heinrich-Balard L, Matera EL, Cros-Perrial E, Bouledrak K, et al. Small molecule inhibitors of ERCC1-XPF protein-protein interaction synergize alkylating agents in cancer cells. Mol Pharmacol. 2013;84(1):12-24.
239. Biau J, Devun F, Verrelle P, Dutreix M. [Dbait: An innovative concept to inhibit DNA repair and treat cancer]. Bull Cancer. 2016;103(3):227-35.